Studying Protein–Glycolipid Interactions and Membrane Peptides and Proteins using Electrospray Ionization Mass Spectrometry and Model Membranes

by

Jun Li

A thesis submitted in partial fulfillment of the requirements for the degree of

Doctor of Philosophy

Department of Chemistry
University of Alberta

Abstract

Membrane systems, including glycolipids (GLs) and membrane peptides and proteins (MPs), play an important role in many cellular processes, such as singling, cellular recognition, transportation, and energy conversion. However, the amphipathic nature of GLs and MPs makes their analysis challenging. Nanoscale lipoprotein model membranes (MMs) provide a native like lipid environment to solubilize them. This thesis focuses on the development of electrospray ionization mass spectrometry (ESI-MS) based methods combined with lipoprotein MMs for discovery and characterization of GL receptors of glycan-binding proteins (GBPs) and to investigate stoichiometry and conformations of MP complexes.

Chapter 2 describes the development of the catch-and-release (CaR) ESI-MS assay, combined with picodiscs (complexes comprised of saposin A and lipids, PDs), to screen GL mixtures against water-soluble GBPs to detect specific interactions. The proof-of-concept experiments were performed by screening PDs containing a small library of purified gangliosides against the B subunit homopentamer of cholera toxin (CTB_5) and a sub-fragment of toxin A from *Clostridium difficile* (TcdA-A2), which demonstrated the simultaneous detection of both high and low affinity interactions. Screening mixture of GLs extracted from porcine brain and a human epithelial cell line against CTB_5 successfully identified high affinity GL ligands present in both GL mixtures. Finally, a comparison of the present results with data obtained with the CaR-ESI-MS assay implemented using nanodiscs (NDs) revealed that the PDs exhibited similar or superior performance to NDs for GBP–GL binding measurements.

Chapter 3 reports the first detailed investigation into the composition, heterogeneity and structure of 1-palmitoyl-2-oleoyl-*sn*-glycero-3-phosphocholine-containing PDs (POPC-PDs) in acquous solutions using high resolution ESI-MS, multi-angle laser light scattering (MALLS) and

molecular dynamics (MD) simulations. The ESI-MS and MALLS data revealed that the size and composition of POPC-PDs are dependent on pH – predominantly as a SapA dimer at acidic pH; predominantly as a SapA tetramer in freshly prepared solutions at neutral pH and converts to SapA trimer over the course of hours. Comparison of measured collision cross sections (Ω) with values calculated for gaseous ions from modelling suggests that the solution structures are largely preserved in the gas phase, although the lipids do not maintain regular bilayer orientations.

Chapter 4 describes the use of passively-loaded PDs (^{PL}PDs), prepared by incubating phospholipid PDs with GL or GL mixture (in the form of glycomicelle) in aqueous solution, for CaR-ESI-MS screening of GLs against CTB_5 and compares their performance with pre-loaded PDs, prepared directly from a mixture of phospholipid and GL(s). GM1 binding to CTB_5 measured for ^{PL}PDs prepared from GM1 is indistinguishable from that observed with pre-loaded GM1 PDs. GL binding to CTB_5 measured for ^{PL}PDs prepared from GLs extracted from pig and mouse brain revealed that the ^{PL}PDs allow for the detection of a greater number of ganglioside ligands than pre-loaded PDs. Together, these results suggest ^{PL}PDs may have advantages over conventionally prepared PDs for screening GLs against GBPs using CaR-ESI-MS.

In Chapter 5, the gas-phase conformations of dimers of the channel-forming membrane peptide gramicidin A (GA), produced from NDs, are investigated using ion mobility separation (IMS)-MS and MD simulations. GA dimer is readily transferred from phospholipid NDs to the gas phase by ESI and it suggested that the ion conducting single stranded head-to-head helical conformation of the dimer was preserved in the gas phase. Notably, the conformation of GA dimers produced from NDs was found to be different from those determined directly from organic solvent and phospholipid vesicles, which suggests that the method used to deliver the peptide complexes from the lipid bilayer to the gas phase may influence the conformations of the gaseous ions.

Preface

My research related to the PDs (Chapters 2 to 4 in this thesis) was conducted in collaboration with Professor Gilbert G. Privé at University of Toronto. My research in Chapter 2 was also collaborated with Professor Christopher W. Cairo at University of Alberta and Professor Kenneth K. S. Ng at University of Calgary. My research in Chapter 3 was also collaborated with Dhanashri Bagal and Dr. Iain D. G. Campuzano at Amgen.

Chapter 2 has been published as: Li, J.; Fan, X.; Kitova, E. N.; Zou, C.; Cairo, C. W.; Eugenio, L.; Ng, K. K. S.; Xiong, Z. J.; Privé, G. G.; Klassen, J. S., "Screening Glycolipids Against Proteins in vitro using Picodiscs and Catch-and-Release Electrospray Ionization Mass Spectrometry", *Anal Chem*. **2016**, *88,* 4742-4750. I was responsible for all the PDs related experiments, data analysis for all experiments and manuscript preparation. The experiments of screening NDs against TcdA-A2 were done by X. Fan. E. N. Kitova assisted with manuscript revision. C. Zou and C. W. Cairo were responsible for GL extraction from the A549 cell line. L. Eugenio and K. K. S. Ng were responsible for the expression and purification of TcdA-A2. Z. J. Xiong and G. G. Privé were responsible for the expression and purification of SapA.

Chapter 3 has been published as: Li, J.; Richards, M. R.; Bagal, D.; Campuzao, D. G.; Kitova, E. N.; Xiong, Z. J.; Privé, G. G.; Klassen, J. S., "Characterizing the Size and Composition of Saposin A Lipoprotein Picodiscs", *Anal Chem*. **2016**, *88,* 9524-9531. I performed all the ESI-MS data using Synapt G2-S and light scattering experiments, analyzed all the experimental data and prepared the manuscript. M. R. Richards performed the MD simulations of POPC-PDs, assisted with the interpretation and calculated the radius of gyration of POPC-PDs. D. Bagal performed the ESI-MS experiments using Exactive Plus Orbitrap. D. G. Campuzao assisted with the spectral deconvolution and theoretical Ω calculation of POPC-PDs. E. N. Kitova assisted with

manuscript revision. Z. J. Xiong and G. G. Privé were responsible for the expression and purification of SapA.

Chapter 4 has been published as: Li, J.; Han, L.; Li, J.; Kitova, E. N.; Xiong, Z. J.; Privé, G. G.; Klassen, J. S., "Detecting Protein–Glycolipid Interactions using CaR-ESI-MS and Model Membranes. Comparison of Pre- and Passively-loaded Picodiscs", *J. Am. Soc. Mass. Spectrom*. **2018**, *29,* 1493-1504. I was responsible for all the experiments, all data analysis and preparation of manuscript. L. Han assisted with the concept formation and design of the ESI-MS experiments. Jianing Li (third author) assisted with the preparation of NDs and PDs. E. N. Kitova assisted with revision of manuscript. Z. J. Xiong and G. G. Privé were responsible for the expression and purification of SapA.

Chapter 5 has been published as: Li, J.; Richards, M. R.; Kitova, E. N.; Klassen, J. S., "Delivering Transmembrane Peptide Complexes to the Gas Phase using Nanodiscs and Electrospray Ionization", *J. Am. Soc. Mass. Spectrom*. **2017**, *28*, 2054-2065. I performed all the ESI-MS experiments, analyzed all experimental data and prepared the manuscript. M. R. Richards performed the MD simulations and calculated theoretical Ω of GA. E. N. Kitova assisted with revision of manuscript.

The supervisory author, J. S. Klassen, was involved throughout all the projects in concept formation and manuscript composition.

Acknowledgement

Looking back to my past five years, I am so lucky to meet and know so many people who helped me and made me today. I would like to express my since gratitude to them.

First, I would like to express the great gratitude to my supervisor, Professor John Klassen, for his continuous support of my Ph.D study and related research, for his guidance, encouragement, and inspiration. His guidance helped me in all the time of research and writing of this thesis. He encouraged me to think critically and independently. He inspired me thinking of the significance of the projects and exploring my own ideas.

I would also like to thank other members of my supervisory and examining committee, Prof. Liang Li, Prof. Christopher Cairo, Prof. Todd Lowary and Prof. Robert Campbell for their invaluable comments and advice on my research. Special thanks must go to Prof. Brandon Ruotolo from University of Michigan, for his participation of my defense and the time spent reviewing my thesis. I am thankful to Prof. Alex Brown for being my non-examining chair of my final exam.

I am very grateful to my collaborators, Prof. Gilbert Privé and his group from University of Toronto for providing us the saposinA (SapA) for PD related projects and helpful suggestions. I would like to thank Prof. Kenneth Ng and his group from University of Calgary for providing TcdA-A2, Prof. Glen Armstrong from University of Calgary for providing shiga toxin (Stx1-B_5), and Prof. Christopher Cairo and his group for providing the GL extract from human cell line, for my library screening project. I am thankful to Dhanashri Bagal and Dr. Iain Campuzano from Amgen for their kind help with ESI-MS experiments on Exactive Plus Orbitrap and the spectral deconvolution and interpretation. I would like to thank Blake Zheng and Gareth Lambkin for their professional trainings and assistance for biological analyses.

I have the honor to work with many excellent colleagues. I would like to thank Dr. Michele Richards for her help with MD simulations and corresponding theoretical calculation. I would like to thank Xuxin Fan for her help with screening experiments using NDs. I would like to thank Dr. Aneika Leney, who taught me a lot of experimental skills, especially the preparation of PDs and NDs. I would like to thank Dr. Ling Han, who taught me a lot in experimental design and data interpretation. I would like to thank Dr. Elena Kitova for kind help with manuscript revision. I would like to thank Jianing Li for her assistance with some sample preparation. Moreover, I would like to acknowledge the support and friendship from other labmates in Klassen group, former or present: Dr. Rambod Daneshfar, Dr. Amr EI-Hawiet, Dr. Emma-Duce Leriche, Jingjing Zhang, Km Shams-Ud-Doha, Reza Rezaei Darestani, Yuyu Yao, Nobar Jalili, Sanaz Nikjah, Xin Wang, Dr. Pavel Kitov, Dr. Heajin Park, Hong Lin, Yajie Chen, Yilin Wang, Zhixiong Li, and Erick Baez Bolivar.

I also would like to thank the National Sciences and Engineering Research Council of Canada and Alberta Glycomics Centre for generous funding and the Alberta Innovates Technology Futures and University of Alberta for graduate scholarships.

I give sincere thanks to my friends, Xiaohui Mao, Qianhui Zhao, Yining Fang, Linwei Wang, Jing liu, Chao Wang and many others for their support. I am deeply thankful to my families for their constant love and support. I give special thanks to my boyfriend, Jingwen Xu, for being my side. I would not have made it this far without his love, strong support and encouragement.

Finally, I acknowledge myself for being strong and always pursuing what I would like to do no matter how difficult it is.

Table of Contents

List of Tables

List of Figures

List of Abbreviations

Ab	Abundance of gas phase ions
ADC	Analog-to-digital
Amphipol	Amphipathic polymer
ATD	Arrival time distribution
BIRD	Blackbody infrared radiative dissociation
BSA	Bovine Serum Albumin
CaR	Catch-and-release
CaR-ESI-MS	Catch-and-release electrospray ionization mass spectrometry
CEM	Chain ejection model
CID	Collision-induced dissociation
CRM	Charged residue model
CTB_5	Cholera toxin B subunit homopentamer
Cyt c	Cytochrome c
Da	Dalton
DC	Direct current
DESI	Desorption electrospray ionization
DMPC	1,2-dimyristoyl-*sn*-glycero-3-phosphocholine
DSDHap	Antiparallel double-stranded double helix
DSDHp	Parallel double-standard double helix
DTIMS	Drift tube ion mobility spectrometry
ECD	Electron capture dissociation
ELISA	Enzyme-linked immunosorbent assay
ESI	Electrospray ionization
ESI-MS	Electrospray ionization mass spectrometry
ETD	Electron transfer dissociation
FAIMS	Field asymmetric waveform ion mobility spectrometry
FT	Fourier transform
Fuc	Fucose

FWHM	Full width half maximum
GA	Gramicidin A
Gal	Galactose
GalNAc	N-acetyl galactosamine
GBP	Glycan-binding protein
GL	Glycolipid
Glc	Glucose
GSL	Glycosphingolipid
HCD	Higher-energy C-trap dissociation
IEM	Ion ejection model
IMS	Ion mobility separation
IMS-MS	Ion mobility mass spectrometry
IRMPD	Infrared radiative multiphoton dissociation
K_a	Association constant
$K_{a,app}$	Apparent association constant
L	Ligand
LDAO	*N,N*-dimethyldodecylamine *N*-oxide
mAb	Monoclonal antibody
MALLS	Multi-angle laser light scattering
MD	Molecular dynamics
MM	Model membrane
m/z	Mass-to-charge ratio
MS	Mass spectrometry
MSP	Membrane scaffold protein
MW	Molecular weight
myo	Myoglobin
nanoESI	Nanoflow electrospray ionization
ND	Nanodisc
Neu5Ac	N-acetyl neuraminic acid

Ni-NTA	Nickel charged nitrilotriacetic acid
NMR	Nuclear magnetic resonance
P	Protein
PA	Phosphatidic acid
PBS	Phosphate buffered saline
PC	Phosphatidylcholine
PD	Picodisc
^{PL}PD	Passively-loaded picodisc
PDB	Protein data bank
PE	Phosphatidylethanolamine
PI	Phosphatidylinositol
PL	Protein–ligand complex
POPC	1-palmitory-2-oleoyl-*sn*-glycero-3-phophoscholine
P_{ref}	Reference protein
PS	Phosphatidylserine
Q	Charge
QELS	Quasi-elastic light scattering
R	Abundance ratio
R_R	Rayleigh limit
R_g	Radius of gyration
R_h	Hydrodynamic radius
RF	Response factor
RF	Radiofrequency
RMS	Root mean square error
SapA	Saposin A
scFv	Single chain variable fragment
SEC	Size exclusion chromatography
SID	Surface induced dissociation
SMA	Styrene maleic acid copolymer

SMALP	Styrene maleic acid copolymer lipid particles
SPR	Surface plasmon resonance spectroscopy
SSHH	Single-stranded head-to-head helix
STD-NMR	Saturation transfer difference-nuclear magnetic resonance
$Stx1B_5$	Shiga toxin type 1 B subunit homopentamer
TcdA	Toxin A from *Clostridium difficile*
TcdA-A2	Sub fragment of toxin A from *Clostridium difficile*
TLC	Thin layer chromatography
TOF	Time-of-flight
TTR	Transthyretin
T-Wave	Travelling wave
TWIMS	Travelling wave ion mobility spectrometry
UV	Ultraviolet
UVPD	Ultraviolet photodissociation
VCFD	Vesicle capture-freeze-drying
Ω	Collision cross section

Chapter 1

Studying Protein–Glycolipid Interactions and Membrane Peptides and Proteins using Electrospray Ionization Mass Spectrometry and Model Membranes

1.1 Introduction

1.1.1 Composition and function of cell membrane

Cell membranes play a critical role in biology. The basic function of the membrane is to physically separate and protect the interior of cells from the extracellular environment.[1] It also controls the movement of substances, regulates information and energy flow in and out of cells and their various compartments. The membrane consists of a variety of biological molecules, notably lipids and proteins. The proportions of each component vary between species, organisms, cell types, and different stages of cell development.[2] Even in a given cell, the composition of membrane is not fixed, but is continuously changing in response to changes in the environment. For the majority of eukaryotic cells, the composition (by weight) of plasma membranes is about half lipids and half proteins. The lipids are arranged as a bilayer held together via non-covalent interactions between their hydrophobic moieties. The membrane is highly fluid and the lipids, as well as the proteins embedded in the bilayer, can move within membrane. The lipids exhibit rapid lateral diffusion along the leaflet in which they are present; however, the exchange of lipids between intracellular and extracellular leaflets of the bilayer is a slow process (generally hours to days).[3,4]

There are three main classes of lipids found in cellular membranes: phospholipids, glycolipids (GLs) and sterols. The amount of each depends on the cell type, but in the most cases,

phospholipids, are the most abundant lipids.[3] The major structural phospholipids in eukaryotic membranes are the glycerophospholipids (Figure 1.1a). They are composed of a hydrophobic diacylglycerol, which contains saturated or cis-unsaturated fatty acyl chains from 14 to 24 atoms, and a hydrophilic phosphate-containing head group.[5] Depending on the head group (Figure 1.1a), they are classified as phosphatidylcholine (PC), phosphatidylethanolamine (PE), phosphatidylserine (PS), phosphatidylinositol (PI) and phosphatidic acid (PA). PC makes up >50 % (by mol) of the phospholipids in most eukaryotic membranes.[6] Most PC molecules have one cis-unsaturated fatty acyl chain, which creates a kink and prevents the fatty acids from packing together too tightly, thus decreasing the melting temperature (increasing the fluidity) of the membrane.[3] Another class of structural phospholipid is sphingophospholipid, which contain a ceramide instead of diacylglycerol as lipid tail. The major sphingophospholipid in animal membranes is sphingomyelin (Figure 1.1b).[6] For example, in humans, sphingomylins comprise nearly 10 – 20% (by mol) of the total plasma membrane lipids.[7] GLs share similar lipid tail with phospholipids, but with a carbohydrate instead of a phosphate-containing head group. There are two main classes of GLs: glyceroglycolipids (such as seminolipid, Figure 1.1c) and glycosphingolipids (GSLs, such as galactosylceramide, Figure 1.1d), with mono-, di, or oligosaccharides attached to glycerol or ceramide, respectively. GLs in animal membranes are mainly GSLs, whereas those in bacterial and plant membranes are principally glyceroglycolipids.[5] In all cases, GLs are only found on the outer leaflet of the plasma membrane with their hydrophilic carbohydrates exposed to aqueous solution and available for binding to glycan-binding proteins (GBPs) and other glycan-recognizing molecules. GLs generally constitute about 5% (by mol) of the lipids in the outer monolayer of animal plasma membranes.[8] Particularly, gangliosides, which are GSLs with terminal sialic acid, are most abundant in the plasma membrane of nerve cells,

where gangliosides constitute 5 – 10% (by mol) of the total lipids and they are also found in much smaller quantities in other cell types.[8] Although GLs account for small proportion of membrane, they are involved in critical biological events in many normal (e.g. signaling, immune response and cell adhesion) and pathological processes (e.g. bacterial and viral infections) through GL recognition by GBPs.[9] As described in more details in section 1.1.2, the characterization and discovery of GBP–GL interactions remain experimentally challenging and the development of new analytical or biochemical methods is needed. The third type of lipid is sterol – the major non-polar lipids of membranes. Predominate class of sterols in mammals is cholesterol (Figure 1.1e),[6] which consists of a four-ring steroid structure together with a short hydrocarbon side-chain and a hydroxyl group. Cholesterol generally makes up about 30% (by mol) of the animal cell membranes and is required to maintain both membrane structural integrity and fluidity.[3]

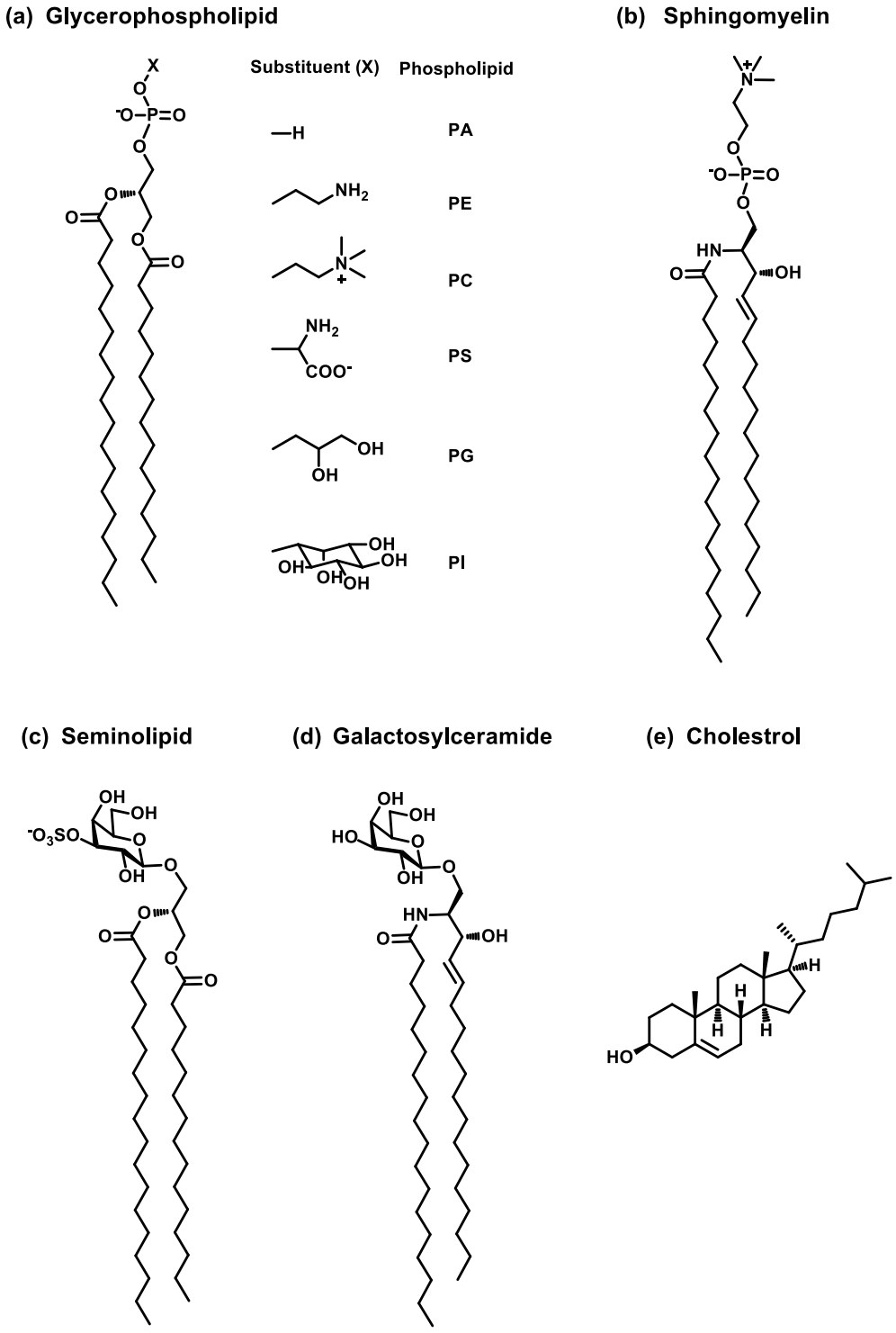

Figure 1.1 The representative structures of (a) glycerophospholipid, (b) sphingomyelin, (c) seminolipid, (d) galactosylceramide, and (e) cholesterol.

The other major component of cell membrane are membrane peptides and proteins (MPs). The amounts and types of MPs vary considerably from cell to cell. MPs associate with the lipid bilayer in several different ways. Many MPs (called integral polytopic proteins or transmembrane protein) span across the lipid bilayer at least once and are permanently anchored. Such MPs have hydrophobic regions which are embedded with the bilayer and interact with the hydrophobic tails of lipids, while the hydrophilic regions of these MPs extend to the aqueous solutions on both sides of the membrane. Some MPs (called integral monotopic proteins) are permanently attached to the membrane, but they are attached to only one side of the membrane. A portion of them is incorporated into the membrane through hydropobic interaction or they covalently bind to a membrane lipid. Integral proteins can only be removed by treatments such as detergents which disrupt the membrane. Some other MPs (called peripheral proteins) are temporarily attach either to the lipid bilayer or to other MPs through non-covalent interactions. Most of the MPs of the plasma membrane have covalently linked carbohydrates (glycosylated MPs) either through the amide group in side chain of the amino acid asparagine or through the hydroxyl group in the side chains of serine or threonine.[5] MPs play an important role in many biological events such as signaling, transport, catalysis, attachment, cell–cell recognition, and energy conversion.[10] Moreover, MPs account for around 20 – 30% of the proteome in most organisms and over 50% of the drug targets.[11,12] As details described in the section 1.1.3, despite their biological importance, the structure and function analysis of MPs are challenging using current methods.

1.1.2 Protein–glycolipid interactions

As described above, recognition of GLs on the surface of cells by GBPs are critical events in many normal and pathological processes.[9] For example, many bacteria and viruses possess GBPs

specific for GL receptors of the target cell, and utilize these interactions for infection. The non-covalent interactions between the GBPs and GLs are driven by the formation of hydrogen bonds and van der Waals contacts between the binding sites of GBPs and carbohydrate moieties of GLs.[13] The affinities of GBPs for individual carbohydrate are typically weak, with association constants (K_a) in the range of 10^3 M^{-1}.[14] However, multivalent binding involving carbohydrates interaction with multiple binding sites on the GBPs result in higher apparent affinities. Due to their biological importance, significant efforts have been made to elucidate the molecular basis of GBP–GL recognition, their binding specificity and affinity, and there is a need for new analytical methods that are capable of identifying and quantifying biologically or therapeutically relevant GBP–GL interactions in vitro. However, the discovery and characterization of GBP–GL interactions are hindered due to the insolubility of GLs in aqueous solution and limited availability of purified GLs. One strategy to overcome these limitations is to study GBP interactions with the water-soluble analogs (i.e., oligosaccharides) of GLs.

GBP-carbohydrate interactions can be analyzed by a variety of surface-based analytical techniques, such as enzyme-linked immunosorbent assays (ELISA), surface plasmon resonance (SPR) spectroscopy, and glycan microarray screening.[15-20] ELISA is a widely used method for quantifying GBP–carbohydrate interactions with moderately high sensitivity and good reproducibility.[15] Typically, carbohydrates are covalently immobilized on a microplate surface and then incubated with solutions containing an enzyme linked target protein, and the enzyme's substrates are added to produce a signal for detection, most commonly a color change. SPR spectroscopy is a very sensitive technique for measuring both the real time kinetic (i.e., association and dissociation rate constants) and the thermodynamic parameters (i.e., affinities) of GBP–carbohydrate interactions.[16-18] Typically, carbohydrates are covalently immobilized on the surface

of a sensor. By flowing the target protein over the sensor, a real time change in the refractive index at the sensor surface is measured. Glycan microarray assay is a high throughput method for screening carbohydrate libraries against GBPs.[19,20] Generally, a library of carbohydrates is covalently printed on a microarray surface and target GBPs are incubated with them. Specific interactions are qualitatively detected either through fluorescence or immunoassays. To some degree, these surface-based techniques, have improved current understanding of GBP-carbohydrate recognition. However, they have some limitations. The orientation of the carbohydrate, the nature of immobilization, carbohydrate density, and the loss of mobility of the immobilized carbohydrates may influence binding.[21,22]

In addition, there are several solution based techniques used to study GBP–carbohydrate interactions, such as isothermal titration calorimetry (ITC), nuclear magnetic resonance (NMR) spectroscopy, and electrospray ionization mass spectrometry (ESI-MS). ITC is the "gold standard" technique for quantifying binding thermochemistry in solution, which can provide a direct measure of the enthalpy of association. However, conventional ITC usually requires large amount (~mg) of protein and ligand for a single analysis.[23,24] NMR spectroscopy is a widely used method for characterizing the protein structure and their complexes in solution.[25] Particularly, the saturation transfer difference (STD)-NMR method,[26-28] in which the detection of the interactions is based on the nuclear Overhauser effect and the observation of the ligand resonance signals, has been applied for studying GBP–carbohydrate interactions and for library screening. It can provide binding affinity as well as structural insights of the binding epitopes. However, NMR measurements are usually limited to relatively small proteins, with molecular weight (MW) up to 40 kDa.[29] In the last two decades, ESI-MS has emerged as a promising method for identifying and quantifying GBP–carbohydrate interactions.[30-34] The soft ionization by ESI enables the transfer and

maintenance of GBP–carbohydrate complexes formed in a solution to the gas-phase for detection. Compared with other techniques, ESI-MS has several advantages such as speed (mass spectra can typically be acquired within a minute), low sample consumption (<fmol of analyte per analysis using nanoflow ESI), simplicity (no labelling or immobilization), and direct insight into binding stoichiometry and multiple binding equilibria simultaneously. A detailed description of the implementation of ESI-MS assay along with some of the limitations of this assay will be given in section 1.3.

Overall, those GBP–carbohydrate binding assays had led to the discovery of a number of carbohydrate receptors. However, information is lost by stripping off the lipid moiety from GLs since the lipid moiety can affect the orientation of the carbohydrate and also can lead glycolipids to cluster in the cell membranes for multivalent binding.[35-37] Alternatively, study of GBP–GL interactions should involve the use of real cellular receptors GLs instead of oligosaccharides. One way is based on immobilization of GLs on surfaces (either through covalent bond or hydrophobic interaction), and their interactions with the target GBP can be probed using those surface-based techniques – ELISA, SPR spectroscopy, and microarrays.[38-42] Recently, GL-based microarray screening was achieved by immobilizing synthetic neoglycolipids and glycosphingolipids onto microarrays, which has been successfully applied for GL receptor discovery.[41] Shotgun microarrays were also used for cellular receptor recognition.[42] Natural GLs and glycoprotein-derived glycans extracted from cells were modified with a bifunctional fluorescent tag and covalently immobilized on microarray surface.[42]

For GL immobilization based assays, covalent modification and immobilization of GLs on surface will affect the structure, orientation, density and accessibility of GL, which therefore may have an influence on their binding. Although in some cases GLs are immobilized through

hydrophobic interactions, the fluidity of the GLs are still limited. Overall, the removal of GLs from a native lipid environment is expected to influence the nature of GBP interactions. It is known that the membrane can influence GBP interactions with GLs,[40,43] For example, the bilayer serves to orient the GLs and enables them to cluster (in the form of microdomains), which leads to a strengthening (due to avidity) or weakening (due to steric effects) of the GBP interactions.[35,36] The GBP–GL interactions may also be affected by the presence of other membrane components, such as cholesterol.[37]

The incorporation of GLs into model membranes (MMs) allows for a more physiological presentation of GLs and a possibility of probing the influence of the lipid environment on binding. GLs can self-assemble into micelles with their hydrophilic heads exposed to a solvent and their hydrophobic tails in the center (Figure 1.2), however, it is not lipid bilayer presentation. Bicelles are a lipid bilayer that is shielded by micelle-like assembly of detergent (Figure 1.2). Besides, a number of MM systems have been developed for solubilization of GLs. Supported lipid bilayer is a planar lipid bilayer localized on a solid surface (Figure 1.2). Liposomes (also known as vesicles) are lipid bilayers in a hollow spherical shell (Figure 1.2). Nanodiscs (NDs) are discoidal phospholipid bilayers surrounded by two copies of an amphipathic membrane scaffold protein (MSP, Figure 1.2).[44] Picodiscs (PDs) are lipid-transporting macromolecular complexes composed of human sphingolipid activator protein saposin A (SapA) and lipids (Figure 1.2).[45]

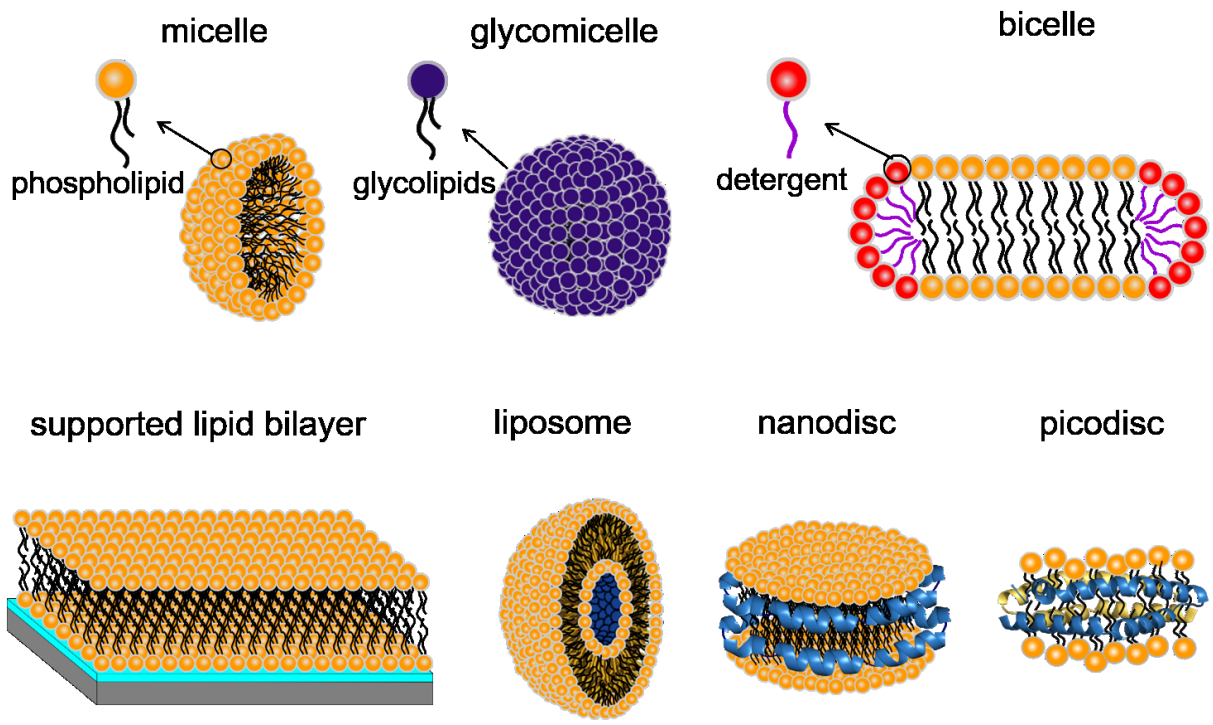

Figure 1.2 The composition and structure of GL self-assembly and model membranes.

Increasingly conventional binding assays, including fluorescence microscopy, NMR spectroscopy, SPR spectroscopy and ESI-MS,[35,36,46-51] are being adapted for use with MMs to allow for GBP–GL interaction studies to be carried out in a membrane-like environment. Fluorescence microscopy is an optical microscopy technique that uses fluorescence and phosphorescence instead of, or in addition to, reflection and absorption to study molecules and their binding events. Particularly, total internal reflection fluorescence microscopy, which allows for selective excitation of the surface-bound fluorophores, was used to explore multivalent interactions between cholera toxin B subunits (CTB_5) and its native receptor ganglioside GM1 incorporated in the supported lipid bilayer.[35] NMR has been combined with the water soluble GM1 containing liposomes to locate the binding sites of the prion protein.[36] SPR spectroscopy has also

been combined with MMs. For example, NDs containing GM1 were immobilized on a surface through binding of the polyhistidine tag of MSP to nickel charged nitrilotriacetic acid (Ni-NTA) and implemented with SPR to measure the kinetics of the CTB_5 binding.[46] Recently, a nanocube sensor was developed by integrating supported lipid bilayer on a silica-coated silver nanocube and localized SPR.[47] Catch-and-release (CaR)-ESI-MS has been combined with NDs for screening GLs against GBPs.[48-50] Both neutral and acidic GLs are readily incorporated into NDs, allowing their interactions with water-soluble GBPs to be investigated. More recently, the new presentation strategy PDs, was also implemented with the CaR-ESI-MS assay to detect both high and low affinity GBP–GL interactions.[51] Studies showed PDs containing GLs have potential advantages over NDs for the detection of some GBP–GL interactions and for studying the kinetics of GL-processing enzymes.[51] Chapter 2 and 4 focus on the development of the CaR-ESI-MS methods, implemented with PDs or passively-loaded PDs, to screen GL libraries against GBPs for discovery and characterization of GL receptors and Chapter 3 focuses on the size and composition characterization of PDs.

1.1.3 Membrane peptides and proteins

As described in section 1.1.1, MPs are implicated in many critical cellular processes, including signal transduction, transportation, and metabolism.[10] Due to the fundamental biological significance of MPs and their importance in drug discovery and disease diagnosis, significant attention has been devoted to investigate the structure and function of MPs. However, the studies are hindered due to their low abundance, poor solubility in aqueous solution, and lack of membrane environment.

The most common solubilization strategy used for MP analysis is the use of amphipathic detergents, which extracts MPs into soluble micelles. Detergents are very effective at extracting proteins from the membrane, however, in some cases, detergents denature the proteins or disrupt their native structure and function.[52,53] Special care must be taken when choosing right detergent and there is no ideal detergent for all MP systems.[54] Amphipathic polymer (amphipol) is an alternative strategy. It has been shown that amphipols can solubilize MPs effectively and preserve their activities.[55,56] However, they are still not native lipid bilayers and may not capture the native form of the protein. Recently, lipoproteins, which are the combinations of lipids and amphipathic proteins that naturally exist in several structural forms, such as NDs,[44] and PDs[57,58] are used to solubilize MP in a native lipid environment. NDs have a diameter of ~10 nm and a thickness of 5–6 nm,[44] which are suitable for incorporation of most MPs. The sizes of NDs are precisely controlled by the size of MSP proteins and can be modified by engineering the MSPs to smaller or larger size. The lipid content of NDs can also be defined to investigate MP–lipid interactions and to probe how lipids modulate MPs.

NDs, combined with diverse structural and biophysical techniques, including NMR,[59-61] optical,[62-64] fluorescence[65-67] and Raman[68,69] spectroscopies, electron microscopy[70,71] and atomic force microscopy,[44,72] small angle x-ray, neutron scattering,[73,74] and electrochemistry,[75,76] have been used to probe the structure and function of MPs, as well as their complexes with other proteins, peptides and lipids. Recently, ESI-MS implemented with NDs, has emerged as a promising tool for studying the binding properties of MPs in a lipid environment.[77-79] Native ESI-MS, which involves the transfer of intact proteins and biomolecular complexes from solution into the gas phase, can provide information on the composition, stoichiometry and interactions in complexes. Moreover, collision cross sections (Ω), measured by ion mobility separation (IMS), provide a

means of assessing possible conformations of the gaseous MPs ions produced from the NDs.[80] Chapter 5 is an application of ESI-MS assay combined with NDs to investigate the structure and stoichiometry of a transmembrane peptide complexes.

1.2 Electrospray Ionization Mass Spectrometry

Before the introduction of different ESI-MS assays for studying GBP–GL interactions and MPs, it is useful to give an overview of the basic concepts of the mass spectrometry (MS) used in this work.

1.2.1 Electrospray ionization

Electrospray ionization (ESI), is a mild ionization method that can transfer analyte, including biological molecule from solution into the gas phase without fragmentation. Of relevance to the work described in this thesis, non-covalent interactions such as those involved in protein–ligand complexes, can be maintained into gas phase. ESI is performed at atmospheric pressure and, in most cases, at room temperature. Three major processes are involved in ESI as shown in Figure1.1.[81-84] A brief description of these processes are described below.

(i) Production of charged droplets at the ESI capillary tip

In conventional ESI, a high voltage is applied to a capillary tube containing the analyte solution that is close to the entrance of the mass spectrometer. A number of charge with the same polarity as the capillary accumulate on the solution surface at the capillary tip and form a Taylor cone. Then a fine filament breaks into a spray of fine droplets.[85] The size and charge of initial droplets mainly depend on the flow rate and solution conditions.[81,83] The voltage (V_{on}) required for the onset of charged droplet emission is given in eq 1.1:

$$V_{on} = 2\times10^{5}(\gamma r_c)^{1/2}\ln(4d/r_c) \quad (1.1)$$

where the γ is the surface tension of the solvent, r_c is the radius of the capillary and d is the distance from capillary tip to the counter electrode.

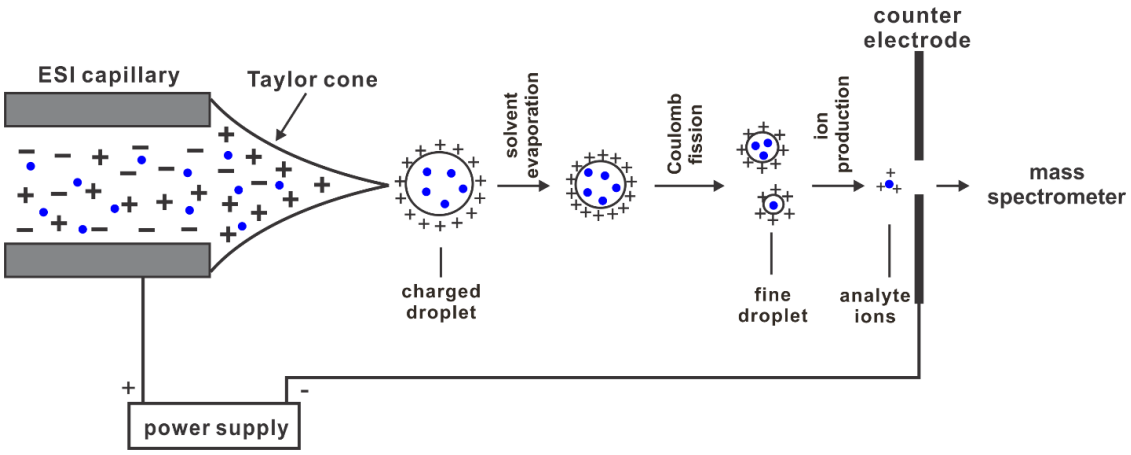

Figure 1.3 Schematic representation of an ESI process performed in the positive ion mode, adapted from reference 83.

(ii) Shrinkage of charged ESI droplets and repeated droplet fission

The charged droplets produced at the capillary shrink due to solvent evaporation. The evaporation occurs until the droplet radius reaches the Rayleigh limit (R_R),[83,84] when the columbic repulsion force just overcomes the surface tension force, then droplets undergo uneven fission into parent and offspring droplets. The Rayleigh equation is:

$$Q_R^2 = 64\pi^2\varepsilon_0\gamma R_R^3 \quad (1.2)$$

where Q_R is the charge of the droplet, ε_0 is the permittivity of vacuum. Typical one droplet produces offspring droplets that carry off 2% of the parent mass and 15% of the parent charge.[81] The droplets undergo repeated shrinkage and fission, and finally, lead to the generation of the

highly charged droplets with diameters in the nm range that are the precursors of the gas phase ions.

(iii) Generation of gas phase ions

Three main theories have been proposed for the formation of gas phase ions from the very small and highly charged droplets, as shown in Figure 1.4:

(a) Ion evaporation model (IEM)

This model was proposed by Iribane and Thomson for small analyte ejection from a highly charged droplet.[86,87] The model predicts that ions emit directly from the droplets when the radius of the droplets shrink to less than 10 nm. Charges are acquired locally by analytes as they evaporate from the droplet.

(b) Charged residue model (CRM)

This model was proposed by Dole and coworkers for the release of a compact macromolecule.[88] It was assumed that, when very small droplets containing a single macromolecule are formed by droplet fission, solvent evaporation from such a droplet leads to a gas-phase analyte ion whose charge originates directly from the charges at the surface of the vanished droplet. CRM is experimentally well-supported for folded globular proteins.[81,82,88,89-91] CRM results in a narrow charge state distribution for folded proteins that is determined by the number of ionizable residues near the droplet surface and the Rayleigh limit.[81,82,89,90]

(c) Chain ejection model (CEM)

This model was proposed by Konermann and coworkers for release of disordered macromolecules, such as denatured proteins.[92-94] The unfolded protein, which is general hydrophobic, will migrate from inside a droplet to the surface to minimize the solvent interactions. One chain terminus then

ejects into the gas-phase carrying some charges, followed by the stepwise ejection of the remaining chain with more charges. CEM results in a wider charge state distribution for unfolded proteins compared to the folded protein ions generated via CRM.[92]

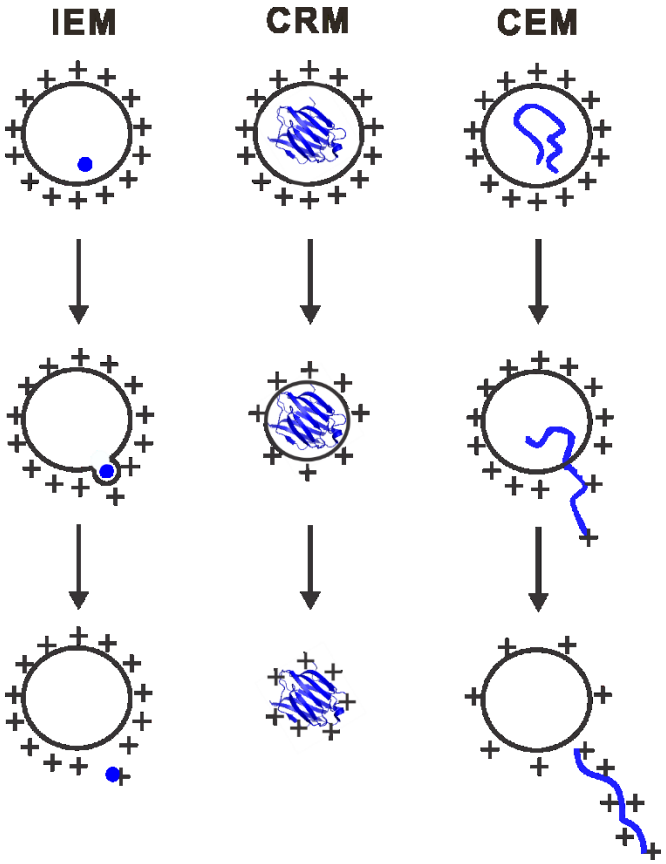

Figure 1.4 ESI models proposed for gas-phase ion formation. Figure is adapted from reference 94.

In this thesis, nanoflow ESI (nanoESI) instead of conventional ESI was used. NanoESI was introduced by Wilm and Mann.[95,96] While the technique uses the same fundamental ion formation mechanisms, it is distinguished from conventional ESI in several aspects.[97,98] First, glass or quartz capillaries with a much smaller diameter are used instead of the metallic capillary in conventional ESI. The flow rate in nanoESI is typically ≤ 10 nL/min compared to µL/min for the conventional

ESI. Therefore, a much smaller quantity of analyte (few μL of solution containing pmol of analyte) is required. Second, a smaller initial droplet size in the nanoESI leads to a shorter lifetime of droplets and a lower number of analyte molecules in each droplet, which may reduce the nonspecific aggregation.[96-99] Moverover, its gentle interface conditions lead to less dissociation and disruption of non-covalent interactions.[100]

1.2.2 MS instrumentation

The ESI-MS measurements described in Chapters 2 to 5 were carried out using a Synapt G2-S quadrupole-ion mobility separation-time-of-flight (Q-IMS-TOF) mass spectrometer (Waters, Manchester, UK) equipped with a nanoESI source, as illustrated in Figure 1.5. The instrument principally consists of several sections: z-spray source section (IntelliStart), ion guide (StepWave), quadrupole, a travelling wave section consisting of Trap, IMS and Transfer (TriWave), and quantitative TOF-reflectron *m/z* analyzer (QuanTof). Droplets and gas phase ions are sampled into the mass spectrometer through a z-shaped source, which minimizes the transfer of the neutral contaminants. Then ions pass through StepWave ion transfer optics, which employs an off-axis design to increase the efficiency of ion transfer from the ion source to the MS analyzer and further minimize the transfer of neutral contaminants at the same time. The ions are then transmitted through the quadrupole mass filter, Trap collision cell, IMS cell, Transfer collision cell, and finally reach the TOF mass analyzer for detection. To perform tandem MS, ions are isolated in quadrupole mass filter and subjected to collision induced dissociation (CID) in the Trap and/or Transfer collision cells. The IMS provides another dimension for separation of isobaric/isomeric ions based on their ion mobility difference. A more detailed description of those parts are given below.

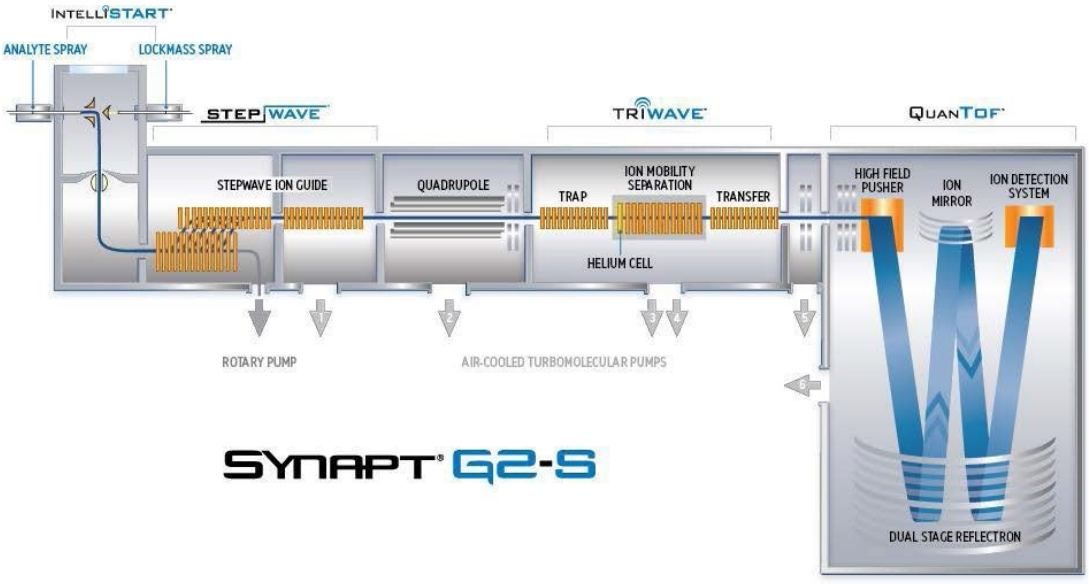

Figure 1.5 A schematic diagram of the Synapt G2-S Q-IMS-TOF mass spectrometer, adapted from the Waters user's manual.

1.2.2.1 Quadrupole mass filter

Quadrupole mass filter separates ions with different *m/z* based on the stability of their trajectories inside an RF field.[101-103] Quadrupole contains four cylindrical rods that create a hyperbolic field. A voltage of (U+Vcos(ωt)) with same polarity is applied to the opposite rods and same voltage with different polarity is applied to adjacent rods, where U is the direct current (DC) voltage, Vcos(ωt) is the radio frequency (RF) voltage with RF amplitude V and RF frequency ω. The stability of the ion trajectory depends on the ion's a and q values, with a and q are defined by eqs 1.3a, 1.3b:

$$a = \frac{8zeU}{mr_0^2\omega^2} \tag{1.3a}$$

$$q = \frac{4zeV}{mr_0^2\omega^2} \tag{1.3b}$$

where the r_0 is the radius of inner surface of the quadrupole. Figure 1.6a depicts the stability diagrams of several ions of different *m/z* values. Normally, when the quadrupole is used as a mass analyzer, the DC and RF voltage are simultaneously increased while the ratio of U/V remain constant, along the scan line as shown in Figure 1.6a. The line scans across the tips of the stability regions of each *m/z* and allows the ions from low to high mass passing the mass filter in turns. For certain U and V, only a small window of a given *m/z* near the vertex of the stability diagram of that *m/z* can have stable trajectories and be transmitted, whereas other ions with *m/z* values out of the small window will hit the rods and are expelled. As suggested by the stability diagram, quadrupoles can be used as ion guides when operated in the RF-only mode since all ions above a certain *m/z* threshold will be transmitted when no DC potential applied (a = 0). Hence, in MS mode, the quadrupole operates in RF-only mode and acts as an ion guide sevice, while in the MS/MS mode, a particular field of DC and RF is applied and only ions with selected *m/z* values are allowed to pass through. Moreover, in the Synapt G2-S mass spectrometer, a quadrupole pre-filter is placed in the front of the quadrupole (Figure 1.6b) to minimize the effects of fringing fields at the entrance to the quadrupole and improve the absolute sensitivity.[104]

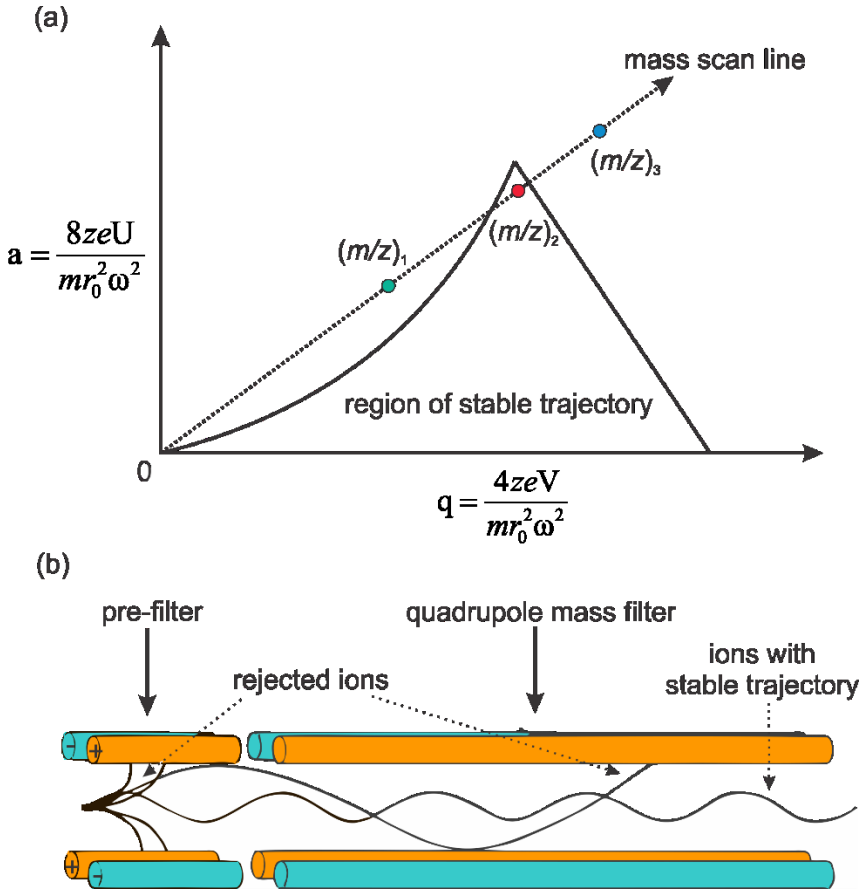

Figure 1.6 (a) a-q stability diagram of quadrupole (adapted from reference 105 for ions with different *m/z* values [$(m/z)_1<(m/z)_2<(m/z)_3$]. (b) Schematic diagram of the quadrupole used in the Waters Synapt G2-S mass spectrometers (adapted from reference 106).

1.2.2.2 Traveling-wave ion guides

A traveling-wave (T-Wave) device consists of an even number of stacked ring-shaped electrodes arranged orthogonally to the ion transmission axis (Figure 1.7).[107,108] An opposite phased of RF voltage is applied to the adjacent electrodes for radial confinement and high transmission of the ions along the axial direction within the device. To propel the ions along the device, a DC voltage is applied to the electrode pairs, to cause a potential barrier that ions within the region cannot cross.

As the DC voltage is stepped to the adjacent pair and sequentially along the rings of the device at regular time intervals, the ion barrier moves forward and creates a "traveling wave" that drives the ions through the device. Using a T-Wave, ions can transfer with a high speed, which allows high data acquisition rates with the high sensitivity maintained. In Synapt G2-S mass spectrometer, T-wave technology is employed for the StepWave ion guide, Trap, IMS and Transfer region.

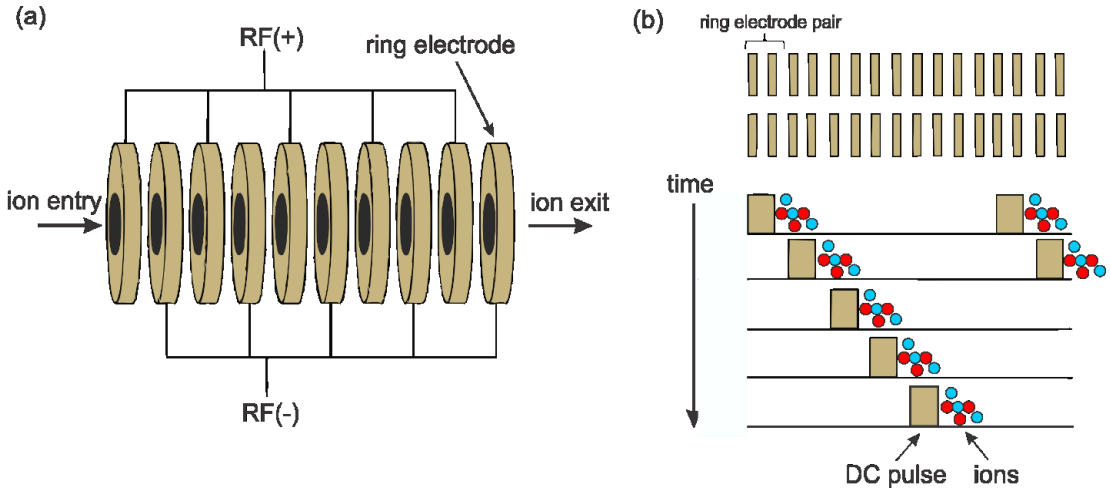

Figure 1.7 Diagrams of (a) stacked rings of a travelling wave device and (b) its operational principle (adapted from reference 107).

1.2.2.3 Ion mobility separation

IMS is a technique to separate ions according to their mobility difference, which based on their charge, size and shape, through an electric filed filled with buffer gas (N_2 or He).[109-111] In IMS, the ions' motion is driven by the electrostatic force through the chamber and opposed by collisions of ions with the buffer gas at the same time. Larger ions with greater Ω undergo more collisions than smaller ions and thereby require longer time to migrate through the drift cell. A more detailed description of IMS is given in Chapter 1.3.3. There are several types of ion mobility

instrumentation that have been successfully coupled with MS such as drift tube IMS (DTIMS),[112] field asymmetric waveform IMS (FAIMS),[113] and T-wave IMS (TWIMS).[107,108,114-117]

The Synapt G2-S mass spectrometer implements a TWIMS technique. Comparing to a uniform static electric field used for classic IMS, a non-uniform, moving electric fields/voltage pulsed (T-Wave technology, see section 1.2.2.2) are performed in TWIMS. Ions are pushed along T-wave and separated based on their mobility in a reverse buffer gas (N_2) flow. Ions with lower mobility experience more friction and eventually slip behind the wave and travel more slowly.[108] Since the ions are given an additional axial velocity by the T-wave, their transit time is reduced (typically in ms). A high-pressure helium-filled cell is placed at the entrance of the IMS T-Wave cell to minimize the scatter and/or fragmentation of ions by collisionally cooling transferred ions.

1.2.2.4 Tandem MS

Tandem MS involves the isolation of ions of interest, activation of them once (MS/MS) or multiple times (MS^n) into fragment ions, and analysis of the fragment ions to elucidate the structure of the precursor ion. Tandem MS may be performed tandem in space, which requires the use of two separate mass analyzers, or in time, where the isolation and fragmentation of precursor ion are achieved in the same mass analyzer. The former was used in the Q-TOF mass spectrometer in this thesis. Ion activation can be achieved in many ways: via collisions with gases or surfaces such as collision-induced dissociation (CID)[118,119] and surface-induced dissociation (SID);[120] via absorption of IR or UV photons such as blackbody infrared radiative dissociation (BIRD),[121,122] infrared multiphoton dissociation (IRMPD)[123,124] and ultraviolet photodissociation (UVPD);[125,126] or via activation by ion-electron interactions such as electron capture dissociation (ECD)[127,128] and

electron transfer dissociation (ETD).[129] Only CID is used in this thesis and the detailed description is given below.

CID is the most commonly used ion activation method in tandem MS. When precursor ions possessing high translational energy collide with neutral gas molecules, a small fraction of their translational energy is converted into internal energy, which causes decomposition of the ions. In Synapt G2-S mass spectrometer, CID can be performed either in Trap or Transfer region, which filled with Ar as a background collision gas with pressure ~10^{-2} mbar. In this case, a constant DC voltage (collision energy) was applied to each ring electrode in addition to the transient DC voltages used to propel ions to the next stage of the instrument (see section 1.2.2.2). A selective ions of interest (precursor ions) are subjected to energetic collisions with Ar in Trap and/or Transfer region accompanied by an accumulation in internal energy of precursor ions. Eventually it induces the decomposition of precursor ions. CID is generally considered as a "slow heating" fragmentation method. Since the energy randomization is faster than the bond decomposition, fragmentation does not occur at a site where the energy is deposited first. Instead, the energy will be redistributed among all the internal modes and when the overall internal energy is raised above activation barrier, fragmentation occurs.[130] CID has been used widely for analysis of non-covalent protein–ligand and protein–protein interactions in the gas phase.[131-135]

1.2.2.5 TOF mass analyzer

TOF mass analyzer separates ions with different *m/z* based on their flight time through a field-free drift region.[136] A linear TOF analyzer is conceptually the simplest type of mass analyzer. All ions are accelerated by an electrical potential V applied between an ion accelerator and a detector. The

velocities of the ions are determined by the kinetic energy of the ion, and can be expressed by the length (L) and flight time (t) through the drift region, as give in eq 1.4:

$$v = \sqrt{\frac{2zeV}{m}} = \frac{L}{t} \tag{1.4}$$

where e is the elementary charge, m and z are the mass and charge of the ion, respectively. Since e, V, L are all constants, m/z of an ion is can be calculated by the flight time.

$$m/z = t^2 \frac{2eV}{L^2} \tag{1.5}$$

In Synapt G2-S mass spectrometer, an orthogonal acceleration-reflectron TOF mass analyzer was used in order to improve the resolution.[137,138] In an orthogonal acceleration, instead of being accelerated along its axis of motion, the ion packet is extracted and accelerated sideways by a pulsed voltage applied, which minimizes the effect of the initial ion kinetic energy spread. Moreover, the use of an ion reflector or ion mirror compensates the initial energy distribution of ions to improve the focusing of high energy ions. A reflector is made of a number of electric plates: ions of the same m/z will penetrate the field at a different depth; fast ions (with more kinetic energy) penetrate deeper into the field and take a longer time to return than slow ions; fast and slow ions are focused to reach the detector at the same time. Synapt G2-S have two modes: the single stage reflectron mode ("V mode") and the dual stage reflectron mode ("W mode"). Although "W mode" with twice ion focus leads to even higher resolution, it results in less sensitivity. "V mode" was used for all the experiments in this thesis. TOF has unlimited mass range, but it is usually limited by the effectiveness of the ion detector. Synapt G2-S adopts an ultra-fast electron multiplier and a hybrid analog-to-digital (ADC) detector for detection.

1.3 ESI-MS Based Assays

1.3.1 Direct ESI-MS assay

The direct ESI-MS assay is used to quantify protein–ligand interactions based on the direct detection of free and ligand-bound protein ions by ESI-MS.[139] For a reversible interaction (eq 1.6) between a monovalent protein (P) and a monovalent ligand (L), the abundance (*Ab*) ratio (*R*) of the ligand-bound protein (PL) to free protein (P) ions measured by ESI-MS is taken to be equal to the equilibrium concentration ratio in a solution (eq 1.7).

$$\mathrm{P} + \mathrm{L} \rightleftharpoons \mathrm{PL} \tag{1.6}$$

$$R = \frac{\sum Ab(\mathrm{PL})}{\sum Ab(\mathrm{P})} = \frac{[\mathrm{PL}]}{[\mathrm{P}]} \tag{1.7}$$

The [P] and [PL] are equilibrium concentrations of the protein and protein–ligand complex in solution, respectively. The apparent association constant (K_a) can be calculated from eq 1.8 with known initial concentrations of protein ($[P]_0$) and ligand ($[L]_0$).[139]

$$\mathrm{K_a} = \frac{[\mathrm{PL}]}{[\mathrm{P}][\mathrm{L}]} = \frac{R}{[\mathrm{L}]_0 - \frac{R}{1+R}[\mathrm{P}]_0} \tag{1.8}$$

Here [L] is the equilibrium concentration of the ligand.

Normally, the affinity (K_a) is determined from measurements performed at different concentrations or titration experiments, where the $[P]_0$ is fixed and the $[L]_0$ is varied. In the latter case, K_a is extracted using nonlinear regression analysis of the experimentally determined concentration dependence of the fraction of the ligand-bound protein, i.e., $R/(R+1)$ flowing eq 1.9.[139]

$$\frac{R}{R+1} = \frac{1 + \mathrm{K}_a[\mathrm{L}]_0 + \mathrm{K}_a[\mathrm{P}]_0 - \sqrt{(1 - \mathrm{K}_a[\mathrm{L}]_0 + \mathrm{K}_a[\mathrm{P}]_0)^2 + 4\mathrm{K}_a[\mathrm{L}]_0}}{2\mathrm{K}_a[\mathrm{P}]_0} \tag{1.9}$$

Experimentally, the values of K_a can be measured accurately with the direct ESI-MS range from ~10^2 to ~10^7 M^{-1}, which fits to most GBP–GL interactions.

For a multivalent protein (P) that can bind up to *h* ligand molecules (i.e., *h* binding sites), the abundance ratio (R_i) of the protein bound to *i* molecules of L (PL_i) to free protein (P) measured by ESI-MS is taken to be equal to the equilibrium concentration ratio in a solution, eq 1.10:[140]

$$R_i = \frac{\sum Ab(\mathrm{PL}_i)}{\sum Ab(\mathrm{P})} = \frac{[PL_i]}{[P]} \tag{1.10}$$

and the apparent association constant ($K_{a,i}$) for the addition of the i^{th} L to P bound to (*i*-1)L can be expressed by eq 1.11:[140]

$$\mathrm{K}_{\mathrm{a},i} = \frac{R_i / R_{i-1}}{[\mathrm{L}]_0 - \dfrac{[\mathrm{P}]_0 \sum_{i=1}^{h} iR_i}{1 + \sum_{i=1}^{h} R_i}} \tag{1.11}$$

The fraction (*f*) of occupied ligand binding sites can be determined from the *Ab* of ligand-bound and free protein ions measured by ESI-MS, eq 1.12:[141]

$$f = \frac{\sum_{q=1}^{5} q \cdot Ab(\mathrm{PL}_i)}{h\left(Ab(\mathrm{P}) + \sum_{i=1}^{h} Ab(\mathrm{PL}_i) \right)} \tag{1.12}$$

1.3.2 Catch-and-Release (CaR)-ESI-MS assay

The CaR-ESI-MS assay is used for screening libraries of ligands against proteins to identify specific protein–ligand interactions.[142-144] The assay involves the direct ESI-MS detection of the protein complexes with a mixture of ligands. In many cases, the identity of the ligands ("caught"

by the protein) can be determined from the ESI mass spectrum based on the MW of the corresponding protein–ligand complexes. In cases where the identity of ligand cannot be accurately determined from the MW of the complexes (due to the size or the heterogeneity of the protein or the number and size of the ligands), the bound ligands are released from the complexes by subjecting the complexes to CID in Trap region. The identity of the bound ligands are determined by the MW of the release ligands or in combination with the isomer separation with IMS or fragmentation pattern of the ligand through another stage of CID in Transfer region.

CaR-ESI-MS assay can be combined with MMs for screening GLs against a target GBP.[48,49,51] Briefly, the assay involves incubating GBP with GL-containing MMs in aqueous solution. The GBP interactions with GLs, which are imbedded in the MMs, is then detected by transferring the intact GBP–GL–MM complexes to the gas phase using ESI. After desolvation, the GBP–GL complexes spontaneously release from the MM ions and are detected by MS. To facilitate the identification of the GL ligands, the GBP–GL complexes are subjected to CID in Trap region to release the GL ions, which can be analyzed subsequently by IMS, another stage CID in Transfer region, and MS. In cases where free and GL-bound GBP ions and those corresponding to the MMs overlapped in the spectrum, IMS is used to separate the GBP and GBP–GL complexes from the MM ions; release of the GL ions was achieved by CID performed in the Transfer region.

1.3.3 IMS-MS

Besides the screening and quantification of protein–ligand interactions in solution by ESI-MS, there is also a great interest in the gas phase studies to investigate structure and conformation of

non-covalent biological complexes. Ion mobility mass spectrometry (IMS-MS) provides information about the structure of gaseous proteins and protein complexes.

IMS is a gas-phase electrophoretic technique used to separate ions based on their charge, size and rotationally averaged Ω (i.e., the effective area for the collision between a target ion and the neutral gas).[109-111] Despite differences in the configuration of IMS-MS instruments (described in section 1.2.2.3), there are common features. In IMS, ions travel through a drift cell with a static electric field that moves the ions towards the cell and a neutral buffer gas flow within the cell that opposes the ions' motion. The mass and charge can be obtained by coupling IMS with MS, allowing the Ω of the ion to be measured. Direct measurement of Ω can be obtained by measuring drift times using a standard drift tube separator (DTIMS-MS) with a careful measurement of temperature and pressure. In cases where the temperature, pressure and gas purity cannot be measured accurately, calibration of the drift time measurements using ions with known Ω is used. This method of calibration, rather than the absolute measurement, is also used for TWIMS-MS since it does not provide Ω directly from drift time. The relationship between Ω and drift time (t_D) in TWIMS can be expressed in eq 1.13:

$$\Omega = A t_D^{\ X} \tag{1.13}$$

where the X is the exponential factor. A number of different calibration approaches have been suggested and they are all based on the use of calibrant standards with known Ω measured in DTIMS-MS instruments.[109] Among them, the most general and widely used approach for calibrating IMS data acquired on TWIMS-MS instruments was reported by Ruotolo and coworkers,[116] which was described in details in section 3.2.4 and used for calibrating Ω values in Chapter 3 and 5.

Although the DTIMS has been extensively used for structural studies of biomolecules, the application of IMS-MS has increased largely since the TWIMS Q-TOF mass spectrometer became commercially available.[107] The instrumental details of TWIMS device are described in section 1.2.2.3. Compared to most drift tubes, the analysis speed of the TWIMS mass spectrometer is significantly increased and the sensitivity is not compromised when operating in the IMS mode through the use of ion accumulation and radial ion confinement.[108,115,147] Various applications of TWIMS technology have been reported. TWIMS have been used to probe the Ω of proteins, unravel protein conformation and folding pathways, access structural and biophysical characteristics of large protein and entire functional assemblies.[146,148-151]

Richer information can be provided by combination of IMS-MS and computational approaches.[152] Experimentally determined Ω data is used to discriminate between different predicted models with different structures but similar energy minima. Alternatively, predicted models can be used to explain and extend the information from IMS-MS.[153,154] The theoretical Ω of a molecule can be calculated based on its structure either directly from available crystal and NMR structures in PDB, or from modelled structures. Several algorithms have been developed using different theoretical assumptions to calculate the theoretical Ω of each structure in order to be compared with determined Ω value from IMS-MS measurement.[155,156] The Diffusion Hard Sphere Scattering method implemented in the IMoS suit of software was used to calculate the theoretical Ω values of PDs in Chapter 3 and the MOBCAL trajectory method was used to calculate the theoretical Ω values for GA dimer in Chapter 5.

1.3.4 Potential pitfalls of ESI-MS assays

Protein–ligand interactions in solution are probed in the ESI-MS binding assays by transferring the free and ligand-bound proteins to gas phase by ESI and detecting the maintained equilibrium abundance of these species. Therefore, any physical or chemical process during ESI and in the gas phase that affects those distributions will lead to incorrect K_a values and, potentially, obscure the true binding stoichiometry. There are four common sources of error associated with ESI-MS assays: (i) in-source dissociation, (ii) nonspecific protein–ligand binding, (iii) non-uniform response factors and (iv) ESI-induced changes in solution pH and temperature.[139] Each of these problems are described below, as well as the available strategies to minimize the effects.

1.3.4.1 In-source dissociation

CID of the gaseous protein–ligand complexes may occur at various stages during the ion sampling process in the ion source (i.e., in-source dissociation), which may affect the relative abundance of free and ligand-bound proteins and, thereby, induce decreased magnitude of K_a values.[157] The extent of the in-source dissociation dependents on the configuration of the ion source used, the choice of instrumental parameters and the gas phase stability of protein–ligand complex. The gas phase stability of PL complex is determined partially by the nature of the specific interactions in a solution but not necessarily parallel to their solution stability.[158] Generally, the greater number of intermolecular interactions the PL complexes possess in a solution, the higher gas phase stability they exhibit.[158-161] In cases where the PL complex is susceptible to in-source dissociation, "gentle" source conditions such as low desolvation temperatures of the sampling capillary, low potentials across lens elements and short accumulation times are needed in order to minimize its influence and obtain reliable K_a values. However, there are trade-offs between the use of "gentle" source

condition and the signal intensity of protein ions. A balance must be found between minimizing the influence of in-source dissociation and achieving adequate protein signals. Decreasing the temperature of the ion source (i.e., cold spray) has been shown to prevent the PL complex ions from in-source dissociation.[162-164]

In cases when gentle source conditions cannot minimize the in-source dissociation, stabilizing additives may be used. For example, the introduction of imidazole (> 1mM) to the solution has been reported to prevent the in-source dissociation of a number of protein–ligand interactions, which is attributed to the enhanced evaporative cooling resulting from the dissociation of nonspecifically bound imidazole from the gaseous PL complex ions.[158,159] Additionally, the use of imidazole may also lead to charge state reduction of the PL complex ions due to its relatively high gas-phase basicity.[165] A potential issue is that the addition of very high concentration of imidazole may suppress the signals of the free and ligand-bound proteins in mass spectra. An alternative solution was reported that the addition of imidazole vapor[159] and sulfur hexafluoride[159] to the ESI source protect some PL complex ions from the in-source dissociation.

In cases when ion-source dissociation still occurs, competitive binding assay such as the reference ligand ESI-MS assay may be used.[161] In this approach, an indirect competitive ESI-MS assay was used, where the direct binding of protein with a reference ligand (L_{ref}) was monitored in order to quantify the interaction between protein and target ligand (L). The L_{ref} binds specifically to the protein at the same binding site with L, with known affinity and forms a kinetic stable complex in the gas phase. This method has proven useful for the analysis of kinetically unstable PL complexes in the gas phase.[166]

1.3.4.2 Nonspecific ligand binding

Free L can bind nonspecifically to P and PL during an ESI process (i.e., nonspecific ligand binding) because of the concentration effect, which results in false positives.[167,168] According to the CRM (Figure 1.8),[139] highly charged offspring droplets will undergo further solvent evaporation to dryness to form multiple charged gaseous ions. Using a monovalent interaction as an example, if one or more free ligand beside the P and PL present in the offspring droplet, nonspecific ionic or neutral intermolecular interactions occur as the droplet evaporate to dryness, leading to the formation of a series of nonspecific complexes PL_q ($q \geq 1$) that is not originated from the solution.

The extent of nonspecific binding can be minimized by decreasing the free L concentration.[167] However, high L concentrations (> 50 μM) are typically required for detection of weak interactions ($K_a < 10^4$ M^{-1}),[139] which is the characteristics of most protein–carbohydrate interactions. Therefore the nonspecific binding is often unavoidable in such cases.

A number of methods are developed to correct the nonspecific interactions,[157,169-173] including the reporter molecule method,[172] the nonspecific probe method,[173] the reference protein method,[157] and the mathematical correction method.[171] While the reporter molecule method and the nonspecific probe method are used to establish whether there are occurrence of the nonspecific binding, the reference protein method allows ESI mass spectra to be quantitatively corrected for the occurrence of thee nonspecific binding. In order to perform the mathematical correction, the number of specific binding sites has to be known.[171] The reference protein method, which is performed in Chapter 2 for nonspecific binding correction of protein–carbohydrate affinity measurements, is described below.

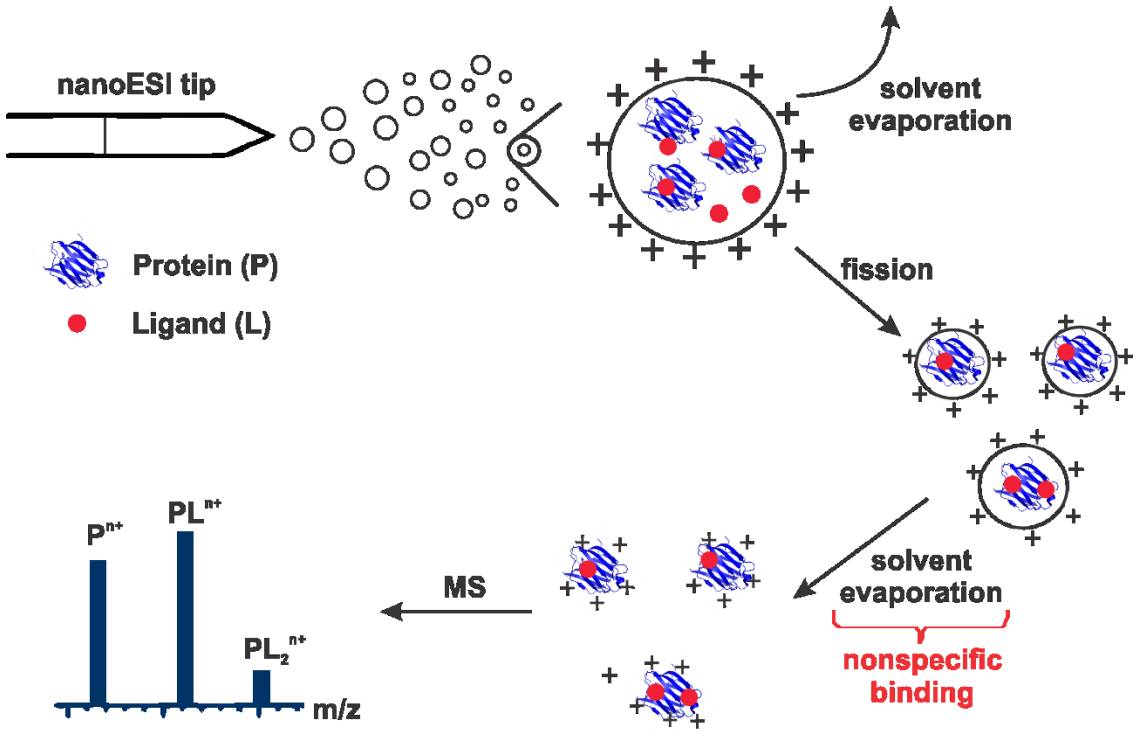

Figure 1.8 Illustration of the nonspecific protein–ligand interactions during an ESI process. Figure is adapted from reference 139.

The reference protein method involves the introduction of a reference protein (P_{ref}) to the solution.[157] The P_{ref} does not bind to target ligand specifically. The method is based on the assumption that nonspecific binding is a random process that affects all proteins in the ESI droplets equally. The fraction of the nonspecific L binding to P_{ref} was used to quantitatively correct the nonspecific binding of target protein P to L.

1.3.4.3 Non-uniform response factors

The abundance of free and ligand-bound proteins measured by ESI-MS is related to their solution concentrations by a response factor (*RF*), as shown in eq 1.18:

$$\frac{[\mathrm{PL}]}{[\mathrm{P}]} = \frac{RF_{\mathrm{P}} \cdot Ab(\mathrm{PL})}{RF_{\mathrm{PL}} \cdot Ab(\mathrm{P})} = RF_{\mathrm{P/PL}} \frac{Ab(\mathrm{PL})}{Ab(\mathrm{P})} \tag{1.14}$$

where the RF_{P} and RF_{PL} are the absolute response factors for P and PL, respectively, and $RF_{\mathrm{P/PL}}$ is the relative response factor. *RF*s depends on many factors including the ionization and detection efficiencies of each species, which account for their size, structure and surface properties, and the instrumental conditions used for the measurements.

The ESI-MS binding measurements (K_a calculation in eq 1.7 and 1.8) relay on the assumption that the protein and protein–ligand complex have uniform *RF* values (i.e., $RF_{\mathrm{P/PL}} \approx 1$). This assumption is held generally if L is much small compared to P, such that the size and the surface properties of P and PL are similar.[139] In most cases, when the MWs of P and PL are similar (more specifically, MW ratio of P and PL ≤ 110%), the P and PL are considered to be similar.[99] The uniform *RF* assumption is applied in the present work for K_a determination of protein–ganglioside oligosaccharide interactions in Chapter 2.

A number of strategies have been developed to minimize this non-uniform *RF* effect on K_a determination. One approach is to fit $RF_{\mathrm{P/PL}}$, as an adjustable parameter, to the experimental data based on an appropriate binding model.[174-177] However, it requires a multiple-parameter regression of the titration data and high quality experimental data to get reliable K_a values.[175] Furthermore, the potential influence of different concentration of analyte on *RF* is not taken into account. Another approach involves the introduction of an appropriate internal standard (IS), which has similar MW and surface activity to P but does not bind to L, to correct the fluctuations in $RF_{\mathrm{P/PL}}$ due to the concentration change, instability of ESI and other factors.[176,177]

1.3.4.4 ESI-induced changes in solution pH and temperature

The protein–ligand affinities are sensitive to pH in a solution. However, the solution pH may be altered during ESI process, caused by electrochemical reactions at the electrode in the ESI tip, resulting in the changes of K_a value.[178,179] The major electrochemical reactions taking place at the electrode are the oxidation of H_2O in the positive mode and reduction of H_2O in the negative mode, as shown in eqs 1.19a, 1.19b, which cause the production of H_3O^+ and OH^-, respectively.

$$3H_2O \rightarrow \frac{1}{2}O_2 + 2H_3O^+ + 2e^- \quad (1.15a)$$

$$2H_2O + 2e^- \rightarrow H_2 + 2OH^- \quad (1.15b)$$

The pH change can be very large (> 1 pH unit after spraying for 30 min) when a low flow rate is used for nanoESI.[178] In order to minimize the effect of pH change, ESI solution with a high buffer capacity and short spraying times (< 10 min) should be used.

Furthermore, an appropriate buffer is important for the protein stability and the protein–ligand interactions. The "physiological" buffers such as phosphate buffered saline (PBS) are good for protein stability, however, those buffers often contain phosphate, sodium, and potassium ions that are not compatible with ESI-MS. Only under special ESI conditions detection and binding measurements of protein can be performed using these buffers. For example, desorption electrospray ionization (DESI), where sample solution containing buffer salts are transferred through collisions to the ESI droplets that are devoid of buffer, enables the quantitative measurements performed using PBS solution.[180] Recently, small Emitter tips (0.5 μm diameter) were shown to be able to desalt protein and protein complex ion formed by ESI directly from a biologically relevant buffer.[181] Instead, most native ESI-MS assays employ buffer like ammonium acetate (1-200 mM). Although ammonium acetate does not effectively buffer the analyte solution

at neutral pH (with pK_a 4.75 for acetic acid and pK_a 9.25 for ammonium), it nonetheless remains a useful additive for native ESI-MS since it is volatile.[182] Ammonium formate is another volatile salt, but it is even less suitable for neutral pH buffering (with pK_a 3.75 for formic acid) than ammonium acetate.[183] Various alkyl-ammonium acetate salts have been used for ESI-MS,[184] however, they still do not provide buffering at neutral pH. Ammonium bicarbonate can buffer near neutral pH (with pK_a 6.4 for bicarbonate).[183] However, ammonium bicarbonate tends to induce protein unfolding during ESI, which makes it unsuitable for native ESI-MS.[185]

1.4 Present Work

The major focus of this thesis is the development of the CaR-ESI-MS assay employing a new class of MMs to facilitate the discovery and characterization of GL receptors of water soluble GBPs. The use of MMs and ESI-IMS-MS to probe the structure and stoichiometry of membrane peptide complexes was also investigated. A more detailed description is given blow.

The goal of Chapter 2 was to evaluate the performance of the CaR-ESI-MS assay, implemented with PDs for screening GLs against water soluble GBPs. PDs were produced either from purified GL mixture or GLs extracted from tissue or cells. To demonstrate the reliability of the method, a small library of purified gangliosides was incorporated, either individually or as a mixture, into PDs and screened against proteins derived from two bacterial toxins: cholera toxin B subunits (CTB_5) and a sub-fragment of toxin A from *Clostridium difficile* (TcdA-A2). The screening results were validated by comparing them with the affinity data measured for the corresponding ganglioside oligosaccharides. The CaR-ESI-MS results demonstrated the simultaneous detection of both high and low affinity interactions and their consistency with measured binding specificities of these GBPs. The assay was then applied for screening mixtures

of lipids extracted from a porcine brain and a human epithelial cell line against CTB_5 and revealed high affinity ligands. Finally, a comparison of the present results with data obtained with the CaR-ESI-MS assay implemented using NDs was made and it revealed that the PDs exhibited similar or superior performance to NDs for GBP-GL binding measurements.

The results described in Chapter 2 suggest that PDs could play a significant role in the discovery of GBP-GL interactions by CaR-ESI-MS. However, the structural composition of PDs have not been thoroughly investigated. Chapter 3 describes the first detailed study of the size, composition, heterogeneity and structure of 1-palmitoyl-2-oleoyl-*sn*-glycero-3-phosphocholine-containing PDs (POPC-PDs) in aqueous solutions at both acidic and neutral pH. Data acquired using high resolution ESI-MS and multi-angle laser light scattering (MALLS) revealed that the size and composition of POPC-PDs are dependent on pH – predominantly as SapA dimer at acidic pH; predominantly as SapA tetramer in freshly prepared solutions at neutral pH 6.8 and converts to SapA trimer over a period of hours. In order to estimate the solution structures of the different POPC-PD species and interpret the Ω data acquired for the gaseous POPC-PD ions, a series of solution and gas-phase molecular dynamics (MD) simulations were performed. The results of MD simulation suggest spheroidal structures for all the three complexes in solution. Comparison of measured Ω with calculated values produced from modelling suggests that the solution structures are largely preserved in the gas phase, although the lipids do not maintain regular bilayer orientations.

The CaR-ESI-MS has been successfully combined with PDs for screening GLs against soluble GBPs in Chapter 2. However, the non-uniform incorporation efficiencies of the various GL present in the mixture is one of the outstanding challenges to using PDs as GL arrays for screening. Chapter 4 compares the use of passively-loaded PDs (^{PL}PDs) with pre-loaded PDs for

CaR-ESI-MS screening of GLs against CTB_5. The ^{PL}PDs were prepared by incubating PDs containing only phospholipid with GL or GL mixture (in the form of glycomicelle) in an aqueous solution, while the pre-loaded PDs were prepared directly from a mixture of purified phospholipid and GL or GL mixture. Time-dependent changes in the composition of the ^{PL}PDs and ^{PL}NDs produced by incubation with GM1 micelle were monitored using CID of the gaseous MM ions and from the extent of GM1 binding to CTB_5 measured by ESI-MS. The ESI-MS results showed that GM1 binding to CTB_5 using ^{PL}PDs is indistinguishable from that observed with pre-loaded PDs produced directly from GM1 and the transfer of GM1 from micelle to NDs is slower than that to PDs. Ganglioside binding to CTB_5 measured for ^{PL}PDs and pre-loaded PDs prepared from GLs extracted from pig and mouse brain was also compared and the ^{PL}PDs allow for the detection of a greater number of ganglioside ligands. Together, the results of this study suggest ^{PL}PDs may have advantages over conventionally prepared PDs for screening GLs against GBPs using CaR-ESI-MS.

NDs and PDs have been successfully used to solubilize GLs for their CaR-ESI-MS screening against GBPs described in above Chapters. They have also been shown to have utility for solubilizing MPs in a native like lipid environment for structural and functional studies.[57-79] The goal of Chapter 5 was to investigate the stoichiometry and conformations of homodimers of the channel-forming membrane peptide gramicidin A (GA) in NDs. ESI-IMS-MS measurements showed that the GA dimer is readily transferred from phospholipid NDs to the gas phase by ESI and suggested that the ion conducting single stranded head-to-dead helical conformation of the dimer was preserved in the gas phase. Notably, the conformation of GA dimer produced from NDs was found to be different from those determined directly from organic solvent and phospholipid

vesicles, which suggests that the method used to deliver the peptide complexes from the lipid bilayer to the gas phase may influence the conformations of the gaseous ions.

1.5 References

1. Singleton, P. *Bacteria in Biology, Biotechnology and Medicine*, 5th ed.; Wiley: New York, 1999.
2. Noutsi, P.; Gratton, E.; Chaieb, S. (2016-06-30). *PLoS ONE*. **2016**, *11*, e0158313.
3. Lodish, H.; Berk, A.; Zipursky, L. S.; Matsudaira, P.; Baltimore, D.; Darnell, J. (2000). Biomembranes: Structural Organization and Basic Functions. *Molecular Cell Biology*, 4th ed.; Freeman, W. H: New York, 2000.
4. Zachowski, A. *Biochem. J*. **1993**, *294*, 1–14.
5. Brown, B. *Biological Membranes*. The Biochemical Society: London, U. K; p. 21.
6. van Meer, G.; Voelker, D. R.; Feigenson, G. W. *Nat. Rev. Mol. Cell Biol*. **2008**, *9*, 112–24.
7. D'Avanzo, N. *Curr. Top. Membr*. **2016**, *78*, 353-407.
8. Alberts, B.; Johnson, A.; Lewis, J.; Raff, M.; Roberts, K.; Walter, P. *Molecular Biology of the Cell*, 4th ed. Garland Science: New York, 2002.
9. Varki, A.; Cummings, R. D.; Esko, J. D.; Freeze, H. H.; Stanley, P.; Bertozzi, C. R.; Hart, G. W.; Etzler, M. E. *Essentials of Glycobiology*, 2nd ed.; Cold Spring Harbor Laboratory Press: Cold Spring Harbor, NY, 2009.
10. Nath, A.; Atkins, W. M.; Sligar, S. G. *Biochemistry*. **2007**, *46*, 2059–2069.
11. von Heijne, G. *J. Intern. Med*. **2007**, *261*, 543–557.
12. Bakheet, T. M.; Doig, A. J. *Bioinformatics* **2009**, *25*, 451–457.
13. Holgersson, J.; Gustafsson, A.; Breimer, M. E. *Immunol. Cell Biol.* **2005**, *83*, 694.

14. Weis, W. I.; Drickamer, K. *Annu. Rev. Biochem.* **1996**, *65*, 441.

15. Larsen, K.; Thygesen, M. B.; Guillaumie, F.; William, G. T.; Willats, W. G. T.; Jensen, K. J. *Carb. Res*. **2006**, *341*, 1209.

16. Homola, J. *Anal. Bioanal. Chem*. **2003**, *377*, 528.

17. Daghestani, H. N.; Day, B. W. *Sensors* **2010**, *10*, 9630.

18. De Crescenzo, G.; Boucher, C.; Durocher, Y.; Jolicoeur, M. *Cell. Mol. Bioeng.* **2008**, *1*, 204.

19. Wang, D. N.; Liu, S. Y.; Trummer, B. J.; Deng, C.; Wang, A. L. *Nat. Biotechnol.* **2002**, *20*, 275.

20. Liu, Y.; Palma, A. S.; Feizi, T. *Biol. Chem.* **2009**, *390*, 647.

21. Grant, O. C.; Smith, H. M.; Firsova, D.; Fadda, E.; Woods, R. J. *Glycobiology* **2014**, *24*, 17.

22. Fais, M.; Karamanska, R.; Russell, D. A.; Field, R. A. *J. Cereal Sci.* **2009,** *50*, 306–311.

23. Saboury, A. A. *J. Iran. Chem. Soc.* **2006**, *3*, 1.

24. Wilcox, D. E. *Inorg. Chim. Acta* **2008**, *361*, 857.

25. Wishart, D. *Curr. Pharm. Biotechnol.* **2005**, *6*, 105.

26. Mayer, M.; Meyer, B. *J. Am. Chem. Soc.* **2001,** *123*, 6108.

27. Haselhorst, T.; Lamerz, A. C.; Itzstein, M. *Methods Mol. Biol.* **2009,** *534*, 375.

28. Viegas, A.; Manso, J.; Nobrega, F. L.; Cabrita, E. J. *J. Chem. Educ.* **2011,** *88*, 990.

29. Wishart, D. *Curr. Pharm. Biotechnol.* **2005**, *6*, 105-120.

30. Ganem, B.; Li, Y. T.; Henion, J. D. *J. Am. Chem. Soc.* **1991**, *113*, 6294.

31. Van Dongen, W. D.; Heck, A. J. R. *Analyst* **2000**, *125*, 583.

32. Kitova, E. N.; Kitov, P. I.; Bundle, D. R.; Klassen, J. S. *Glycobiology* **2001**, *11*, 605.

33. Cederkvist, F. H.; Zamfir, A. D.; Bahrke, S.; Eijsink, V. G.; Sorlie, M.; Peter-Katalinic, J.; Peter, M. G., *Angew. Chem. Int. Ed.* **2006,** *45*, 2429.

34. Jecklin, M. C.; Touboul, D.; Jain, R.; Toole, E. N.; Tallarico, J.; Drueckes, P.; Ramage, P.; Zenobi, R. *Anal. Chem.* **2009**, *81*, 408.

35. Shi, J.; Yang, T.; Kataoka, S.; Zhang, Y.; Diaz, A. J.; Cremer, P. S. *J. Am. Chem. Soc*. **2007**, *129*, 5954−5961.

36. Sanghera, N.; Correia, B. E.; Correia, J. R.; Ludwig, C.; Agarwal, S.; Nakamura, H. K.; Kuwata, K.; Samain, E.; Gill, A. C.; Bonev, B. B.; Pinheiro, T. J. *Chem. Biol.* **2011**, *18*, 1422–1431.

37. Lingwood, D.; Binnington, B.; Rog, T.; Vattulainen, I.; Grzybek, M.; Coskun, U.; Lingwood, C. A.; Simons, K. *Nat. Chem. Biol.* **2011**, *7*, 260–262.

38. Lopez, H. H. H.; Schnaar, R. L. *Methods Enzymol*. **2006**, *417*, 205–220.

39. Lipid–Protein Interactions. In *Methods and Protocols*; Kleinschmidt, J. H., Ed.; Springer: New York, 2014; Vol. *974*.

40. Evans, S. V.; Roger MacKenzie. C. *J. Mol. Recognit*. **1999**, *12*, 155–68.

41. Feizi, T.; Chai, W. *Nat. Rev. Mol. Cell Biol.* **2004**, *5*, 582.

42. Song, X.; Lasanajak, Y.; Xia, B.; Heimburg–Molinaro, J.; Rhea, J. M.; Ju, H.; Zhao, C.; Molinaro, R. J.; Cummings, R. D.; Smith, D. F. *Nat Methods*. **2011**, *8*, 85–90

43. Lingwood, C. A.; Manis, A.; Mahfoud, R.; Khan, F.; Binnington, B.; Mylvaganam, M. *Chem. Phys. Lipids*. **2010**, *163*, 27–35.

44. Bayburt, T. H.; Grinkova, Y. V.; Sligar, S. G. *Nano Lett*. **2002**, *2*, 853−856.

45. Popovic, K.; Holyoake, J.; Pomès, R.; Privé, G.G. *Prot. Natl. Acad. Sci.* **2012**, *109*, 2908–2912.

46. Borch, J.; Torta, F.; Sligar, S. G.; Roepstorff, P. *Anal. Chem.* **2008**, *80*, 6245–6252.

47. Wu, H. J.; Henzie, J.; Lin, W. C.; Rhodes, C.; Li, Z.; Sartorel, E.; Thorner, J.; Yang, P.; Groves, J. T. *Nat Methods*. **2012**, *9*, 1189.

48. Zhang, Y.; Liu, L.; Daneshfar, R.; Kitova, E. N.; Li, C.; Jia, F.; Cairo, C.W.; Klassen, J. S. *Anal. Chem.* **2012**, *84*, 7618–7621.

49. Leney, A.; Fan, X.; Kitova, E.N.; Klassen, J. S. *Anal. Chem.* **2014**, *86*, 5271–5277.

50. Han, L.; Kitova, E. N.; Li, J.; Nikjah, S.; Lin, H.; Pluvinage, B.; Boraston, A. B.; Klassen, J. S. *Anal. Chem.* **2015,** *87,* 4888–4896.

51. Leney, A. C.; Darestani, R. R.; Li, J.; Nikjah, S.; Kitova, E. N.; Zou, C.; Cairo, C. W.; Xiong, Leney, A.; Fan, X.; Kitova, E. N.; Klassen, J. S. *Anal. Chem.* **2015**, *87*, 4402–4408.

52. Garavito, R. M.; Ferguson-Miller, S. *J. Biol. Chem*. **2001**, *276*, 32403–32406.

53. Seddon, A. M.; Curnow, P.; Booth, P. J. *Biochim. Biophys. Acta.* **2004**, *1666*, 105–117.

54. Duquesne, K.; Sturgis, J. N. *Humana Press*. **2010**, *601*, 205–217.

55. Popot, J. L. *Annu. Rev. Biochem*. **2010**, *79*, 737–775.

56. Calabrese, A. N.; Watkinson, T. G.; Henderson, P. J. F.; Radford, S. E.; Ashcroft, A. E. *Anal. Chem*. **2015**, *87*, 1118–1126.

57. Frauenfeld, J.; Löving, R.; Armache, J. P.; Sonnen, A. F.; Guettou, F.; Moberg, P.; Zhu, L.; Jegerschöld, C.; Flayhan, A.; Briggs, J. A.; Garoff, H.; Löw, C.; Cheng, Y.; Nordlund, P. *Nat Methods*. **2016**, *13*, 345–51.

58. Lyons, J. A.; Bøggild, A.; Nissen, P.; Frauenfeld, J. *Methods Enzymol*. **2017**, *594*, 85–99.

59. Hagn, F.; Etzkorn, M.; Raschle, T.; Wagner, G. J. *Am. Chem. Soc*. **2013**, *135*, 1919-1925.

60. Kijac, A.; Shih, A. Y.; Nieuwkoop, A. J.; Schulten, K.; Sligar, S. G.; Rienstra, C. M. *Biochemistry.* **2010**, *49*, 9190–9198.

61. Wang, X.; Mu, Z.; Li, Y.; Bi, Y.; Wang, Y. *Protein J*. **2015**, *34*, 205–211.

62. Baas, B. J.; Denisov, I. G.; Sligar, S. G. *Arch. Biochem. Biophys*. **2004**, *430*, 218–228.

63. Bayburt, T. H.; Grinkova, Y. V.; Sligar, S. G. *Arch. Biochem. Biophys*. **2006**, *450*, 215–222.

64. Mak, P. J.; Gregory, M. C.; Denisov, I. G.; Sligar, S. G.; Kincaid, J. R. *Proc. Natl. Acad. Sci. USA.* **2015**, *112*, 15856–15861.

65. Bayburt, T. H.; Vishnivetskiy, S. A.; McLean, M. A.; Morizumi, T.; Huang, C.-C.; Tesmer, J. J. G.; Ernst, O. P.; Sligar, S. G.; Gurevich, V. V. *J. Biol. Chem*. **2011**, *286*, 1420–1428.

66. Chougnet, A.; Grinkova, Y.; Ricard, D.; Sligar, S.; Woggon, W.-D. *ChemMedChem.* **2007**, *2*, 717–724.

67. Nath, A.; Trexler, A. J.; Koo, P.; Miranker, A. D.; Atkins, W. M.; Rhoades, E. *Methods Enzymol*. **2010**, *472*, 89–117.

68. Mak, P. J.; Denisov, I. G.; Grinkova, Y. V.; Sligar, S. G.; Kincaid, J. R. *J. Am. Chem. Soc*. **2011**, *133*, 1357–1366.

69. Gregory, M.; Mak, P. J.; Sligar, S. G.; Kincaid, J. R. *Angew. Chem. Int. Ed*. **2013**, *52*, 5342–5345.

70. Ye, F.; Hu, G.; Taylor, D.; Ratnikov, B.; Bobkov, A. A.; McLean, M. A.; Sligar, S. G.; Taylor, K. A.; Ginsberg, M. H. *J. Cell Biol*. **2010**, *188*, 157–173.

71. Akkaladevi, N.; Hinton-Chollet, L.; Katayama, H.; Mitchell, J.; Szerszen, L.; Mukherjee, S.; Gogol, E. P.; Pentelute, B. L.; Collier, R. J.; Fisher, M. T. *Protein Sci*. **2013**, *22*, 492–501.

72. Civjan, N. R.; Bayburt, T. H.; Schuler, M. A.; Sligar, S. G. *Biotechniques.* **2003**, *35*, 556–563.

73. Skar-Gislinge, N.; Arleth, L. *Phys. Chem. Chem. Phys*. **2011**, *13*, 3161–3170.

74. Denisov, I. G.; McLean, M. A.; Shaw, A. W.; Grinkova, Y. V.; Sligar, S. G. *J. Phys. Chem. B.* **2005**, *109*, 15580–15588.

75. Das, A.; Sligar, S. G. *Biochemistry.* **2009**, *48*, 12104–12112.

76. Das, A.; Grinkova, Y. V.; Sligar, S. G. *J. Am. Chem. Soc*. **2007**, *129*, 13778–13779.

77. Hopper, J. T.; Yu, Y. T.; Li, D.; Raymond, A.; Bostock, M.; Liko, I.; Mikhailov, V.; Laganowsky, A.; Benesch, J. L.; Caffrey, M.; Nietlispach, D.; Robinson, C. V. *Nat Methods*. **2013**, *10*, 1206–1208.

78. Hebling, C. M.; Morgan, C. R.; Stafford, D. W.; Jorgenson, J. W.; Rand, K. D.; Engen, J. R. *Anal. Chem*. **2010**, *82*, 5415–5419.

79. Marty, M. T.; Hoi, K. K.; Gault, J.; Robinson, C. V. *Angew. Chem., Int. Ed*. **2016**, *55*, 550−554.

80. Bernstein, S. L.; Dupuis, N. F.; Lazo, N. D.; Wyttenbach, T.; Condron, M. M.; Bitan, G.; Teplow, D. B.; Shea, J. E.; Ruotolo, B. T.; Robinson, C. V.; Bowers, M. T. *Nature Chem*. **2009**, *1*, 326−331.

81. Kebarle, P.; Tang, L. *Anal. Chem*. **1993**, *65*, 972A–986A.

82. Fenn, J. B. *Angew. Chem. Int. Ed.* **2003**, *42*, 3871.

83. Kebarle, P. *J. Mass Spectrom.* **2000,** *35*, 804.

84. Kebarle, P.; Verkerk, U. H. *Mass Spectrom. Rev.* **2009***, 28*, 898.

85. Taylor, G. I. *J. Fluid Mech.* **1965***, 2*, 1.

86. Iribarne, J. V.; Thomson, B. A. *J. Chem. Phys.* **1976***, 64*, 2287.

87. Iribarne, J. V.; Thomson, B. A. *J. Chem. Phys.* **1979***, 71*, 4451.

88. Dole, M.; Mack, L. L.; Hines, R. L. *J. Chem. Phys.* **1968**, *49*, 2240.

89. Smith, J. N.; Flagan, R. C.; Beauchamp, J. L. *J. Phys. Chem. A* **2002**, *106*, 9957.

90. Peschke, M.; Verkerk, U. H.; Kebarle, P. *J. Am. Soc. Mass Spectrom.* **2004**, *15*, 1424.

91. de la Mora, J. F. *Anal. Chim. Acta* **2000**, *406*, 93.

92. Konermann, L.; Rodriguez, A. D.; Liu, J. *Anal. Chem.* **2012**, *84*, 6798.

93. Ahadi, E.; Konermann, L. *J. Phy. Chem. B* **2012**, *116*, 104.

94. Konermann, L.; Ahadi, E.; Rodriguez, A. D.; Vahidi, S. *Anal. Chem.* **2013**, *85*, 2.

95. Wilm, M. S.; Mann, M. *Int J Mass Spectrom Ion Processes*. **1994**, *136*, 167–180.

96. Wilm, M.; Mann, M. *Anal. Chem.* **1996**, *68*, 1.

97. Karas, M.; Bahr, U.; Dulcks, T. *Fresenius J. Anal. Chem.* **2000**, *366*, 669.

98. Juraschek, R.; Dulcks, T.; Karas, M. *J. Am. Soc. Mass Spectrom.* **1999**, *10*, 300.

99. Jecklin, M. C.; Touboul, D.; Bovet, C.; Wortmann, A.; Zenobi, R. *J. Am. Soc. Mass Spectrom*. **2008**, *19*, 332.

100. Benesch, J. L. P.; Ruotolo, B. T.; Simmons, D. A.; Robinson, C. V. *Chem Rev*. **2007**, 107, 3544–3567.

101. Dawson, P. H. *Quadrupole Mass Spectrometry and Its Applications*. Springer: New York, 1995.

102. March, R. E.; Hughes, R. J. *Quadrupole Storage Mass Spectrometry*. John Wiley & Sons: New York, 1989.

103. De Hoffmann, E.; Stroobant, V. *Mass Spectrometry Principles and Applications,* 3th ed.; John Wiley & Sons: New York, 2007.

104. Pedder, R. E. *Ardara Technologies Technical Note* **2009**, TN_3005A.

105. Wilfried, M. A.; Niessen, Ricardo A.; Correa C. Interpretation of MS-MS Mass Spectra of Drugs and Pesticides.; John Wiley & Sons: New York, 2017.

106. Lu, D. PhD. Dissertation, University of Alberta, 2013.

107. Pringle, S. D.; Giles, K.; Wildgoose, J. L.; Williams, J. P.; Slade, S. E.; Thalassinos, K.; Bateman, R. H.; Bowers, M. T.; Scrivens, J. H. *Int. J. Mass Spectrom.* **2007***, 261*, 1.

108. Giles, K.; Pringle, S. D.; Worthington, K. R.; Little, D.; Wildgoose, J. L.; Bateman, R. H. *Rapid Commun. Mass Spectrom.* **2004***, 18*, 2401–2414.

109. Karasek, F. W. *Anal. Chem.* **1974***, 46*, 710A.

110. McCullough, B. J.; Kalapothakis, J.; Eastwood, H.; Kemper, P.; MacMillan, D.; Taylor, K.; Dorin, J.; Barran, P. E. *Anal. Chem.* **2008**, *80*, 6336.

111. Sergio, A.; Manel, A.; Marcelo, B. *Anal. Chim. Acta.* **2011***, 703*, 114.

112. Cohen, M. J.; Karasek, F. W. *J. Chromatogr. Sci.* **1970***, 8*, 330.

113. Buryakov, I. A.; Krylov, E. V.; Nazarov, E. G.; Rasulev, U. K. *Int. J. Mass Spectrom. Ion Processes.* **1993***, 128*, 143.

114. Shvartsburg, A. A.; Smith, R. D. *Anal. Chem.* **2008**, *80*, 9689.

115. Wildgoose, J.; McKenna, T.; Hughes, C.; Giles, K.; Pringle, S.; Campuzano, I.; Langridge, J.; Bateman, R. H. *Mol. Cell. Proteomics.* **2006**, *5*, S14.

116. Ruotolo, B. T.; Benesch, J. L. P.; Sandercock, A. M.; Hyung, S.-J.; Robinson, C. V. *Nat. Protocols.* **2008**, *3*, 1139.

117. Giles, K.; Williams, J. P.; Campuzano, I. *Rapid Commun. Mass Spectrom.* **2011**, *25*, 1559.

118. McLuckey, S. A. *J. Am. Soc. Mass. Spectrom.* **1992**, *3*, 599.

119. Papayannopoulos, I. A. *Mass Spectrom. Rev.* **1995**, *14*, 49.

120. Dongre, A. R.; Somogyi, A.; Wysocki, V. H. *J. Mass Spectrom.* **1996,** *31*, 339.

121. Price, W. D.; Schnier, P. D.; Jockusch, R. A.; Strittmatter, E. F.; Williams, E. R. *J. Am. Chem. Soc.* **1996**, *118*, 10640.

122. Dunbar, R. C.; McMahon, T. B. *Science* **1998**, *279*, 194.

123. Price, W. D.; Schnier, P. D.; Williams, E. R. *Anal. Chem.* **1996**, *68*, 859.

124. Polfer, N. C. *Chem. Soc. Rev.* **2011**, *40*, 2211.

125. Madsen, J. A.; Boutz, D. R.; Brodbelt, J. S. *J. Proteome Res.* **2010,** *9*, 4205.

126. Shaw, J. B.; Li, W.; Holden, D. D.; Zhang, Y.; Griep-Raming, J.; Fellers, R. T.; Early, B. P.; Thomas, P. M.; Kelleher, N. L.; Brodbelt, J. S. *J. Am. Chem. Soc.* **2013,** *135*, 12646.

127. Zubarev, R. A.; Kelleher, N. L.; McLafferty, F. W. *J. Am. Chem. Soc.* **1998**, *120*, 3265.

128. Zubarev, R. A.; Kruger, N. A.; Fridriksson, E. K.; Lewis, M. A.; Horn, D. M.; Carpenter, B. K.; McLafferty, F. W. *J. Am. Chem. Soc.* **1999**, *121*, 2857.

129. Syka, J. E. P.; Coon, J. J.; Schroeder, M. J.; Shabanowitz, J.; Hunt, D. F. *Proc. Natl. Acad. Sci. U. S. A.* **2004,** *101*, 9528.

130. Wyttenbach, T.; Bowers, M. T. *Annu. Rev. Phys. Chem.* **2007**, *58*, 511.

131. Sharon, M.; Taverner, T.; Ambroggio, X. I.; Deshaies, R. J.; Robinson, C. V. *PLoS. Biol.* **2006,** *4*, 1314.

132. Benesch, J. L. P.; Aquilina, J. A.; Ruotolo, B. T.; Sobott, F.; Robinson, C. V. *Chem. Biol*. **2006**, *13*, 597.

133. Lorenzen, K.; Vannini, A.; Crarner, P.; Heck, A. J. R. *Structure.* **2007,** *15*, 1237.

134. Tešić, M.; Wicki, J.; Poon, D. K. Y.; Withers, S. G.; Douglas, D. J. *J. Am. Soc. Mass Spectrom.* **2007**, *18*, 64. El-Hawiet, A.;

135. Shoemaker, G. K.; Daneshfar, R.; Kitova, E. N.; Klassen, J. S. *Anal. Chem.* **2012,** *84*, 50.

136. Guilhaus, M.; Selby, D.; Mlynski, V. *Mass Spectrom. Rev.* **2000**, *19*, 65.

137. Chernushevich, I. V.; Loboda, A. V.; Thomson, B. A. J Mass Spectrom. **2001**, *36*, 849–865.

138. Mamyrin, B. A. *Int. J. Mass Spectrom.* **2001,** *206*, 251.

139. Kitova, E. N.; El-Hawiet, A.; Schnier, P. D.; Klassen, J. S. *J. Am. Soc. Mass Spectrom.* **2012**, *23*, 431–441.

140. Kitova, E. N.; Kitov, P. I.; Paszkiewicz, E.; Kim, J.; Mulvey, G. L.; Armstrong, G. D.; Bundle, D. R.; Klassen, J. S. *Glycobiology* **2007**, *17*, 1127.

141. Han, L.; Kitova, E. N.; Klassen, J. S. *J. Am. Soc. Mass Spectrom*. **2016**, *27*, 1878–1886.

142. Abzalimov, R. R.; Dubin, P. L.; Kaltashov, I. A. *Anal. Chem.* **2007**, *97*, 6055–6063.

143. Cederkvist, F.; Zamfir, A. D.; Bahrke, S.; Eijsink, V. G. H.; Sorlie, M.; Peter-Katalinic, J.; Peter, M. G. *Angew. Chem. Int. Ed.* **2006,** *45*, 2429–2434.

144. El-Hawiet, A.; Shoemaker, G. K.; Daneshfar, R.; Kitova, E. N.; Klassen, J. S. *Anal. Chem.* **2012,** *84*, 50–58.

145. Creaser, C. S. ; Griffiths, J. R.; Bramwell, C. J.; Noreen, S.; Hill, C. A. ; Paul Thomas, C. L. *Analyst.* **2004***, 129*, 984.

146. Uetrecht, C., Rose, R. J., van Duijn, E., Lorenzen, K., Heck, A. J. R. *Chem. Sov. Rev*. **2010**, *39*, 1633–1655.

147. Scarff, C. A.; Thalassinos, K.; Hilton, G. R.; Scrivens, J. H. *Rapid Commun. Mass Spectrom*. **2008**, *22*, 3297–3304.

148. Thalassinos, K.; Slade, S. E.; Jennings, K.R.; Scrivens, J. H.; Giles, K.; Wildgoose, J.; Hoyes, J.; Bateman, R. H.; Bowers, M. T. *Int. J. Mass Spectrom*. **2004**, *236*, 55–63.

149. Smith, D. P.; Giles, K.; Bateman, R. H.; Radford, S. E.; Ashcroft, A. E. *J. Am. Soc. Mass Spectrom*. **2007**, *18*, 2180–2190.

150. Ruotolo, B. T.; Giles, K.; Campuzano, I.; Sandercock, A. M.; Bateman, R. H.; Robinson, C. V. *Science*, **2005**, *310*,1658–1661.

151. Uetrecht, C.; Versluis, C.; Watts, N. R.; Wingfield, P. T.; Steven, A. C.; Heck, A. J. *Angew. Chem. Int. Ed*. **2008**, *47*, 6247–6251.

152. Pacholarz, K. J.; Garlish, R. A.; Taylor, R. J.; Barran, P. E. *Chem. Soc. Rev.* **2012**, *41*, 4335–4355.

153. Arteca, G. A.; Reimann, C. T.; Tapia, O.; *Mass Spectrom. Rev*. **2001**, *20*, 402–422.

154. Daggett, V. *Chem. Rev*. **2006**, *106*, 1898–1916.

155. Clemmer, D. E.; Jarrold, M. F. *J. Mass Spectrom.* **1997**, *32*, 577–592.

156. Wyttenbach, T.; Witt, M.; Bowers, M. T. *J. Am. Chem. Soc.* **2000**, *122*, 3458–3464.

157. Sun, J.; Kitova, E. N.; Klassen, J. S. *Anal. Chem*. **2006**, *79*, 416–425.

158. Sun, J.; Kitova, E. N.; Klassen, J. S. *Anal. Chem*. **2007**, *79*, 416.

159. Bagal, D.; Kitova, E. N.; Liu, L.; El-Hawiet, A.; Schnier, P. D.; Klassen, J. S. *Anal. Chem.* **2009**, *81*, 7801.

160. Robinson, C. V.; Chung, E. W.; Kragelund, B. B.; Knudsen, J.; Aplin, R. T.; Poulsen, F. M.; Dobson, C. M. *J. Am. Chem. Soc.* **1996***, 118*, 8646.

161. El-Hawiet, A.; Kitova, E. N.; Liu, L.; Klassen J. S. *J. Am. Soc. Mass Spectrom.* **2010**, *21*, 1893.

162. Sakamoto, S.; Fujita, M.; Kim, K.; Yamaguchi, K. *Tetrahedron*. **2000**, *56*, 955–964.

163. Nishimura, S. -I.; Nagahori, N.; Takaya, K.; Tachibana, Y.; Miura, N.; Monde, K. *Angew. Chem. Int. Ed*. **2005**, *44*, 571–575.

164. Miras, H. N.; Wilson, E. F.; Cronin, L. *Chem. Commun*. **2009**, *11*, 1297–1311.

165. Hunter, E. P.; Lias, S. G. *Phys. Chem. Ref. Data.* **1998**, *27*, 413.

166. Liu, L.; Kitova, E. N.; Klassen, J. S. *J. Am. Soc. Mass Spectrom*. **2011**, *22*, 310–318.

167. Wang, W.; Kitova, E. N.; Klassen, J. S. *Anal. Chem.* **2005,** *77*, 3060.

168. Hossain, B. M.; Konermann, L. *Anal. Chem.* **2006**, *78*, 1613.

169. Daubenfeld, T.; Bouin, A. P.; van der Rest, G. *J. Am. Soc. Mass Spectrom.* **2006**, *17*, 50 1239.

170. Lane, L. A.; Ruotolo, B. T.; Robinson, C. V.; Favrin, G.; Benesch, J. L. P. *J. Mass Spectrom.* **2009**, *283*, 169.

171. Shimon, L.; Sharon, M.; Horovitz, A. *Biophys. J.* **2010,** *99*, 1645.

172. Sun, N.; Sun, J.; Kitova, E. N.; Klassen, J. S. J. *Am. Soc. Mass Spectrom.* **2009**, *20*, 1242.

173. Kitova, E. N.; Soya, N.; Klassen, J. S. *Anal. Chem.* **2011**, *83*, 5160.

174. Wilcox, J. M.; Rempel, D. L.; Gross, M. L. *Anal. Chem.* **2008**, *80*, 2365.

175. Gabelica, V.; Galic, N.; Rosu, F.; Houssier, C.; De Pauw, E. *J. Mass Spectrom.* **2003**, *38*, 491.

176. Gabelica, V.; Rosu, F.; De Pauw, E. *Anal. Chem.* **2009**, *81*, 6708.

177. Mathur, S.; Badertscher, S.; Scott, M.; Zenobi, R. *Phys. Chem. Chem. Phys.* **2007**, *9*, 6187.

178. Wang, W.; Kitova, E. N.; Klassen, J. S. *Anal. Chem.* **2003**, *75*, 4945.

179. Van Berkel, G. J.; Asano, K. G.; Schnier, P. D. *J. Am. Soc. Mass Spectrom.* **2001**, *12*, 853.

180. Yao, Y.; Shams-Ud-Doha, K.; Daneshfar, R.; Kitova, E. N.; Klassen, J. S. *J. Am. Soc. Mass. Spectrom.* **2015,** *26*, 98.

181. Susa, A. C.; Xia, Z.; Williams, E. R. *Anal. Chem*. **2017**, *89*, 3116.

182. Konermann, L. *J. Am. Soc. Mass Spectrom*. **2017**, *28*, 1827–1835.

183. Lide, D. R. *CRC Handbook of chemistry and physics*, 82nd ed. CRC Press: Boca Raton, London, New York, Washington, 2001.

184. Zhuang, X.; Gavriilidou, A. F. M.; Zenobi, R. *J. Am. Soc. Mass Spectrom*. **2017**, *28*, 341–346.

185. Hedges, J. B.; Vahidi, S.; Yue, X.; Konermann, L. *Anal. Chem*. **2013**, *85*, 6469–6476.

Chapter 2

Screening Glycolipids against Proteins in vitro using Picodiscs and Catch-and-Release Electrospray Ionization Mass Spectrometry*

2.1 Introduction

The interactions between glycan-binding proteins (GBPs) and glycolipids (GLs), which consist of a mono-, oligo- or polysaccharides covalently attached to a lipid moiety, represent an important class of cellular recognition processes.[1-4] Despite their importance in normal and pathological cellular processes, the identification and characterization of GBP–GL interactions remains challenging and new experimental techniques are needed.[5-6] The key challenges to the detection and characterization of GBP–GLs complexes are the relative insolubility of the GLs in water, which imposes limitations on how the binding measurements are performed; the low affinities characteristic of monovalent GBP–carbohydrate interactions, which require sensitive detection methods and the expected dependence of the properties of the interactions on the nature of the lipid environment.[7-9] Commonly used methods for detecting GBP–GL binding, such as thin layer chromatography (TLC) overlay, enzyme-linked immunosorbent assays (ELISA) and surface plasmon resonance (SPR) spectroscopy, employ GLs immobilized on a solid surface.[5] While convenient, such a presentation of GLs differs significantly from the native lipid environment of

* A version of this chapter has been published: Li, J.; Fan, X.; Kitova, E. N.; Zou, C.; Cairo, C. W.; Eugenio, L.; Ng, K. K. S.; Xiong, Z. J.; Privé, G. G.; Klassen, J. S. *Anal Chem*. **2016**, *88*, 4742–4750.

cell membranes. The incorporation of GLs into model membranes (*e.g.* micelles, bicelles, liposomes and nanodiscs (NDs)) allows for a more physiological presentation of GLs and the possibility of probing the influence of the lipid environment on binding. Increasingly conventional binding assays, including electrospray ionization-mass spectrometry (ESI-MS), are being adapted for use with model membranes to allow for GBP–GL interaction studies to be carried out in a membrane-like environment.[10-13]

Recently protein interactions with gangliosides (sialic acid containing glycosphingolipids) were detected using the catch-and-release (CaR)-ESI-MS assay implemented with NDs.[10-11] Briefly, the assay involves transferring the GBP–GL–ND complexes, which are present in solution, to the gas phase using ESI. Intact GBP–GL complexes are released from the NDs in the ion source, isolated and then subjected to collision-induced dissociation (CID) to release the GL ligands for identification purposes. Both neutral and acidic GLs are readily incorporated into NDs, which are ~150 kDa water-soluble discoidal phospholipid bilayers surrounded by two copies of an amphipathic membrane scaffold protein (MSP), thereby allowing their interactions with water-soluble proteins to be investigated.[10-11,14] Because of their size, each ND can accommodate a significant number of GLs (NDs containing up to thirty gangliosides have been reported) and allow for binding studies to be carried out using a wide range of lipid compositions.[11-12] Moreover, NDs can serve as GL arrays and can be combined with the CaR-ESI-MS assay to rapidly screen known and unknown mixtures of GLs against target GBPs.[11] However, the use of NDs has several drawbacks, such as their tendency to disassemble in aqueous solution at room temperature and the inherent challenges in accurately characterizing their lipid composition. More recently, the implementation of the CaR-ESI-MS assay with lipid-transporting macromolecular complexes called picodiscs (PDs) to detect both high and low affinity GBP–GL interactions was described.[13]

PDs are reported to be composed of two copies of the human sphingolipid activator protein saposin A (SapA) and a small number (8-12) of phospholipids.[15] PDs containing GLs have been shown to have advantages over NDs for the detection of some GBP–GL interactions and for studying the kinetics of GL-processing enzymes.[13] Furthermore, PDs are stable at room temperature for periods of weeks[13] and, therefore, are attractive as GL arrays for *in vitro* screening.

The goal of the present study was to investigate the feasibility of implementing the CaR-ESI-MS assay with PDs to screen libraries of GLs against water-soluble GBPs. The B subunit homopentamer of cholera toxin (CTB_5) and a sub-fragment of toxin A (TcdA-A2) from *Clostridium difficile* (TcdA), served as model GL-binding proteins for this work. The CTB subunits, each possessing a single, dominant, carbohydrate binding site, are responsible for cellular recognition.[16] The interactions between CTB_5 with its native receptor GM1, as well as other gangliosides and their corresponding oligosaccharides, have been extensively studied.[17-18] The apparent association constants (K_a) for the stepwise binding of the GM1 pentasaccharide (β-D-Gal-(1→3)-β-D-GalNAc-(1→4)-[α-D-Neu5Ac-(2→3)]-β-D-Gal-(1→4)-D-Glc, Figure 2.1) to CTB_5 range from 2×10^6 to 2×10^7 M^{-1}.[19] Binding of CTB_5 to other ganglioside oligosaccharides is suggested to be much weaker, although quantitative binding data have not been reported.[18] The exotoxin TcdA, which is one of the main virulence factors of *C. difficile*, consists of four regions: a N-terminal domain which is responsible for the glucosylating activity of the toxin, a cysteine protease domain, a delivery/pore forming domain, and a C-terminal domain containing combined repetitive oligopeptides, which is responsible for receptor binding on target cell surfaces.[20-21] Although the functional human receptors of TcdA have not been conclusively identified, it is known that TcdA binds to a variety of carbohydrate structures, including the trisaccharide α-D-Gal-(1→3)-β-D-Gal-(1→4)-D-GlcNAc,[22] several Lewis X, Y and I glycan sequences,[23-24] the

glycosphingolipid β-D-GalNAc-(1→3)-β-D-Gal-(1→4)-β-D-GlcNAc-(1→3)-β-D-Gal-(1→4)-β-D-Glc-cer[25-26] and several ganglioside oligosaccharides (*e.g.* $GM1a_{os}$, $GM2_{os}$, $GM3_{os}$, $GT1b_{os}$, $GD3_{os}$, $GD1a_{os}$, $GT3_{os}$, $GT1a_{os}$, $GT1b_{os}$).[27] In the present study, the CaR-ESI-MS assay was used to screen a small library of gangliosides (GM1, GM2, GM3, GD1a, GD1b, GD2 and GT1b) against CTB_5 and TcdA-A2; the screening results were validated using binding data measured for the corresponding ganglioside oligosaccharides. The assay was also used to screen mixtures of GLs extracted from porcine brain, as well as a human epithelial cell line, against CTB_5 to demonstrate the applicability of the assay for analysis of natural GL libraries.

2.2 Experimental Section

2.2.1 Proteins

Cholera toxin B subunit homopentamer from *Vibrio cholerae* (CTB_5, homopentamer molecular weight (MW) 58,020 Da) was purchased from Sigma-Aldrich Canada (Oakville, Canada). The A2 subfragment of *Clostridium difficile* toxin (TcdA-A2, MW 29,575 Da) and the single chain variable fragment (scFv, MW 26,539 Da) of the monoclonal antibody (mAb) Se155-4 were expressed in *Escherichia coli* and purified as described previously.[28-29] Saposin A (SapA, two major isoforms with MWs 8,918 Da and MW 9,049 Da) and recombinant MSP (MSP1E1, MW 27,494 Da) were expressed and purified as previously described.[14-15] Shiga toxin type 1 B subunit homopentamer ($Stx1B_5$, MW 38,455 Da) was a gift from Prof. G. Armstrong (University of Calgary).

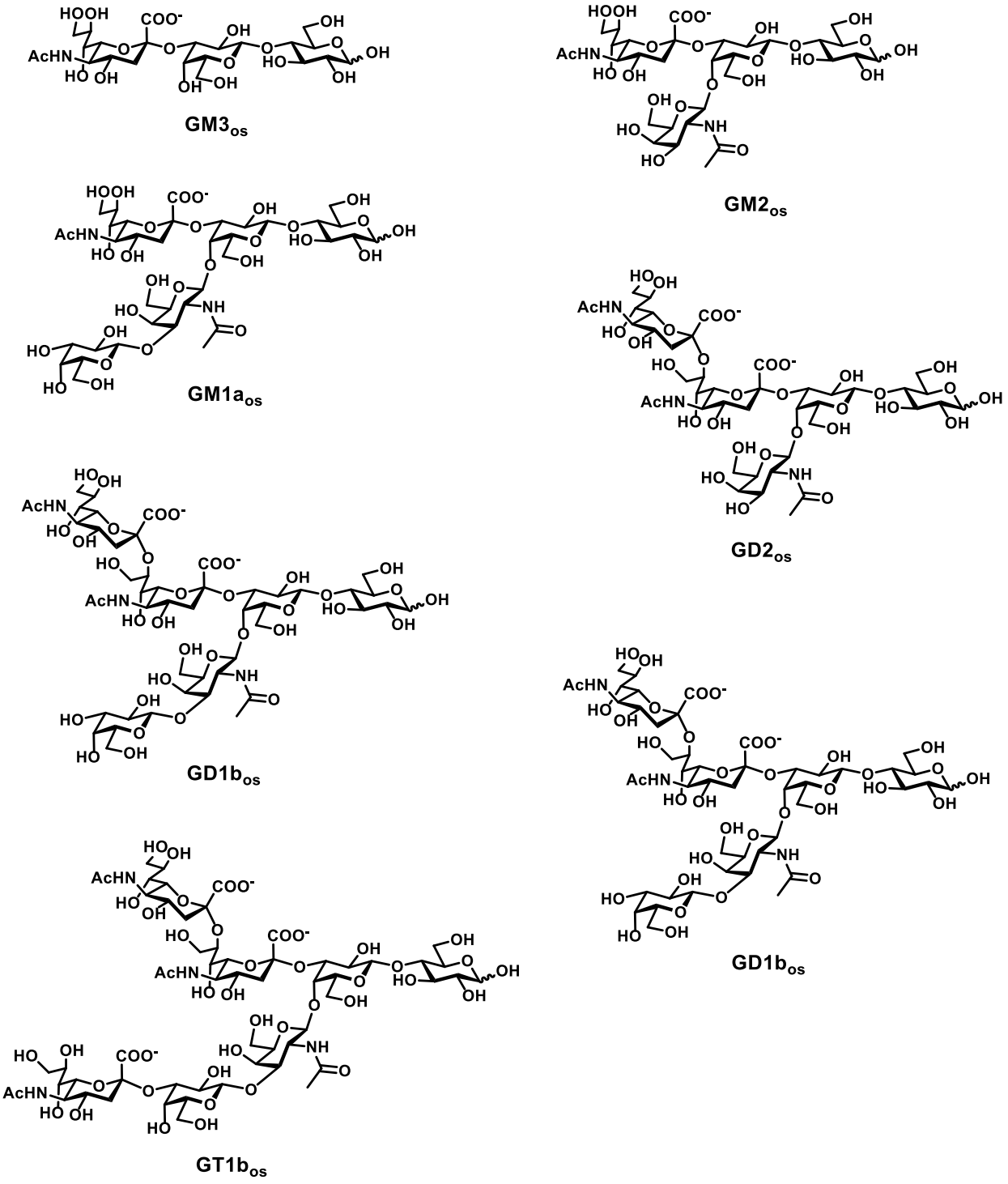

Figure 2.1 Structures of the ganglioside oligosaccharides $GM3_{os}$, $GM2_{os}$, $GD2_{os}$, $GD1a_{os}$, $GD1b_{os}$ and $GT1b_{os}$.

2.2.2 Lipids and glycolipids

The gangliosides β-D-Gal-(1→3)-β-D-GalNAc-(1→4)-[α-D-Neu5Ac-(2→3)]-β-D-Gal-(1→4)-D-Glc-ceramide (GM1, major isoforms *d*18:1-18:0 and *d*20:1-18:0 have MWs 1545.8 Da, 1573.9 Da), β-D-GalNAc-(1→4)-[α-D-Neu5Ac-(2→3)]-β-D-Gal-(1→4)-D-Glc-ceramide (GM2, major isoforms *d*18:1-18:0 and *d*20:1-18:0 have MWs 1383.7 Da, 1411.7 Da) and α-D-Neu5Ac-(2→3)-β-D-Gal-(1→4)-D-Glc-ceramide (GM3, major isoforms *d*18:1-18:0 and *d*20:1-18:0 have MWs 1180.5 Da, 1208.5 Da) were purchased from Cedarlane Labs (Burlington, Canada); α-D-Neu5Ac-(2→3)-β-D-Gal-(1→3)-β-D-GalNAc-(1→4)-[α-D-Neu5Ac-(2→3)]-β-D-Gal-(1→4)-D-Glc-ceramide (GD1a, major isoforms *d*18:1-18:0 and *d*20:1-18:0 have MWs 1836.1 Da, 1864.1 Da), (β-D-Gal-(1→3)-β-D-GalNAc-(1→4)-[α-D-Neu5Ac-(2→8)-α-D-Neu5Ac-(2→3)]-β-D-Gal-(1→4)-D-Glc-ceramide (GD1b, major isoforms *d*18:1-18:0 and *d*20:1-18:0 have MWs 1836.1 Da, 1864.1 Da), α-Neu5Ac-(2-3)-β-D-Galp-(1-3)-β-D-GalNAc-(1-4)-[α-Neu5Ac-(2-8)-α-Neu5Ac-(2-3)]-β-D-Galp-(1-4)-D-Glc-ceramide (GT1b, major isoforms *d*18:1-18:0 and *d*20:1-18:0 have MWs 2126.4 Da, 2154.4 Da) were purchased from Sigma-Aldrich Canada (Oakville, Canada), and β-D-GalNAc-(1→4)-[α-D-Neu5Ac-(2→8)-α-D-Neu5Ac-(2→3)]-β-D-Gal-(1→4)-D-Glc-ceramide (GD2, major isoforms *d*18:1-18:0 and *d*20:1-18:0 have MWs 1674.0 Da, 1702.0 Da) were purchased from MyBioSource Inc. (San Diego, CA). The phospholipid 1-palmitoyl-2-oleoyl-*sn*-glycero-3-phosphocholine (POPC) and porcine brain extract were purchased from Avanti Polar Lipids Inc. (Alabaster, AL). The structures of the gangliosides and POPC are shown in Figure 2.2. The procedure for extracting GLs from the A549 cell line culture was described previously.[10]

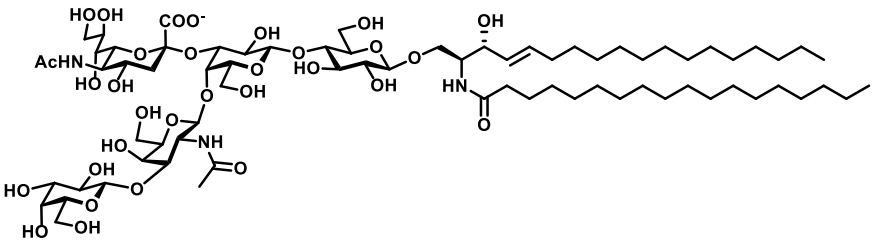

*d*18:1-18:0

GM1

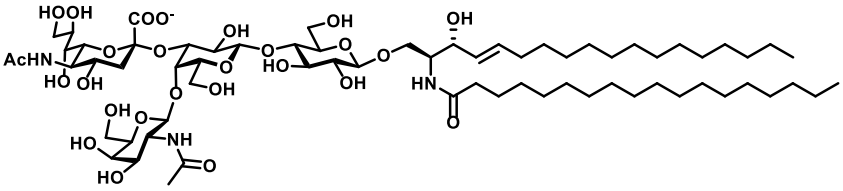

*d*18:1-18:0

GM2

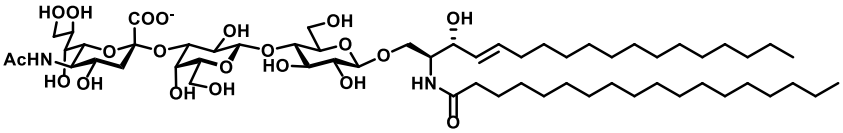

*d*18:1-18:0

GM3

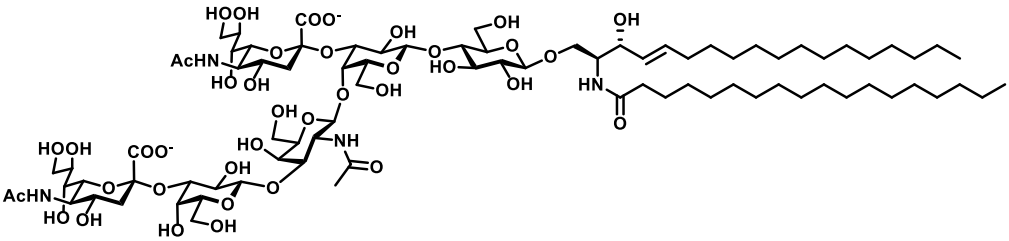

*d*18:1-18:0

GD1a

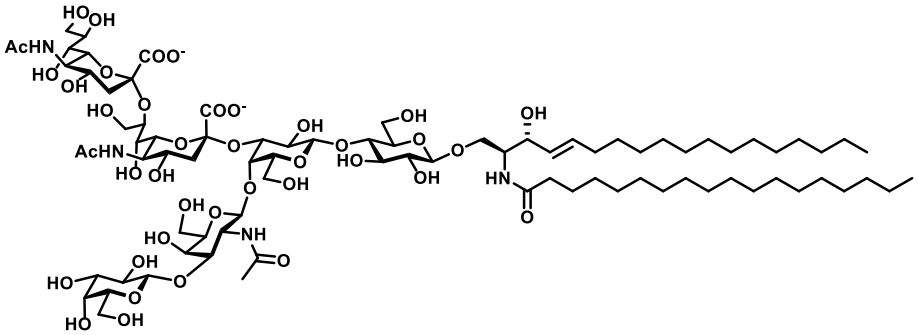

*d*18:1-18:0

GD1b

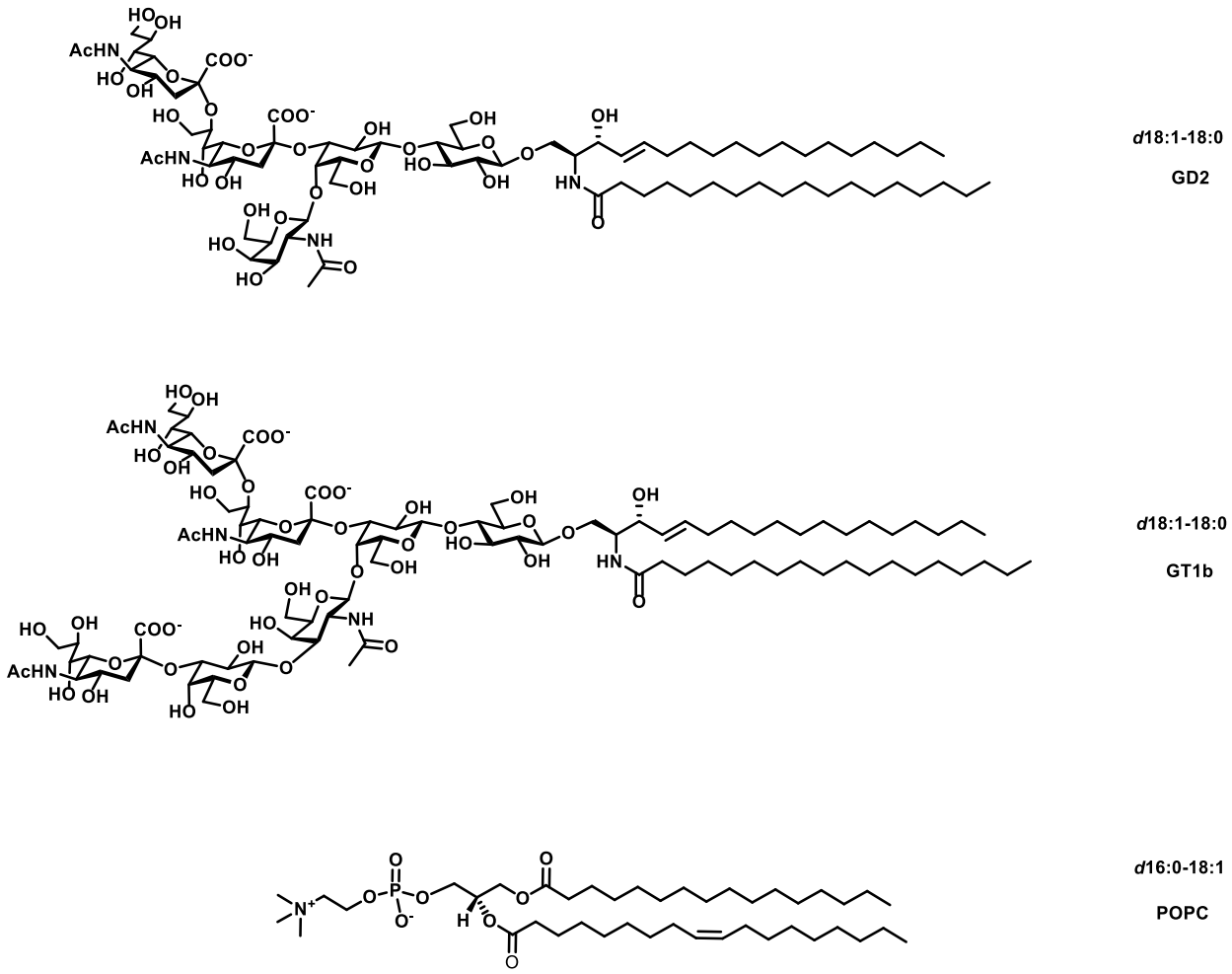

Figure 2.2 Structures of the gangliosides GM1, GM2, GM3, GD2, GD1a, GD1b and GT1b and the phospholipid POPC.

2.2.3 Oligosaccharides

The ganglioside oligosaccharides β-D-Gal-(1→3)-β-D-GalNAc-(1→4)-[α-D-Neu5Ac-(2→3)]-β-D-Gal-(1→4)-D-Glc ($GM1_{os}$, MW 998.34 Da); β-D-GalNAc-(1→4)-[α-D-Neu5Ac-(2→3)]-β-D-Gal-(1→4)-D-Glc ($GM2_{os}$, MW 836.29 Da); α-D-Neu5Ac-(2→3)-β-D-Gal-(1→4)-D-Glc ($GM3_{os}$, MW 633.21 Da); α-D-Neu5Ac-(2→3)-β-D-Gal-(1→3)-β-D-GalNAc-(1→4)-[α-D-Neu5Ac-(2→3)]-β-D-Gal-(1→4)-D-Glc ($GD1a_{os}$, MW 1289.44 Da); β-D-Gal-(1→3)-β-D-GalNAc-(1→4)-[α-D-Neu5Ac-(2→8)-α-D-Neu5Ac-(2→3)]-β-D-Gal-(1→4)-D-Glc ($GD1b_{os}$, MW 1289.44 Da); β-D-GalNAc-(1→4)-[α-D-Neu5Ac-(2→8)-α-D-Neu5Ac-(2→3)]-β-D-Gal-(1→4)-D-Glc ($GD2_{os}$, MW 1127.39 Da); α-Neu5Ac-(2-3)-β-D-Galp-(1-3)-β-D-GalNAc-(1-4)-[α-Neu5Ac-(2-8)-α-Neu5Ac-(2-3)]-β-D-Galp-(1-4)-D-Glc ($GT1b_{os}$, MW 1581.39 Da) were purchased from Elicityl SA (Crolles, France). The structures of the oligosaccharides are shown in Figure 2.1. Stock solutions (1 mM in Milli-Q water (Millipore, MA)) of each of the oligosaccharides were stored at -20 °C until needed.

2.2.4 Picodisc preparation

PDs containing GLs were prepared using a protocol reported previously[15] and only a brief overview is given here. The phospholipid POPC, dissolved in chloroform, was mixed with either an individual ganglioside, a mixture of gangliosides (GM1, GM2, GM3, GD1a, GD1b, GD2, GT1b) or a GL extract, dissolved in 2:1 chloroform:methanol, in a 4:1 molar ratio. The lipids were dried using nitrogen and kept in a vacuum desiccator overnight at room temperature to form a lipid film. The film was re-dissolved in a buffer of 50 mM sodium acetate and 150 mM NaCl (pH 4.8) followed by sonication and around 10 freeze/thaw cycles to form liposomes. PD formation was

initiated by adding SapA protein, at 1:10 molar ratio of SapA-to-total lipid, and incubating at 37 °C for 60 min. A Superdex 75 10/300 size-exclusion column (GE Healthcare Bio-Science, Uppsala, Sweden), equilibrated in 50 mM sodium acetate and 150 mM NaCl (pH 4.8), was used for purification of the PDs. The PD fractions were pooled, concentrated and buffer exchanged into 200 mM ammonium acetate (pH 6.8). The concentration of SapA monomer was determined by measuring the UV absorbance at 280 nm and using an extinction coefficient of 8855 M^{-1} cm^{-1}. The PDs were concentrated to approximately 100 μM and stored at room temperature until used.

2.2.5 Nanodisc preparation

NDs were prepared according to a protocol reported previously.[30-32] Briefly, DMPC (dissolved in chloroform) was mixed with seven gangliosides GM1, GM2, GM3, GD1a, GD1b, GT1b, GD2 (dissolved in 2:1chloroform:methanol) in the desired ratio (2% for each ganglioside and 86% for DMPC). The lipids were dried under nitrogen and kept in a vacuum desiccator overnight at room temperature to form a lipid film. Lipids were then re-suspended in 20 mM TrisHCl, 0.5 mM EDTA, 100 mM NaCl, 25 mM sodium cholate (pH 7.4) and sonicated for 15 min. MSP1E1 was added at 1:100 molar ratio of MSP1E1-to-total lipid followed by incubation at room temperature for 15 min. An equal volume of Bio-Beads (Bio-Rad Laboratories Ltd., Mississauga, Canada) was added to initiate ND formation and the solution was incubated at room temperature for 3 h to remove all detergent. Finally, a Superdex 200 10/300 size exclusion column (GE Healthcare Bio-Sciences, Uppsala, Sweden), which was equilibrated in 200 mM ammonium acetate (pH 6.8), was used for purification of the NDs. The concentration of NDs was determined from the concentration of MSP1E1 dimer. NDs were concentrated to approximately 60 μM and stored at -80 °C until needed.

2.2.6 Mass spectrometry

The ESI-MS and CaR-ESI-MS measurements were carried out using a Synapt G2-S quadrupole-ion mobility separation-time-of-flight (Q-IMS-TOF) mass spectrometer (Waters, Manchester, UK) equipped with a nanoESI source. The CaR-ESI-MS assay was implemented in negative ion mode, whereas the direct ESI-MS assay was performed in positive ion mode. Borosilicate capillaries (1.0 mm o.d., 0.68 mm i.d.) were pulled using a P-1000 micropipette puller (Sutter Instruments, Novato, CA). A platinum wire was inserted into the nanoESI tip and a capillary voltage of -0.9 kV (negative ion mode) or 1.0 kV (positive ion mode) was applied to carry out ESI. The source temperature was 60 °C for both two modes. A cone voltage of 30 V was used and the Trap and Transfer collision energies were set to 5 and 2 V, respectively, for ESI-MS analysis. All data were processed using MassLynx software (version 4.1) and Driftscope *v.*2.5 (Waters, Manchester, UK).

2.2.6.1 CaR-ESI-MS assay

To implement the CaR-ESI-MS assay, the quadrupole mass filter was set (to HM 15 and LM 4) to pass ions with a range of mass-to-charge ratios (*m/z*) (actual window, which was determined based on changes in background signal, ranges from 100 to 200 *m/z*) that encompasses the ions corresponding to the free and GL-bound GBP of interest at a given charge state. Collision-induced dissociation (CID) was performed in the Trap region using collision energies of 50 to 100 V. The released ganglioside anions were identified based on their measured MWs. Where MW alone was insufficient for positive GL identification, CID of the corresponding ions, produced directly from solution, was carried out in the Transfer region using a collision energy of 75 V. In cases where the free and GL-bound GBP ions and those corresponding to the PDs overlapped in the mass spectrum, IMS was used to separate the GBP (and GBP–GL complexes) from the PD ions; release

of the GL ions was achieved by CID performed in the Transfer region using collision energies of between 50 V and 75 V. For IMS measurements, a wave height of 40 V and a wave velocity of between 650 m s^{-1} and 850 m s^{-1} were applied and helium and nitrogen (IMS gas) gas flow rates of 50 mL min^{-1} and 60 mL min^{-1}, respectively, were used.

2.2.6.2 Direct ESI-MS assay

The direct ESI-MS assay was used to quantify the binding of seven ganglioside oligosaccharides (GM1os, $GM2_{os}$, $GM3_{os}$, GD1aos, GD1bos, $GD2_{os}$, $GT1b_{os}$) to CTB_5.[33] Binding measurements were carried out in triplicate using a fixed protein concentration and five different oligosaccharide concentrations. The reference protein (P_{ref}) method was used to correct the mass spectra for the occurrence of non-specific carbohydrate–protein binding during ESI.[34] The scFv, which does not bind to the oligosaccharides tested, served as P_{ref}. Although CTB_5 has five carbohydrate binding sites, only a single site was found to be occupied under the solution conditions used. Consequently, a 1:1 protein (P)–ligand (L) binding model (eq 2.1) was used to analyze the ESI-MS data. The apparent association constant ($K_{a,app}$) was calculated using eq 2.2:

$$\mathrm{P} + \mathrm{L} \rightleftharpoons \mathrm{PL} \tag{2.1}$$

$$\mathrm{K_{a,app}} = \frac{R}{[\mathrm{L}]_0 - \frac{R}{1+R}[\mathrm{P}]_0} \tag{2.2}$$

where $[P]_0$ and $[L]_0$ are the initial concentrations of P and L, respectively. The abundance ratio (R) of the ligand-bound protein (PL) to free protein (P) ions measured by ESI-MS (after correction for non-specific binding)[34] is taken to be equal to the equilibrium concentration ratio in solution, eq 2.3:

$$R = \frac{\sum Ab(\mathrm{PL})}{\sum Ab(\mathrm{P})} = \frac{[\mathrm{PL}]}{[\mathrm{P}]} \tag{2.3}$$

2.3 Results and Discussion

The main objective of this study was to establish the feasibility of using PDs to solubilize mixtures of GLs and screen them against water-soluble target GBPs using the CaR-ESI-MS assay. With this goal in mind, four libraries of GL-containing PDs were prepared. Two of the libraries (*Library 1* and *Library 2,* Table 2.1) contained seven gangliosides (GM1, GM2, GM3, GD1a, GD1b, GD2 and GT1b) - *Library 1* consisted of an equimolar mixture of seven different PDs, each prepared with a single ganglioside, while *Library 2* consisted of PDs prepared from an equimolar mixture of the seven gangliosides. To confirm that all seven gangliosides were incorporated into the PDs, the two libraries were analyzed by ESI-MS and the PD ions subjected to CID. Shown in Figure 2.3 are the ESI mass spectra for aqueous ammonium acetate solutions (200 mM, pH 6.8) of each library (total ganglioside concentration 140 μM). In both cases, a broad unresolved peak centered at approximately *m/z* 4800 was observed. This feature is attributed to the intact PD ions.[13] The quadrupole was set to pass ions with *m/z* > 4000, which were then subjected to CID in the Trap region. At collision energies of 30 V to 100 V, signal corresponding to all seven deprotonated ganglioside ions was detected. At energies ≥50 V, secondary fragmentation of the ganglioside ions resulted in the appearance of deprotonated Neu5Ac (*m/z* 290) and deprotonated α-D-Neu5Ac-(2→8)-α-D-Neu5Ac (*m/z* 581) (Figure 2.4). These results confirm that all seven gangliosides were successfully incorporated into the PDs. *Library 3* and *Library 4* (Table 2.1) consisted of a mixture of GLs extracted from porcine brain and a mixture of GLs extracted from cultured human epithelial A549 cell line, respectively. All four libraries were screened against CTB_5, only *Library* 2 was screened against TcdA-A2.

Previously, the GLs found in *Library 2*, *Library 3* and *Library 4* were screened against CTB_5 using the CaR-ESI-MS assay implemented with NDs.[1,2] In order to have a complete set of comparative data, the CaR-ESI-MS assay, implemented with NDs, was also used in the present study to screen a mixture of seven gangliosides against TcdA-A2. The NDs used for these measurements consisted of equimolar amounts (2% of each ganglioside) of GM1, GM2, GM3, GD1a, GD1b, GD2, GT1b. These NDs are referred to as the 7G NDs. Shown in Figure 2.5a is a representative ESI mass spectrum acquired for an aqueous ammonium acetate (200 mM, pH 6.8) solution of 7G ND (6 μM). The broad peak centered at *m/z* ~11000 is attributed to intact ND. CID was carried out on all ions with *m/z* >5600 in the Trap region with a collision energy of 150 V and resulted in the appearance of all seven deprotonated ganglioside ions, confirming their incorporation into the NDs (Figure 2.5b).

Table 2.1 Composition of lipids (phospholipid and glycosphingolipid) in *Library 1*, *Library 2*, *Library 3* and *Library 4*, which were used to produce the PDs.

Library	Phospholipid	Glycolipids
Library 1	POPC	GM1, GM2, GM3, GD2, GD1a, GD1b and GT1b
Library 2	POPC	GM1, GM2, GM3, GD2, GD1a, GD1b and GT1b
Library 3	POPC	GLs extract from porcine brain
Library 4	POPC	GLs extract from cultured human epithelial A549 cell line

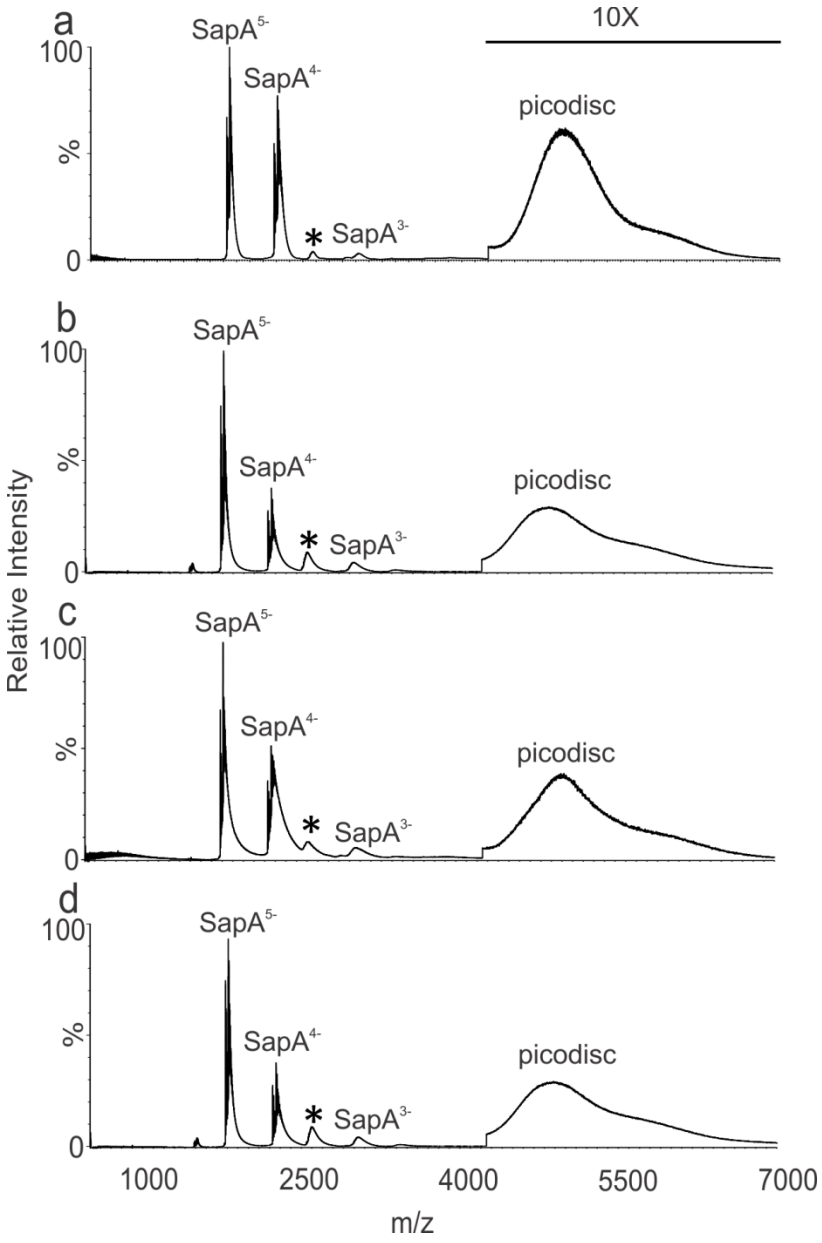

Figure 2.3 ESI mass spectra acquired in negative ion mode for aqueous ammonium acetate solutions (200 mM, pH 6.8) of (a) *Library 1* (20 μM of each PD), (b) *Library 2* (140 μM), (c) *Library 3* (40 μM) and (d) *Library 4* (140 μM). Peaks labelled * correspond to (SapA + POPC) complexes.

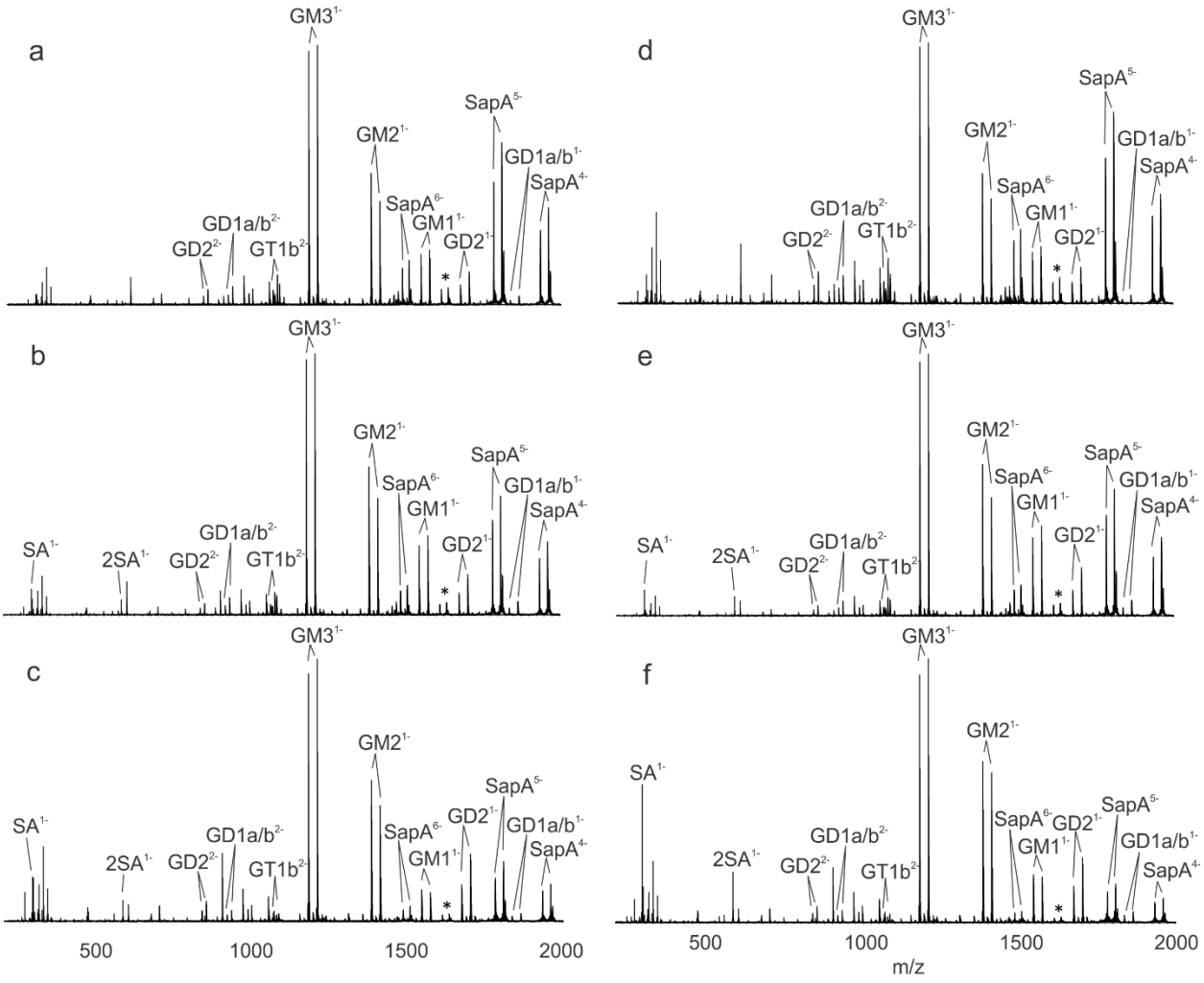

Figure 2.4 CID mass spectra of ions with *m/z* >4000, produced by ESI performed in negative ion mode on aqueous ammonium acetate solutions (200 mM, pH 6.8) of *Library 1* (20 μM each PD), at collision energies (in Trap) of (a) 30 V, (b) 50 V and (c) 100 V, and of *Library 2* (140 μM) at collision energies (in Trap) of (d) 30 V, (e) 50 V, and (f) 100 V. Peaks labelled * correspond to (SapA + POPC) complexes.

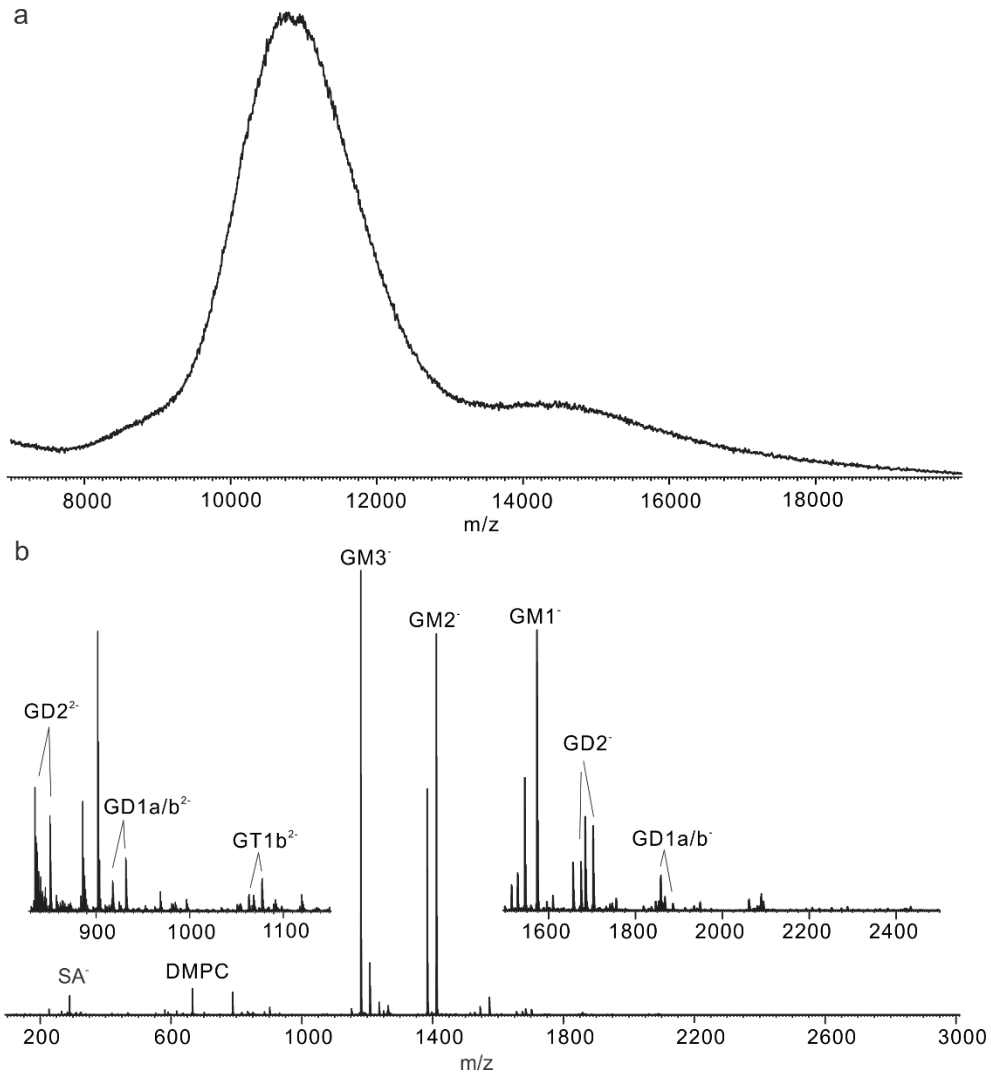

Figure 2.5 (a) ESI mass spectrum acquired in negative ion mode for an aqueous ammonium acetate solution (200 mM, pH 6.8) of 7G ND (6 μM, 2% of each ganglioside). (b) CID mass spectrum of ions with *m/z* >5600, produced by ESI for the solution described in (a), using a collision energy (in Trap) of 150 V.

2.3.1 Screening ganglioside-containing PDs against CTB_5

The CaR-ESI-MS assay was used to screen *Library 1* and *Library 2* against CTB_5. Shown in Figure 2.6a is a representative ESI mass spectrum acquired in negative ion mode for an aqueous ammonium acetate solution (200 mM, pH 6.8) of CTB_5 (3 μM) and *Library 1* (6 μM, each ganglioside). Signal corresponding to the -12 to -15 charge states of the deprotonated ions of CTB_5 and CTB_5 bound to one or two ganglioside molecules (i.e., $(CTB_5 + L)^{n-}$ and $(CTB_5 + 2L)^{n-}$), as well as PD ions, is evident. Peak assignments were made using the measured and theoretical *m/z* values and assuming that L corresponds predominantly to GM1. Because of spectral overlap of ions corresponding to the free and GL-bound CTB_5 and those of the PDs, IMS was used to separate the CTB_5 ions from PD ions (Figures 2.6b & c). To identify the gangliosides bound to CTB_5, CID (in the Transfer region) was performed simultaneously on the $(CTB_5 + L)^{n-}$ and $(CTB_5 + 2L)^{n-}$ ions, at charge states -12 to -15, post-IMS. Using a collision energy of 75 V, CID resulted predominantly in the release of singly deprotonated GM1 ions, with singly deprotonated GM2, GM3, GD1a and/or GD1b ions and doubly deprotonated GT1b detected, but at lower abundance (Figure 2.6d). Because GD1a and GD1b are structural isomers, they cannot be distinguished based on mass. Moreover, because CID was performed post-IMS, it was not possible to confirm the identity of the two gangliosides based on differences in IMS arrival times. Therefore, the CaR-ESI-MS measurements were repeated using PDs containing only GD1a or GD1b. These results confirmed that both GD1a and GD1b bind to CTB_5 under these solution conditions (Figure 2.7). Based on the results of this analysis, it is concluded that GM1, GM2, GM3, GT1b, GD1a and GD1b bind to CTB_5, with no evidence of GD2 binding. Moreover, the relative abundances of the released ligands are consistent with GM1 having a higher affinity than the other gangliosides. These findings are

consistent with binding data measured for CTB_5 and the oligosaccharides of these seven gangliosides, *vide infra*.

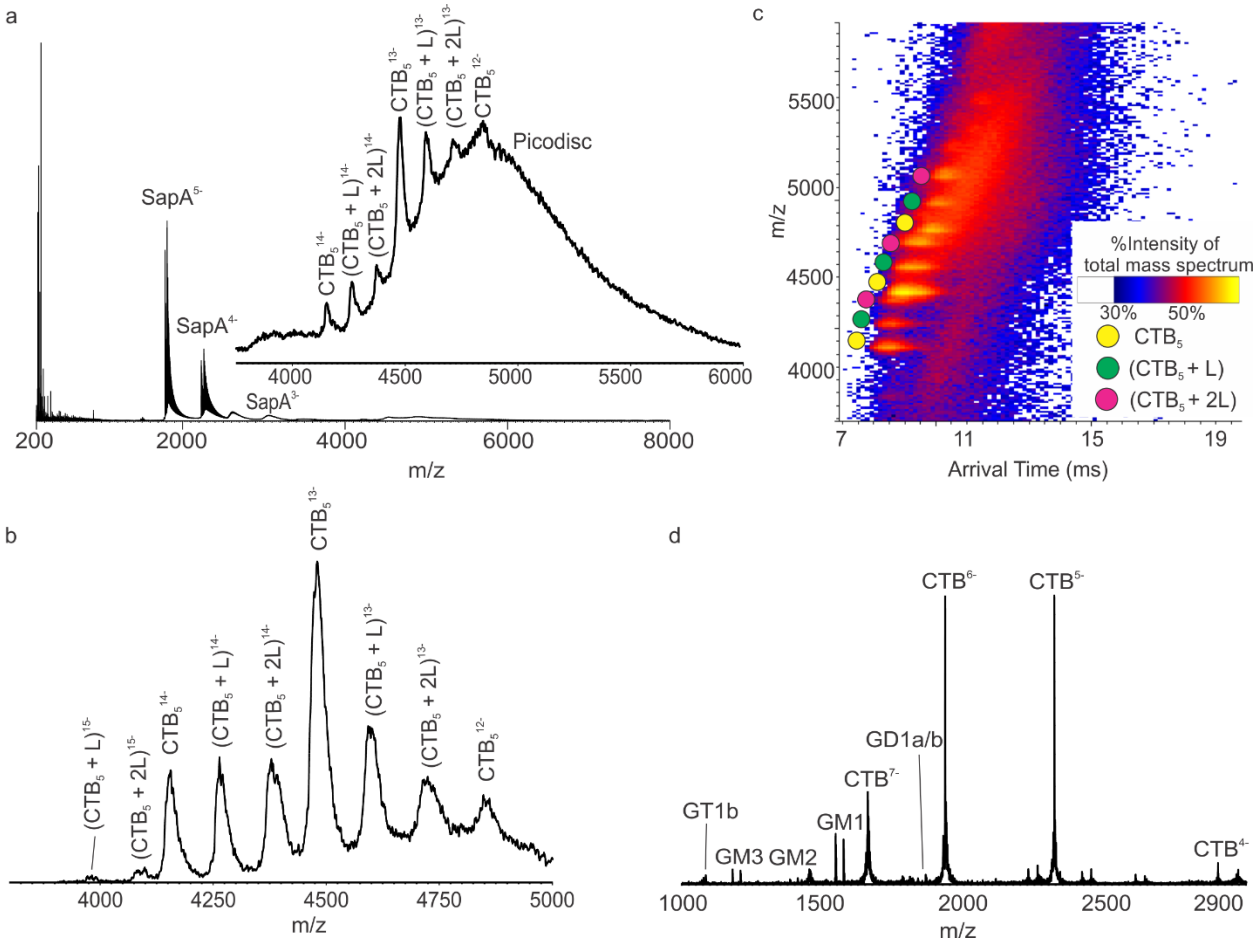

Figure 2.6 ESI mass spectra acquired in negative ion mode for a 200 mM aqueous ammonium acetate solution (pH 6.8, 22 °C) containing CTB_5 (3 μM) and *Library 1* (6 μM) (a) before and (b) after separation of the CTB_5 ions from the PD ions using IMS. (c) Corresponding IMS heat map (plot of ion *m/z*, ion intensity and IMS arrival times). (d) CID mass spectrum acquired in the Transfer region (post IMS) for the CTB_5 ions, produced from the solution described in (a) and (b), performed in the Transfer region using a collision energy of 75 V.

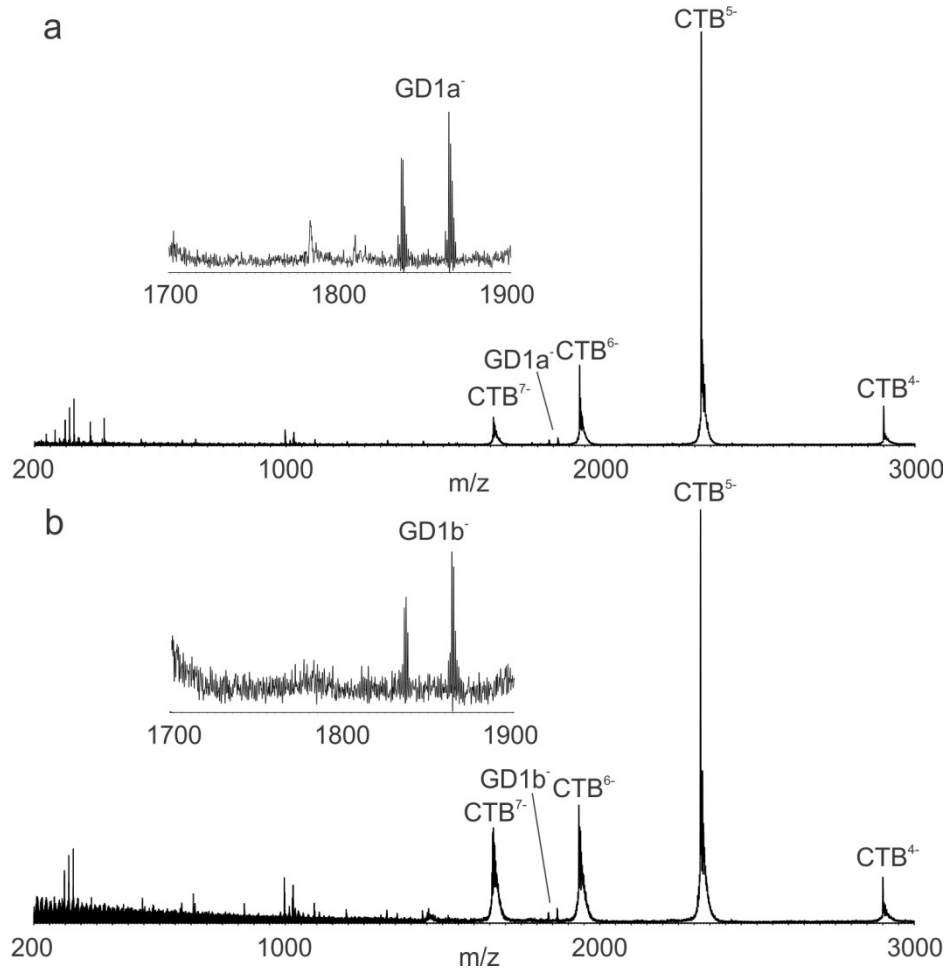

Figure 2.7 CID mass spectra of free and any ligand-bound CTB_5 ions, at charge states -12 to -15, produced in negative ion mode by ESI performed on an aqueous ammonium acetate solutions (200 mM, pH 6.8) containing CTB_5 (3 μM) and 6 μM of (a) GD1a PD or (b) GD1b PD. CID was performed with a collision energy of 75 V in the Transfer region following IMS separation of CTB5 ions from the PD ions.

Measurements were also carried out on an aqueous ammonium acetate solution (200 mM, pH 6.8) of CTB_5 (3 μM) and *Library 2* (42 μM, 6 μM of each ganglioside). The ESI mass spectrum acquired post-IMS, Figure 2.8a, is qualitatively similar to that measured for solutions containing

Library 1. At these concentrations, signals corresponding to the -12 to -15 charge states of free CTB_5 and CTB_5 bound to one or two ganglioside molecules (i.e., $(CTB_5 + L)^{n-}$ and $(CTB_5 + 2L)^{n-}$ were detected. CID of all the $(CTB_5 + L)^{n-}$ and $(CTB_5 + 2L)^{n-}$ ions in the Transfer region, using a collision energy of 75 V, led primarily in the appearance of singly deprotonated GM1 ions, with signal corresponding to GM2, GM3, GT1b ions also evident (Figure 2.8b). Signal corresponding to deprotonated ions of GD1a and/or GD1b was also detected. Based on the results described above, it is reasonable to assume that the signal corresponds to the presence of both isomers. The CaR-ESI-MS measurements were also performed using a higher concentration of *Library 2*. Shown in Figure 2.8c is a representative ESI mass spectrum acquired for an aqueous ammonium acetate solution (200 mM, pH 6.8) of CTB_5 (3 μM) and *Library 2* (63 μM, 9 μM of each ganglioside). Notably, at the higher library concentration, CTB_5 was found to bind between one and five gangliosides. Post-IMS CID of the $(CTB_5 + iL)^{n-}$ ions, where i = 1 to 5, at charge states -12 to -15 resulted primarily in the appearance of singly deprotonated GM1 ions, with GM2, GM3, GT1b, GD1a/GD1b ions also detected (Figure 2.8d). These results are consistent with those obtained at the lower *Library 2* concentration (Figure 2.8a).

To exclude the possibility of false positives resulting from the formation non-specific GBP-ganglioside interactions during the ESI process, the CaR-ESI-MS assay was also used to screen *Library 2* against Stx1-B_5, which served as a negative control. Stx1, like CT, belongs to the family of AB_5 bacterial toxins. However, to the best of our knowledge, Stx1-B_5 (and Stx1) has no affinity for gangliosides. Shown in Figure 2.9 is a representative ESI mass spectrum acquired for an aqueous ammonium acetate solution (200 mM, pH 6.8) of Stx1-B_5 (5 μM) and *Library 2* (56 μM, 8 μM of each ganglioside). Notably, no signal corresponding to Stx1-B_5 bound to any of the gangliosides was detected; instead, the only protein ion signal corresponded to free Stx1-B_5. The

absence of ganglioside binding was further shown by CID, performed in the Trap region on the Stx1-B_5 ions, which failed to produce any signal corresponding to ganglioside ions. These results suggest that nonspecific binding of proteins to GLs contained within the PDs during the ESI process is negligible.

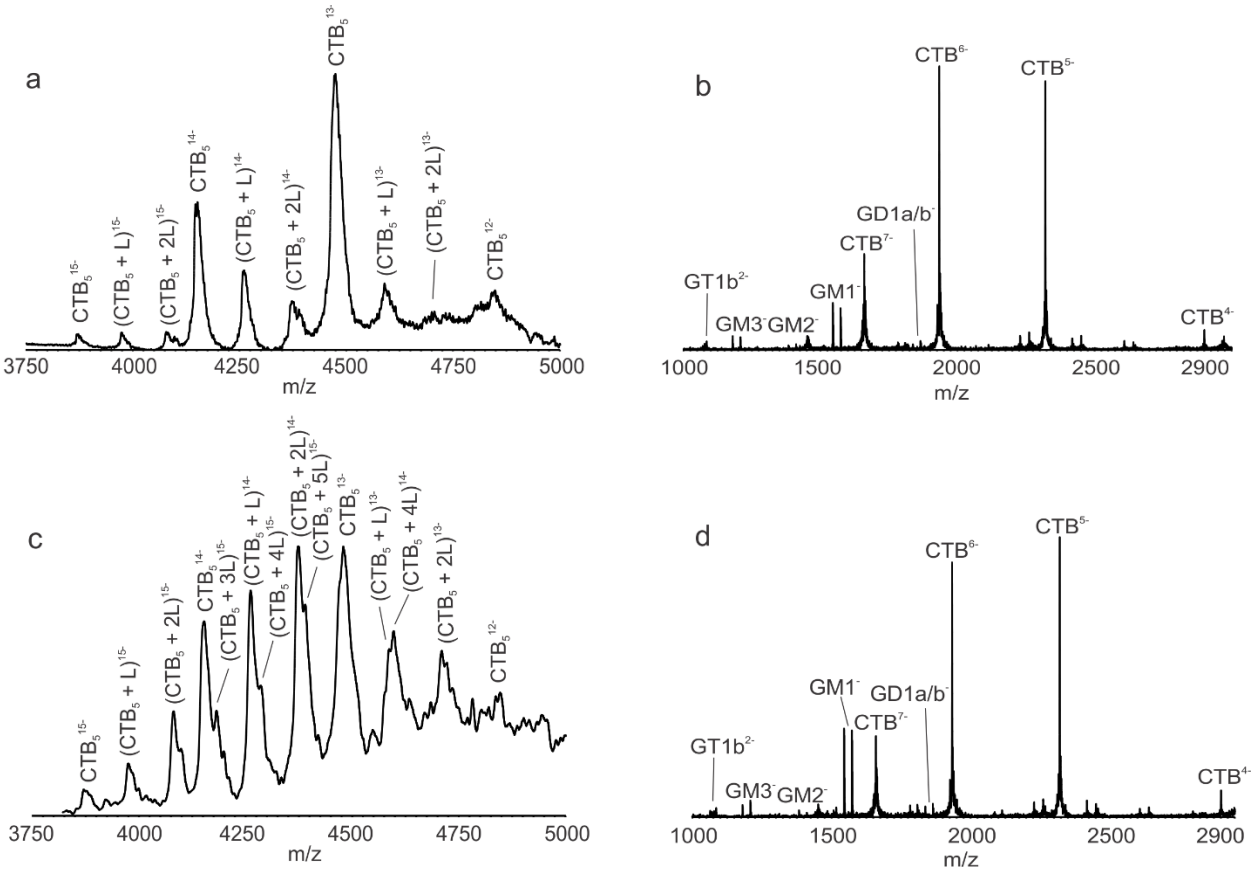

Figure 2.8 ESI mass spectra acquired in negative ion mode for a 200 mM aqueous ammonium acetate solution (pH 6.8) containing CTB_5 (3 μM) and *Library 2* at (a) 42 μM or (c) 63 μM; PD ions were excluded from the mass spectrum using IMS. (b) and (d) CID mass spectra acquired in the Transfer region (post IMS separation) for the CTB_5 ions, produced from the solution described in (a) and (c), respectively, performed in the Transfer region using a collision energy of 75 V.

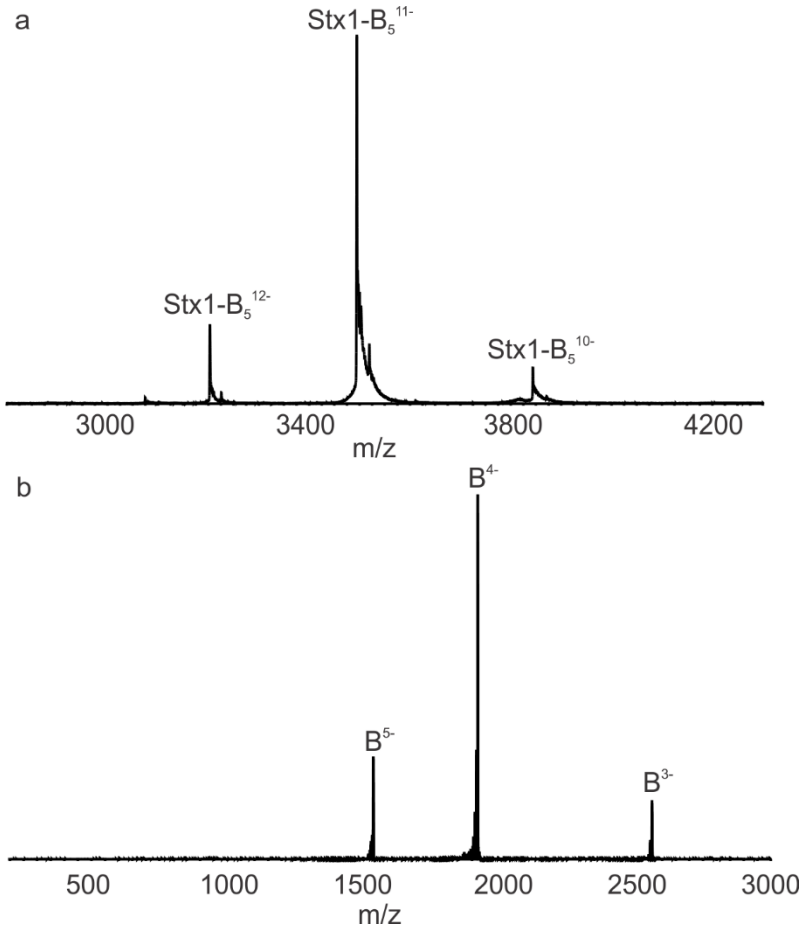

Figure 2.9 (a) ESI mass spectrum acquired in negative ion mode for an aqueous ammonium acetate solution (200 mM, pH 6.8) of Stx1-B5 (5 μM) and *Library 2* (56 μM). (b) CID mass spectrum acquired in the Trap region on possible (Stx1-B5 + L)11- ions using a collision energy of 50 V.

Based on the results described above, it is concluded that CTB_5 binds to GM1, GM2, GM3, GT1b, GD1a and GD1b, but not GD2. Interestingly, screening this same mixture of gangliosides against CTB_5 using the CaR-ESI-MS assay implemented with NDs revealed binding to GM1, GM2, GM3, GD1a and GD1b, but not to GT1b or GD2.[11] The relative affinities of six of these gangliosides for CTB_5 were previously investigated using SPR spectroscopy and found to be in

the order: GM1 > GM2 > GD1a > GM3 > GT1b > GD1b;[18] no binding to GD2 has been reported.[35-36] Consequently, it would seem that the CaR-ESI-MS results obtained using the PDs are in better agreement with the reported CTB_5 binding data than those measured using NDs. To further support this conclusion, affinity measurements were carried out using the direct ESI-MS assay on CTB_5 and the oligosaccharides of the seven gangliosides found in *Library 1* and *Library 2*. To the best of our knowledge, quantitative affinity data for CTB_5 binding to ganglioside oligosaccharides are only available for the GM1 pentasaccharide ($GM1_{os}$).[19] Because the affinities of the other ganglioside oligosaccharides for CTB_5 are low, the ESI-MS binding measurements were carried out using a titration format, wherein the concentration of CTB_5 was fixed at 6 μM and the concentration of oligosaccharide was varied from 0 to 100 μM. A reference protein (P_{ref}) was added in all experiments to correct nonspecific protein–carbohydrate interactions during the ESI process.[34] Representative ESI mass spectra acquired for an aqueous ammonium acetate (200 mM, pH 6.8) solution of CTB_5 (6 μM), P_{ref} (2 μM), and each of the oligosaccharides (60 μM) are shown in Figure 2.10; the corresponding titration plots are shown in Figure 2.11. From the ESI-MS data, apparent K_a values were calculated for each oligosaccharide (Table 2.2). Inspection of Table 2.2 reveals that $GM2_{os}$, $GM3_{os}$, $GD1a_{os}$, $GD1b_{os}$ and $GT1b_{os}$ exhibit low, but measurable, affinities, in the 500 M^{-1} range, while GD2 does not bind. Notably, these results are in agreement with the results obtained from the CaR-ESI-MS assay implemented with the PDs. At present it is not known why the GT1b interaction with CTB_5 was not detected when using NDs; however, it should be noted that the CaR-ESI-MS assay implemented with NDs has produced false negatives for other low affinity GBP–GL interactions.[11]

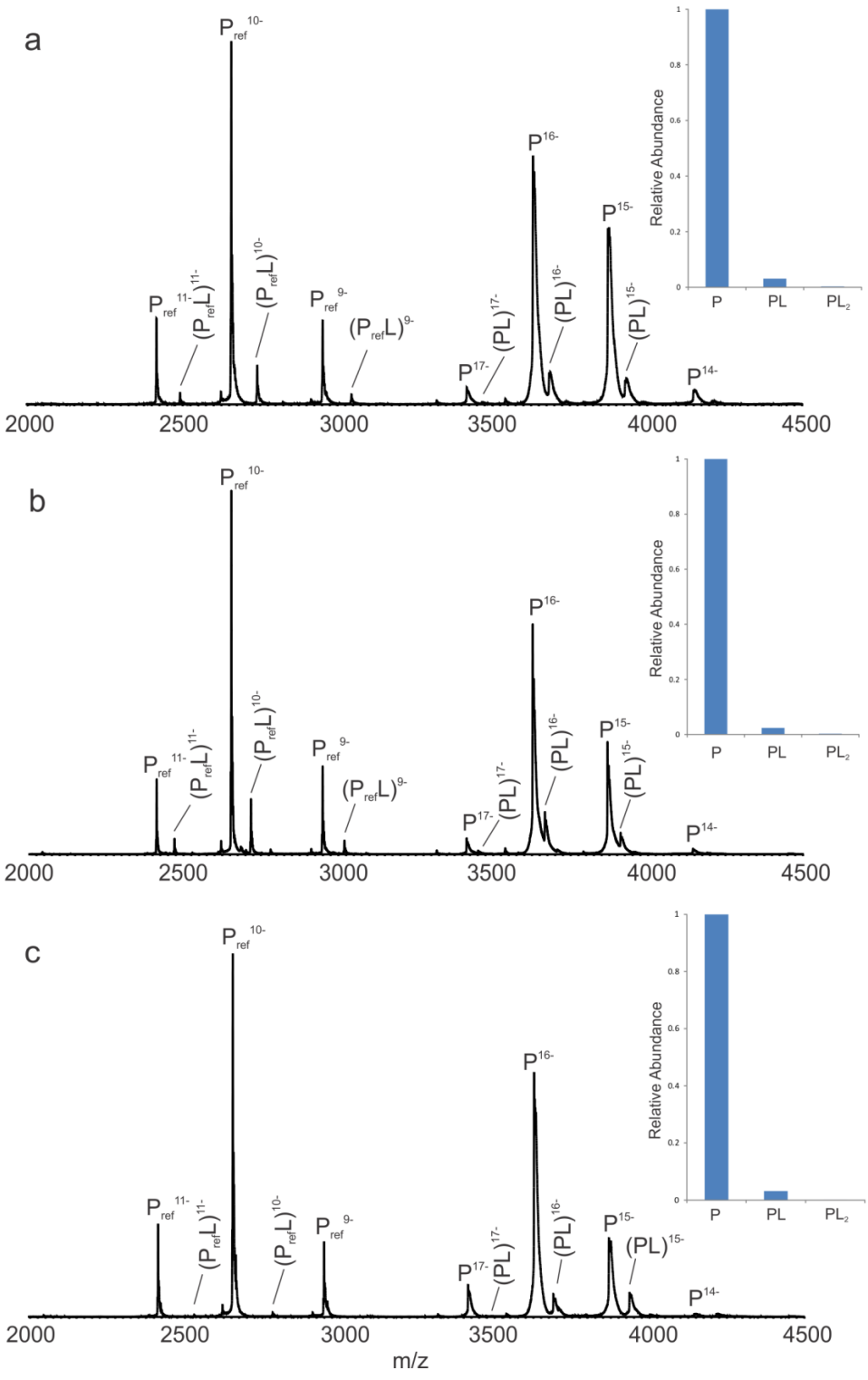
a
b
c
P_{ref}^{10-}
P_{ref}^{11-}
$(P_{ref}L)^{11-}$
$(P_{ref}L)^{10-}$
P_{ref}^{9-}
$(P_{ref}L)^{9-}$
P^{17-}
$(PL)^{17-}$
P^{16-}
$(PL)^{16-}$
P^{15-}
$(PL)^{15-}$
P^{14-}
Relative Abundance
P
PL
PL_2
2000
2500
3000
3500
4000
4500
m/z

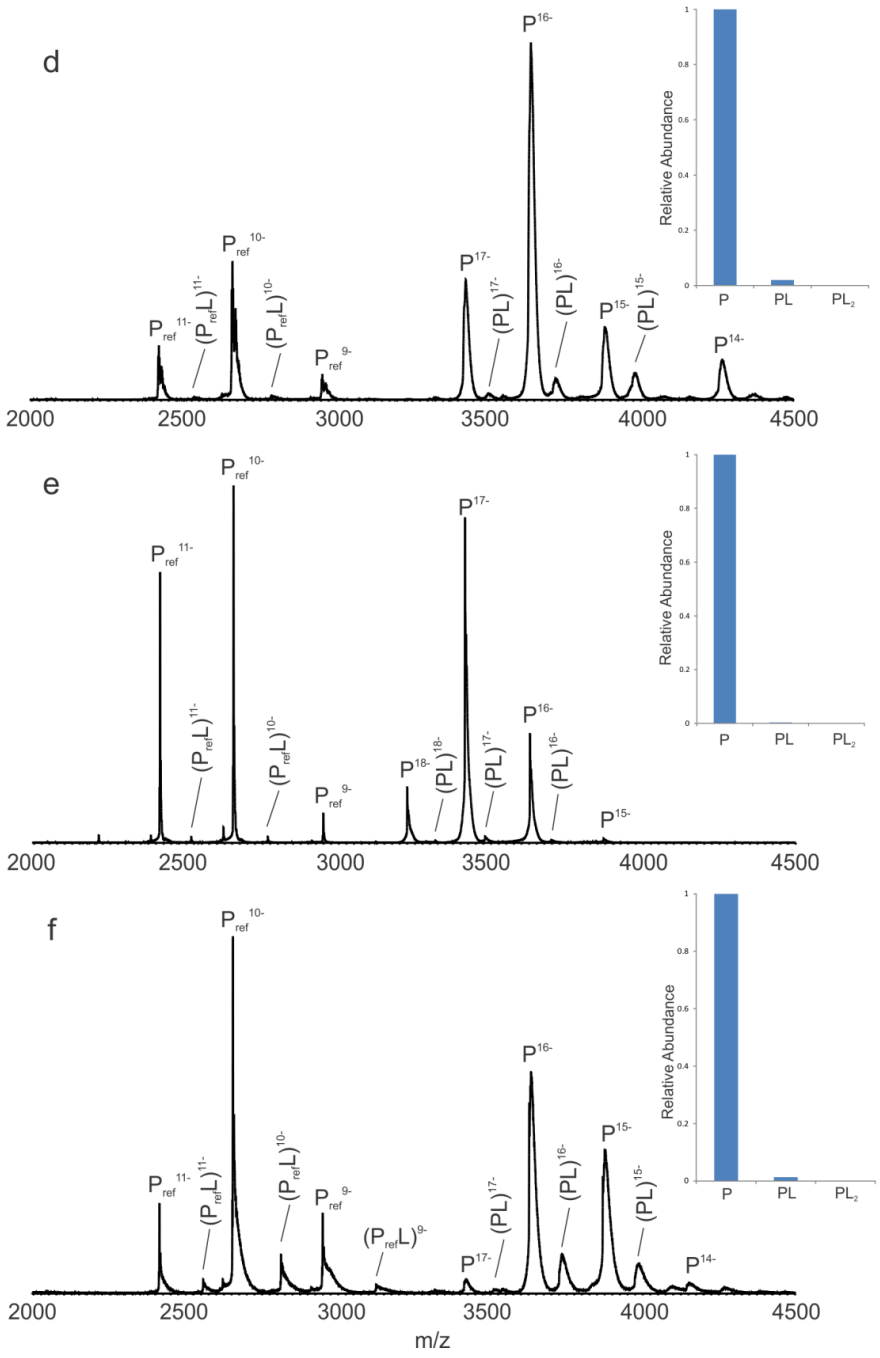

Figure 2.10 ESI mass spectra acquired in positive ion mode for aqueous ammonium acetate solutions (200 mM, pH 6.8) of CTB_5 (6 µM), P_{ref} (2 µM), and the ganglioside oligosaccharide (60 µM) (a) $GM2_{os}$, (b) $GM3_{os}$, (c) $GD1a_{os}$, (d) $GD1b_{os}$, (e) $GD2_{os}$ or (f) $GT1b_{os}$. Insets show the normalized distributions of free and ligand-bound forms of CTB_5.

a

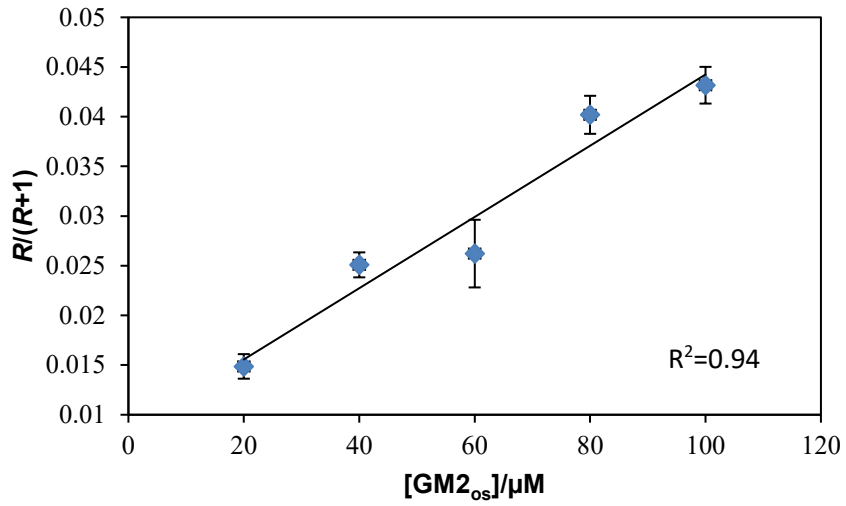
0.05
0.045
0.04
0.035
0.03
0.025
0.02
0.015
0.01
R/(R+1)
R²=0.94
0
20
40
60
80
100
120
[GM2os]/μM

b

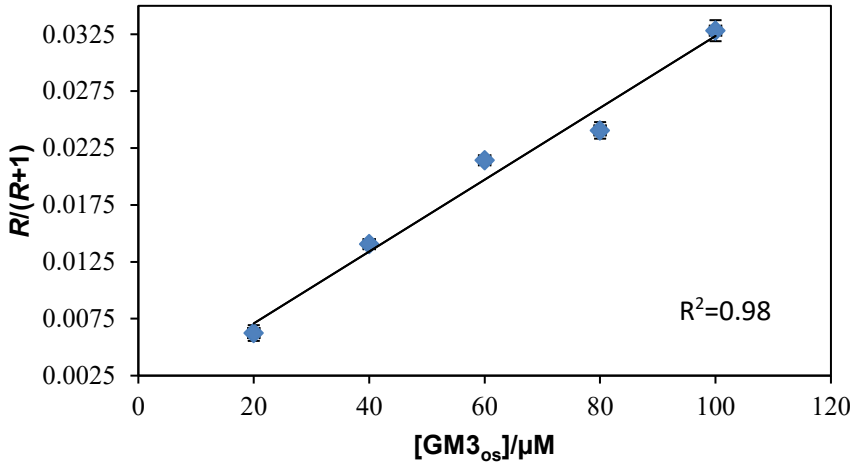
0.0325
0.0275
0.0225
0.0175
0.0125
0.0075
0.0025
R/(R+1)
R²=0.98
0
20
40
60
80
100
120
[GM3os]/μM

c

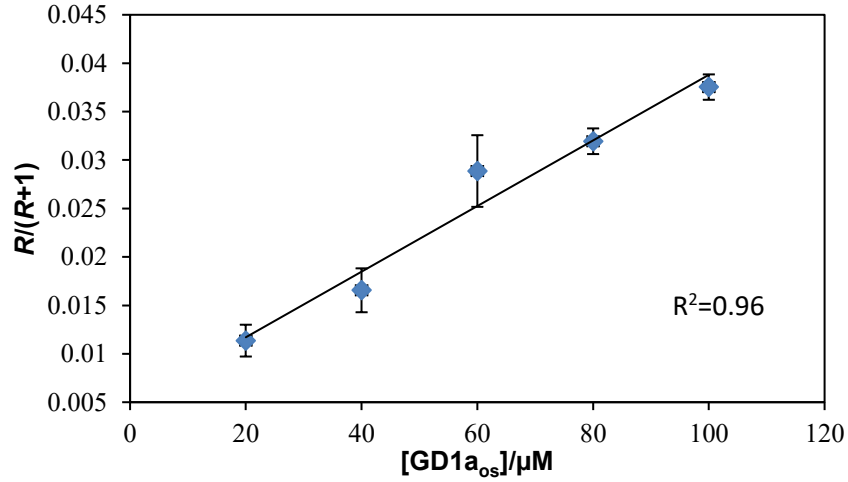
0.045
0.04
0.035
0.03
0.025
0.02
0.015
0.01
0.005
R/(R+1)
R²=0.96
0
20
40
60
80
100
120
[GD1aos]/μM

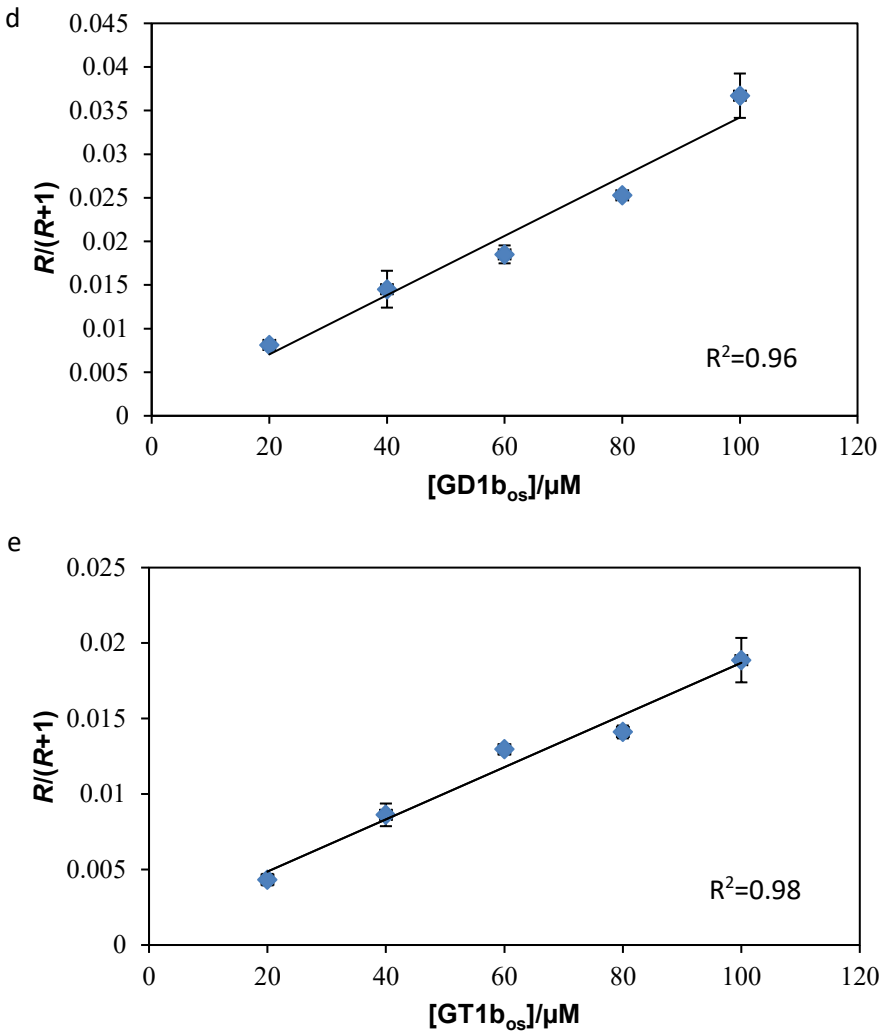

Figure 2.11 Plot of the fraction of ligand-bound CTB_5 (i.e., $R/(R+1)$) versus ligand concentration measured for the ganglioside oligosaccharides (a) $GM2_{os}$, (b) $GM3_{os}$, (c) $GD1a_{os}$, (d) $GD1b_{os}$ and (e) $GT1b_{os}$. The concentration of CTB_5 was fixed at 6 μM and the concentration of oligosaccharide varied from 0 to 100 μM. The error bars correspond to one standard derivation.

Table 2.2 Apparent association constants ($K_{a,app}$) for CTB_5 binding to the oligosaccharides (L) of seven gangliosides measured in an aqueous ammonium acetate solution (200 mM) at pH 6.8 and 25 °C using the direct ESI-MS assay.[a]

L	$K_{a,app}$ (M^{-1})
$GM1_{os}$	$(16.0 \pm 1.2) \times 10^{6}$ [b]
$GM2_{os}$	580 ± 130
$GM3_{os}$	370 ± 40
$GD1a_{os}$	480 ± 150
$GD1b_{os}$	350 ± 50
$GD2_{os}$	NB [c]
$GT1b_{os}$	240 ± 60

a. The reported errors are one standard deviation. b. Apparent association constants for the binding of a single $GM1_{os}$ to CTB_5. c. NB ≡ No binding detected.

2.3.2 Screening PDs and NDs containing known GLs against TcdA-A2

Taken together, the results obtained for CTB_5 and the PD-based ganglioside libraries show that the CaR-ESI-MS assay combined with PDs can be used to screen mixtures of GLs against GBPs and simultaneously detect both low and high affinity GBP–GL interactions. To demonstrate the general utility of the assay, it was also applied to screen *Library 2* against TcdA-A2. Shown in Figure 2.12a is a representative ESI mass spectrum acquired for an aqueous ammonium acetate (200 mM, pH 6.8) solution of TcdA-A2 (6 μM) and *Library 2* (120 μM, 17 μM each ganglioside). Signals corresponding to the -9 to -12 charge states of free and ganglioside-bound TcdA-A2 (i.e., $(TcdA\text{-}A2 + L)^{n-}$) ions were detected (along with a broad feature attributed to the PD ions, *vide*

supra). CID, carried out in Trap, of the $(TcdA\text{-}A2 + L)^{10-}$ ions resulted in the appearance of singly deprotonated GM3, GM2, GM1, GD1a and/or GD1b ions and doubly deprotonated GT1b, GD1a and/or GD1b ions, as well as TcdA-A2 ions (Figure 2.12c). These results suggest that TcdA-A2 exhibits broad specificity for gangliosides and binds GM1, GM2, GM3, GT1b, GD1a and/or GD1b, although, presumably, with low affinity. CaR-ESI-MS measurements performed using PDs containing only GD1a or GD1b revealed that only GD1a bind to TcdA-A2 under these solution conditions (Figure 2.13). Like CTB_5, TcdA-A2 was found not to bind GD2. These results are in qualitative agreement with affinity measurements, which reveal that the oligosaccharides of GM1, GM2, GM3, GT1b and GD1a, but not GD2, bind to TcdA-A2, with association constants in the 1000 M^{-1} range.[27]

To further compare the performance of PDs to NDs for GL screening, the CaR-ESI-MS assay was implemented using NDs to screen the same seven gangliosides against TcdA-A2. Shown in Figure 2.12d is a representative ESI mass spectrum acquired in negative ion mode for an aqueous ammonium acetate (200 mM, pH 6.8) solution of TcdA-A2 (6 μM) and 7G NDs (20 μM, which contain 2% of each of the seven gangliosides). A broad peak centered at *m/z* ~10000, which is attributed to intact ND ions, as well as signals corresponding to $TcdA\text{-}A2^{n-}$ and $(TcdA\text{-}A2 + L)^{n-}$ ions, at charge states -8 to -11, can be identified in the mass spectrum. Also present are ion signals corresponding to TcdA-A2 bound to DMPC, which was used to prepare the NDs. To ascertain the identity of the GL ligands, the quadrupole mass filter was set to pass all possible $(TcdA\text{-}A2 + L)^{10-}$ ions; these were then subjected to CID in the Trap. Analysis of the CID results revealed TcdA-A2 binding to GM1, GM2, GM3 (Figure 2.12f). However, the assay failed to detect binding to GT1b or GD1a. These results, taken together with the false negatives reported above and elsewhere,[13]

suggest that PDs are to be preferred over NDs for detection of low affinity GBP-GL interactions by ESI-MS.

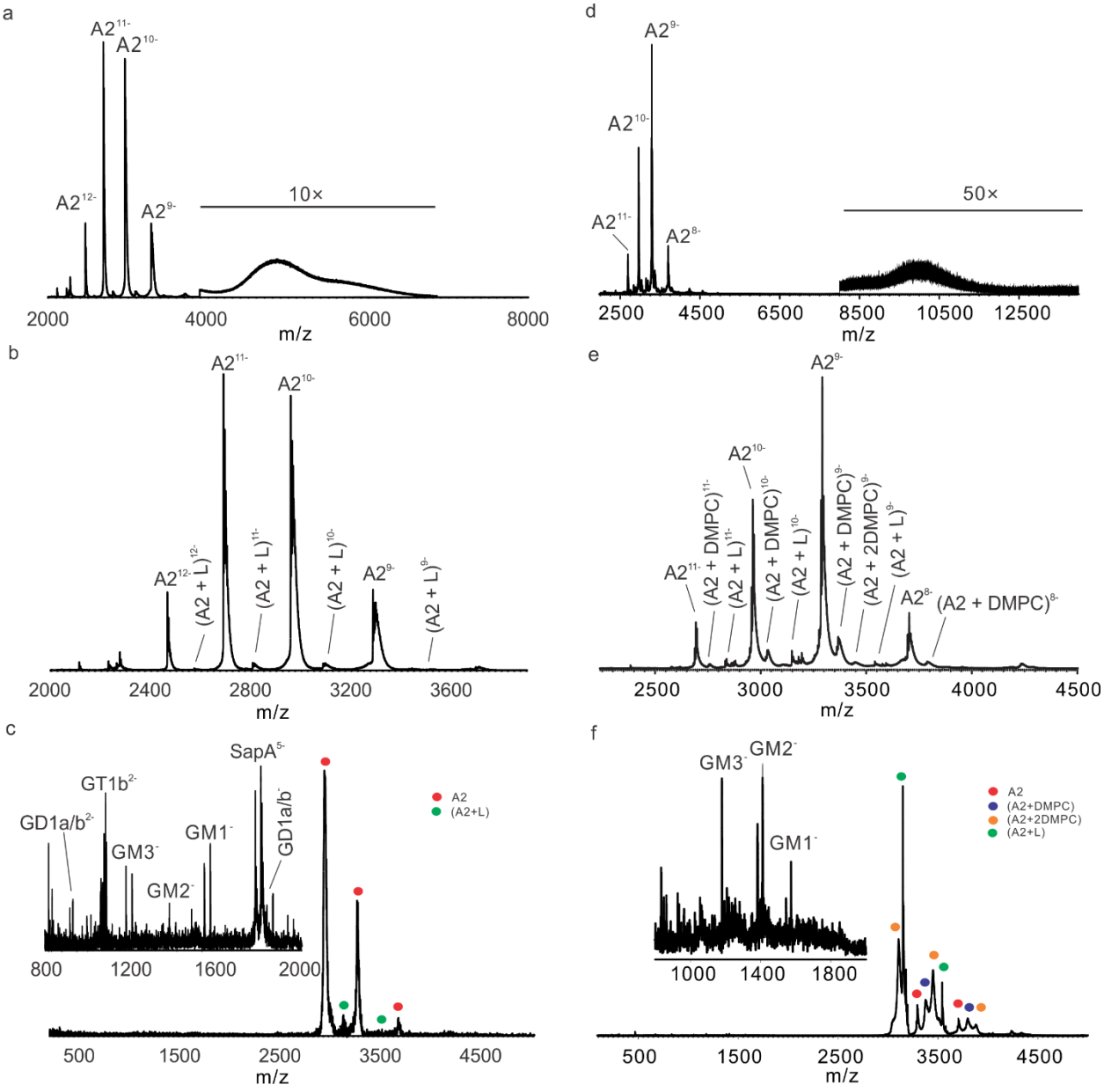

Figure 2.12 (a) and (b) ESI mass spectrum acquired in negative ion mode for a 200 mM aqueous ammonium acetate solution (pH 6.8, 22 °C) containing TcdA-A2 (6 µM) and *Library 2* (120 µM,

17 μM each ganglioside). (c) CID mass spectrum acquired in the Trap region for the (TcdA-A2 + L)$^{10-}$ ions using a collision energy of 50 V. (d) and (e) ESI mass spectrum acquired in negative ion mode for a 200 mM aqueous ammonium acetate solution (pH 6.8, 22 °C) containing TcdA-A2 (6 μM) and 7G ND (20 μM, 2% for each ganglioside). (f) CID mass spectrum acquired in the Trap region for the (TcdA-A2 + L)$^{10-}$ ions using a collision energy of 50 V.

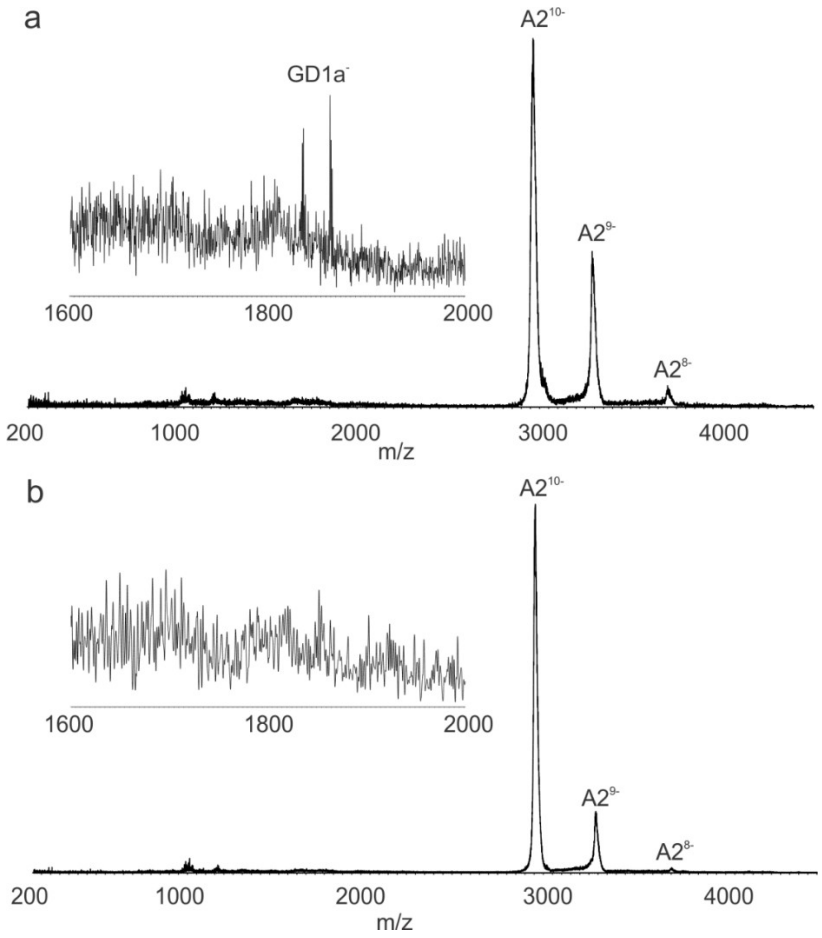

Figure 2.13 CID mass spectra acquired for ions with *m/z* between 2944 and 3344 produced by ESI performed in negative ion mode on aqueous ammonium acetate solutions (200 mM, pH 6.8) of TcdA-A2 (6 μM) and (a) GD1a PD (17 μM) or (b) GD1b PD (17 μM). CID was performed in the Trap region using a collision energy of 50 V.

2.3.3 Screening PDs prepared from glycolipid extracts against CTB_5

The results described above establish the reliability of the CaR-ESI-MS assay, implemented with PDs of known composition, to screen libraries of GLs against target proteins *in vitro*. To further illustrate the utility of the assay, measurements were also carried out using PDs prepared using GLs extracted from porcine brain (*Library 3*). This extract is known to consist primarily of ten different gangliosides and seventeen sulphatides.[37] ESI mass spectra acquired post-IMS for an aqueous ammonium acetate (200 mM, pH 6.8) solution of CTB_5 (5 μM) and *Library 3* (at an estimated (based on the mass concentration of extract and an estimated average MW for the lipids) concentration of 78 μM) revealed signal corresponding to free CTB_5^{n-} and $(CTB_5 + L)^{n-}$ ions (Figure 2.14a). CID performed simultaneously on $(CTB_5 + L)^{n-}$ ions at charge states -12 to -15 in the Transfer region resulted in the appearance of deprotonated GM1 ions (isoform *d*18:1-18:0, *m/z* 1545.09 and isoform *d*20:1-18:0, *m/z* 1573.12), as well as singly charged ions at *m/z* 1690.83 (L_{a1}) and *m/z* 1718.86 (L_{b1}), along with CTB monomer (Figure 2.14b). The identities of the L_{a1} and L_{b1} were established by subjecting these ions (produced directly from a methanol solution of the extracted lipids) to CID. Based on the fragment ions produced, $(B_0\text{-}H_2)^-$, Y_0^-, Y_1^-, Y_2-Neu5Ac$^-$ and Y_4^- (Figure 2.15) it was concluded that L_{a1} and L_{b1} are two isoforms (*d*18:1-18:0 and *d*20:1-18:0) of fucosyl-GM1 (α-L-Fuc-(1→2)-β-D-Gal-(1→3)-β-D-GalNAc-(1→4)-[α-D-Neu5Ac-(2→3)]-β-D-Gal-(1→4)-D-Glc-ceramide). It has been previously reported that CTB_5 binds with fucosyl-GM1 oligosaccharide with high affinity.[38]

Measurements were also carried out on PDs prepared from GLs extracted from the A549 carcinomic human alveolar basal epithelial cell line (*Library 4*). CaR-ESI-MS performed on an aqueous ammonium acetate (200 mM, pH 6.8) solution of CTB_5 (5 μM) and *Library 4* yielded signal corresponding to free CTB_5 and CTB_5 bound to one GL (Figure 2.14c). CID performed in

the Transfer region on $(CTB_5 + L)^{n-}$ ions, at charge states -12 to -15, resulted in the appearance of CTB monomer and singly deprotonated ions with *m/z* 1517.02 (L_{a2}), *m/z* 1545.07 (L_{b2}), *m/z* 1573.09 (L_{c2}) and *m/z* 1629.15 (L_{d2}). CID of the L_{a2}^-, L_{b2}^-, L_{c2}^- and L_{d2}^- ions, produced by ESI performed on a methanol solution of A549 cell line extract, produced $(B_0\text{-}H_2)^-$, Y_0^-, Y_1^-, and Y_2-Neu5Ac$^-$ fragment ions (Figure 2.16). Based on the CID results, the four ions were identified as isoforms of GM1 (*d*16:1-18:0 (or *d*18:1-16:0), *d*18:1-18:0, *d*20:1-18:0, *d*20:1-22:0 (or *d*18:1-24:0), Figure 2.14b). Notably, these results are consistent with those obtained previously using the CaR-ESI-MS assay implemented with NDs.[11]

2.4 Conclusions

The results of the present study demonstrate the utility of the CaR-ESI-MS assay, implemented with PDs, for screening libraries of GLs against water-soluble GBPs *in vitro* to identify specific interactions. Application of the assay to screen a small library of gangliosides against CTB_5 and TcdA-A2 demonstrated that both high and low affinity interactions can be detected simultaneously. Notably, comparison of the screening results with affinity data for the corresponding ganglioside oligosaccharides indicates that the assay produced no false positives or false negatives. Moreover, implementation of the assay using PDs prepared from GLs extracted from tissue or cell culture successfully identified high affinity ganglioside ligands present in both GL mixtures. Finally, a comparison of the present results with data obtained with the CaR-ESI-MS assay implemented using NDs revealed that the PDs exhibit similar or superior performance to NDs for GBP–GL binding measurement and that PDs are to be preferred over NDs for detection of low affinity GBP–GL interactions.

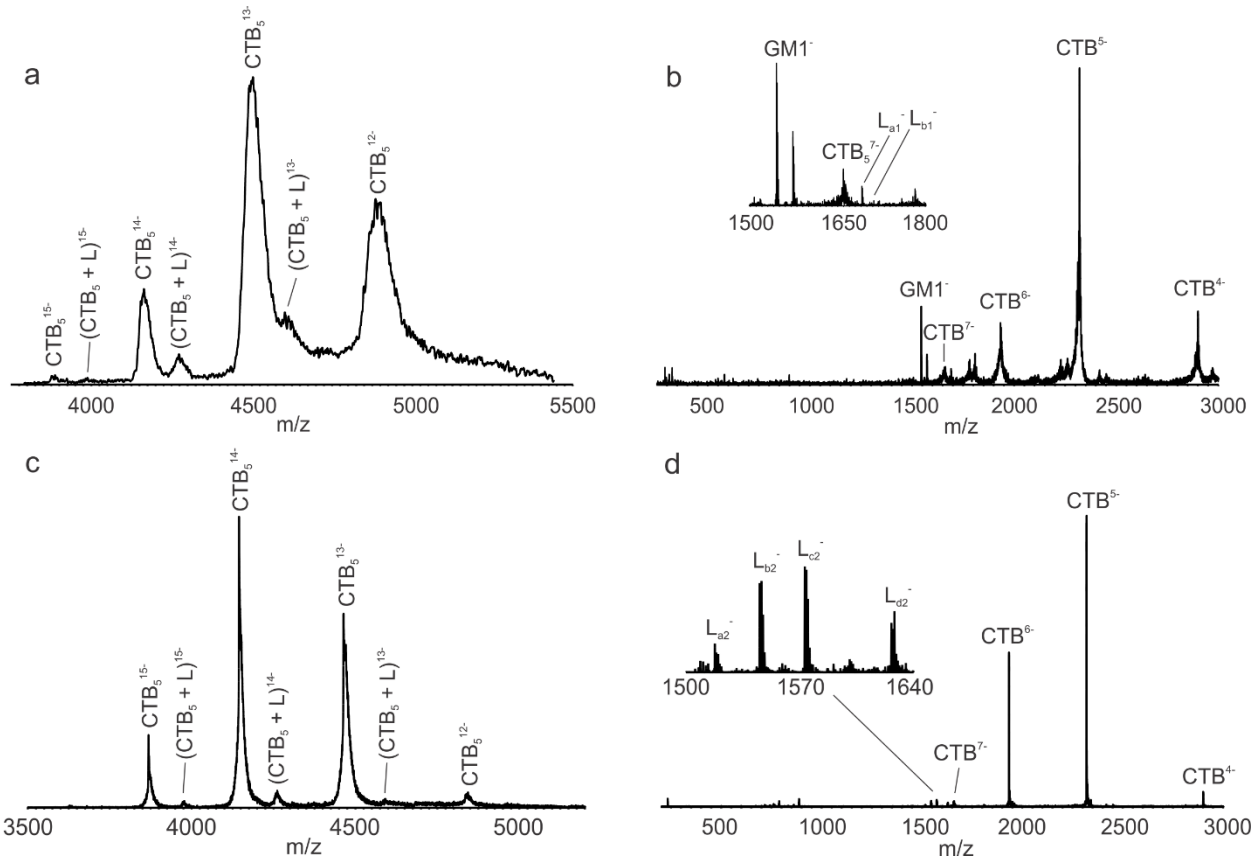

Figure 2.14 ESI mass spectra acquired in negative ion mode for a 200 mM aqueous ammonium acetate solution (pH 6.8, 22 °C) containing CTB_5 (5 μM) and (a) *Library 3* (78 μM) or (c) *Library 4*, after separation of the CTB_5 ions from the PD ions using IMS. (b) and (d) CID mass spectra acquired in the Transfer region (post IMS separation) for the CTB_5 ions, produced from the solution described in (a) and (c), respectively, performed in the Transfer region using a collision energy of 75 V.

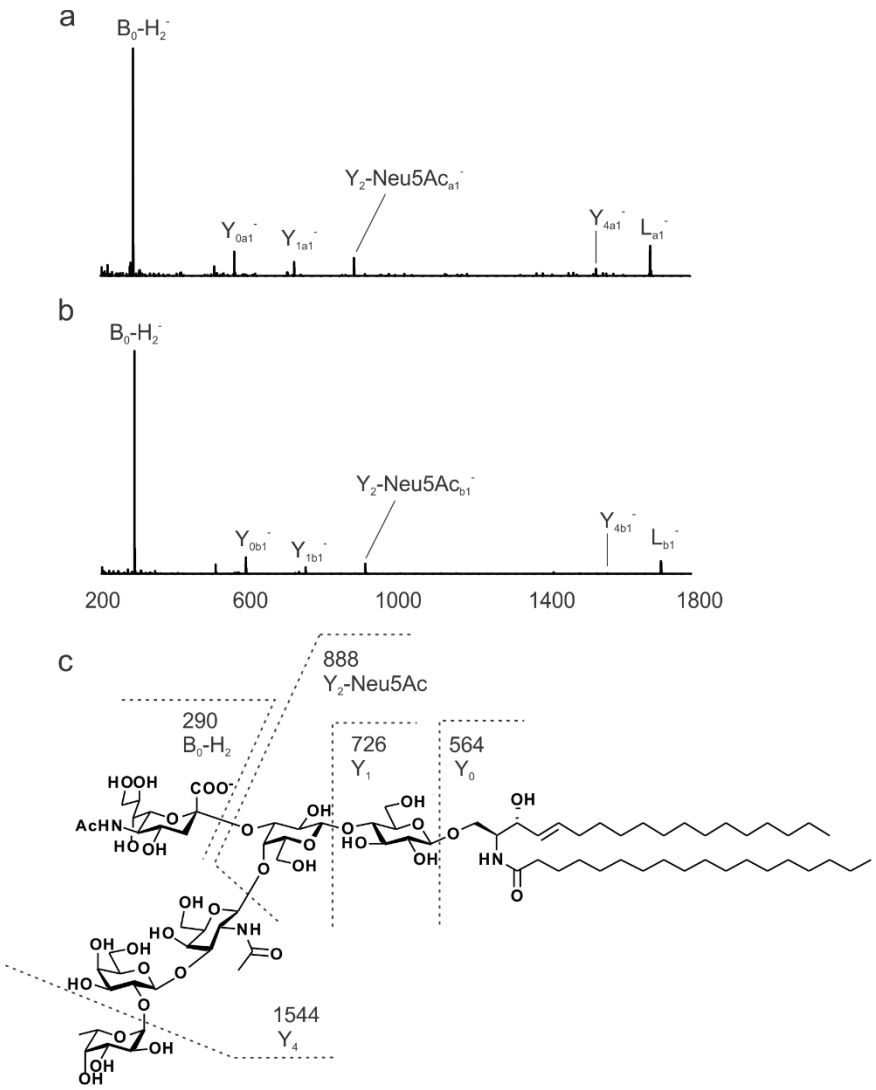

Figure 2.15 CID mass spectra acquired for (a) the L_{a1}^- ion (*m/z* 1690.8) or (b) the L_{b1}^- ion (*m/z* 1718.8), produced by ESI performed in negative ion mode on a methanol solution of *Library 3*. $B_0\text{-}H_2^-$ corresponds to deprotonated 5-N-acetyl-neuraminic acid (Neu5Ac); Y_{4a1}^- and Y_{4b1}^- result from loss of the fucosyl moiety from L_{a1}^- and L_{b1}^-, respectively; $Y_2\text{-Neu5Ac}_{a1}^-$ and $Y_2\text{-Neu5Ac}_{b1}^-$ result from loss of the Fuc, Gal, GalNAc and Neu5Ac residues from L_{a1}^- and L_{b1}^-, respectively; Y_{1a1}^- and Y_{1b1}^- result from the loss of Gal residue from $Y_2\text{-NeuAc}_{a1}^-$ and $Y_2\text{-NeuAc}_{b1}^-$, respectively; and Y_{0a1}^- and Y_{0b1}^- result from the loss of Glc residue from Y_{1a1}^- and Y_{1b1}^-, respectively. (c) Fragmentation scheme shown for L_{a1}^- (d 18:1-18:0).

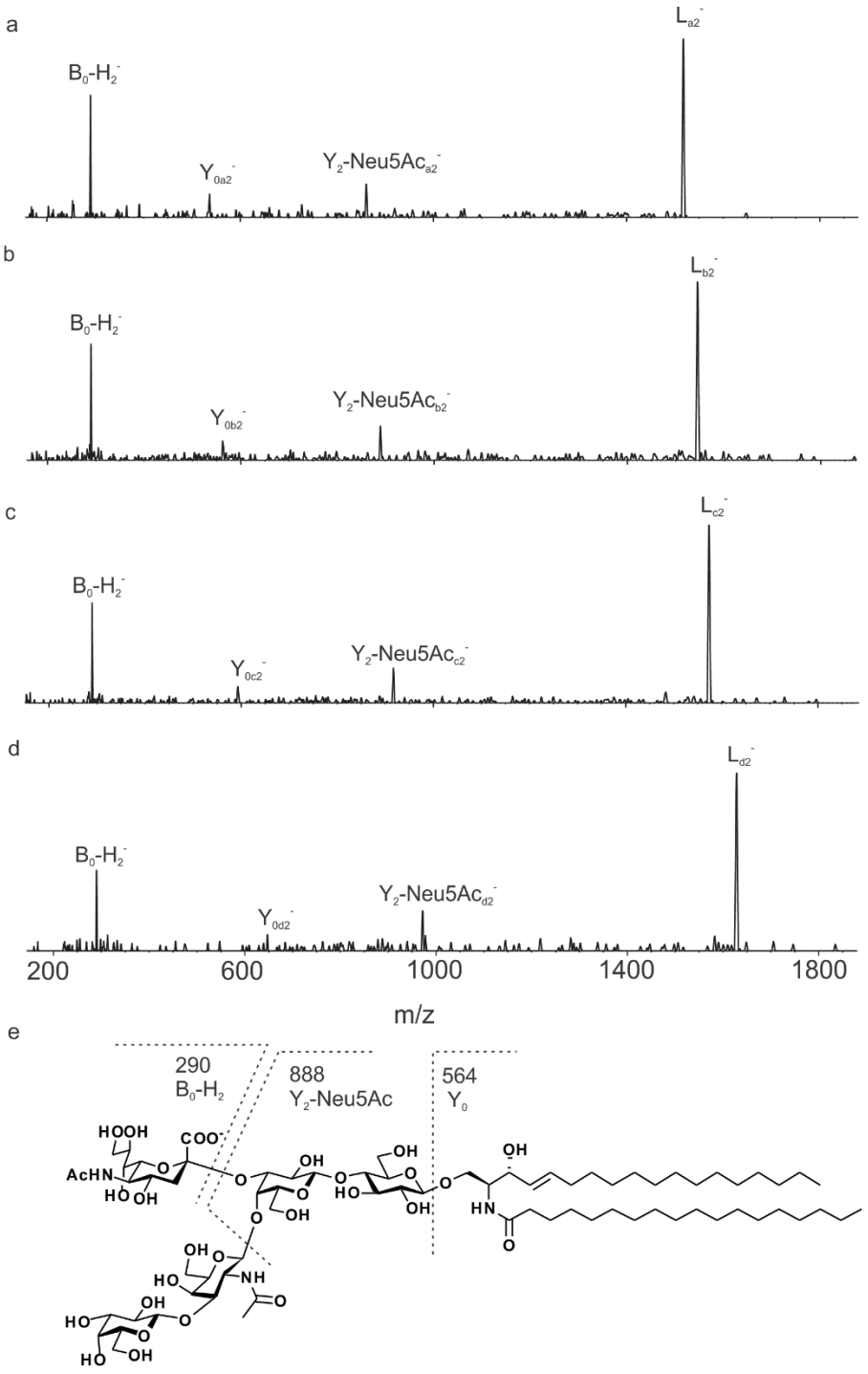

Figure 2.16 CID mass spectra acquired for the (a) the L_{a2}^- (at *m/z* 1517.0), (b) L_{b2}^- (at *m/z* 1545.1), (c) L_{c2}^- (at *m/z* 1573.1) and (d) L_{d2}^- (at *m/z* 1629.1) ion, produced by ESI performed in negative ion mode on a methanol solution of *Library 4*. B_0-H_2^- corresponds to deprotonated Neu5Ac; Y_2-

Neu5Ac$_{a2}^-$, Y$_2$-NeuA5c$_{b2}^-$, Y$_2$-Neu5Ac$_{c2}^-$ and Y$_2$-Neu5Ac$_{d2}^-$result from loss of the Gal, GalNAc and Neu5Ac residues from L$_{a2}^-$, L$_{b2}^-$, L$_{c2}^-$ and L$_{d2}^-$, respectively; Y$_{0a2}^-$, Y$_{0b2}^-$, Y$_{0c2}^-$ and Y$_{0d2}^-$ result from the loss of Gal and Glc residues from Y$_2$-NeuAc$_{a2}^-$ and Y$_2$-NeuAc$_{b2}^-$, Y$_2$-NeuAc$_{c2}^-$ and Y$_2$-NeuAc$_{d2}^-$, respectively. (e) Fragmentation scheme shown for L$_{a2}^-$ (d18:1-18:0).

2.5 References

1. Hakomori, S. *Curr. Opin. Hematol.* **2003**, *10*, 16–24.
2. Varki, A.; Cummings, R. D.; Esko, J. D.; Freeze, H. H.; Stanley, P.; Bertozzi, C. R.; Hart, G. W.; Etzler, M. E. *Essentials of Glycobiology*, 2nd ed.; Cold Spring Harbor Laboratory Press: Cold Spring Harbor, NY, 2009.
3. Malhotra, R. *Biochem Anal Biochem* **2012**, *1*, 108.
4. Schulze, H.; Sandhoff, K. *Biochim. Biophys. Acta* **2014**, *1841*, 799–810.
5. Lopez, H. H. H.; Schnaar, R. L. *Methods Enzymol*. **2006**, *417*, 205–220.
6. Lipid-Protein Interactions. In *Methods and Protocols*; Kleinschmidt, J. H., Ed.; Springer: New York, 2014; Vol. *974*.
7. Evans, S. V.; Roger MacKenzie. C. *J. Mol. Recognit*. **1999**, *12*, 155–68.
8. Lingwood, C. A.; Manis, A.; Mahfoud, R.; Khan, F.; Binnington, B.; Mylvaganam, M. *Chem. Phys. Lipids*. **2010**, *163*, 27–35.
9. Czogalla, A.; Grzybek, M.; Jones, W.; Coskun, U. *Biochim. Biophys. Acta* **2014**, *1841*, 1049–1859.
10. Zhang, Y.; Liu, L.; Daneshfar, R.; Kitova, E. N.; Li, C.; Jia, F.; Cairo, C.W.; Klassen, J. S. *Anal. Chem.* **2012**, *84*, 7618–7621.
11. Leney, A.; Fan, X.; Kitova, E.N.; Klassen, J. S. *Anal. Chem.* **2014**, *86*, 5271–5277.

12. Han, L.; Kitova, E. N.; Li, J.; Nikjah, S.; Lin, H.; Pluvinage, B.; Boraston, A. B.; Klassen, J. S. *Anal. Chem.* **2015,** *87,* 4888–4896.

13. Leney, A. C.; Darestani, R. R.; Li, J.; Nikjah, S.; Kitova, E. N.; Zou, C.; Cairo, C. W.; Xiong, Leney, A.; Fan, X.; Kitova, E. N.; Klassen, J. S. *Anal. Chem.* **2015**, *87*, 4402–4408.

14. Bayburt, T. H.; Grinkova, Y. V.; Sligar, S. G. *Nano Lett*. **2002**, *2*, 853−856.

15. Popovic, K.; Holyoake, J.; Pomès, R.; Privé, G.G. *Prot. Natl. Acad. Sci.* **2012**, *109*, 2908–2912.

16. Merritt, E. A.; Sarfaty, S.; Van Den Akker, F.; L'Hoir, C.; Martial, J. A.; Hol, W. G. J. *Protein Sci*. **1994**, *3*, 166−175.

17. Holmgren, J.; Lö nnroth, I.; Svennerholm, L. *Infect. Immun*. **1973**, *8*, 208–214.

18. Kuziemko, G. M.; Stroh, M.; Stevens, R. C. *Biochemistry* **1996**, *35*, 6375–6384.

19. Lin, H.; Kitova, E. N.; Klassen, J. S. *J. Am. Soc. Mass Spectrom*. **2014**, *25*, 104−110.

20. Just, I.; Gerhard, R. Large clostridial cytotoxins. In *Reviews of Physiology, Biochemistry and Pharmacology*, Springer Berlin Heidelberg: **2005**, *152*, 23–47.

21. Dallas, S. D.; Rolfe, R. D. *J. Med. Microbiol*. **1998**, *47*, 879–888.

22. Krivan, H. C.; Clark, G. F.; Smith, D. F.; Wilkins, T. D. *Infect. Immun*. **1986**, *53*, 573–581.

23. Smith, J. A.; Cooke, D. L.; Hyde, S.; Borriello, S. P.; Long, R. G. *J. Med. Microbiol*. **1997**, *46*, 953–958.

24. Tucker, K. D.; Wilkins, T. D. *Infect. Immun*. **1991**, *59*, 73–78.

25. Karlsson, K. A. *Curr. Opin. Struct. Biol*. **1995**, *5*, 622–635.

26. Teneberg, S.; Lonnroth, I.; Lopez, J. F. T.; Galili, U.; Halvarsson, M. O.; Angstrom, J.; Karlsson, K. A. *Glycobiology* **1996**, *6*, 599–609.

27. Fan, X.; Kitova, E. N.; Eugenio, L.; Ng, K. K. S; Klassen, J. S. *manuscript in preparation*

28. Greco, A.; Ho, J. G. S.; Lin, S. J.; Palcic, M. M.; Rupnik, M.; Ng, K. K. S. *Nat. Struct. Mol. Biol.* **2006**, *13*, 460–461.

29. Zdanov, A.; Li Y.; Bundle, D. R.; Deng, S. J.; Mackenzie, C. R.; Narang, S. A.; Young, N. M.; Cygler, M. *Proc. Natl. Acad. Sci. USA.* **1994**, *91*, 6423–6427.

30. Bayburt, T. H.; Grinkova, Y. V.; Sligar, S. G. *Nano Lett*. **2002**, *2*, 853−856.

31. Borch, J.; Torta, F.; Sligar, S. G.; Roepstorff, P. *Anal. Chem*. **2008**, *80*, 6245−6252.

32. Bayburt, T. H.; Sligar, S. G. *FEBS Lett*. **2010**, *584*, 1721−1727.

33. Kitova, E. N.; El-Hawiet, A.; Schnier, P. D.; Klassen, J. S. *J. Am. Soc. Mass Spectrom.* **2012**, *23*, 431–441.

34. Sun, J.; Kitova, E. N.; Wang, W.; Klassen, J. S. *Anal. Chem*. **2006**, *78*, 3010–3018.

35. Teneberg, S.; Hirst, T. R.; Angström, J.; Karlsson, K. A.; *Glycoconj. J*. **1994**, *11*, 533–540.

36. MacKenzie, C. R.; Hirama, T.; Lee, K. K.; Altman, E.; Young, N. M. *J. Biol. Chem*. **1997**, *272*, 5533–5538.

37. Ikeda, K.; Shimizu, T.; Taguchi, R. *J. Lipid Res*. **2008**, *49*, 2678−2689.

38. Masserini, M.; Freire, E.; Palestini, P.; Calappi, E.; Tettamanti, G. *Biochemistry*. **1992**, *31*, 2422–2426.

Chapter 3

Characterizing the Size and Composition of Saposin A Lipoprotein Picodiscs[†]

3.1 Introduction

Glycan-binding protein (GBPs) interactions with glycolipids (GLs) present in the plasma membrane represent an important class of recognition events that are implicated in a wide variety of cellular processes, including cell–cell adhesion, signalling, immune response and pathogen infection.[1–4] Although the biological importance of GBP−GL binding is well established, the identification of the functional GL receptors for many proteins, including bacterial and viral lectins, and the characterization of these interactions is challenging. The detection of GBP−GL interactions is commonly performed using techniques such as enzyme-linked immunosorbent assay (ELISA), surface plasmon resonance (SPR) spectroscopy, thin-layer chromatography (TLC) with immuno-overlay or microarrays of naturally-occurring or synthetic GLs.[5,6] A potential limitation of these surface-based approaches is that GBP−GL binding may be affected by the nature of the surface coupling (immobilization), GL density, the loss of mobility and the orientation of the carbohydrate moiety in the immobilized GLs.[7]

An alternative strategy to probe GBP−GL interactions is to present the GLs in a lipid environment. A number of different model membranes have been used for such purposes, including supported lipid bilayers, liposomes, micelles and nanodiscs (NDs).[8–11] Recently, the use of saposin A (SapA)-containing discs to solubilize GLs and present them for protein binding

[†] A version of this chapter has been published: Li, J.; Richards, M. R.; Bagal, D.; Campuzao, D. G.; Kitova, E. N.; Xiong, Z. J.; Privé, G. G.; Klassen, J. S. *Anal Chem*. **2016**, *88,* 9524–9531.

studies was reported.[12,13] These binding studies were carried out using the catch-and-release electrospray ionization-mass spectrometry (CaR-ESI-MS) assay.[12,13] SapA, a sphingolipid activator protein involved in the transport and degradation of galactosylceramide by lysosomal hydrolases,[14–15] is a small (molecular weight (MW) ~9 kDa) alpha helical protein that, upon incubation with detergent or lipid, self-assembles into disc-like structures.[15] These SapA discs, which are also referred to as picodiscs (PDs), share some structural similarities with NDs (which are ~150 kDa water-soluble discoidal (diameter ~10 nm) phospholipid bilayers surrounded by two copies of an amphipathic membrane scaffold protein (MSP)),[10] but are reported to be smaller in physical size and MW.[15] According to a reported crystal structure (PDB ID: 4ddj), SapA discs of *N,N*-dimethyldodecylamine *N*-oxide (LDAO) are composed of two SapA and forty detergent molecules (twenty-four and sixteen LDAO per leaflet), with a MW ~27 kDa.[15] In the presence of liposomes of the phospholipid 1-palmitoyl-2-oleoyl-*sn*-glycero-3-phosphocholine (POPC, Figure 3.1) at pH 4.8, which is the expected pH within lysosomes, discs with hydrodynamic radii of ~3.2 nm, MWs of 35–45 kDa (determined by size exclusion chromatography (SEC)) and a 5:1 ratio of lipid/SapA have been detected.[15]

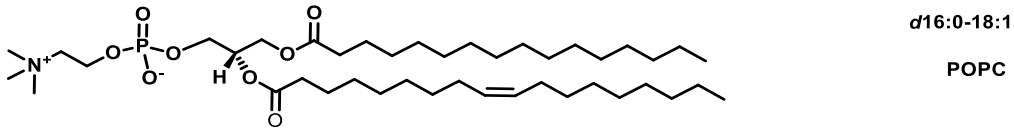

Figure 3.1 Structure of 1-palmitoyl-2-oleoyl-sn-glycero-3-phosphocholine (POPC).

PDs have been shown to be attractive alternatives to NDs for the presentation of GLs for GBP binding studies *in vitro*, particularly for low affinity interactions.[12,13] For example, the weak

interaction ((0.27 ± 0.08) × 10^3 M^{-1})[16] between the B subunit homopentamer of shiga toxin type 1 and a known cellular receptor, the globotriaosylceramide Gb3, was successfully detected using ESI-MS and Gb3-containing PDs, but not with NDs.[12] Given the significant role that PDs are likely to play in the discovery and characterization of GBP−GL interactions, there is a clear need to accurately establish the size and composition of lipid-PDs in aqueous solutions.[12,13] Here, we describe the results of a detailed investigation into the composition, heterogeneity and structure of POPC-containing PDs in aqueous ammonium acetate solutions at pH 4.8 and 6.8 using high resolution ESI-MS, multi-angle laser light scattering (MALLS) and molecular dynamics (MD) simulations. Collision cross sections (Ω) were also determined from ion mobility separation (IMS) measurements to assess the structures of PD ions in the gas phase.

3.2 Experimental Section

3.2.1 Proteins, lipids and detergent

Cytochrome c from equine heart (Cyt c, MW 12 384 Da), transthyretin from human plasma (TTR, MW 56 kDa), and avidin from chicken egg white (Avidin, MW 64 kDa), which were used to construct the Ω calibration curve for IMS measurements, were purchased from Sigma-Aldrich Canada (Oakville, Canada). Stock solutions of Cyt c, TTR and Avidin in 200 mM aqueous ammonium acetate were prepared by dissolving a known mass of protein. All stock solutions were stored at –20 °C until needed. Saposin A (SapA, two major isoforms with MWs 8 918 Da and MW 9 049 Da), was expressed and purified as previously described.[15] The phospholipid POPC (MW 760.08 Da) was purchased from Avanti Polar Lipids Inc. (Alabaster, AL).

3.2.2 Picodisc preparation

POPC-containing PDs were prepared as previously described.[15] and the detail of PDs preparation was provided in Chapter 2, section 2.2.1. POPC-PDs were buffer exchanged into 200 Mm ammonium acetate (pH 4.8 or 6.8) concentrated to approximately 150 μM and stored at room temperature until used.

3.2.3 Mass spectrometry

MS measurements were performed on an Exactive Plus (with extended mass range) Orbitrap Fourier-transform (FT) mass spectrometer (Thermo Fisher Scientific, Bremen, Germany)[17,18] and a Synapt G2-S quadrupole-ion mobility separation-time-of-flight (Q-IMS-TOF) mass spectrometer (Waters, Manchester, UK). Both instruments were equipped with nanoflow ESI (nanoESI) sources. A brief overview of the instrumental conditions used is given below.

3.2.3.1 Exactive Plus Orbitrap

Instrument calibration was performed using a 25 μg μL^{-1} 50% (v/v) aqueous isopropanol solution of cesium iodide over the mass-to-charge ratio (*m/z*) range 1000 to 20,000. NanoESI, at a flow rate of about 1–2 μL h^{-1} using 4 μm id GlassTip Emitters (New Objective, Woburn, MA), was used to spray aqueous ammonium acetate (200 mM) solutions of PDs (5 μM). The capillary voltage was set to 1.8 kV; ions formed by nanoESI were sampled through a stainless steel capillary (ion transfer tube) maintained at 250 ºC into an S-Lens stacked ring ion guide with an applied RF-amplitude (peak-to-peak) of 200 V. Ions then travel through a transport multipole and enter the HCD cell where they were stored at a high pressure before they were returned to the C-trap. This feature allows efficient trapping and desolvation of large protein ions and dramatically improves

sensitivity. Nitrogen gas was used in the C-trap, as well as the HCD cell. Utilising a trapping gas pressure setting of 7.0 (software determined) the C-trap pressure is approximately $2x10^{-4}$ mbar and the pressure in the OrbiTrap analyser was $7.5x10^{-10}$ mbar. The voltage offsets on the transport multipoles were manually tuned to increase the transmission of large complexes (C-trap entrance lens; -2 V or 0 V, bent flatapole DC, 4 V; inter-flatapole DC, 4 V; injection flatapole DC, 4 V. Mass spectra were acquired under varying in-source CID voltage conditions ranging from 50 V to 200 V and varying HCD voltages from 20 V to 150 V to achieve efficient sample desolvation. Transients detected were processed using enhanced Fourier transformation (eFT™) for converting the time domain into frequency domain and then into *m/z* values.[19] The instrument was set at a nominal resolving power of 8,750 at *m/z* 200 and mass spectra were acquired for 1 min by averaging 10 microscans per one analytical scan. Data was analyzed using xcaliber™2.2. No additional data processing (smoothing) was performed.

Spectral deconvolution was performed with the UniDec[20] deconvolution algorithm using the following parameters: *m/z* range – 4000 to 6000, however depending on the samples and observed *m/z* range, this range can vary; Subtract Curved - 10.0; Gaussian Smoothing - 1.0; Linear *m/z* (constant delta *m/z*); Bin every 1.0; Charge Range - 1 to 20; Mass range 10,000 to 100,000; Sample Mass Every 1.0 Da; Peak FWHM (Th) 4.0; Peak Shape Function - Gaussian; Charge Smooth Window - 0.0; Mass Difference - 760.0; Mass Smooth Window - 1.0; Maximum number of iterations - 1000. Spectral files were loaded as text files containing intensity and *m/z* values.

3.2.3.2 Synapt G2-S

The ESI-MS carried out in Synapt G2-S were described in Chapter 2, section 2.2.6. To dissociate PDs, the *m/z* region corresponding to PD ions were selected by quadrupole mass filter and

subjected to collision-induced dissociation (CID) in the Trap region using a series of collision energies from 5 V to 100 V. For IMS, a wave height of 40 V and a wave velocity of 1000 m s^{-1} were applied along with a helium and nitrogen (IMS gas) gas flow of 50 and 60 mL min^{-1}, respectively. All data was processed using MassLynx software (*v*4.1) in combination with Driftscope *v*2.5.

3.2.4 Collision cross section analysis

The Ω of the gaseous PD ions were determined from the IMS measurements using a protocol described elsewhere.[21,22] Briefly, the relationship between drift times (t_D) and Ω was established by analyzing calibrant proteins (Cyt c, TTR and Avidin) with known Ω (in N_2) under the same experimental conditions.

The measured t_D values were corrected using eq 3.1:[22]

$$t'_D = t_D - c\sqrt{m/z}/1000 - 10l_{transfer}/WV_{transfer} \quad (3.1)$$

where t_D' is the corrected drift time (in ms), t_D is the measured drift time (in ms), *m/z* is the mass-to-charge ratio of the observed ion and the constant *c* (enhanced duty cycle delay coefficient),[22] $l_{transfer}$ is the length of the transfer T-wave region (in cm), and $WV_{transfer}$ is the transfer wave velocity (in m s^{-1}). The literature Ω (in N_2) values for the calibrant protein ions were corrected for charge and reduced mass (μ) by eq 3.2:[22]

$$\Omega' = \Omega\sqrt{\mu}/z \quad (3.2)$$

where Ω′ is the corrected collision cross section in N_2 (nm^2), Ω is the literature collision cross section in N_2 (nm^2), μ and *z* is the reduced mass and charge of the observed ion. The final corrected drift times (t_D'') were calculated from eq 3.3:

$$t''_D = (t'_D)^X(z/\sqrt{\mu}) \quad (3.3)$$

where t_D'' is the final corrected drift times (in ms) and X is the exponential factor, which corresponds to the slope of the plot of $\ln(\Omega')$ versus $\ln(t_D')$. The Ω values of the protonated PD ions were determined from the calibration curve of literature Ω values versus t_D''.

3.2.5 Size-exclusion chromatography/multi-angle laser light scattering (SEC-MALLS)

PDs in 200 mM aqueous ammonium acetate (pH 4.8 or pH 6.8) were injected into a Superose^{TM} 12 HR 10/30 column, which was equilibrated using the same aqueous ammonium acetate solution. PD elution was detected via refractive index using an in-line Optilab rEX^{TM} differential refractive index detector and DAWN EOS^{TM} MALLS, which includes both MALLS and Quasi-Elastic Light Scattering (QELS) detectors (Wyatt Technologies, Santa Barbara, CA). The combined MALLS-QELS can measure simultaneously radius of gyration (R_g, from 10–500 nm), hydrodynamic radius (R_h, from 1–500 nm) and MW. However, for PDs, the R_g was below the angular variation detection limit of 10 nm, so only R_h and MW were obtained. Data were processed using ASTRA version 5.3.4.14 software. Average values of the MW and R_h for PDs were calculated form data collected over the elution peak and MW predictions were normalized to a BSA standard.

3.2.6 Molecular dynamics (MD) simulations

MD simulations were performed on four different POPC-containing PDs – (SapA dimer + 10POPC), (SapA dimer + 26POPC), (SapA trimer + 33POPC) and (SapA tetramer + 42POPC). Initial conformations for MD (Figure 3.2) were generated in Chimera[23] using SapA coordinates from Popovic *et al*. (PDB ID: 4ddj),[15] and various POPC bilayers generated using the membrane plugin for VMD.[24,25] The SapA proteins were manually placed around each bilayer to allow for minimal close contacts and minimal extra vacuum space (initial coordinates are included as

Supporting Information). The MD simulations were performed in aqueous solution and the gas phase for all four systems using the AMBER12[26] software package. Simulations in aqueous solution were run in boxes of TIP3P[27] water using the PMEMD module in AMBER12 for 50 ns under NPT conditions at 1 atm and 300 K. The solution cut-off for nonbonding interactions was 8 Å. The gas-phase MD simulations were run using the SANDER module in AMBER12 for 20 ns at 300 K, with cut-off for nonbonding interactions set to 999 Å. For the gas-phase complexes, each SapA protein was at a +4 charge state. The positive charges were placed evenly over the surface of the protein with R68, K19, K33, and K40 protonated. The remaining lysine residues (K8, K48, and K63) were neutral, as were all aspartic acid and glutamic acid residues. The equilibrated structures from solution simulations were used as the initial structures for the gas-phase simulations.

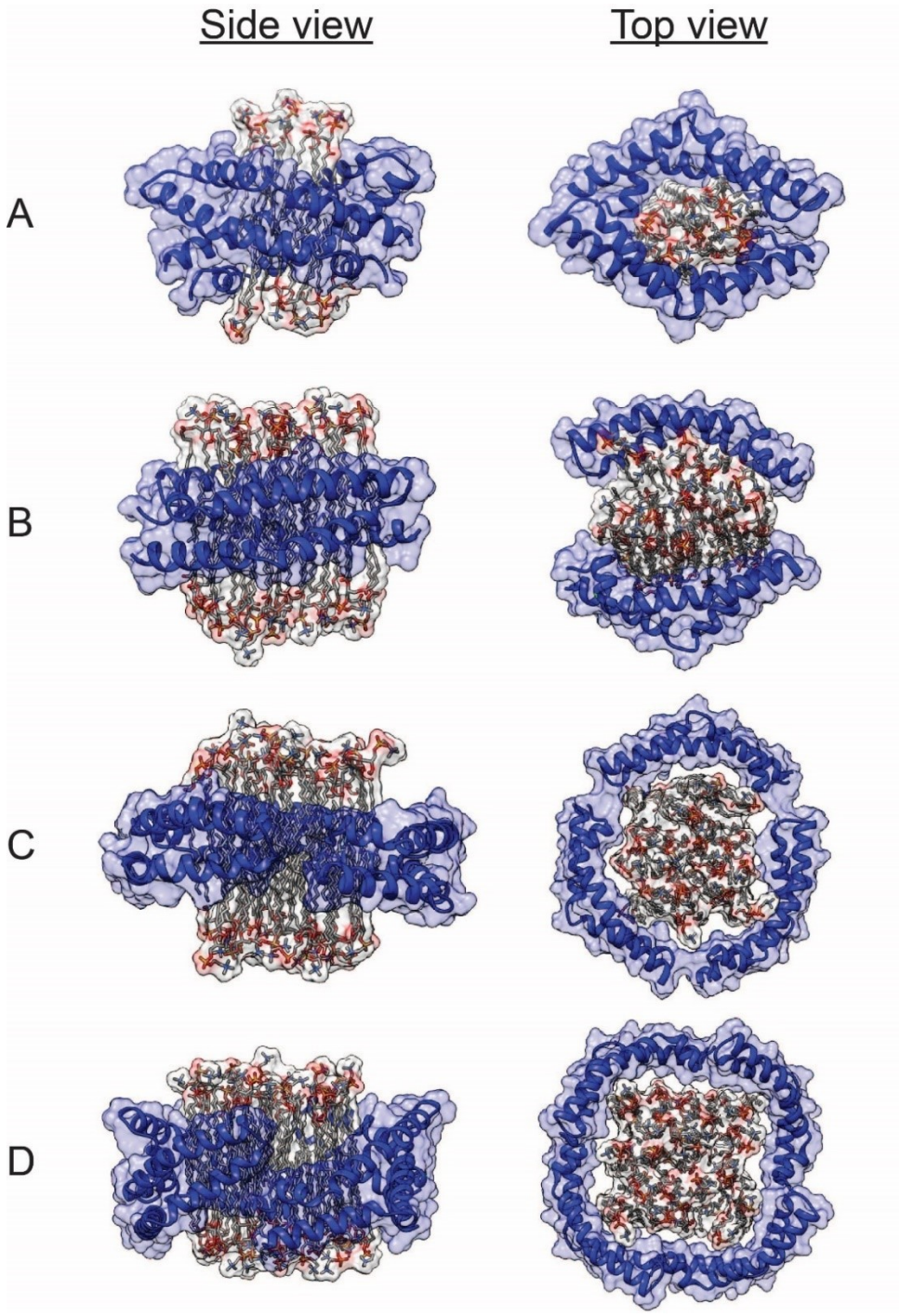

Figure 3.2 Initial configurations of POPC-PDs used for the solution MD simulations – (a) (SapA dimer + 10POPC) complex, (b) (SapA dimer + 26POPC) complex, (c) (SapA trimer + 33POPC)

complex, and (d) (SapA tetramer + 42POPC) complex. SapA proteins are shown as blue ribbons and POPC molecules are shown as sticks.

In all simulations, the ff03[28] force field was used for SapA and the lipid11[29] force field used for POPC. The time step for all simulations was 2 fs, and the temperature was maintained with the Berendsen[30] (*ntt = 1*) thermostat with velocities rescaled every 1 ps. All bonds containing hydrogen were fixed using the SHAKE[31] algorithm, except during the minimization step. To prepare the system for dynamics, the entire system was minimized, via 5000 steps of steepest descent followed by 5000 steps of conjugate gradient minimization. An equilibration period was carried out that included heating the system from 5 K to 300 K over 50 ps, then cooling to 5 K over 50 ps. This simulated annealing step was followed by a second, slower heating from 5 K to 300 K over 100 ps. The production simulation began after an additional 100 ps of equilibration at 300 K. Once the simulations were complete, R_g was calculated with AmberTools12,[32] and for the gas-phase simulations, theoretical N_2-based **Ω** values were calculated using the Diffuse Hard Sphere Scattering method implemented in the IMoS suite of software[33] using the following parameters: radgas 1.5; Mgas 28; Temperature 310; Nrotations EHSS 3; NgastotalEHSS 1000000; Accommodation 1.0; Diffuse 1; EHSS/DHSS 1. Coordinates were read in as PDB files.

3.3 Results and Discussion

3.3.1 Composition and size of POPC-PDs

To probe the composition and polydispersity of POPC-PDs in acidic and neutral solutions, ESI-MS measurements were carried out using both ToF-MS (Synapt G2-S) and FT-MS (Exactive Plus Orbitrap). Shown in Figure 3.3 are representative ESI mass spectra acquired in positive mode for aqueous solutions of POPC-PD in 200 mM aqueous ammonium acetate, at pH 4.8 or pH 6.8,

measured using the Synapt mass spectrometer. The mass spectrum shown in Figure 3.3a was acquired for a freshly prepared acidic (pH 4.8) solution containing 10 μM PD (the PD stock solution was diluted from 150 μM to a final concentration of 10 μM in the 200 mM aqueous ammonium acetate). Signal corresponding to protonated POPC and SapA monomer ions was detected, as well as a broad feature centred at *m/z* ~3500, which could not be fully resolved. All ions with *m/z* >2500 were selected using the quadrupole mass filter and simultaneously subjected to CID in the Trap region using a moderate (50 V) collision energy. Collisional activation, which caused the POPC-PDs signal to be distributed over a broader range of *m/z* values (with a shift towards higher *m/z*), resulted in peaks that were partially resolved. The peak identities were made based on the theoretical and measured *m/z* values (Table 3.1). It should be noted that the SapA used to produce the PDs consists of two major isoforms (Figure 3.4). Consequently, the SapA dimer exists at three distinct MWs, corresponding to two homodimers and one heterodimer, while the SapA trimer exists at four MWs, corresponding to two homotrimers and two heterotrimers. Analysis of the mass spectrum revealed the presence of protonated ions of POPC, SapA monomer and the (SapA monomer + *i*POPC) complexes, where *i* = 1 to 3, at charge states +3 to +6, SapA dimer and the (SapA dimer + *i*POPC) complexes, where *i* = 1 to 4, at charge state +4 to +5, and the (SapA dimer + *i*POPC) complexes, where *i* = 23 to 28, at charge state +6 to +7, and the SapA trimer and (SapA trimer + *i*POPC) complexes, where *i* = 1 to 2, at charge states +6 (Figure 3.3b). The presence of POPC-bound SapA dimer is consistent with the crystal structure reported for LDAO-PDs prepared at acidic pH.[15] However, the presence of free and POPC-bound SpaA trimer ions suggests that, at least, some fraction of the POPC-PDs at pH 4.8 exist as SapA trimers or larger multimers. Measurements carried out on the same solution as described above, but following incubation for 3 h at room temperature, revealed no significant differences (Figures 3.3c & d, Table

3.2). This finding suggests that the POPC-PDs species are kinetically stable (over the timescale of the measurements) at acidic pH.

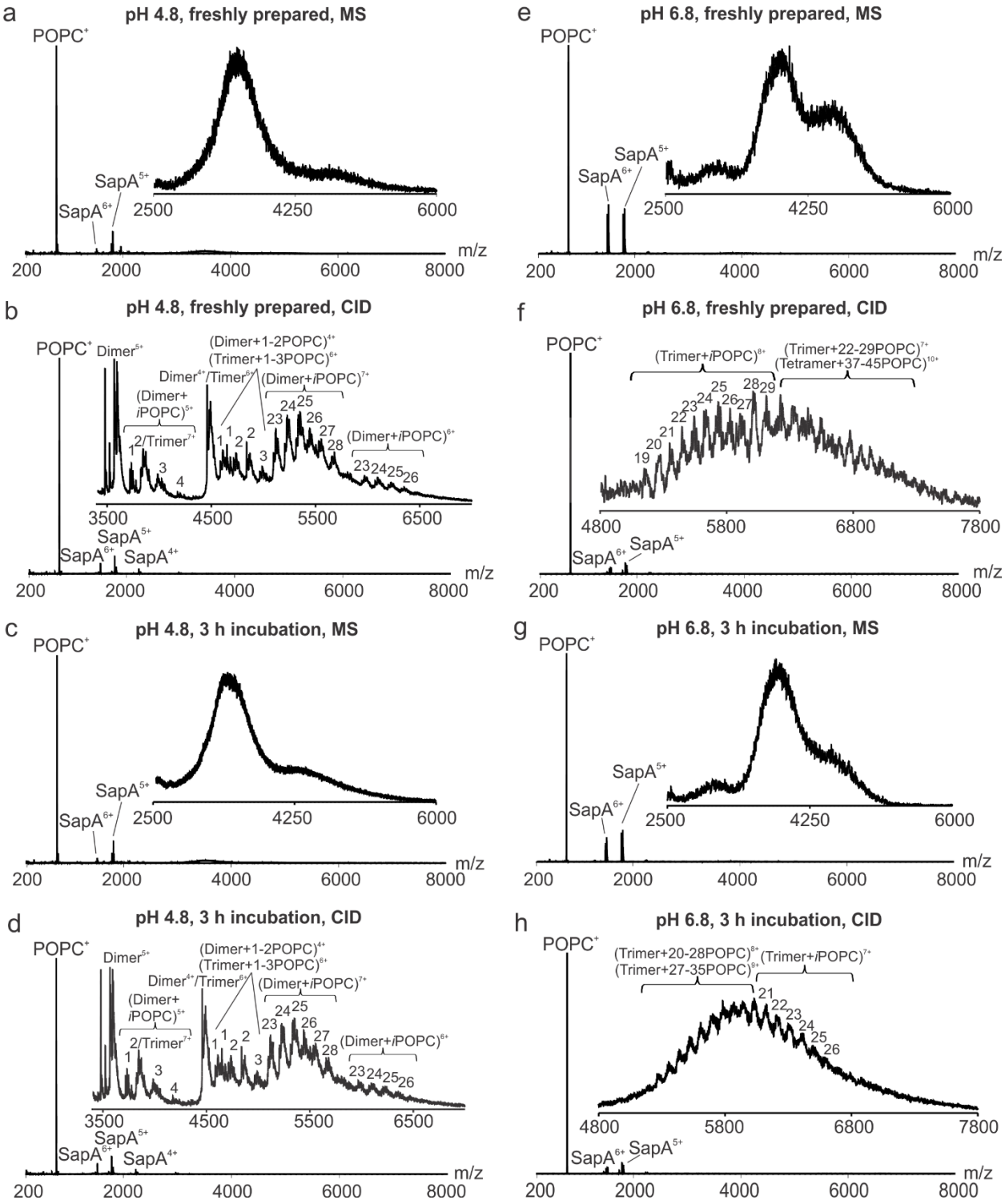

Figure 3.3 ESI mass spectra acquired by ToF-MS in positive ion mode for freshly prepared 200 mM aqueous ammonium acetate solutions of POPC-PDs (10 μM) at (a) pH 4.8 or (e) pH 6.8. (b) and (f) CID mass spectra (50 V in Trap) for the POPC-PD ions produced from the solutions described in (a) and (e), respectively. (c) and (g) ESI mass spectra acquired for the solutions described in (a) and (e), respectively, after 3 h incubation. (d) and (h) CID mass spectra (50 V in Trap) for POPC-PD ions produced from the solutions described in (c) and (g), respectively.

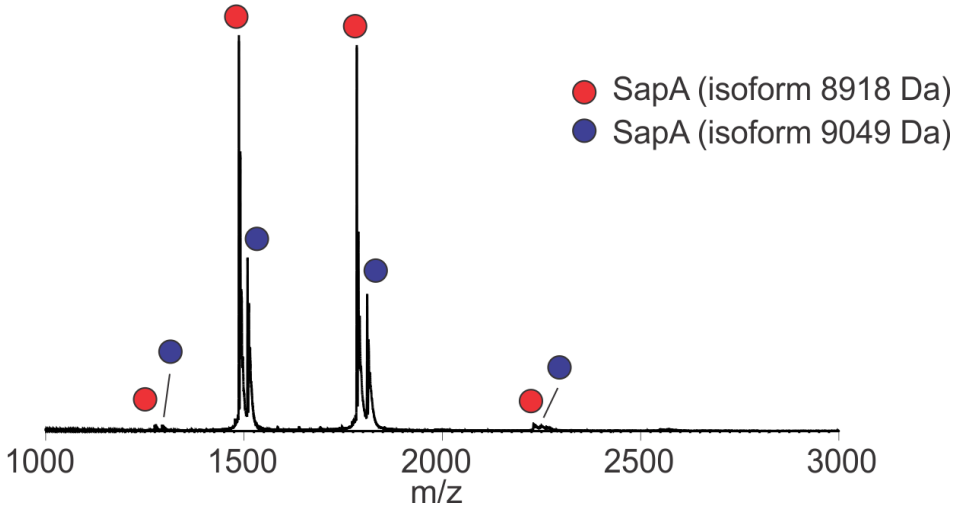

Figure 3.4 ESI mass spectrum acquired for SapA (10 μM) in a 200 mM aqueous ammonium acetate solution at pH 6.8.

Table 3.1 Composition of POPC-PDs. Comparison of theoretical and measured *m/z* values (based on average MWs) for signals observed in CID (Trap energy 50 V) mass spectrum (Figure 3.3b) acquired for a 200 mM aqueous ammonium acetate solution of POPC-PD (10 μM) at pH 4.8.

Composition	Theoretical *m/z*	Measured *m/z*	Composition	Theoretical *m/z*	Measured *m/z*
$(POPC + H)^{+}$	760.6	760.5	$(2SapA + 2POPC + 5H)^{5+}$	3898.0	3898.4
$(2POPC + H)^{+}$	1520.2	1520.1	$(2SapA + 3POPC + 5H)^{5+}$	4050.0	4050.2
$(SapA + 6H)^{6+}$	1486.0	1486.0	$(2SapA + 4POPC + 5H)^{5+}$	4202.0	4202.5
$(SapA + 6H)^{6+}$	1508.2	1508.2	$(2SapA + 4H)^{4+}$	4459.0	4459.2
$(SapA + 5H)^{5+}$	1784.2	1784.2	$(3SapA + 6H)^{6+}$	4459.0	
$(SapA + 5H)^{5+}$	1810.8	1810.8	$(3SapA + POPC + 6H)^{6+}$	4607.8	4608.4
$(SapA + 4H)^{4+}$	2230.0	2230.0	$(2SapA + POPC + 4H)^{4+}$	4649.0	4649.7
$(SapA + 4H)^{4+}$	2263.3	2263.3	$(3SapA + 2POPC + 6H)^{6+}$	4756.7	4756.7
$(SapA + POPC + 4H)^{4+}$	2420.0	2420.1	$(2SapA + 2POPC + 4H)^{4+}$	4839.0	4839.2
$(SapA + POPC + 4H)^{4+}$	2453.3	2453.4	$(3SapA + 3POPC + 6H)^{6+}$	4839.0	
$(SapA + 2POPC + 4H)^{4+}$	2610.0	2610.1	$(3SapA + 4POPC + 6H)^{6+}$	5010.0	5010.1
$(SapA + 2POPC + 4H)^{4+}$	2643.3	2643.3	$(2SapA + 3POPC + 4H)^{4+}$	5062.3	5062.5
$(SapA + 3POPC + 4H)^{4+}$	2800.0	2800.0	$(2SapA + 23POPC + 7H)^{7+}$	5120.1	5120.9
$(SapA + 3POPC + 4H)^{4+}$	2833.3	2833.3	$(2SapA + 24POPC + 7H)^{7+}$	5228.7	5228.8
$(SapA + 3H)^{3+}$	2973.0	2973.1	$(2SapA + 25POPC + 7H)^{7+}$	5337.3	5337.7
$(SapA + 3H)^{3+}$	3017.3	3017.4	$(2SapA + 26POPC + 7H)^{7+}$	5445.9	5445.2
$(SapA + POPC + 3H)^{3+}$	3226.3	3226.6	$(2SapA + 27POPC + 7H)^{7+}$	5554.4	5554.8
$(SapA + POPC + 3H)^{3+}$	3270.7	3270.3	$(2SapA + 28POPC + 7H)^{7+}$	5663.0	5662.8
$(SapA + 2POPC + 3H)^{3+}$	3479.7	3479.8	$(2SapA + 23POPC + 6H)^{6+}$	5973.3	5973.5
$(SapA + 2POPC + 3H)^{3+}$	3524.0	3523.9	$(2SapA + 24POPC + 6H)^{6+}$	6100.0	6100.1
$(2SapA + 5H)^{5+}$	3594.0	3594.1	$(2SapA + 25POPC + 6H)^{6+}$	6226.7	6226.1
$(2SapA + POPC + 5H)^{5+}$	3746.0	3746.2	$(2SapA + 26POPC + 6H)^{6+}$	6353.3	6353.5
$(3SapA + 7H)^{7+}$	3860.1	3860.5			

Table 3.2 Composition of POPC-PDs. Comparison of theoretical and measured *m/z* values (based on average MWs) for signals observed in CID (Trap energy 50 V) mass spectrum (Figure 3.3d) acquired for a 200 mM aqueous ammonium acetate solution of POPC-PD (10 μM) after 3 hours incubation at pH 4.8.

Composition	Theoretical *m/z*	Measured *m/z*	Composition	Theoretical *m/z*	Measured *m/z*
$(POPC + H)^{+}$	760.6	760.5	$(2SapA + 2POPC + 5H)^{5+}$	3898.0	3898.4
$(2POPC + H)^{+}$	1520.2	1520.1	$(2SapA + 3POPC + 5H)^{5+}$	4050.0	4050.2
$(SapA + 6H)^{6+}$	1486.0	1486.0	$(2SapA + 4POPC + 5H)^{5+}$	4202.0	4202.5
$(SapA + 6H)^{6+}$	1508.2	1508.2	$(2SapA + 4H)^{4+}$	4459.0	4459.2
$(SapA + 5H)^{5+}$	1784.2	1784.2	$(3SapA + 6H)^{6+}$	4459.0	
$(SapA + 5H)^{5+}$	1810.8	1810.8	$(3SapA + POPC + 6H)^{6+}$	4607.8	4608.4
$(SapA + 4H)^{4+}$	2230.0	2230.0	$(2SapA + POPC + 4H)^{4+}$	4649.0	4649.7
$(SapA + 4H)^{4+}$	2263.3	2263.3	$(3SapA + 2POPC + 6H)^{6+}$	4756.7	4756.7
$(SapA + POPC + 4H)^{4+}$	2420.0	2420.1	$(2SapA + 2POPC + 4H)^{4+}$	4839.0	4839.2
$(SapA + POPC + 4H)^{4+}$	2453.3	2453.4	$(3SapA + 3POPC + 6H)^{6+}$	4839.0	
$(SapA + 2POPC + 4H)^{4+}$	2610.0	2610.1	$(3SapA + 4POPC + 6H)^{6+}$	5010.0	5010.1
$(SapA + 2POPC + 4H)^{4+}$	2643.3	2643.3	$(2SapA + 3POPC + 4H)^{4+}$	5062.3	5062.5
$(SapA + 3POPC + 4H)^{4+}$	2800.0	2800.0	$(2SapA + 23POPC + 7H)^{7+}$	5120.1	5120.9
$(SapA + 3POPC + 4H)^{4+}$	2833.3	2833.3	$(2SapA + 24POPC + 7H)^{7+}$	5228.7	5228.8
$(SapA + 3H)^{3+}$	2973.0	2973.1	$(2SapA + 25POPC + 7H)^{7+}$	5337.3	5337.7
$(SapA + 3H)^{3+}$	3017.3	3017.4	$(2SapA + 26POPC + 7H)^{7+}$	5445.9	5445.2
$(SapA + POPC + 3H)^{3+}$	3226.3	3226.6	$(2SapA + 27POPC + 7H)^{7+}$	5554.4	5554.8
$(SapA + POPC + 3H)^{3+}$	3270.7	3270.3	$(2SapA + 28POPC + 7H)^{7+}$	5663.0	5662.8
$(SapA + 2POPC + 3H)^{3+}$	3479.7	3479.8	$(2SapA + 23POPC + 6H)^{6+}$	5973.3	5973.5
$(SapA + 2POPC + 3H)^{3+}$	3524.0	3523.9	$(2SapA + 24POPC + 6H)^{6+}$	6100.0	6100.1
$(2SapA + 5H)^{5+}$	3594.0	3594.1	$(2SapA + 25POPC + 6H)^{6+}$	6226.7	6226.1
$(2SapA + POPC + 5H)^{5+}$	3746.0	3746.2	$(2SapA + 26POPC + 6H)^{6+}$	6353.3	6353.5
$(3SapA + 7H)^{7+}$	3860.1	3860.5			

Measurements analogous to those described above were carried out on a freshly prepared neutral (pH 6.8) aqueous ammonium acetate solution containing 10 μM PD (Figure 3.3e). In addition to signal corresponding to protonated ions of POPC and SapA monomer, two broad features centred at *m/z* ~4000 and ~4300 were observed. CID (collision energy of 50 V in the Trap) performed on ions with *m/z* >3500 resulted in the appearance of POPC, SapA monomer and the (SapA monomer + *i*POPC) complex, where *i* = 1 to 4, at charge states +3 to +6, the (SapA trimer + *i*POPC) ions, where *i* = 19 to 29, at charge states +7 to +8 and/or the (SapA tetramer + *i*POPC) ions, where *i* = 37 to 45, at charge states +10 (Figure 3.3f, Table 3.3). Notably, there was no evidence of ions corresponding to SapA dimer, either on its own or bound to POPC. These results suggest that the POPC-PDs do not exist as SapA dimer at neutral pH and, instead, contain ≥3 copies of SapA. Measurements performed on this same solution, but following incubation for 3 h, at room temperature revealed subtle changes in the relative abundance of the two broad features noted above (Figure 3.3g). Moreover, CID produced POPC, SapA monomer and the (SapA monomer + *i*POPC) complex, where *i* = 1 to 3, at charge states +3 to +6, and SapA trimer ions bound to a number of POPC, i.e., (SapA trimer + *i*POPC) ions, where *i* = 20 to 28, at charge states +7 to +8 and/or (SapA trimer + *i*POPC) ions, where *i* = 27 to 35, at charge states +9 (Figure 3.3h, Table 3.4). These results suggest that, upon dilution, the composition of the POPC-PDs in neutral solution changes with time, whereby tetrameric POPC-PDs convert to trimer.

Table 3.3 Composition of POPC-PDs. Comparison of theoretical and measured *m/z* values (based on average MWs) for signals observed in CID (Trap energy 50 V) mass spectrum (Figure 3.3f) acquired for a 200 mM aqueous ammonium acetate solution of POPC-PD (10 μM) at pH 6.8.

Composition	Theoretical *m/z*	Measured *m/z*	Composition	Theoritical *m/z*	Measured *m/z*
$(POPC + H)^{+}$	760.6	760.6	$(3SapA + 23POPC + 8H)^{8+}$	5562.8	5561.4
$(2POPC + H)^{+}$	1520.2	1520.3	$(3SapA + 24POPC + 8H)^{8+}$	5657.8	5656.7
$(SapA + 6H)^{6+}$	1486.0	1486.0	$(3SapA + 25POPC + 8H)^{8+}$	5752.8	5752.5
$(SapA + 6H)^{6+}$	1508.2	1508.2	$(3SapA + 26POPC + 8H)^{8+}$	5847.8	5843.1
$(SapA + 5H)^{5+}$	1784.2	1784.2	$(3SapA + 27POPC + 8H)^{8+}$	5942.8	5942.4
$(SapA + 5H)^{5+}$	1810.8	1810.7	$(3SapA + 28POPC + 8H)^{8+}$	6037.8	6037.7
$(SapA + 4H)^{4+}$	2230.0	2230.0	$(3SapA + 29POPC + 8H)^{8+}$	6132.8	6133.2
$(SapA + 4H)^{4+}$	2263.3	2263.1	$(3SapA + 22POPC + 7H)^{7+}$	6248.7	6251.5
$(SapA + POPC + 4H)^{4+}$	2420.0	2420.0	$(3SapA + 23POPC + 7H)^{7+}$	6357.3	6356.8
$(SapA + POPC + 4H)^{4+}$	2453.3	2453.3	$(3SapA + 23POPC + 7H)^{7+}$	6376.3	6377.0
$(SapA + 2POPC + 4H)^{4+}$	2610.0	2610.1	$(4SapA + 37POPC + 10H)^{10+}$	6379.4	
$(SapA + 2POPC + 4H)^{4+}$	2643.3	2643.3	$(3SapA + 24POPC + 7H)^{7+}$	6465.9	6465.9
$(SapA + 3POPC + 4H)^{4+}$	2800.0	2800.0	$(4SapA + 38POPC + 10H)^{10+}$	6468.7	
$(SapA + 3POPC + 4H)^{4+}$	2833.3	2833.3	$(3SapA + 25POPC + 7H)^{7+}$	6555.4	6557.4
$(SapA + 3H)^{3+}$	2973.0	2973.1	$(4SapA + 39POPC + 10H)^{10+}$	6558.0	
$(SapA + 3H)^{3+}$	3017.3	3017.1	$(3SapA + 26POPC + 7H)^{7+}$	6645.0	6646.1
$(SapA + 4POPC + 4H)^{4+}$	2990.0	2990.2	$(4SapA + 40POPC + 10H)^{10+}$	6647.3	
$(SapA + 4POPC + 4H)^{4+}$	3023.3	3023.4	$(3SapA + 26POPC + 7H)^{7+}$	6702.0	6710.8
$(SapA + POPC + 3H)^{3+}$	3226.3	3226.6	$(4SapA + 41POPC + 10H)^{10+}$	6710.0	
$(SapA + POPC + 3H)^{3+}$	3270.7	3270.3	$(3SapA + 27POPC + 7H)^{7+}$	6810.6	6813.2
$(SapA + 2POPC + 3H)^{3+}$	3479.7	3479.9	$(4SapA + 42POPC + 10H)^{10+}$	6812.6	
$(SapA + 2POPC + 3H)^{3+}$	3524.0	3523.9	$(3SapA + 28POPC + 7H)^{7+}$	6862.1	6865.6
$(SapA + 3POPC + 3H)^{3+}$	3733.0	3733.3	$(4SapA + 43POPC + 10H)^{10+}$	6862.0	
$(SapA + 3POPC + 3H)^{3+}$	3777.3	3777.1	$(3SapA + 29POPC + 7H)^{7+}$	6970.7	6963.6
$(3SapA + 19POPC + 8H)^{8+}$	5182.8	5183.3	$(4SapA + 44POPC + 10H)^{10+}$	6964.6	
$(3SapA + 20POPC + 8H)^{8+}$	5277.8	5277.7	$(3SapA + 29POPC + 7H)^{7+}$	7027.7	7033.7
$(3SapA + 21POPC + 8H)^{8+}$	5372.8	5371.8	$(4SapA + 45POPC + 10H)^{10+}$	7027.3	
$(3SapA + 22POPC + 8H)^{8+}$	5467.8	5466.3			

Table 3.4 Composition of POPC-PDs. Comparison of theoretical and measured *m/z* values (based on average MWs) for signals observed in CID (Trap energy 50 V) mass spectrum (Figure 3.3h) acquired for a 200 mM aqueous ammonium acetate solution of POPC-PD (10 μM) after 3 hours incubation at pH 6.8.

Composition	Theoretical *m/z*	Measured *m/z*	Composition	Theoritical *m/z*	Measured *m/z*
$(POPC + H)^{+}$	760.6	760.6	$(3SapA + 21POPC + 8H)^{8+}$	5356.1	5354.3
$(2POPC + H)^{+}$	1520.2	1520.2	$(3SapA + 28POPC + 9H)^{9+}$	5352.2	
$(SapA + 5H)^{6+}$	1486.0	1486.0	$(3SapA + 22POPC + 8H)^{8+}$	5451.1	5453.0
$(SapA + 5H)^{6+}$	1508.2	1508.2	$(3SapA + 29POPC + 9H)^{9+}$	5451.4	
$(SapA + 5H)^{5+}$	1784.2	1784.3	$(3SapA + 23POPC + 8H)^{8+}$	5546.1	5539.6
$(SapA + 5H)^{5+}$	1810.8	1810.7	$(3SapA + 30POPC + 9H)^{9+}$	5535.9	
$(SapA + 4H)^{4+}$	2230.0	2230.0	$(3SapA + 24POPC + 8H)^{8+}$	5624.5	5621.2
$(SapA + 4H)^{4+}$	2263.3	2263.1	$(3SapA + 31POPC + 9H)^{9+}$	5620.3	
$(SapA + POPC + 4H)^{4+}$	2420.0	2420.0	$(3SapA + 25POPC + 8H)^{8+}$	5719.5	5723.3
$(SapA + POPC + 4H)^{4+}$	2453.3	2453.3	$(3SapA + 32POPC + 9H)^{9+}$	5719.6	
$(SapA + 2POPC + 4H)^{4+}$	2610.0	2610.1	$(3SapA + 26POPC + 8H)^{8+}$	5814.5	5806.2
$(SapA + 2POPC + 4H)^{4+}$	2643.3	2643.3	$(3SapA + 33POPC + 9H)^{9+}$	5804.0	
$(SapA + 3POPC + 4H)^{4+}$	2800.0	2800.0	$(3SapA + 26POPC + 8H)^{8+}$	5864.4	5860.7
$(SapA + 3POPC + 4H)^{4+}$	2833.3	2833.3	$(3SapA + 34POPC + 9H)^{9+}$	5858.9	
$(SapA + 3H)^{3+}$	2973.0	2973.1	$(3SapA + 27POPC + 8H)^{8+}$	5926.1	5928.5
$(SapA + 3H)^{3+}$	3017.3	3017.3	$(3SapA + 35POPC + 9H)^{9+}$	5928.6	
$(SapA + 4POPC + 4H)^{4+}$	2990.0	2990.2	$(3SapA + 28POPC + 8H)^{8+}$	6037.8	6037.5
$(SapA + 4POPC + 4H)^{4+}$	3023.3	3023.4	$(3SapA + 21POPC + 7H)^{7+}$	6140.1	6140.8
$(SapA + POPC + 3H)^{3+}$	3226.3	3226.6	$(3SapA + 22POPC + 7H)^{7+}$	6248.7	6248.7
$(SapA + POPC + 3H)^{3+}$	3270.7	3270.3	$(3SapA + 23POPC + 7H)^{7+}$	6338.3	6337.9
$(SapA + 2POPC + 3H)^{3+}$	3479.7	3479.9	$(3SapA + 24POPC + 7H)^{7+}$	6465.9	6465.6
$(SapA + 2POPC + 3H)^{3+}$	3524.0	3523.9	$(3SapA + 25POPC + 7H)^{7+}$	6574.4	6572.2
$(SapA + 3POPC + 3H)^{3+}$	3733.0	3733.3	$(3SapA + 26POPC + 7H)^{7+}$	6664.0	6663.3
$(SapA + 3POPC + 3H)^{3+}$	3777.3	3777.1	$(3SapA + 21POPC + 8H)^{8+}$	5356.1	5354.3
$(3SapA + 20POPC + 8H)^{8+}$	5277.8	5278.1			
$(3SapA + 27POPC + 9H)^{9+}$	5282.6				

In order to more precisely establish the composition and degree of heterogeneity of the POPC-PDs under acidic and neutral conditions, high resolution ESI-MS analysis was performed using FT-MS. Shown in Figure 3.5a is a representative ESI mass spectrum acquired for a freshly prepared 200 mM aqueous ammonium acetate solution, at pH 4.8, containing 5 μM PD; the mass spectrum shown in Figure 3.5d was acquired after 3 h at room temperature. An expanded view of the *m/z* 4400 – 5800 portions of the two mass spectra is given in Figure 3.5b and Figure 3.5e, respectively. In both Figure 3.5a and Figure 3.5d, the POPC dimer ion was detected, along with two distributions of ions corresponding to (SapA dimer + *i*POPC) complexes, where $i = 23$ to 29, at charge states +7 to +8. Shown in Figure 3.5c and Figure 3.5f are the zero-charge mass spectra corresponding to the mass spectral data shown in Figure 3.5a and Figure 3.5d, respectively. In addition to the dominant (SapA dimer + *i*POPC) species, with $i = 23$ to 29 and a weighted average MW of 38.2 ± 3.3 kDa, there is evidence of smaller (SapA dimer + *i*POPC) complexes, with $i =$ 12 to 20, (SapA trimer + *i*POPC) complexes with $i = 32$ to 37, and (SapA tetramer + *i*POPC) complexes with $i = 48$ to 60. The zero-charge mass spectrum shown in Figure 3.5f, acquired after 3 h of incubation, revealed a similar distribution of species. This observation, which is consistent with results obtained by ToF-MS, suggests that the distribution of POPC-PD species remains relatively constant over time at acidic pH.

High resolution ESI mass spectra acquired for a 200 mM aqueous ammonium acetate solution (pH 6.8) of 5 μM PD POPC-PDs, acquired immediately after preparation and after 3 h incubation, are shown in Figures 3.6a and 3.6d, respectively; expanded views of the region of the mass spectra containing signal for the POPC-PDs are given in Figure 3.6b (*m/z* 6200 – 7800) and Figure 3.6e (*m/z* 4200 – 6000), respectively. The corresponding zero-charge mass spectra are shown in Figure 3.6c and Figure 3.6f, respectively. Analysis of the mass spectral data suggests

that, for the freshly prepared neutral solution, POPC-PDs exist predominantly as (SapA tetramer + *i*POPC) complexes with i = 37 to 47 and an average MW of 68.0 ± 2.7 kDa; (SapA tetramer + *i*POPC) complexes with i = 55 to 60 were also detected but at low abundance. After incubation for 3 h, there is an obvious change in the distribution of POPC-PD species – a significant fraction of the (SapA tetramer + *i*POPC) complexes appears to have transformed to (SapA trimer + *i*POPC) complexes, with i = 29 to 36 and an average MW of 51.1 ± 2.9 kDa (Figure 3.6f).

The size and MWs of the POPC-PDs in neutral and acidic solutions were also investigated using MALLS coupled with SEC. Shown in Figure 3.7 are the chromatograms and corresponding MW distributions acquired for 200 mM aqueous ammonium acetate solutions, at pH 4.8 (Figure 3.7a) or 6.8 (Figure 3.7b), containing 225 μM POPC-PDs. It can be seen that, at acidic pH, the POPC-PDs have MWs ranging from approximately 35 kDa to 50 kDa, with an average MW of 40.9 ± 1.6 kDa. These results are consistent with the values (35–45 kDa) estimated for POPC-PDs based on SEC measurements.[15] Of more significance, the average MW determined by MALLS is in good agreement with the value determined by ESI-MS (38.2 ± 3.3 kDa). It can also be seen from the MALLS data that POPC-PDs are more heterogeneous and span a much wider range of MWs (approximately 50 kDa to 90 kDa) at neutral pH, and have an average MW of 73.7 ± 0.4 kDa. This average MW is in good agreement with the value of 68.0 ± 2.7 kDa determined by ESI-MS performed on the freshly prepared POPC-PD solution. It can be concluded, therefore, that, at neutral pH, POPC-PDs exist predominantly as (SapA tetramer + *i*POPC) complexes. As described above, the ESI-MS data suggest that the (SapA tetramer + *i*POPC) complexes are unstable at neutral pH and, over a period of hours, convert to (SapA trimer + *i*POPC) complexes. In addition to providing insight into the MWs of the POPC-PDs, the MALLS data also provide an estimate of R_h. According to the measured data, the POPC-PDs have an R_h of 31.0 ± 1.5 Å at acidic pH and

an R_h of 39.0 ± 0.2 Å at neutral pH. The value measured at pH 4.8 agrees with the R_h value (32.5 Å) reported previously.[15]

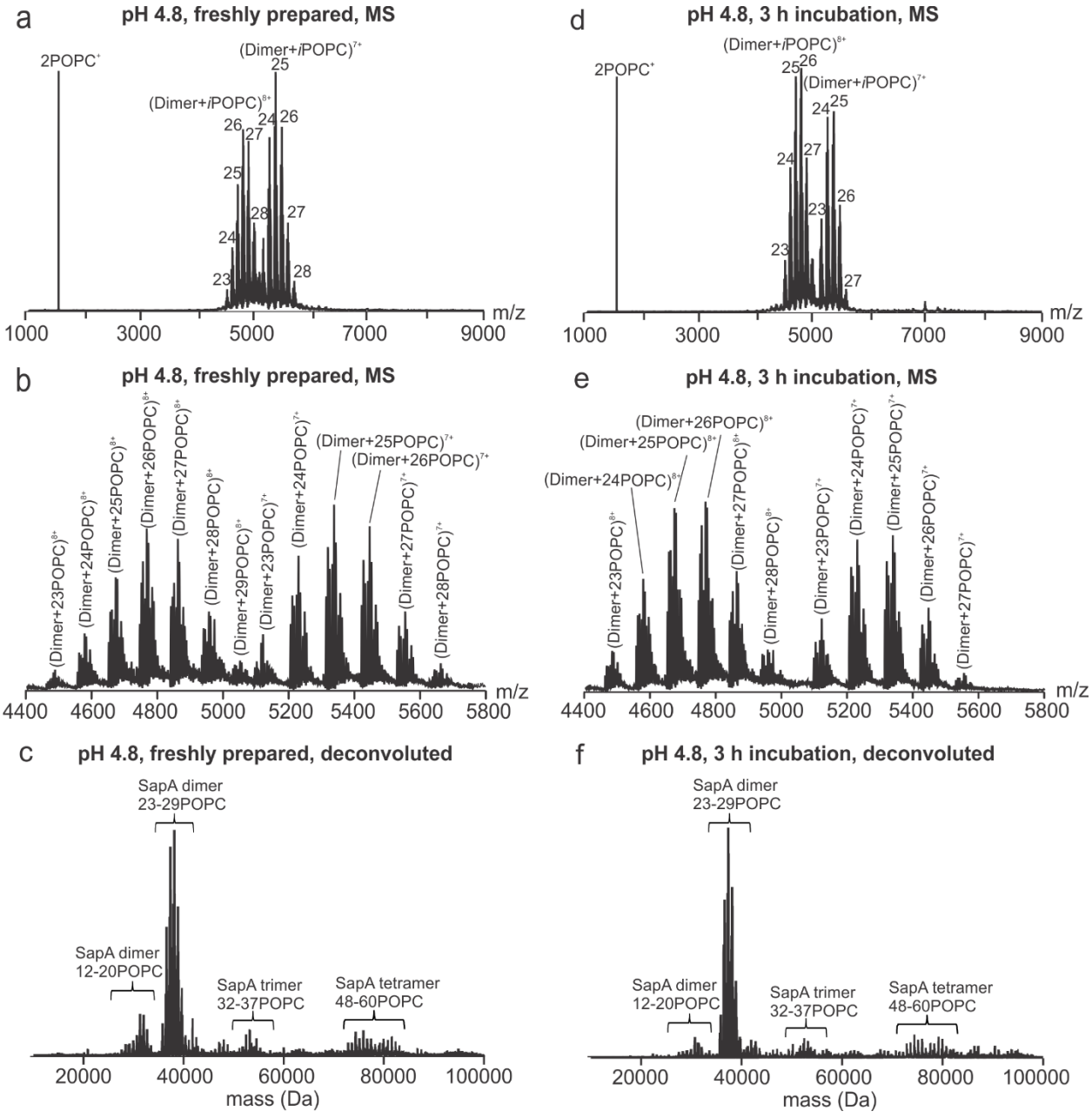

Figure 3.5 ESI mass spectra acquired by FT-MS in positive ion mode for a 200 mM aqueous ammonium acetate solution of POPC-PDs (5 μM) at pH 4.8 (a) immediately after preparation of

the solution and (d) after 3 h incubation. (b) and (e) Expanded view of the mass spectra shown in (a) and (d), respectively. (c) and (f) Zero-charge mass spectrum corresponding to (a) and (d), respectively.

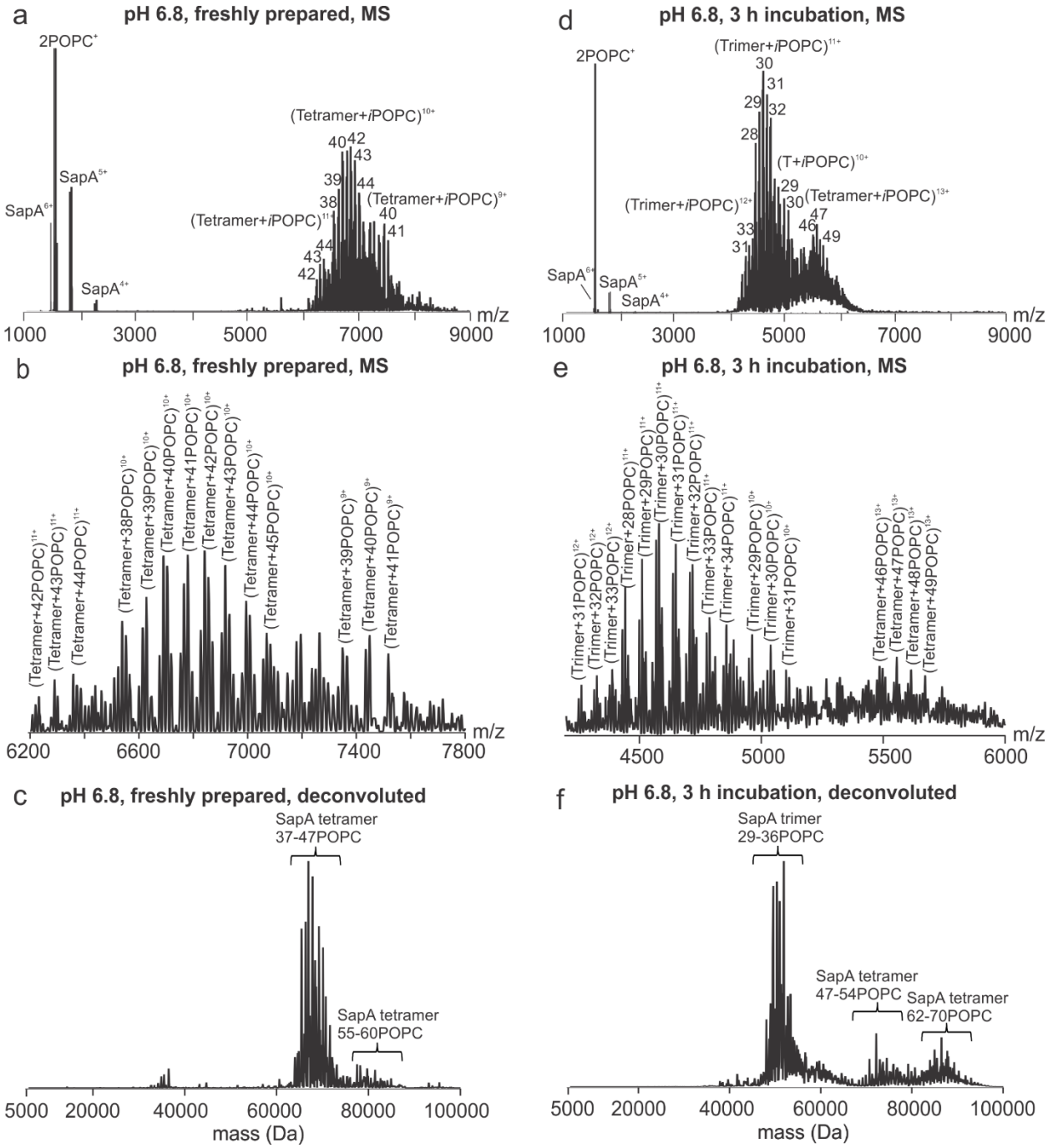

Figure 3.6 ESI mass spectra acquired by FT-MS in positive ion mode for a 200 mM aqueous ammonium acetate solution of POPC-PDs (5 μM) at pH 6.8 (a) immediately after preparation of the solution and (d) after 3 h incubation. (b) and (e) Expanded viewes of the mass spectra shown in (a) and (d), respectively. (c) and (f) Zero-charge mass spectrum corresponding to (a) and (d), respectively.

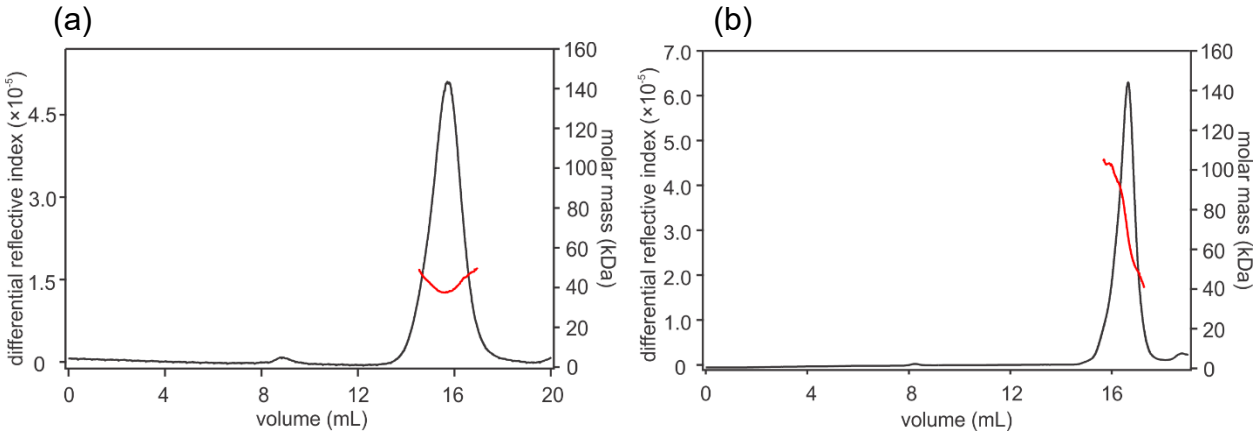

Figure 3.7 SEC-MALLS analysis of POPC-PDs (225 μM) solution in 200 mM ammonium acetate at (a) pH 4.8 or (b) 6.8. The black line represents the SEC elution profile monitored by refractive index and the red line across the elution peak indicates the MW calculated by MALLS.

3.3.2 Structures of POPC-PDs in solution

A series of MD simulations were performed with the goal of estimating the solution structures of the different POPC-PD species identified by ESI-MS and MALLS. The simulations were carried out with four different species – (SapA dimer + 10POPC), (SapA dimer + 26POPC), (SapA trimer + 33POPC) and (SapA tetramer + 42POPC). The initial structure of the (SapA dimer + 10POPC) complex was based on the reported model for POPC-PDs (Figure 3.2).[15] Initial structures for the

other three complexes, which are among the most abundant species detected by ESI-MS, were built by manually arranging SapA proteins around a bilayer of POPC (Figure 3.2). Analysis of the 50-ns simulations performed on the hydrated POPC-PDs shows that, while the complexes undergo a slight compaction, the POPCs remain in a bilayer-like arrangement throughout the simulation (Figure 3.8). The R_g values of the four POPC-PD complexes were monitored over the course of the simulation and found to remain relatively constant; with average values of 17.6 ± 0.2 Å (SapA dimer + 10POPC), 20.6 ± 0.2 Å (SapA dimer + 26POPC), 23.3 ± 0.3 Å (SapA trimer + 33POPC), and 26.0 ± 0.2 Å (SapA tetramer + 42POPC) (Table 3.5 and Figure 3.9).

As described above, R_g values for the POPC-PDs could not be measured using MALLS. Consequently, a direct comparison of the R_g values determined from the structures generated from modelling with experimental values was not possible. The R_g/R_h ratios, based on the R_g values calculated for the (SapA dimer + 26POPC) and (SapA tetramer + 42POPC) complexes and the experimental R_h values determined at pH 4.8 and 6.8 are 0.66–0.67 (Table 3.5). These values are somewhat smaller than the theoretical value of 0.775 expected for hard spheres.[33] However, it is known that core weighting of the density distributions of spheres, as might be expected in the case of the PDs, leads to R_g/R_h ratios <0.775.[34] Moreover, the ratios calculated for the POPC-PDs are similar to values (0.68–0.69) reported for poly(amidoamine) (PAMAM) dendrimers of comparable size (e.g. R_g = 17.1 Å and 26.3 Å for generation 4 and 6).[35] While the aforementioned analysis does not enable any conclusions to be drawn regarding the shapes (structures) of the solvated POPC-PDs, it does raise the possibility that the (SapA dimer + *i*POPC), (SapA tetramer + *i*POPC) and, presumably, (SapA trimer + *i*POPC) complexes adopt spheroidal structures, of the type shown in Figure 3.8, in solution.

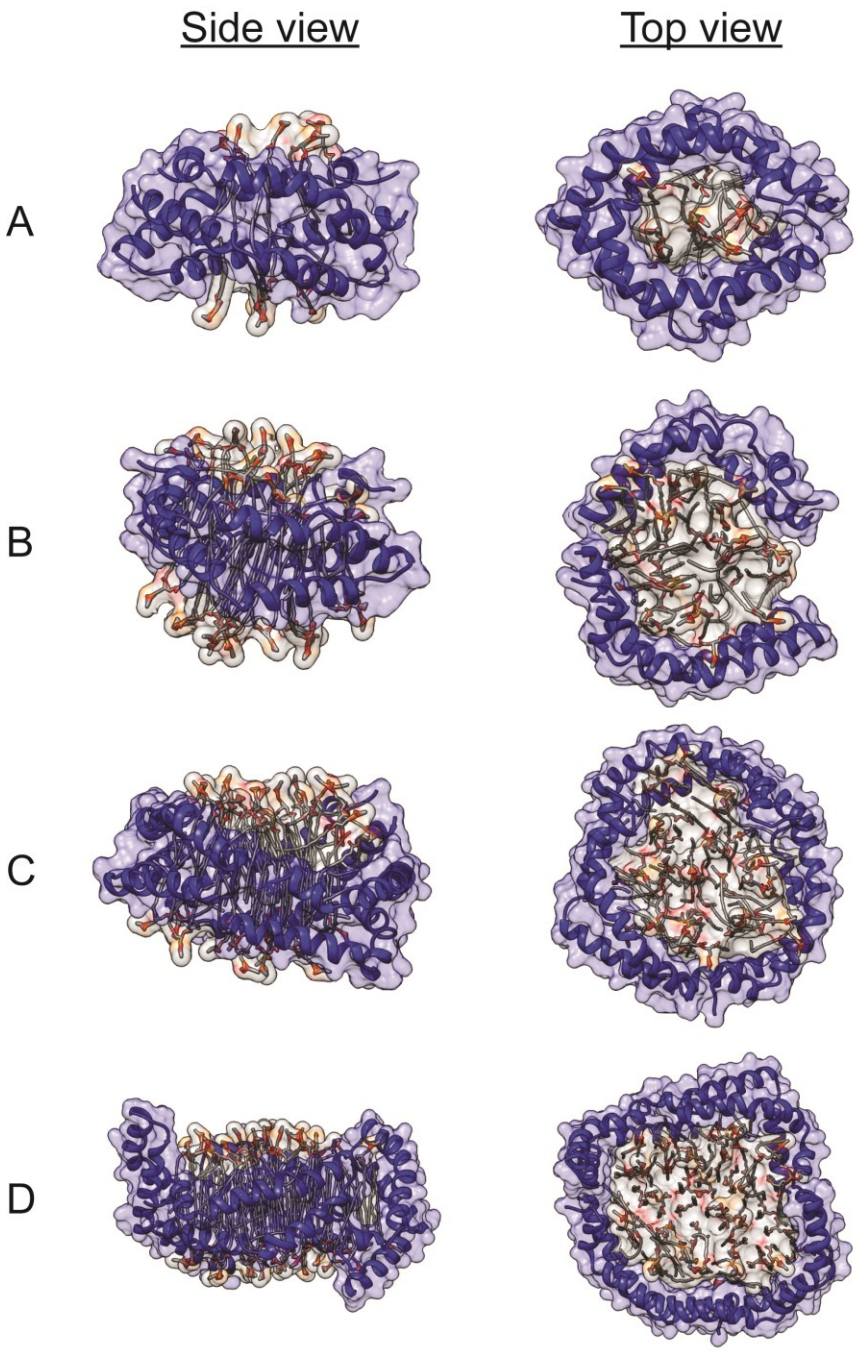

Figure 3.8 Averaged structures of POPC-PDs obtained by MD simulations performed in solution over 50 ns (SapA shown as blue ribbon and POPC shown as sticks). (a) (SapA dimer + 10POPC) complex, (b) (SapA dimer + 26POPC) complex, (c) (SapA trimer + 33POPC) complex, and (d) (SapA tetramer + 42POPC) complex.

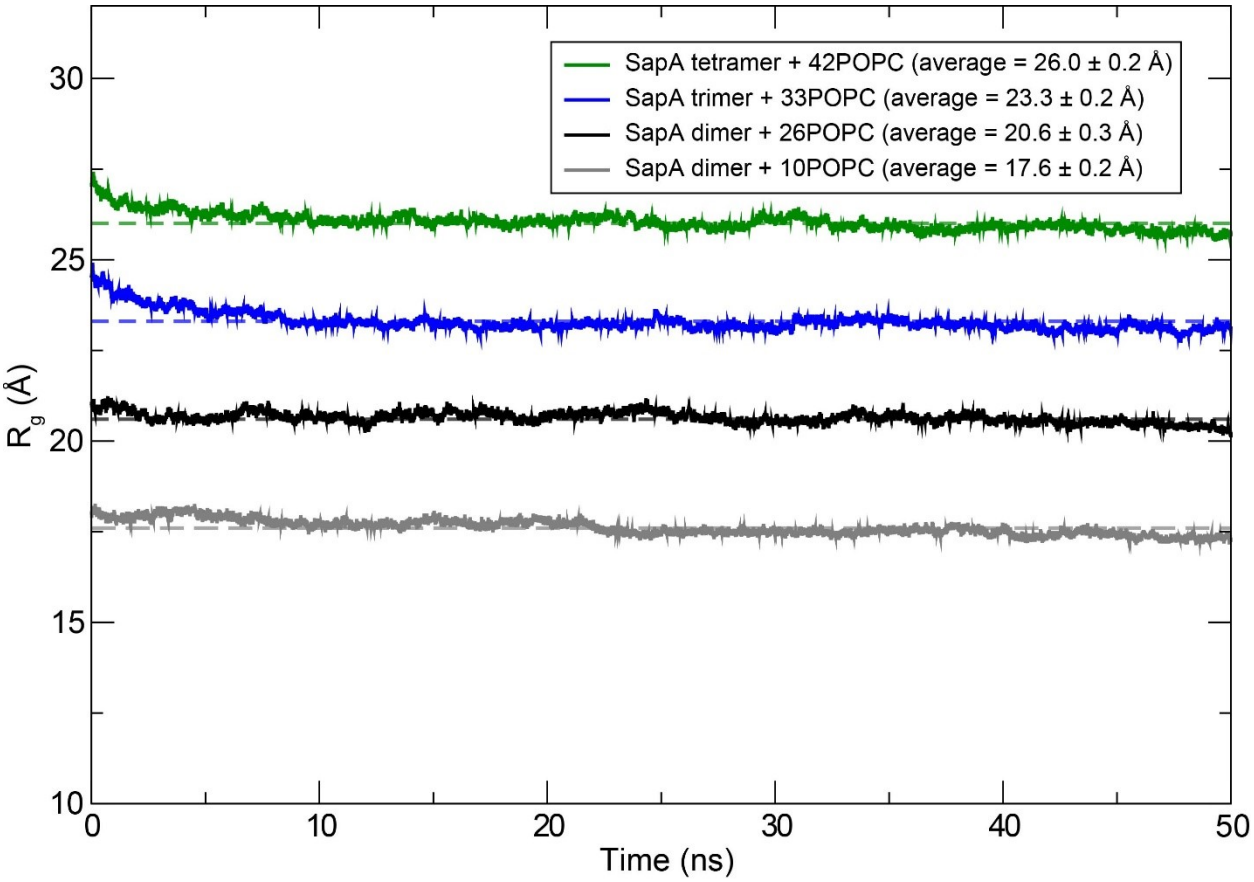

Figure 3.9 Radius of gyration (R_g) for the 50-ns solution MD simulations. The (SapA dimer + 10POPC) complex is shown in grey, (SapA dimer + 26POPC) complex is shown in in black, the (SapA trimer + 33POPC) complex is shown in blue, and the (SapA tetramer + 42POPC) complex is shown in green. The average R_g values, determined over the course of the simulations, are shown as dashed lines – (SapA dimer + 10POPC), $R_g = 17.6 \pm 0.2$ Å; (SapA dimer + 26POPC), $R_g = 20.6 \pm 0.2$ Å; (SapA trimer + 33POPC), $R_g = 23.3 \pm 0.3$ Å; and (SapA tetramer + 42POPC), $R_g = 26.0 \pm 0.2$ Å.

Table 3.5 Solution properties of POPC-PD species evaluated by ESI-MS, SEC-MALLS, and MD simulations.[a]

POPC-PD	*i*	Average MW (kDa)	Measured R_h (Å)	Average R_g (Å)	R_g/R_h
(SapA dimer + *i*POPC)	10	ND	ND	17.6 ± 0.2 [d]	ND
(SapA dimer + *i*POPC)	23–29 [b]	38.2 ± 3.3 [b] 40.9 ± 1.6 [c]	31.0 ± 1.5 [c]	20.6 ± 0.2 [d] (*i* = 26)	0.66 [e]
(SapA trimer + *i*POPC)	29–36 [b]	51.1 ± 2.9 [b]	ND	23.3 ± 0.3 [d] (*i* = 33)	ND
(SapA tetramer + *i*POPC)	37–47 [b]	68.0 ± 2.7 [b] 73.7 ± 0.4 [c]	39.0 ± 0.2 [c]	26.0 ± 0.2 [d] (*i* = 42)	0.67 [e]

a. ND ≡ Not determined. b. Values measured by FT-MS. c. Values measured by SEC-MALLS. d. Values calculated by MD simulations in solution and averaged over 50 ns. e. Ratio of calculated R_g to measured R_h.

3.3.3 Structures of POPC-PDs in the gas phase

It is also relevant, in the context of the CaR-ESI-MS assay, to ask what happens to the structures of the POPC-PD complexes once they are transferred to the gas phase. As a step towards answering this question, Ω values of the gaseous POPC-PD ions produced by ESI were determined by measuring the IMS drift times and comparing those values with drift times measured for calibrant protein ions (with known Ω values). The corresponding calibration plot, produced using Cyt c, TTR and Avidin, is shown in Figure 3.10. It can be seen that there is a linear correlation (correlation coefficient (R^2) of 0.996) between the drift times (corrected drift times, t_D'') and known

Ω values. Shown in Figure 3.11 are the ESI mass spectra and the corresponding 3D IMS heat maps (*m/z* versus IMS drift times) measured for POPC-PD ions produced from 200 mM ammonium acetate aqueous solutions at pH 4.8 (Figures 3.11a and 3.11b) or 6.8 (Figures 3.11c and 3.11d). The results shown in Figure 3.11a and Figure 3.11c were acquired immediately after preparing the POPC-PD solutions; those shown in Figure 3.11b and Figure 3.11d were acquired following 3 h incubation. Listed in Tables 3.6, 3.7, 3.8 are the Ω values for the POPC-PD ions determined from their corrected drift times (t_D'') and the calibration curve shown in Figure 3.10.

Summarized in Table 3.9 are the average Ω values of gaseous POPC-PD ions, taken over all compositions and all charge states. It can be seen that, as expected, Ω scales with the number of SapA proteins contained in the POPOC-PD ions. The (SapA dimer + *i*POPC) complexes with *i* = 23 to 29, the dominant species in acidic solution, have an average Ω of 29.5 ± 0.6 nm^2. The (SapA tetramer + *i*POPC) complexes with *i* = 37 to 47, which are dominant in freshly diluted solution at neutral pH, have an average Ω of 48.6 ± 1.1 nm^2, while the (SapA trimer + *i*POPC) complexes with *i* = 29 to 36, which dominate at longer times, have an average Ω of 37.1 ± 0.7 nm^2. Shown in Figure 3.12 are the measured Ω values plotted versus composition (number of POPC) at given charge states. It can also be seen that, for POPC-PDs with the same charge state, Ω increases, approximately linearly, with the number of POPCs. On average (considering all POPC-PD ions), Ω increases by 0.25 ± 0.12 nm^2 per POPC; for (SapA dimer + *i*POPC) ions (*i* = 24 to 29), Ω increases by 0.22 ± 0.10 nm^2 per POPC at charge states +10 and +11 (Table 3.6); for (SapA trimer + *i*POPC) ions Ω increases by 0.25 ± 0.14 nm^2 per POPC at charge state +12 and +13 (Table 3.8); for the (SapA tetramer + *i*POPC) ions Ω increases by 0.28 ± 0.11 nm^2 per POPC at charge states +14 to +17 (Table 3.7).

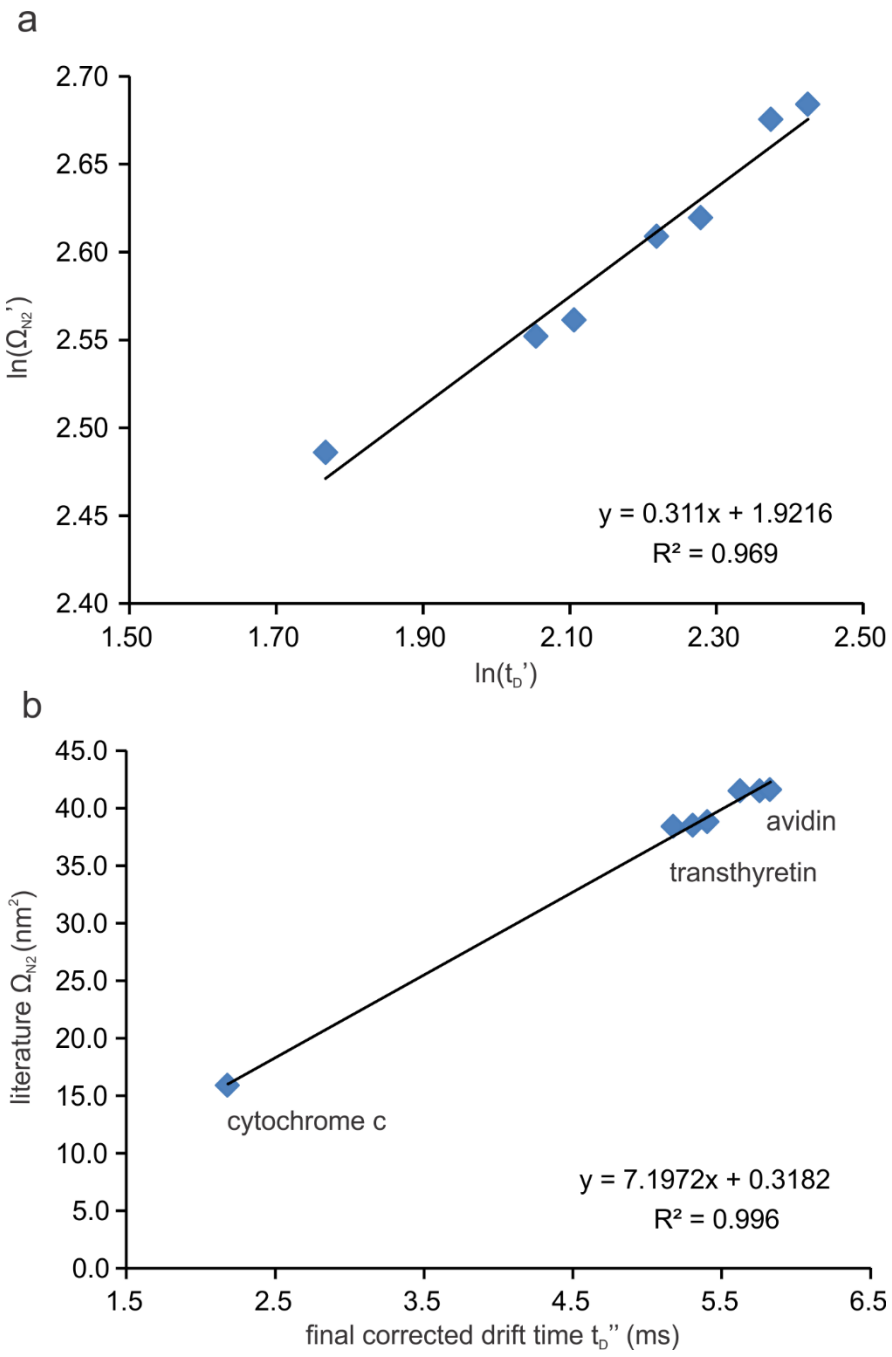

Figure 3.10 (a) Plot of $\ln(\Omega_{N2}')$ versus $\ln(t_D')$ for the calibrants: cytochrome c, transthyretin and avidin. An exponential factor (X) of 0.311 was determined from the slope of the plot. (b) Calibration displayed as a linear plot of literature Ω_{N2} values and final corrected drift times (t_D'').

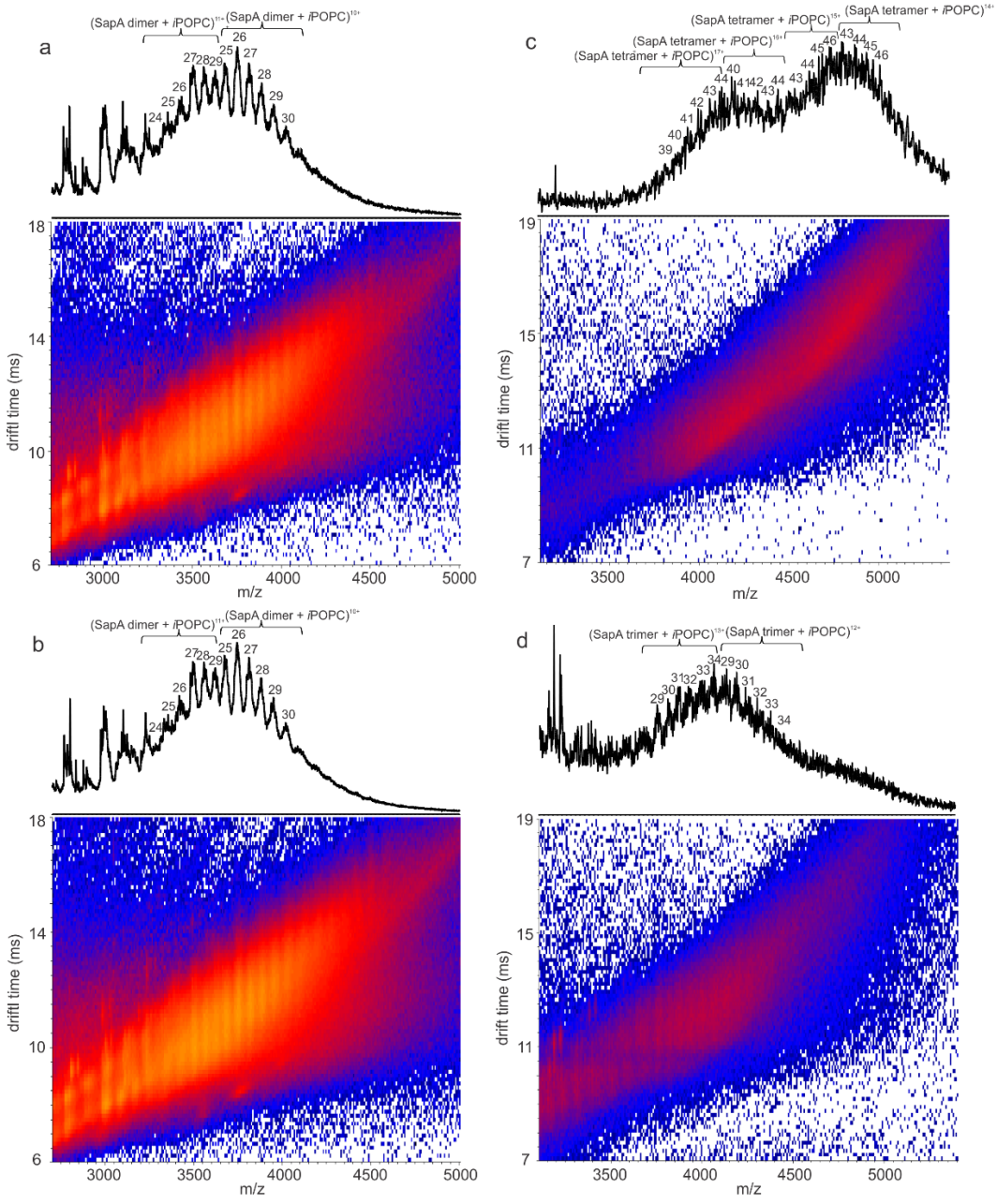

Figure 3.11 ESI mass spectra and corresponding IMS heat maps (*m/z* versus IMS drift times) measured in positive ion mode for (a) freshly prepared 200 mM aqueous ammonium acetate solutions (pH 4.8) of POPC-PDs (10 μM) and (b) after 3 h incubation. ESI mass spectra and corresponding IMS heat maps measured in positive ion mode for (c) freshly prepared 200 mM aqueous ammonium acetate solutions (pH 6.8) of POPC-PDs (10 μM) and (d) after 3 h incubation.

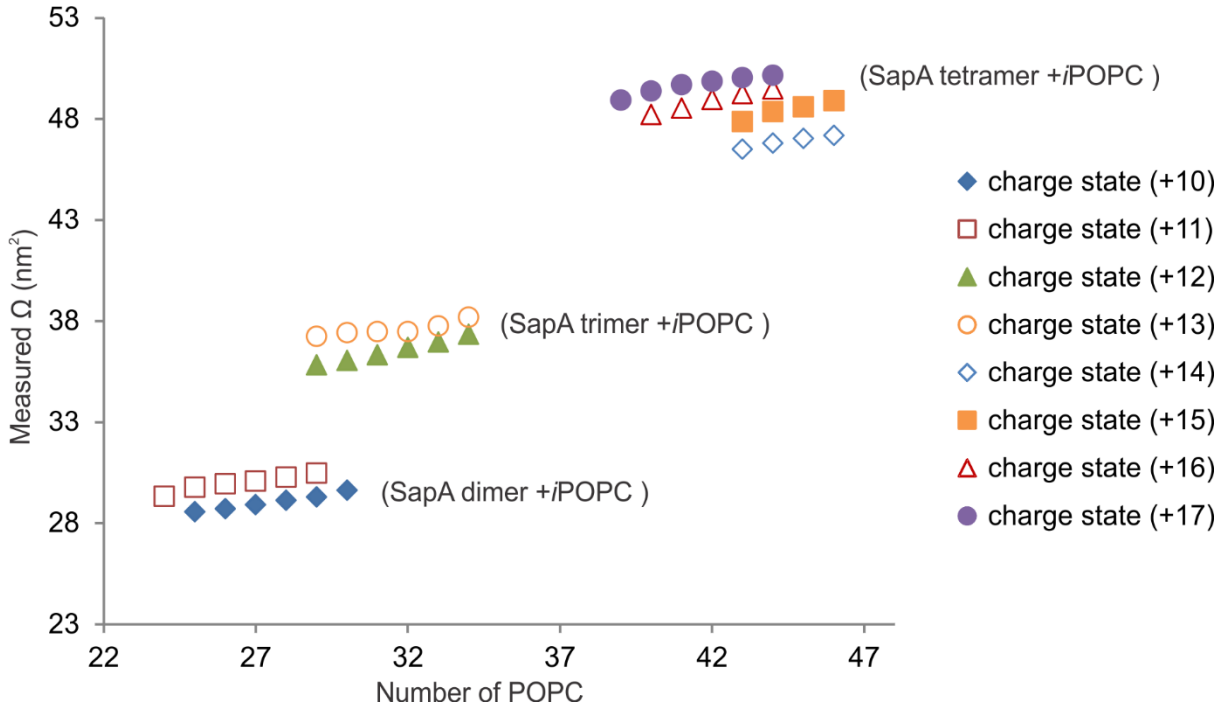

Figure 3.12 Measured Ω values plotted versus composition (number of POPC) at given charge states for POPC-PD ions: (SapA dimer + iPOPC)$^{n+}$ ions, (SapA trimer + iPOPC)$^{n+}$ ions, and (SapA tetramer + iPOPC)$^{n+}$ ions.

Table 3.6 Measured drift times (t_D), corrected drift times (t_D' and t_D'') and collision cross sections (Ω) for (SapA dimer + *i*POPC)$^{n+}$ ions.

Charge state (n)	*m/z*	Drift time (t_D, ms)	Corrected drift time (t_D', ms)	Final corrected drift time (t_D'', ms)	Calculated Ω (nm^2)
11	3286.5	8.75	8.40	4.03	29.32
11	3353.6	9.18	8.83	4.09	29.78
11	3412.5	9.35	9.00	4.12	29.95
11	3480.1	9.48	9.13	4.14	30.08
11	3556.4	9.67	9.32	4.16	30.27
11	3621.3	9.87	9.52	4.19	30.47
10	3681.3	10.82	10.46	3.92	28.55
10	3740.0	10.99	10.63	3.94	28.69
10	3809.9	11.24	10.88	3.97	28.90
10	3883.1	11.51	11.15	4.00	29.12
10	3950.0	11.72	11.36	4.02	29.28
10	4019.9	12.13	11.77	4.07	29.60

Table 3.7 Measured drift times (t_D), corrected drift times (t_D' and t_D'') and collision cross sections (Ω) for (SapA tetramer + iPOPC)$^{n+}$.

Charge state	*m/z*	Drift time (t_D, ms)	Corrected drift time (t_D', ms)	Final corrected drift time (t_D'', ms)	Calculated Ω (nm^2)
17	3867.8	11.26	10.90	6.75	48.92
17	3936.1	11.59	11.23	6.82	49.38
17	4012.1	11.83	11.47	6.86	49.70
17	4059.6	11.95	11.59	6.88	49.86
17	4105.0	12.09	11.73	6.91	50.04
17	4158.8	12.18	11.82	6.93	50.16
16	4213.0	12.98	12.62	6.65	48.19
16	4263.1	13.26	12.90	6.70	48.52
16	4316.2	13.63	13.27	6.76	48.94
16	4366.1	13.88	13.52	6.80	49.23
16	4410.3	14.09	13.73	6.83	49.46
15	4578.7	15.55	15.18	6.61	47.86
15	4628.4	16.08	15.71	6.68	48.37
15	4681.2	16.32	15.95	6.71	48.60
15	4732.7	16.64	16.27	6.75	48.89
14	4832.1	17.62	17.25	6.41	46.49
14	4896.3	17.99	17.62	6.46	46.79
14	4942.7	18.27	17.90	6.49	47.02
14	5000.3	18.46	18.09	6.51	47.17

Table 3.8 Measured drift times (t_D), corrected drift times (t_D' and t_D'') and collision cross sections (Ω) for (SapA trimer + iPOPC)$^{n+}$.

Charge state	*m/z*	Drift time (t_D, ms)	Corrected drift time (t_D', ms)	Final corrected drift time (t_D'', ms)	Calculated Ω (nm^2)
13	3794.6	11.03	10.67	5.13	37.25
13	3850.3	11.20	10.84	5.16	37.43
13	3910.5	11.24	10.88	5.16	37.47
13	3965.6	11.25	10.89	5.16	37.48
13	4034.2	11.52	11.16	5.20	37.76
13	4082.3	11.93	11.57	5.26	38.18
12	4140.6	12.51	12.15	4.93	35.81
12	4200.8	12.75	12.39	4.96	36.02
12	4264.3	13.07	12.71	5.00	36.31
12	4377.1	13.49	13.13	5.05	36.67
12	4394.8	13.81	13.45	5.09	36.94
12	4452.3	14.27	13.91	5.14	37.33

Table 3.9 Collision cross sections (Ω) of POPC-PD species from ESI-IMS-MS measurements and MD simulations.

POPC-PD	Measured Ω (nm^2) [a,b]	Measured Ω (nm^2) [a]	Calculated Ω (nm^2) [c]
(SapA dimer + *i*POPC)	29.5 ± 0.6 (*i* = 23–29)	29.3 ± 0.9 (*i* = 26)	31.5 (*i* = 26)
(SapA trimer + *i*POPC)	37.1 ± 0.7 (*i* = 29–36)	37.4 ± 0.6 (*i* = 33)	41.8 (*i* = 33)
(SapA tetramer + *i*POPC)	48.6 ± 1.1 (*i* = 37–47)	49.4 ± 0.6 (*i* = 42)	49.3 (*i* = 42)

a. Values measured by ESI-IMS-MS. b. Values averaged over all measured compositions. c. Value calculated for averaged structure from MD simulations.

In order to interpret the Ω data acquired for the gaseous POPC-PD ions, MD simulations were performed on the (SapA dimer + 26POPC)$^{8+}$, (SapA trimer + 33POPC)$^{12+}$, and (SapA tetramer + 42POPC)$^{16+}$ ions. All of the POPC-PD ions maintain a spheroidal shape, similar to the solutions structures, throughout the simulation, although the lipids do not maintain regular bilayer orientations, especially on the edges of the lipid packet (Figures 3.13 and 3.14. The gaseous ions also tend to be slightly more compact than their solution counterparts. For example, the average R_g for (SapA dimer + 26POPC)$^{8+}$ and (SapA tetramer + 42POPC)$^{16+}$ ions are 0.7 Å smaller than the solution complexes; the (SapA trimer + 33POPC)$^{12+}$ ion has the same average R_g, within error, as the hydrated complex (Figures 3.9 and 3.15). Theoretical values of Ω were also calculated for averaged structures of gaseous POPC-PD complexes over the course of the simulations. The theoretical Ω for the gas-phase (SapA dimer + 26POPC)$^{8+}$, (SapA trimer + 33POPC)$^{12+}$, and (SapA tetramer + 42POPC)$^{16+}$ ions are 31.5 nm^2, 41.8 nm^2, and 49.3 nm^2, respectively (Table 3.9). Notably, these values are within 12% of the average experimental Ω values determined for POPC-PDs with the same composition (29.3 ± 0.9 nm^2, 37.4 ± 0.6 nm^2 and 49.4 ± 0.6 nm^2, respectively, Table 3.9) and within 15% of the average values at all measured compositions (29.5 ± 0.6 nm^2, 37.1 ± 0.7 nm^2 and 48.6 ± 1.1 nm^2, respectively). These results suggest that the calculated structures, in particular those of (SapA dimer + 26POPC)$^{8+}$ and (SapA tetramer + 42POPC)$^{16+}$, might provide a reasonable representation of the structures of the POPC-PD ions in the gas phase.

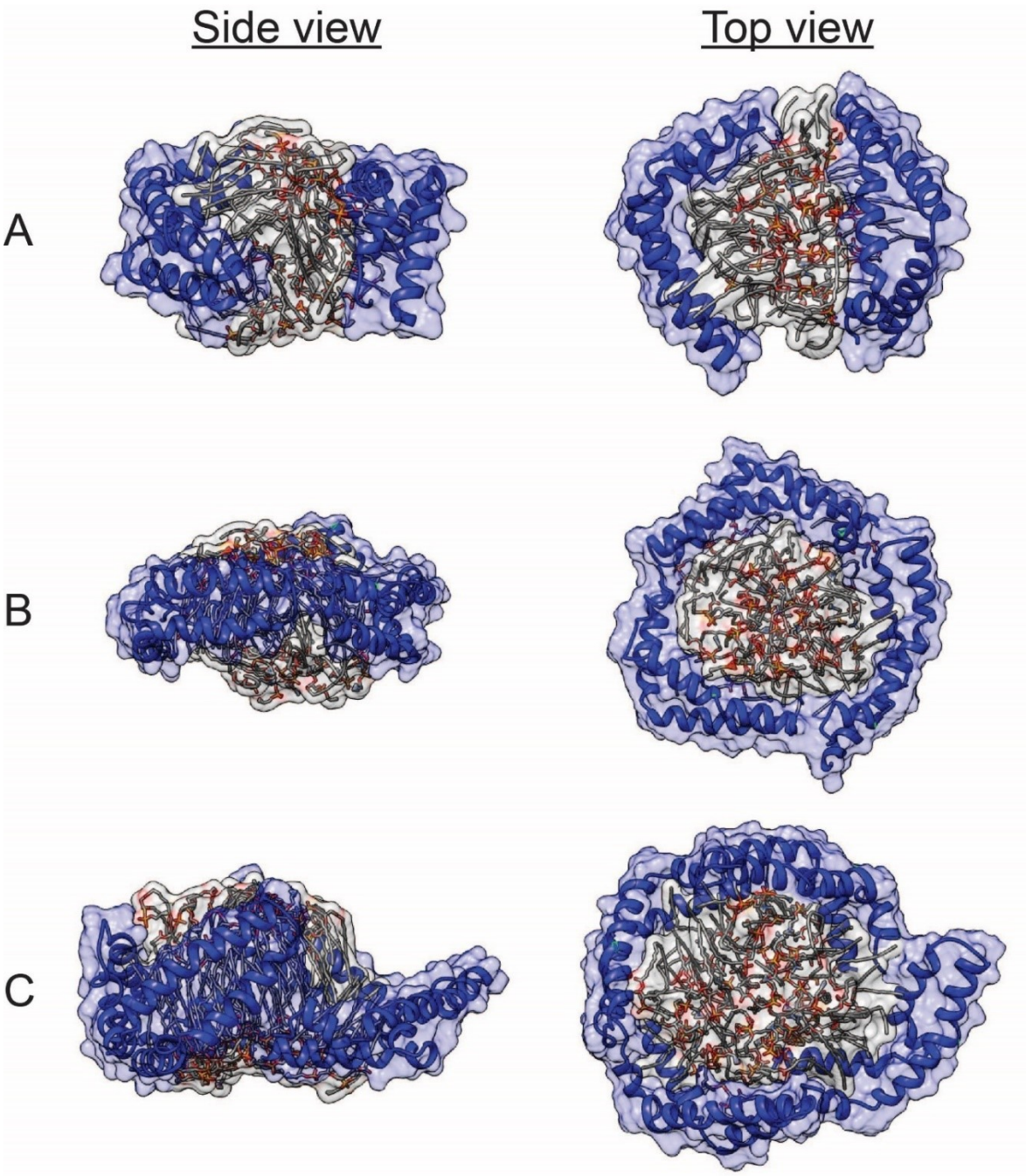

Figure 3.13 The averaged structures of the POPC-PD complexes from 20-ns gas-phase MD simulations. (a) (SapA dimer + 26POPC)$^{8+}$ ion, (b) (SapA trimer + 33POPC)$^{12+}$ ion, and (c) (SapA tetramer + 42POPC)$^{16+}$ ion.

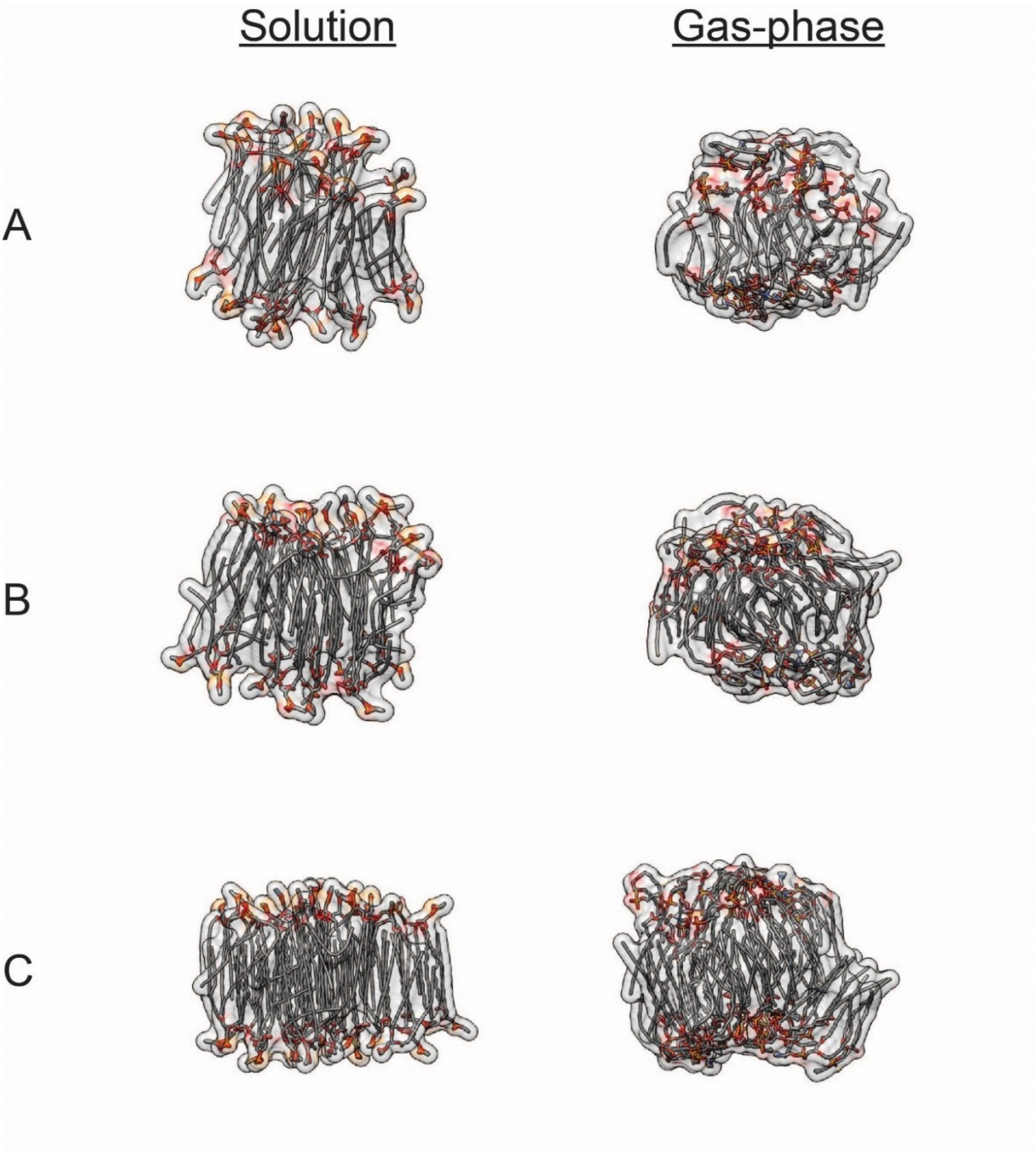

Figure 3.14 The averaged lipid conformations for POPC-PDs complexes from solution and gas-phase MD simulations – (a) (SapA dimer + 26POPC), (b) (SapA trimer + 33POPC) ion, and (c) (SapA tetramer + 42POPC). The gas-phase simulations were performed on the (a) (SapA dimer + 26POPC)$^{8+}$, (b) (SapA trimer + 33POPC)$^{12+}$ and (c) (SapA tetramer + 42POPC)$^{16+}$ ions.

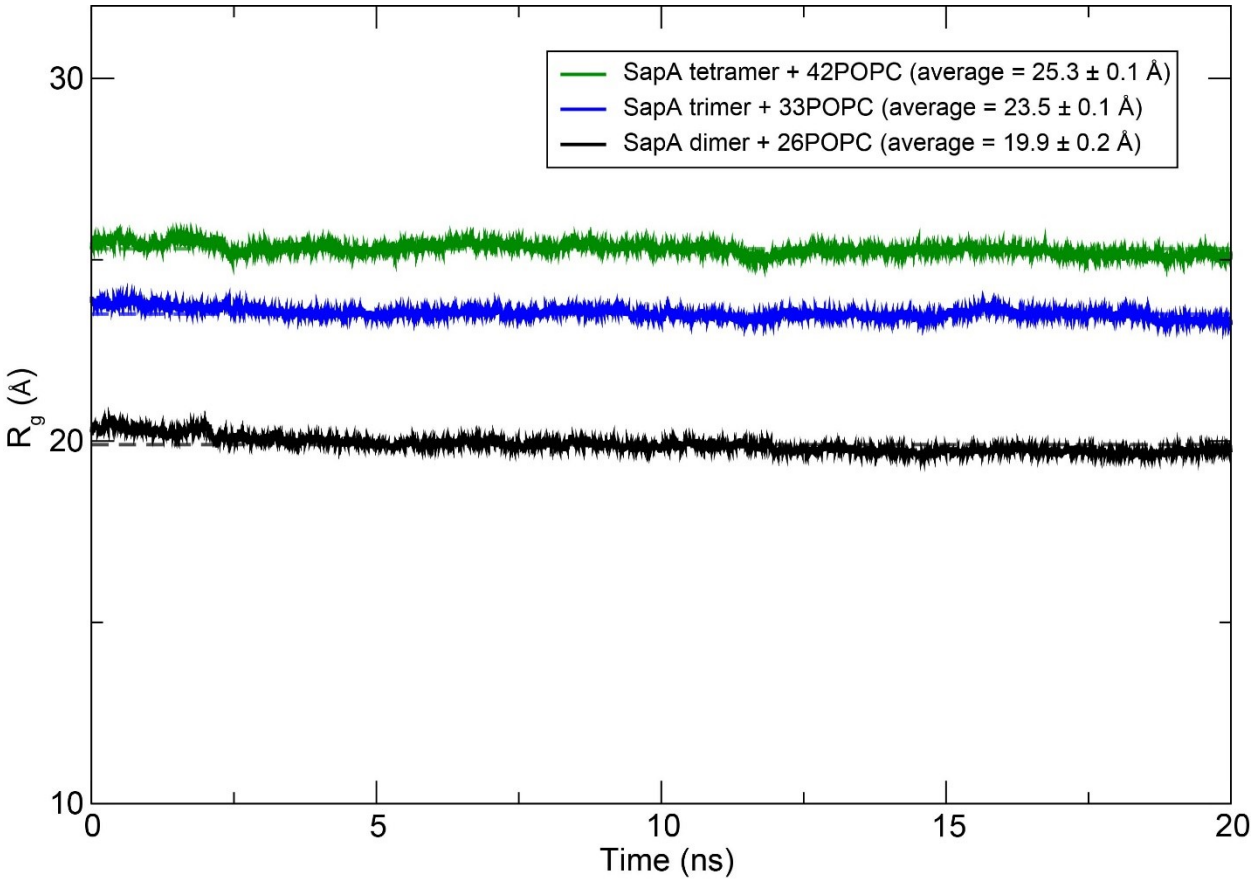

Figure 3.15 Radius of gyration (R_g) for the 20-ns gas-phase MD simulations. Results for the (SapA dimer + 26POPC)$^{8+}$ ion is shown in black, the (SapA trimer + 33POPC)$^{12+}$ ion is shown in blue, and the (SapA tetramer + 42POPC)$^{16+}$ ions is shown in green. The average R_g values, determined over the course of the simulations, are shown as dashed lines – (SapA dimer + 26POPC), R_g = 19.9 ± 0.2 Å; (SapA trimer + 33POPC), R_g = 23.5 ± 0.1 Å; and (SapA tetramer + 42POPC), R_g = 25.3 ± 0.1 Å.

3.4 Conclusions

The results of the first detailed investigation into the size and composition of POPC-PDs in neutral and acidic solution are reported. The ESI-MS and MALLS data acquired at pH 4.8 revealed that POPC-PDs consist predominantly of (SapA dimer + *i*POPC) complexes, where i = 23 to 29, and have an average MW of 38.2 ± 3.3 kDa and an average R_h of 31.0 ± 1.5 Å. In contrast, data acquired at pH 6.8 revealed that, in freshly prepared solutions, POPC-PDs exist predominantly as (SapA tetramer + *i*POPC) complexes, where i = 37 to 60, and have an average MW of 68.0 ± 2.7 kDa and an average R_h of 39.0 ± 0.2 Å. It was also found that the (SapA tetramer + *i*POPC) complexes convert, over a period of hours, to (SapA trimer + *i*POPC) complexes, with i = 29 to 36 and an average MW of 51.1 ± 2.9 kDa. At present, the mechanism underlying this conversion process is not understood and will be the focus of future study. The results of molecular modelling suggest spheroidal structures for the (SapA dimer + *i*POPC), (SapA trimer + *i*POPC) and (SapA tetramer + *i*POPC) complexes in solution. Comparison of experimentally determined **Ω** with values calculated for gaseous $(\text{SapA dimer} + 26\text{POPC})^{8+}$, $(\text{SapA trimer} + 33\text{POPC})^{12+}$ and $(\text{SapA tetramer} + 42\text{POPC})^{16+}$ ions produced from modelling suggests that the solution structures are largely preserved in the gas phase, although the lipids do not maintain regular bilayer orientations. Finally, it should be noted that the results of this study lay the foundation for future investigations into the structures of GL-loaded PDs and their use in GBP−GL interaction studies.

3.5 References

1. Malhotra, R. *Biochem. Anal. Biochem.* **2012**, *1*, 108.
2. Hakomori, S. *Curr. Opin. Hematol.* **2003**, *10*, 16−24.
3. Sharon, N.; Lis, H. *Sci. Am*. **1993**, *268*, 82−89.

4. Varki, A.; Cummings, R. D.; Esko, J. D.; Freeze, H. H.; Stanley, P.; Bertozzi, C. R.; Hart, G. W.; Etzler, M. E. *Essentials of Glycobiology*, 2nd ed.; Cold Spring Harbor Laboratory Press: Cold Spring Harbor, NY, 2009.

5. Lopez, H. H. H.; Schnaar, R. L. *Methods Enzymol*. **2006**, *417*, 205–220.

6. Feizi, T. *Ann. N.Y. Acad. Sci*. **2013**, *1292*, 33−44.

7. Grant, O. C.; Smith, H. M.; Firsova, D.; Fadda, E.; Woods, R. J. *Glycobiology* **2014**, *24*, 17−25.

8. Shi, J.; Yang, T.; Kataoka, S.; Zhang, Y.; Diaz, A. J.; Cremer, P. S. *J. Am. Chem. Soc*. **2007**, *129*, 5954−5961.

9. Jayaraman, N.; Maiti, K.; Naresh, K. *Chem. Soc. Rev*. **2013**, *42*, 4640 −4656.

10. Bayburt, T. H.; Grinkova, Y. V.; Sligar, S. G. *Nano Lett*. **2002**, *2*, 853−856.

11. Zhang, Y.; Liu, L.; Daneshfar, R.; Kitova, E. N.; Li, C.; Jia, F.; Cairo, C.W.; Klassen, J. S. *Anal. Chem.* **2012**, *84*, 7618−7621.

12. Leney, A. C.; Darestani, R. R.; Li, J.; Nikjah, S.; Kitova, E. N.; Zou, C.; Cairo, C. W.; Xiong, Z. J.; Privé, G. G.; Klassen, J. S. *Anal. Chem.* **2015**, *87*, 4402−4408.

13. Li, J.; Fan, X.; Kitova, E. N.; Zou, C.; Cairo, C. W.; Eugenio, L.; Ng, K. K. S.; Xiong, Z. J.; Privé, G. G.; Klassen, J. S. *Anal. Chem.* **2016**, *88*, 4742**–**4750.

14. Locatelli-Hoops, S.; Remmel, N.; Klingenstein, R.; Breiden, B.; Rossocha, M. Schoeniger, M.; Koenigs, C.; Saenger, W.; Sandhoff, K. *J. Biol. Chem*. **2006**, *281*, 32451.

15. Popovic, K.; Holyoake, J.; Pomès, R.; Privé, G. G. *Prot. Natl. Acad. Sci.* **2012**, *109*, 2908−2912.

16. Sun, J.; Kitova, E.N.; Wang, W.; Klassen, J. S. *Anal. Chem.* **2006**, *78*, 3010−3018.

17. Rose, R. J.; Damoc, E,; Denisov, E.; Makarov, A.; Heck, A. J. R. *Nat. Methods* **2012**, *9*,

1084−1086.

18. Rosati, S.; Rose, R. J.; Thompson, N. J.; Van Duijn, E.; Damoc, E.; Denisov, E.; Makarov, A.; Heck, A. J. *Angew. Chem. Int. Ed*. **2012**, *51*, 12992−12996.

19. Michalski, A.; Damoc, E.; Hauschild, J. P.; Lange, O.; Wieghaus, A.; Makarov, A.; Nagaraj, N.; Cox, J.; Mann, M.; Horning, S. *Mol. Cell. Proteomics*. **2011**, *10*, M111.011015.

20. Marty, M. T.; Baldwin, A. J.; Marklund, E. G.; Hochberg, G. K.; Benesch, J. L.; Robinson, C. V. *Anal. Chem.* **2015**, *87*, 4370–4376.

21. Bush, M. F.; Hall, Z.; Giles, K.; Hoyes, J.; Robinson, C. V.; Ruotolo, B. T. *Anal. Chem*. **2010**, *82*, 9557−9565.

22. Ruotolo, B. T.; Benesch, J. L. P.; Sandercock, A. M.; Hyung, S. J.; Robinson, C. V. *Nat. Protoc*. **2008**, *3*, 1139−1152.

23. Pettersen, E. F.; Goddard, T. D.; Huang, C. C.; Couch, G. S.; Greenblatt, D. M.; Meng, E. C.; Ferrin, T. E. *J. Comput. Chem.* **2004**, *25*, 1605–1612.

24. Balabin, I. Membrane Plugin, Version 1.1. http://www.ks.uiuc.edu/Research/vmd/plugins/membrane/ (accessed 11/21/2014).

25. Humphrey, W.; Dalke, A.; Schulten, K. *J. Mol. Graphics* **1996**, *14*, 33–38.

26. Case, D. A.; Darden, T. A.; Cheatham III, T. E.; Simmerling, C. L.; Wang, J.; Duke, R. E.; Luo, R.; Walker, R. C.; Zhang, W.; Merz, K. M.; Roberts, B.; Hayik, S.; Roitberg, A.; Seabra, G.; Swails, J.; Götz, A. W.; Kolossváry, I.; Wong, K. F.; Paesani, F.; Vanicek, J.; Wolf, R. M.; Liu, J.; Wu, X.; Brozell, S. R.; Steinbrecher, T.; Gohlke, H.; Cai, Q.; Ye, X.; Wang, J.; Hsieh, M.-J.; Cui, G.; Roe, D. R.; Mathews, D. H.; Seetin, M. G.; Salomon-Ferrer, R.; Sagui, C.; Babin, V.; Luchko, T.; Gusarov, S.; Kovalenko, A.;

Kollman, P. A. AMBER 12, University of California: San Fancisco, CA, 2012.

27. Jorgensen, W. L.; Chandrasekhar, J.; Madura, J. D.; Impey, R. W.; Klein, M. L. *J. Chem. Phys.* **1983**, *79*, 926–935.

28. Duan, Y.; Wu, C.; Chowdhury, S.; Lee, M. C.; Xiong, G.; Zhang, W.; Yang, R.; Cieplak, P.; Luo, R.; Lee, T.; Caldwell, J.; Wang, J.; Kollman, P. *J. Comput. Chem*. **2003**, *24*, 1999−2012.

29. Skjevik, Å. A.; Madej, B. D.; Walker, R. C.; Teigen, K. *J. Phys. Chem. B* **2012**, *116*, 11124−11136.

30. Berendsen, H. J. C.; Postma, J. P. M.; Gunsteren, W. F. v.; DiNola, A.; Haak, J. R. *J. Chem. Phys*. **1984**, *81*, 3684–3690.

31. Ryckaert, J.-P.; Ciccotti, G.; Berendsen, H. J. C. *J. Comput. Phys*. **1977**, *23*, 327–341.

32. Contributors to Amber. http://ambermd.org/contributors.html (accessed 1/26/2016).

33. Larriba, C.; Hogan, C. J. Jr. *J. Phys. Chem. A* **2013**, *117*, 3887–3901.

34. Antonietti, M.; Bremser, W.; Schmidt, M. *Macromolecules* **1990**, *23*, 3796−3805.

35. Tande, B. M.; Wagner, N. J.; Mackay, M. E.; Hawker, C. J.; Jeong, M. *Macromolecules* **2001**, *34*, 8580−8585.

Chapter 4

Detecting Protein–Glycolipid Interactions using CaR-ESI-MS and Model Membranes. Comparison of Pre- and Passively-loaded Picodiscs[‡]

4.1 Introduction

Many important cellular processes, such as recognition, signaling, development and differentiation, as well as bacterial and viral infections, rely on non-covalent interactions between glycan-binding proteins (GBPs) and glycolipid (GL) ligands.[1,2] Most GLs found in animals are glycosphingolipids, wherein the carbohydrate (mono- or oligosaccharide) is attached to a ceramide lipid moiety.[2] The ceramide imbeds in the cell membrane, leaving the carbohydrate exposed to aqueous solution and available for binding to GBPs. Although the carbohydrate moiety is primarily responsible for recognition, it is known that the membrane can influence GBP interactions with GLs.[3,4] For example, the bilayer serves to orient the GLs and enables them to cluster, which can lead to a strengthening (due to avidity) or weakening (due to steric effects) of the GBP interactions.[5,6] The presence of other membrane components, such as cholesterol, may also affect the strength of GBP binding.[7]

GL interactions with water soluble GBPs can be studied under native-like conditions using model membranes (MMs), such as supported lipid bilayers, liposomes, nanodiscs (NDs), which are discoidal phospholipid bilayers surrounded by two copies of a membrane scaffold protein (MSP), and picodiscs (PDs) which are lipid-transporting macromolecular complexes composed of

[‡] A version of this chapter has been published: Li, J.; Han, L.; Li, J. N.; Kitova, E. N.; Xiong, Z. J.; Privé, G. G.; Klassen, J. S. *J. Am. Soc. Mass. Spectrom*. **2018**, *29,* 1493-1504.

human sphingolipid activator protein saposin A (SapA) and lipids.[5,8-12] The GBP interactions with GLs can be detected by a variety of methods, including fluorescence, surface plasmon resonance and nuclear magnetic resonance spectroscopy, quartz crystal microbalance or flow cytometry.[5,6,13-15] Recently, catch-and-release electrospray ionization mass spectrometry (CaR-ESI-MS) has emerged as a promising method for screening GLs against GBPs.[10,12,16,17] Briefly, the assay involves incubating GBPs with GL-containing NDs or PDs, in aqueous solution. The GBP interactions with GLs (imbedded in the MM) are then detected by transferring the intact GBP–GL–MM complexes to the gas phase using ESI. After desolvation, the GBP–GL complexes spontaneously release from the MM ions and can be detected by MS. To facilitate the identification of the GL ligands, the GBP–GL complexes are collisionally-activated in order to release the GL (as ions), which are subsequently analyzed by ion mobility separation (IMS), collision-induced dissociation (CID) and MS.[10] While both NDs and PDs have been used to detect moderate-to-high affinity GBP–GL interactions by CaR-ESI-MS, PDs have been shown to be superior for detecting low affinity ($\leq 10^3$ M^{-1}) interactions.[16,17]

One of the outstanding challenges to using NDs and PDs as GL arrays for screening, particularly when produced from GL/lipid mixtures extracted from cell culture or tissue, is the non-uniform incorporation efficiencies of the various GLs present in the mixture. For example, PDs are typically formed by incubating SapA with liposomes, formed from GL/phospholipid mixtures, followed by purification using size exclusion chromatography.[12,17] If the GLs present in the mixture have different incorporation efficiencies, the composition of the "pre-loaded" PDs will not quantitatively reflect the original composition of the mixture and, in cases of low incorporation efficiencies, this could result in false negative binding results.

It is known that phospholipids can spontaneously transfer between organized lipid membrane assemblies (e.g., micelles or lipid bilayers), on timescales ranging from hours (h) to days (d).[18-20] Lipid exchange is thought to occur either through a lipid monomer diffusion model, whereby lipid monomers partition between the lipid assemblies and aqueous solution and, through diffusion, are taken up by other lipid assemblies, or a collision model, whereby a collision complex forms between different lipid assemblies and allowing for lipid diffusion within the complex.[19-21] Moreover, it has been shown that lipids and GLs are rapidly exchanged, on the timescale of minutes (min), between NDs and PDs and that SapA can efficiently transfer GLs from liposomes to proteins.[22-24] Therefore, it may be possible to mitigate, at least to some extent, the deleterious effects of non-uniform GL incorporation efficiencies using spontaneous GL transfer from micelles to pre-formed, phospholipid PDs to alter their composition and enhance their utility for GL screening.

Here, we compare the use of conventional, pre-loaded PDs, prepared from a mixture of purified GL and phospholipid or lipids extracted from tissue, with passively-loaded PDs (^{PL}PDs), prepared by incubating phospholipid PDs with GLs (in the form of GL micelles)[25] in aqueous solution, for CaR-ESI-MS screening of GLs against cholera toxin B subunit homopentamer (CTB_5). The results were compared with CTB_5 binding data acquired for pre-loaded PDs, prepared directly from the GL/lipid mixtures to assess the performance of the ^{PL}PDs for GL screening. A small number of comparative measurements were also performed on pre- and passively-loaded NDs.

4.2 Experimental Section

4.2.1 Proteins

CTB5, SapA and recombinant MSP were expressed and purified as previously described,[9,11] and detailed information provided in Chapter 2, section 2.2.1.

4.2.2 Lipids and oligosaccharides

The gangliosides GM1, GM2, GM3, GD1a, GD1b, GT1b, GD2 and phospholipid POPC were used for this study and the detailed information on their structures, MWs and sources were provided in Chapter 2, section 2.2.2. The phospholipid 1,2-dimyristoyl-sn-glycero-3-phosphocholine (DMPC, MW 677.9 Da) and pig brain GL extract were purchased from Avanti Polar Lipids Inc. (Alabaster, AL). The structures of the phospholipids and the gangliosides used in this are shown in Figure 4.1.

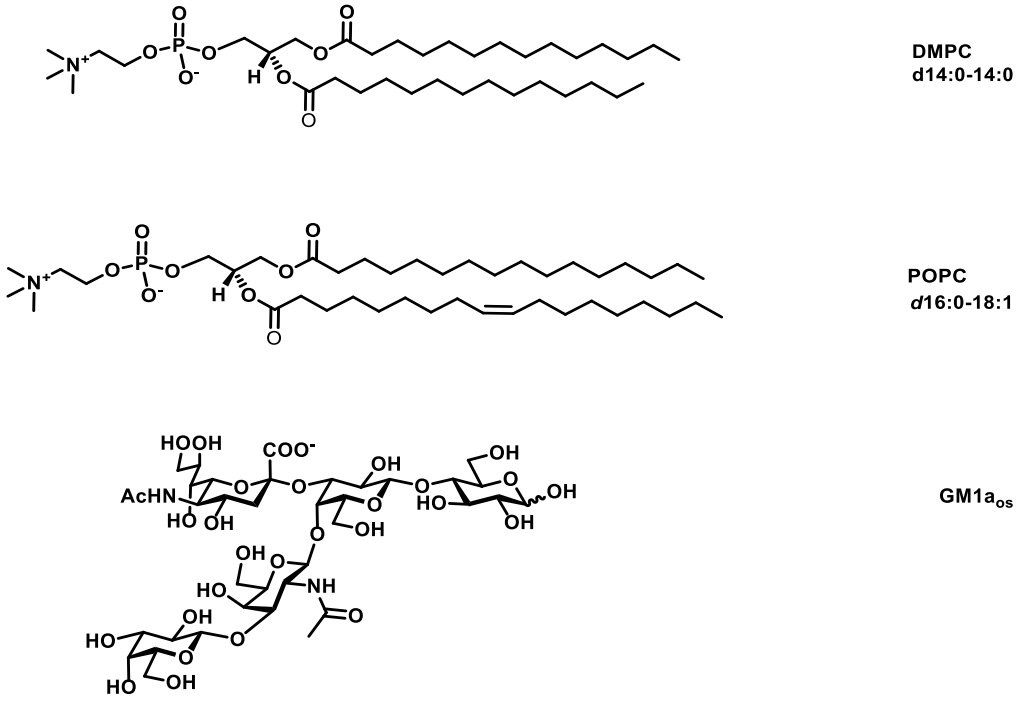

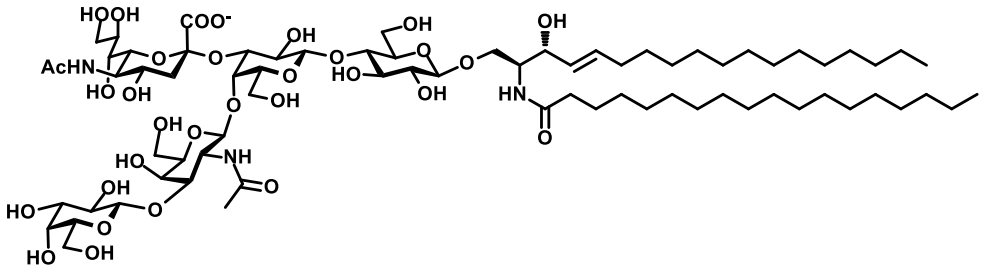

*d*18:1-18:0

GM1a

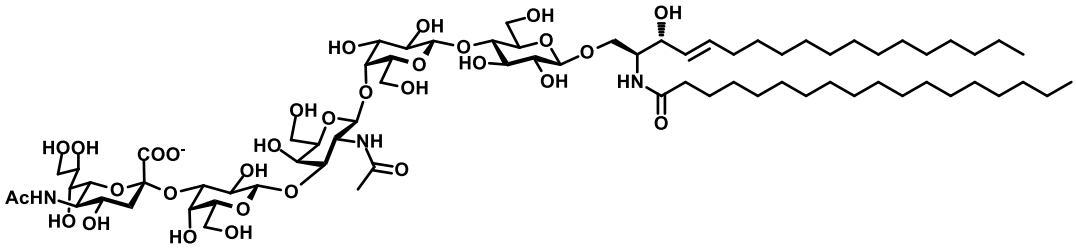

*d*18:1-18:0

GM1b

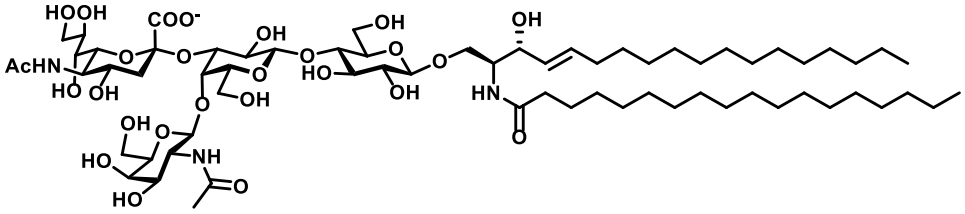

*d*18:1-18:0

GM2

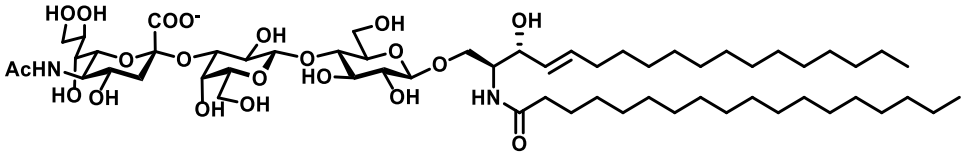

*d*18:1-18:0

GM3

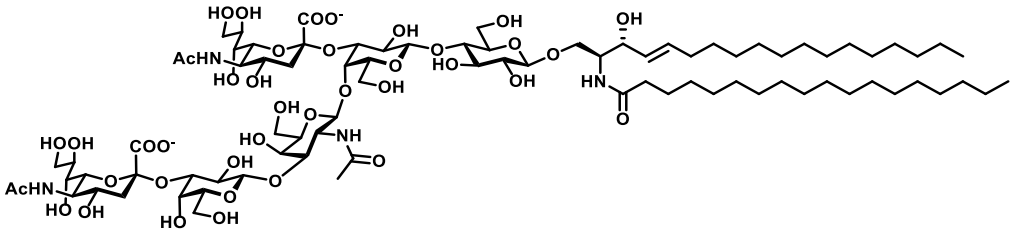

*d*18:1-18:0

GD1a

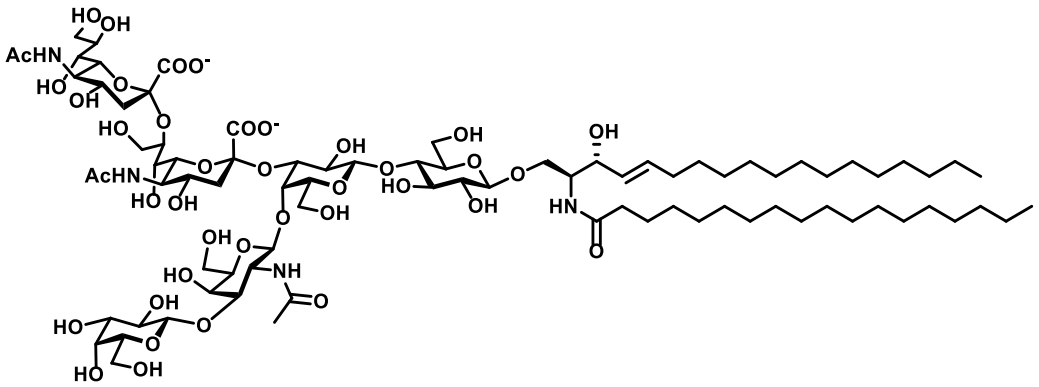

*d*18:1-18:0

GD1b

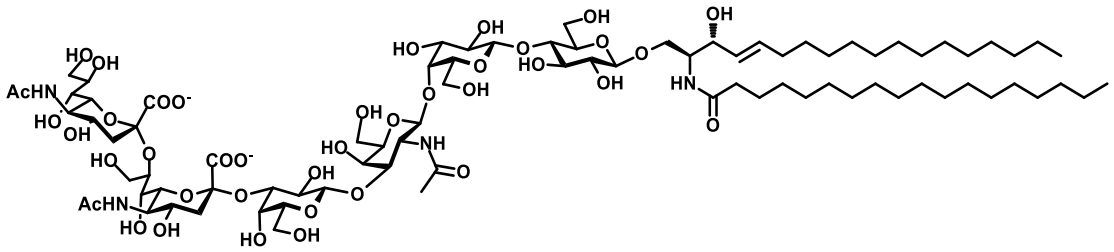

*d*18:1-18:0

GD1c

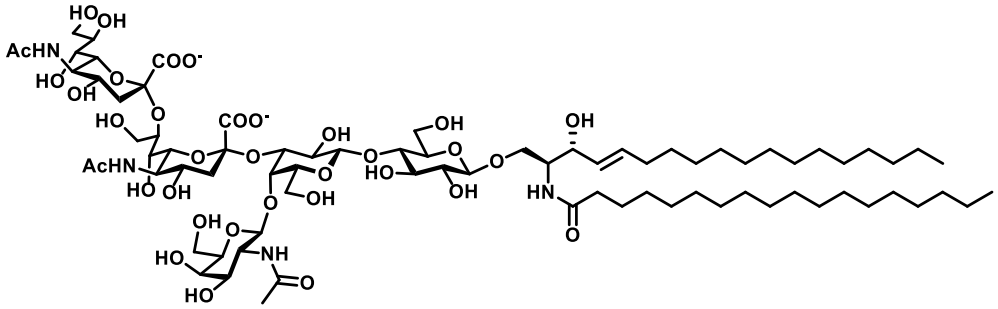

*d*18:1-18:0

GD2

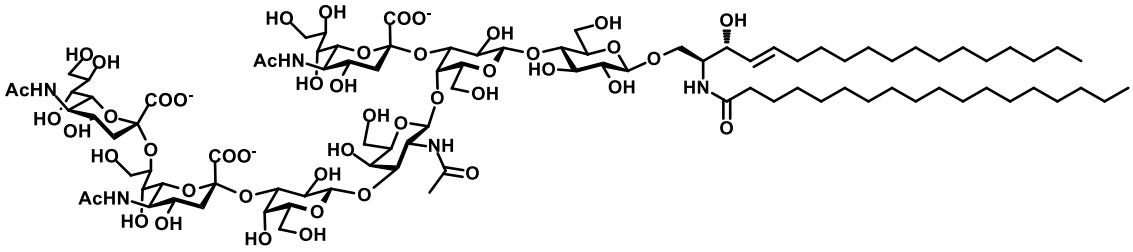

*d*18:1-18:0

GT1a

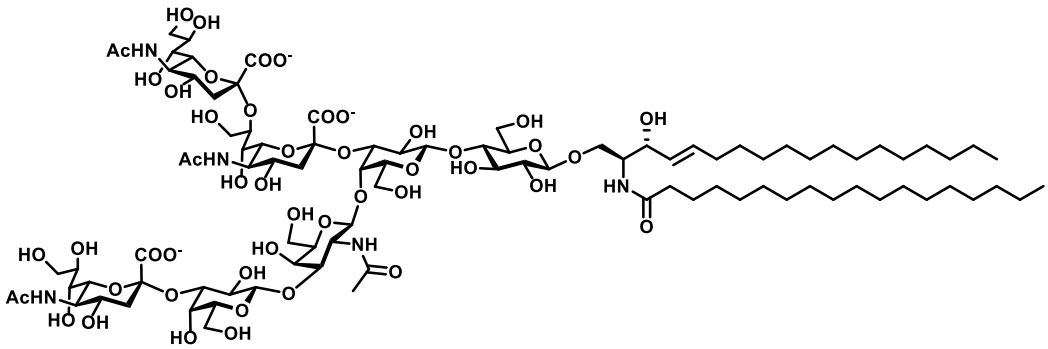

*d*18:1-18:0

GT1b

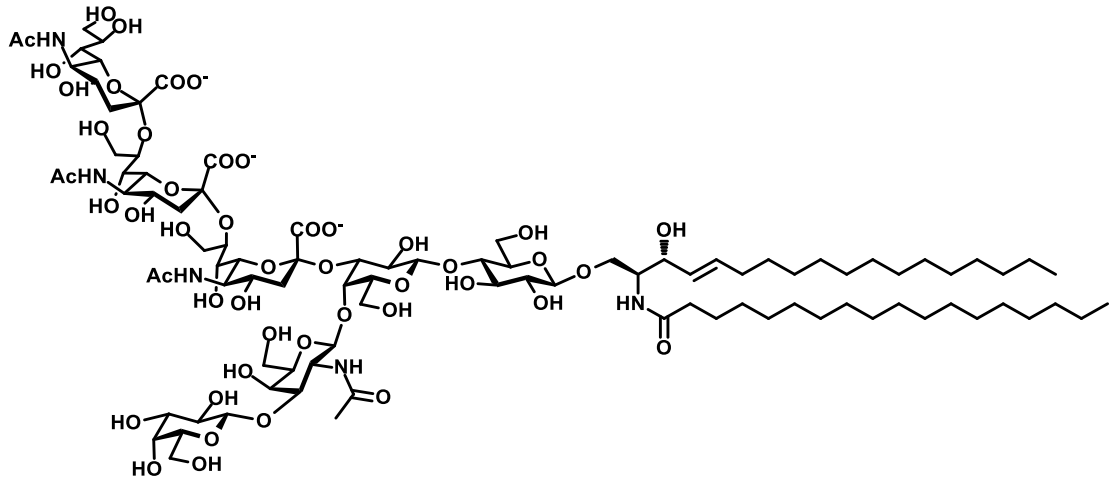

*d*18:1-18:0

GT1c

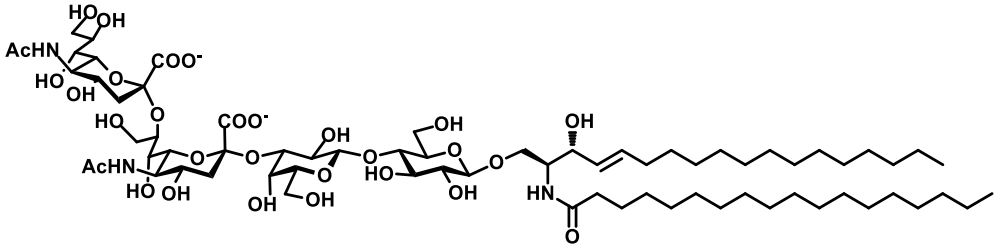

*d*18:1-18:0

GD3

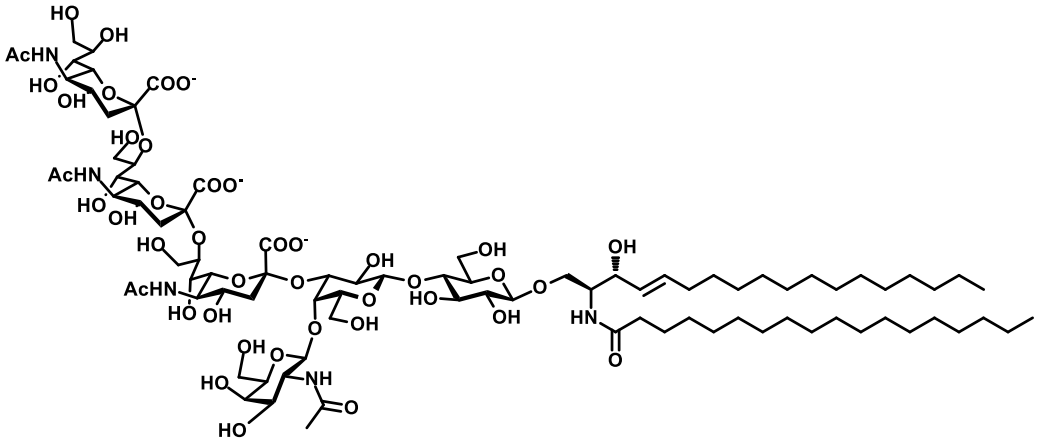

*d*18:1-18:0

GT2

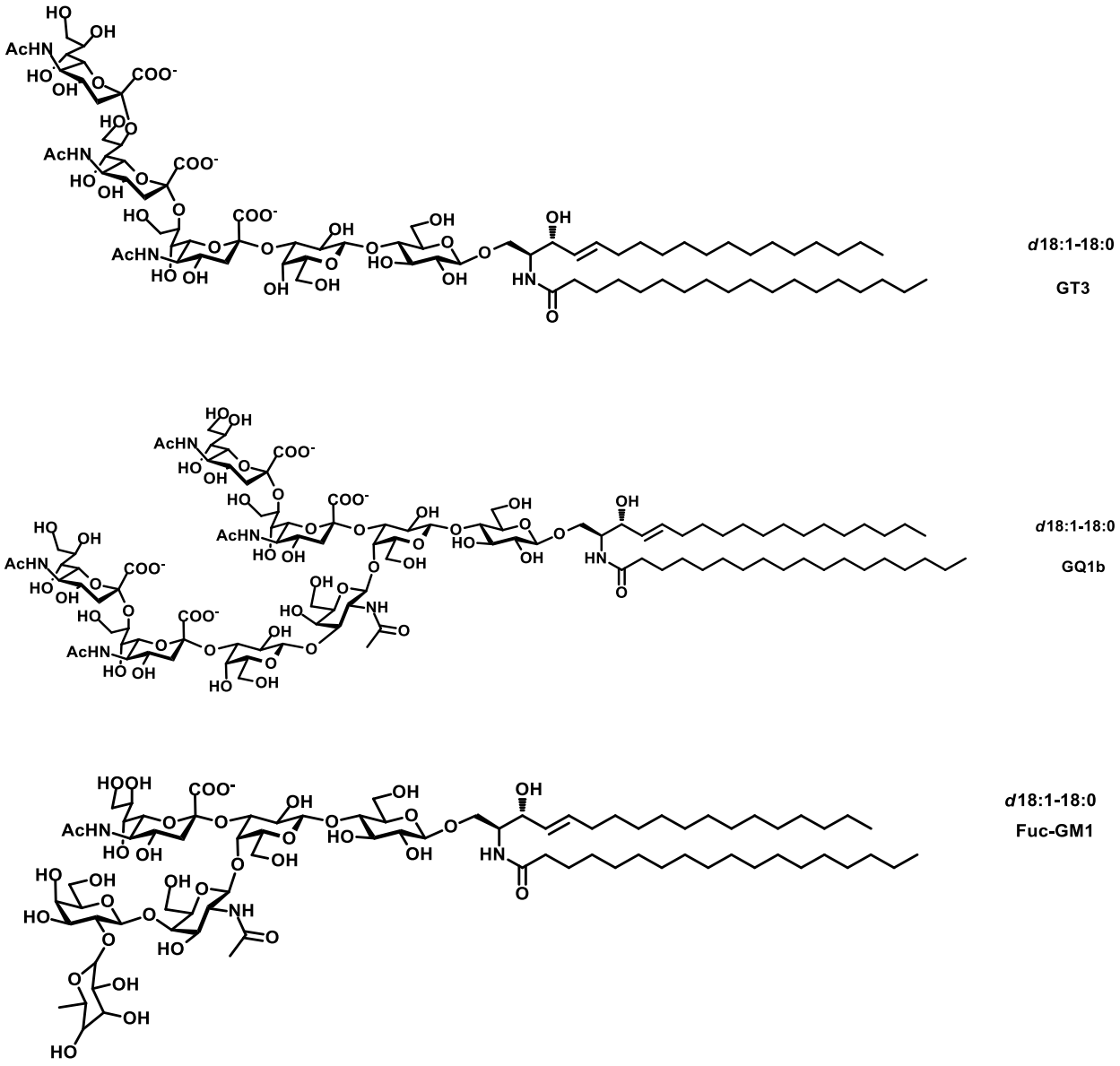

Figure 4.1 Structures of the phospholipids DMPC and POPC, the gangliosides GM1a, GM1b, GM2, GM3, GD1a, GD1b, GD1c, GD2, GT1a, GT1b, GT1c, GD3, GT2, GT3, GQ1b and Fuc-GM1 and the GM1a pentasaccharide ($GM1_{aos} \equiv GM1_{os}$).

4.2.3 Mouse brain glycolipids extraction

Mouse brain (US origin CD-1) was purchased from Cedarlane Laboratories (Burlington, Canada) and stored at -80 °C until used. The procedure for extracting the GLs was described previously.[26] Briefly, the whole brain was weighed, thawed on ice, and added to 4 volumes of ice-cold water and homogenized. Methanol was added to give a methanol/water volume ratio of 8:3, and the mixture vortexed and brought to room temperature. Chloroform was added to give a chloroform/methanol/water volume ratio of 4:8:3. The suspension was further mixed and centrifuged at room temperature for 15 min. The supernatant was transferred, measured, mixed with 0.173 volumes of water, and separated by centrifugation again. The supernatant was collected and loaded onto a pre-washed tC18 Sep-Pak. The GLs were eluted with methanol, which was then evaporated under a stream of nitrogen; the GLs were then re-dissolved in methanol.

4.2.4 Glycolipid micelle preparation

Ganglioside (or GL/lipid mixture), dissolved in 1:1 volume ratio of methanol/chloroform, was dried using nitrogen and kept in a vacuum desiccator overnight at room temperature to form a lipid film. The film was then re-dissolved in 200 mM aqueous ammonium acetate (pH 6.8, 25 °C), vortexed for 5 min and sonicated for 30 min.[25,27] The micellar solution was stored at room temperature until used.

4.2.5 Picodisc preparation

PDs composed of POPC (POPC-PDs), DMPC (DMPC-PDs), POPC and GM1 (GM1-containing POPC-PDs), POPC and library of 7 gangliosides (≡7G library - GM1, GM2, GM3, GD1a, GD1b, GD2 and GT1b) and POPC with GL extracts from pig or mouse brain were prepared using a

protocol described by Popovic and co-workers[11] and a detailed description was provided in Chapter 2, section 2.2.4. The PD concentration was determined from the concentration of SapA, assuming that the PDs contain predominantly (at time of preparation) four copies of SapA.[28] For the GM1-containing PDs, the GM1 content was measured using ESI-MS and a stable isotope labeled internal standard approach described elsewhere.[29] The PDs were concentrated to 40 μM and stored at room temperature until needed.

4.2.6 Nanodisc preparation

NDs composed of POPC (POPC-NDs), DMPC (DMPC-NDs) or POPC and GM1 (5% GM1-containing POPC-NDs), were prepared following a protocol described by Bayburt and co-workers.[9,30] and a detailed description was given in Chapter 2, section 2.2.5. For the GM1-containing NDs, the GM1 content was determined using ESI-MS and a stable isotope labeled internal standard.[29] The NDs were concentrated to 60 μM and stored at -80 °C until needed.

4.2.7 Mass spectrometry

The ESI-MS and CaR-ESI-MS measurements were carried out using a Synapt G2-S with a detailed description given in Chapter 2, section 2.2.6.

4.2.7.1 Direct ESI-MS assay

The direct ESI-MS assay was used to measure the extent of GL binding to CTB_5. The GBP possesses five equivalent ganglioside binding sites.[31] In the case of GM1 and GM1 pentasaccharide (β-D-Gal-(1→3)-β-D-GalNAc-(1→4)-[α-D-Neu5Ac-(2→3)]-β-D-Gal-(1→4)-D-Glc, $GM1_{os}$, Figure 4.1), stepwise binding is known to exhibit positive cooperativity with

apparent association constants (for $GM1_{os}$) ranging from 2×10^6 to 2×10^7 M^{-1}.[31] As described elsewhere,[25] the fraction (*f*) of CTB_5 ligand binding sites that are occupied can be determined from the abundances (*Ab*) of ligand (L)-bound and free CTB_5 ions measured by ESI-MS, eq 4.1:

$$f = \frac{\sum_{q=1}^{5} q \cdot Ab(\mathrm{CTB_5L}_q)}{5\left(Ab(\mathrm{CTB_5}) + \sum_{q=1}^{5} Ab(\mathrm{CTB_5L}_q) \right)} \tag{4.1}$$

where *q* is the number of L bound.

4.2.7.2 CaR-ESI-MS assay

The details description of the CaR-ESI-MS measurements was provided in Chapter 2, section 2.2.6.1. For the IMS measurements, a wave height of 40 V and a wave velocity of 650 m s^{-1} were used and the helium and nitrogen gas flow rates were 50 mL min^{-1} and 60 mL min^{-1}, respectively.

4.3 Results and Discussion

4.3.1 CTB_5 binding to GM1 in pre-loaded picodiscs and nanodiscs and glycomicelles

As a starting point for the present study, the binding of CTB_5 with the high affinity ganglioside ligand GM1 in aqueous solution (in the form of glycomicelles)[25] or introduced into PDs and NDs was investigated. Shown in Figure 4.2a is a representative ESI mass spectrum acquired in positive mode for an aqueous ammonium acetate solution (200 mM, pH 6.8, 25 °C) of CTB_5 (6 μM) and GM1 (40 μM). Notably, only free CTB_5 ions, i.e., CTB_5^{n+} at $n = 14 – 16$, were detected under these conditions; this is in striking contrast to the, essentially, complete occupancy of CTB_5 binding sites expected for $GM1_{os}$ when present in solution at the same concentration.[31] The absence of any detectable GM1-bound CTB_5 ions produced directly from the solution of GM1 micelle is

consistent with the findings of a recent study, which showed that the detection of CTB_5-GM1 interactions by ESI-MS using glycomicelles requires higher GM1 concentrations.[25]

Representative mass spectra measured for aqueous ammonium acetate solutions (200 mM, pH 6.8, 25 °C) of CTB_5 (6 μM) with GM1-containing POPC-PDs and GM1-containing POPC-NDs are shown in Figures 4.2b and 4.2c, respectively. The total GM1 concentration was 40 μM in both cases and the average number of GM1 per PD was 8.32 ± 0.48 and 5.70 ± 0.20 per ND. When CTB_5 was incubated with the PDs, signal corresponding predominantly to CTB_5 bound to three to five GM1 was detected, i.e., $(CTB_5 + qGM1)^{n+}$ with $q = 3 – 5$ and $n = 15 – 17$ (Figure 4.2b). The significant background observed from *m/z* 3500 to *m/z* 4500 is attributed to PD ions containing variable numbers of SapA and phospholipid, over a range of charge states.[28] As described elsewhere, it is possible to separate the $(CTB_5 + qGM1)^{n+}$ ions from the PD ions, based on differences in their IMS arrival times.[12,17] However, the distributions of $(CTB_5 + qGM1)$ species determined from the mass spectra acquired using IMS filtering (to remove the contribution of PD ions) are similar to those obtained by simply performing background subtraction. For example, the relative abundances of the $(CTB_5 + qGM1)$ species, with $q = 3$, 4 and 5, determined from the mass spectrum shown in Figure 4.2b after background subtraction are 0.03, 0.35 and 0.62, respectively and 0.04, 0.38 and 0.58, respectively, after IMS filtering (Figure 4.2b, insets). Because IMS filtering provided no significant advantage over background subtraction, only the latter approach was used for the determination of the relative abundances of the $(CTB_5 + qGM1)$ species from solutions containing PDs. The ESI-MS results obtained for the solution of CTB_5 incubated with NDs are qualitatively similar to those obtained for the solution containing PDs - ions corresponding to CTB_5 bound to between three and five GM1 were observed (Figure 4.2c). In this

case, there was no overlap between the $(CTB_5 + qGM1)^{n+}$ and ND ions and, consequently, no IMS filtering or background subtraction was needed.

The normalized distributions of $(CTB_5 + qGM1)$ species determined from the mass spectra described above, and the distribution expected for $GM1_{os}$ under the same conditions, are shown in Figure 4.2d. From this plot it can be seen that, when GM1 is present in PDs, the binding site occupancy is slightly higher than observed with NDs, but does not reach the near-complete occupancy achieved with $GM1_{os}$.[31] For ease of comparison, these distributions can be converted into the fraction (f) of CTB_5 binding sites that are occupied. For $GM1_{os}$, f is ~1.0; for GM1 in aqueous solution, is f ~0 (i.e., no detectable complexes). For GM1-containing PDs and NDs, f is 0.90 and 0.87, respectively.

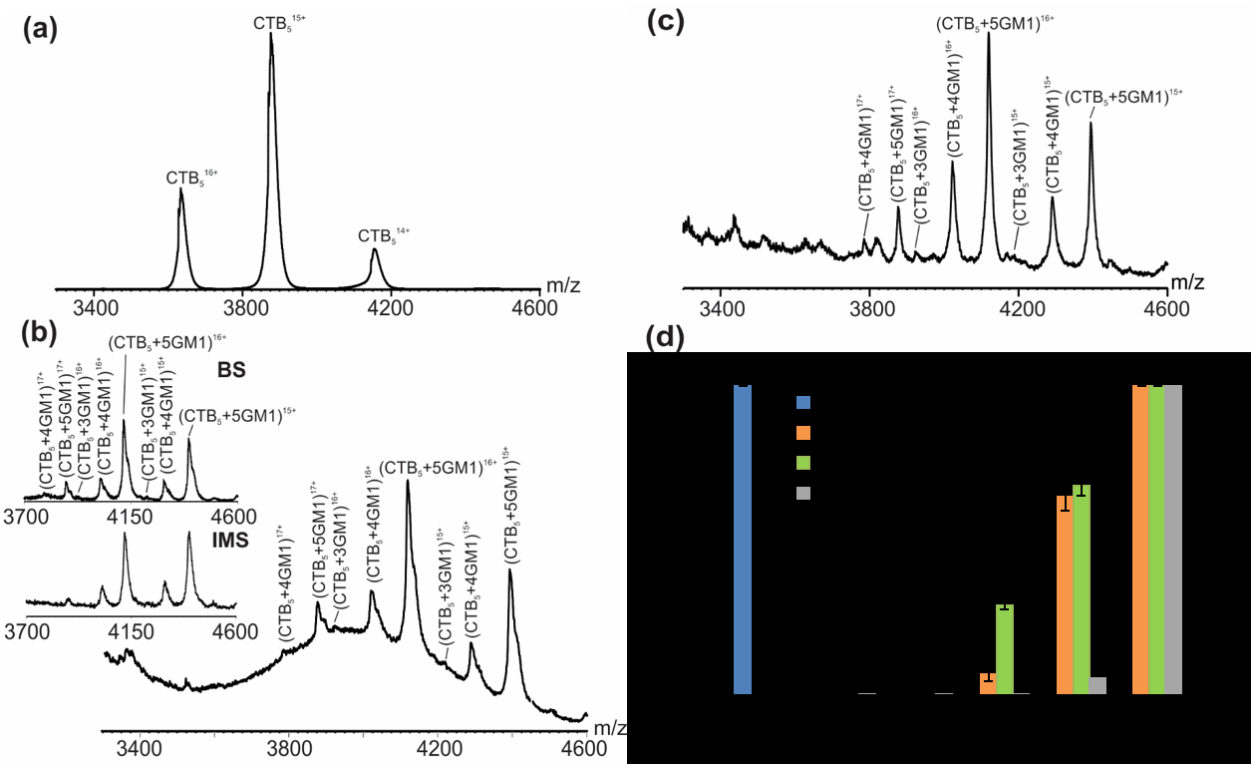

Figure 4.2 ESI mass spectra acquired in positive ion mode for aqueous ammonium acetate solutions (200 mM, pH 6.8, 22 °C) of CTB_5 (6 μM) with (a) GM1 (40 μM), (b) GM1-containing POPC-PDs (40 μM GM1) and (c) GM1-containing POPC-NDs (40 μM GM1). The two inserts shown in (b) correspond to the mass spectrum after background subtraction (BS) or IMS filtering (IMS). (d) Normalized distributions of free and GM1-bound CTB_5 – experimental distributions measured for solutions described in (a), (b) and (c) are shown in blue (■), orange (■) and green (■), respectively; theoretical distribution shown in gray (■) was calculated using association constants reported in reference 31 for the stepwise binding of $GM1_{os}$ to CTB_5. The error bars correspond to one standard deviation.

4.3.2 Comparison of CTB_5 binding to GM1 in pre- and passively-loaded PDs

To test the feasibility of preparing GM1-containing PDs from phospholipid-PDs and GM1 glycomicelles, POPC-PDs (12.5 μM) were incubated in aqueous ammonium acetate solutions (200 mM, pH 6.8, 25 °C) of GM1 (50 μM) at room temperature for 5 min, 4 h, 2.5 d, 7 d, 10 d, 14 d, 17 d, and 20 d. Following incubation, an aliquot of solution was removed and the PDs analyzed for GM1 content (Figure 4.3). The solution was then mixed with CTB_5 (final concentrations: 6 μM CTB_5, 10 μM POPC-PD and 40 μM GM1) and the extent of GM1 binding measured (Figure 4.4).

To monitor GM1 incorporation into the POPC-PDs (as a function of incubation time), CID was performed in negative ion mode on ions with *m/z* values of 6100 (±100). As controls, measurements were also performed, using identical conditions, on ions produced from solutions containing only GM1 or POPC-PDs. As can be seen from the ESI mass spectra shown in Figure 4.3, the *m/z* of the GM1 micelle ions (approximately *m/z* 8000 to *m/z* 12000) are larger than those of the PDs (approximately *m/z* 4500 to *m/z* 7000). In the absence of POPC-PDs, CID of ions at *m/z* 6100 (±100) produced no GM1 ions (Figures 4.3a and 4.3k), while in the absence of GM1, CID of the POPC-PD ions produced only free and POPC-bound SapA ions (Figures 4.3b and 4.3l). Following 5 min incubation of the PDs with the GM1 glycomicelles, GM1 ions were detected in the CID mass spectra (Figures 4.3c and 4.3m). With increasing incubation time the abundance of the GM1 ions, relative to free and POPC-bound SapA ions, increased and, at incubation times of ≥10 d, they were the most abundant ions in the CID mass spectra (Figures 4.3d-4.3j and 4.3n-4.3t). Taken together, these results suggest that incubation of POPC-PDs with GM1 glycomicelles results in the spontaneous transfer of GM1 to the PDs and that the amount of GM1 incorporated increases with incubation time (up to ~10 d).

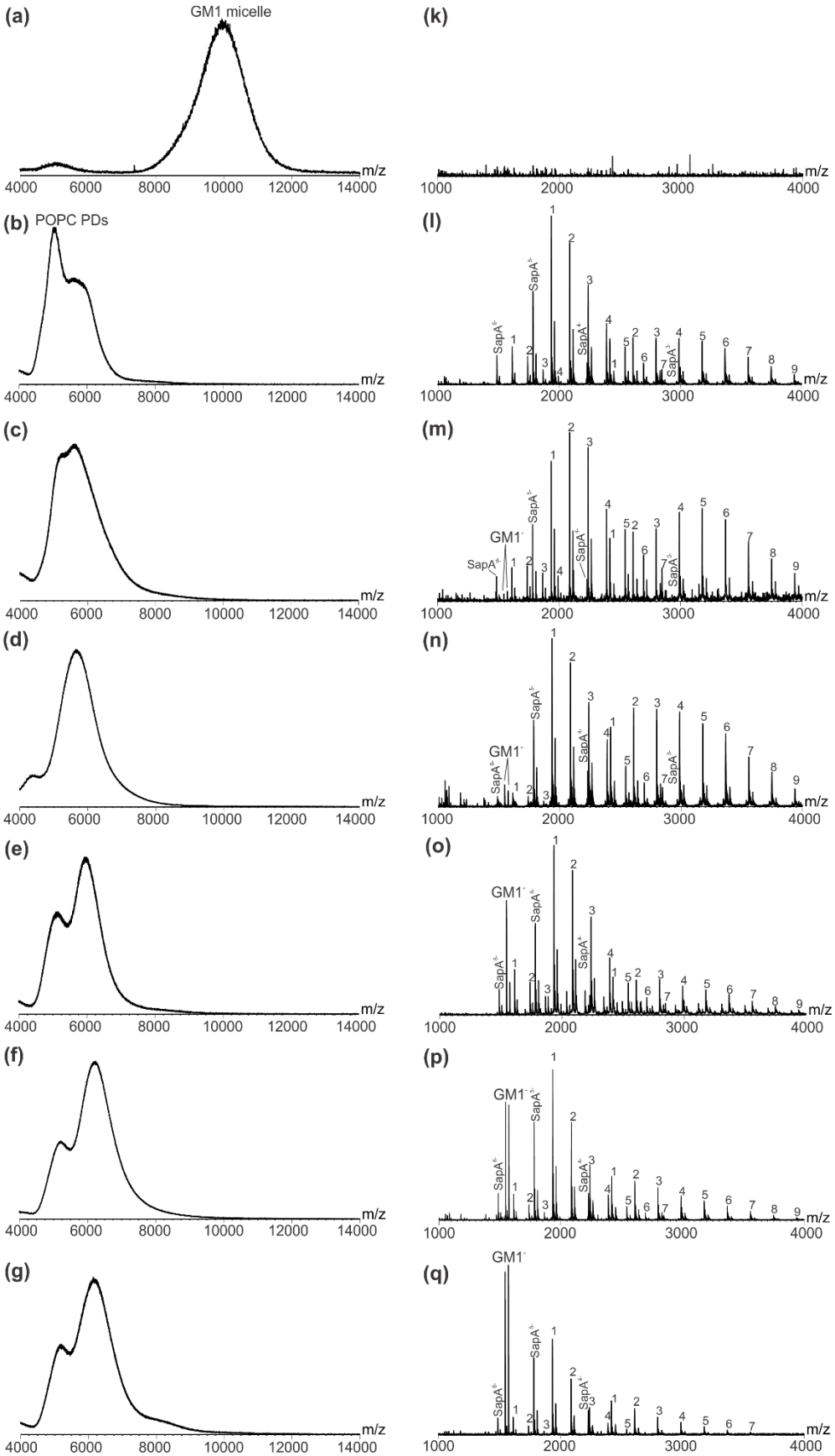
(a)
GM1 micelle
(b) POPC PDs
(c)
(d)
(e)
(f)
(g)
(k)
(l)
(m)
(n)
(o)
(p)
(q)
m/z
4000 6000 8000 10000 12000 14000
1000 2000 3000 4000
GM1-
SapA-
SapA+

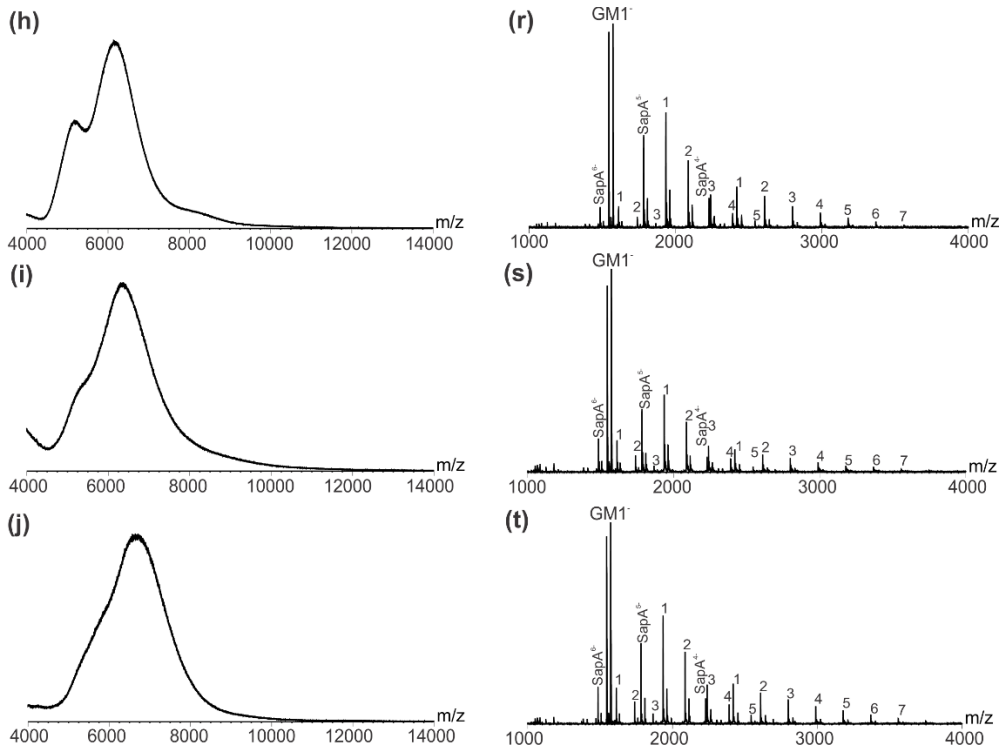

Figure 4.3 ESI mass spectra acquired in negative ion mode for aqueous ammonium acetate solutions (200 mM, pH 6.8, 22 °C) of (a) GM1 (50 μM) and (b) POPC-PDs (12.5 μM) alone or incubated with GM1 (50 μM) for (c) 5 min, (d) 4 h, (e) 2.5 d. (f) 7 d, (g) 10 d, (h) 14 d, (i) 17 d or (j) 20 d. (k) ~ (t) CID mass spectra measured for ions centered at *m/z* 6100 and produced from the solutions described in (a) ~ (j), respectively, in the Trap region (75 V). Peaks labeled as numbers (= i) correspond to $(SapA + iPOPC)^{6-/5-/4-}$ ions.

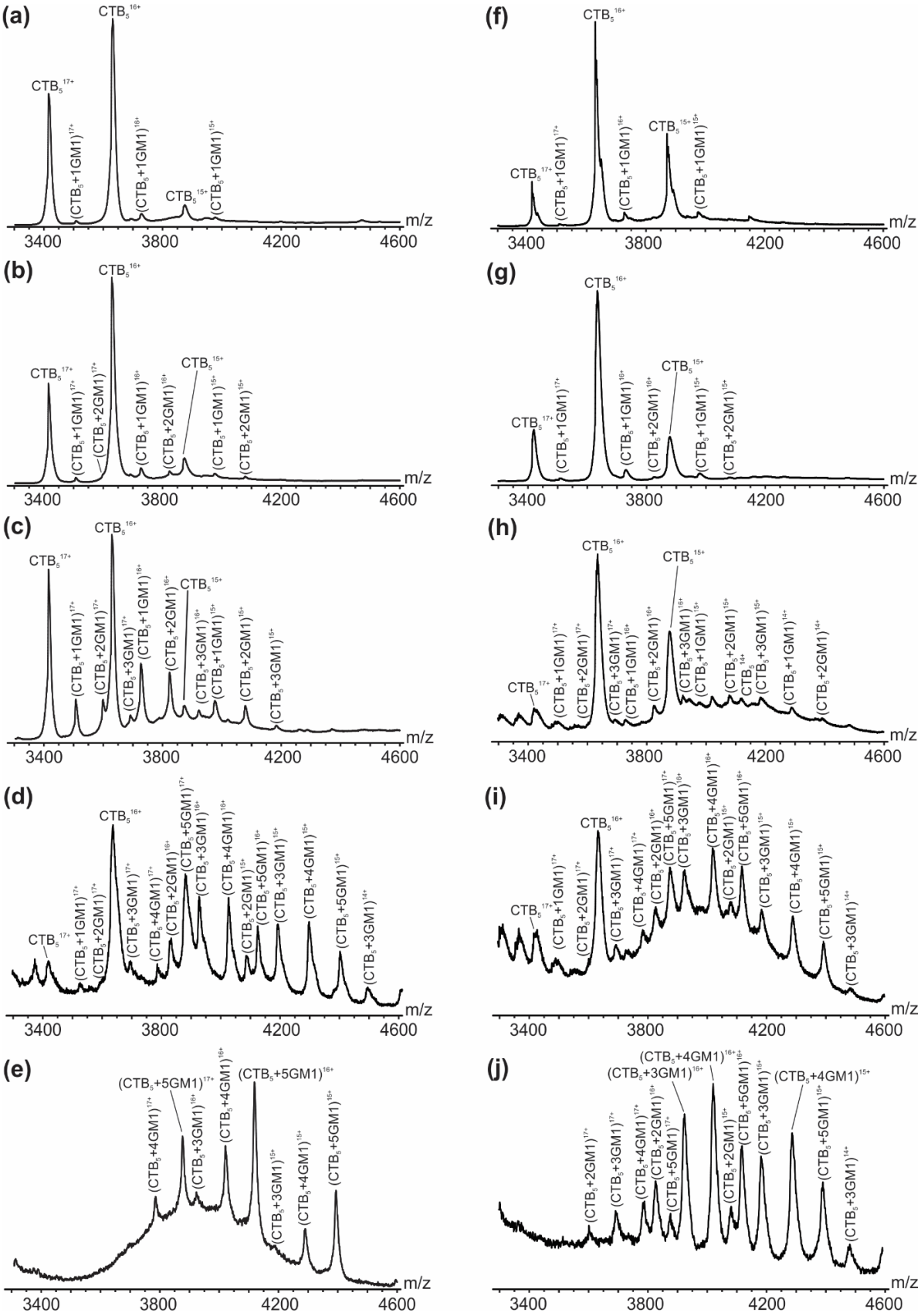
(a)
(b)
(c)
(d)
(e)
(f)
(g)
(h)
(i)
(j)
m/z
3400
3800
4200
4600

Figure 4.4 ESI mass spectra acquired in positive ion mode for aqueous ammonium acetate solutions (200 mM, pH 6.8, 22 °C) of CTB_5 (6 μM) with ^{PL}PDs (10 μM) produced by incubating GM1 (40 μM) and POPC-PDs (10 μM) for (a) 5 min, (b) 4 h, (c) 2.5 d, (d) 7 d or (e) 10 d. ESI mass spectra acquired in positive ion mode for aqueous ammonium acetate solutions (200 mM, pH 6.8, 22 °C) of CTB_5 (6 μM) with ^{PL}PDs (10 μM) produced by incubating GM1 (40 μM) and DMPC-PDs (10 μM) for (f) 5 min, (g) 4 h, (h) 2.5 d, (i) 7 d or (j) 10 d.

Analysis of the solution of CTB_5 and the 5 min ^{PL}PD revealed abundant free CTB_5 ions, as well as a minor amount of CTB_5 bound to one GM1 (Figure 4.4a). This result contrasts with the absence of detectable CTB_5-GM1 complexes for the solution containing only CTB_5 and GM1 glycomicelle (Figure 4.2a). With increasing incubation time, the extent of GM1 binding to CTB_5 increased, reaching a maximum at 10 d (Figures 4.4b–4.4d and 4.5). At incubation times of ≥10 d, ions corresponding to CTB_5 bound to four and five GM1 dominated the mass spectra (Figure 4.4e and Figures 4.6a–4.6c). These results are consistent with GM1 being incorporated into the POPC-PD and becoming available for binding to CTB_5. Analogous measurements carried out using PDs prepared from DMPC produced results that closely match those obtained for the POPC-PDs (Figures 4.4f–4.4j and Figures 4.6d–4.6f). This finding suggests that the GM1 transfer process (from glycomicelle to PD) is relatively insensitive to differences in the structures of the two phosphatidylcholines used to prepare the PDs.

Plotted in Figure 4.5a are the time-dependent *f* calculated from the mass spectra shown in Figures 4.4 and 4.6. Also shown are *f* values measured for solutions of CTB_5 (6 μM) and ^{PL}PDs prepared using different initial concentrations of POPC-PD (10 μM or 20 μM) and GM1 (40 μM or 50 μM). Notably, the time-dependent *f* data obtained from the four ^{PL}PD solutions are

indistinguishable, within experimental error. For incubation times between 5 min and 10 d, *f* increases essentially linearly with time (Figure 4.7a). At >10 d, a limiting value of *f* is reached (from 0.82 to 0.87 for the POPC-PDs and 0.82 for the DMPC-PDs). Given the fast kinetics of CTB_5 (which is added to the solution immediately before the ESI-MS measurements are performed) binding with GM1 in the PDs,[12,17] it can be reasonably suggested that the time-dependence of *f* reflects the rate at which GM1 is transferred from glycomicelles to the PDs. Moreover, given that the time-dependent *f* plots are linear (at incubation times of 5 min to 10 d) and independent of the initial concentrations of GM1 and PDs used to produce the ^{PL}PDs, it can be further suggested that the rate limiting step for the formation of the passively-loaded GM1 PDs is a zero-order process, with apparent rate constants of $(3.4 \pm 0.1) \times 10^{-3}$ *f* h^{-1} (Figure 4.7a).

To establish whether the nature of the lipoprotein disc influences the extent and rate of GM1 incorporation, analogous measurements were performed on NDs, prepared from POPC or DMPC. Representative mass spectra are shown in Figure 4.8 and the corresponding *f* values are shown in Figure 4.5. Qualitatively, the results obtained for the NDs are similar to those reported above for the PDs – the extent of binding site occupancy increases linearly with incubation time. However, as can be seen from Figure 4.5b, at all incubation times investigated, the *f* values are smaller than those measured for the PDs. For example, at 10 d, the *f* values for the NDs are 0.32 (POPC) and 0.27 (DMPC) and 0.86 (POPC) and 0.81 (DMPC) for the PDs. These results suggest that the net rate of GM1 transfer to NDs is approximately one-third of that for PDs, with apparent zero-order rate constants of $(1.3 \pm 0.1) \times 10^{-3}$ *f* h^{-1} (POPC-NDs) and $(1.2 \pm 0.1) \times 10^{-3}$ *f* h^{-1} (DMPC-NDs) (Figure 4.7b).

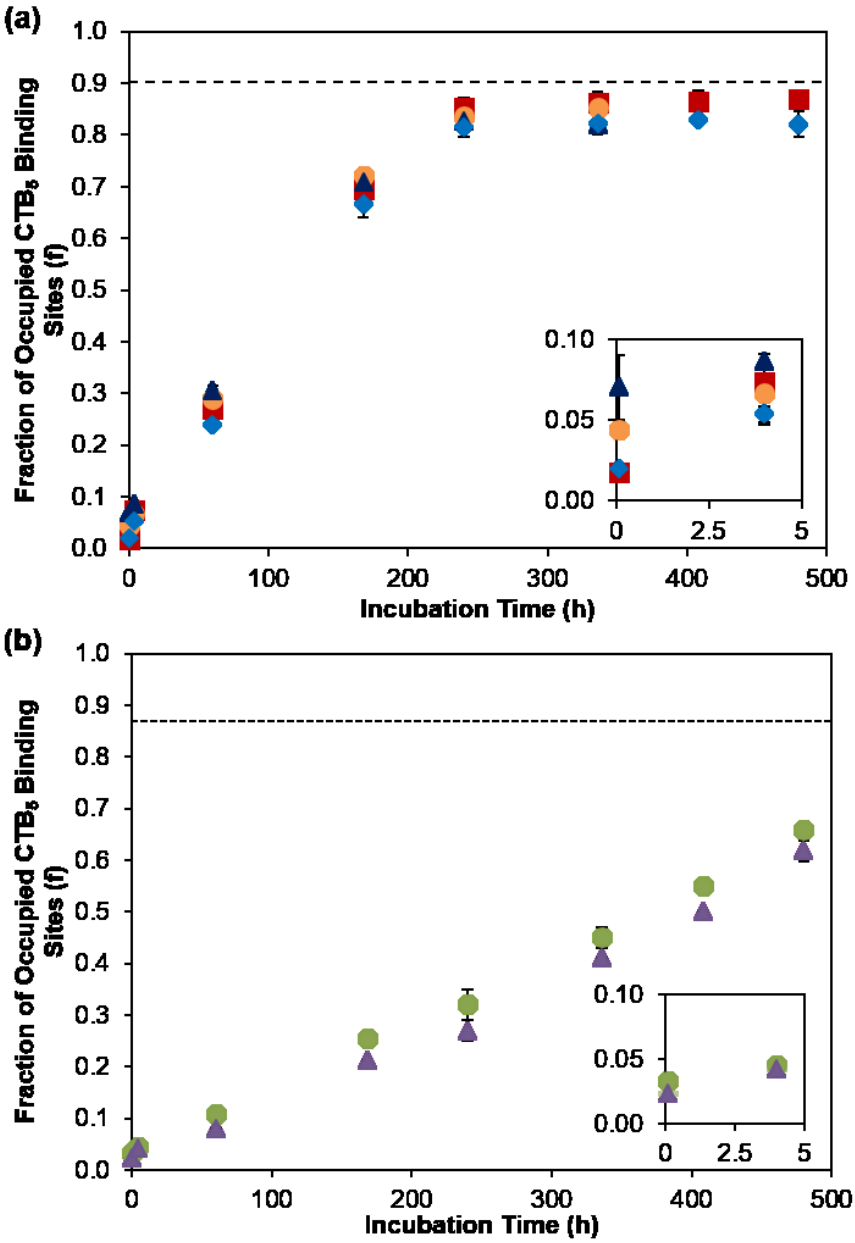

Figure 4.5 (a) Plots of fraction of occupied CTB_5 binding sites (f) versus incubation time (used to prepare ^{PL}PDs) measured by ESI-MS for solutions of CTB_5 (6 μM) and ^{PL}PDs produced from: (■) POPC-PDs (10 μM) and GM1 (40 μM); (●) POPC-PDs (10 μM) and GM1 (50 μM); (▲) POPC-PDs (20 μM) and GM1 (40 μM) and (◆) DMPC-PDs (10 μM) and GM1 (40 μM). Dashed lines indicate values measured for pre-loaded GM1-containing PDs (40 μM GM1). (b) Plots of fraction of occupied CTB_5 binding sites (f) versus incubation time (used to prepare ^{PL}NDs) measured by

ESI-MS for solutions of CTB_5 (6 μM) and ^{PL}NDs produced from: (●) POPC-NDs (10 μM) and GM1 (40 μM) and (▲) DMPC-NDs (20 μM) and GM1 (40 μM). Dashed lines indicate values measured for pre-loaded GM1-containing NDs (40 μM GM1). The error bars correspond to one standard deviation.

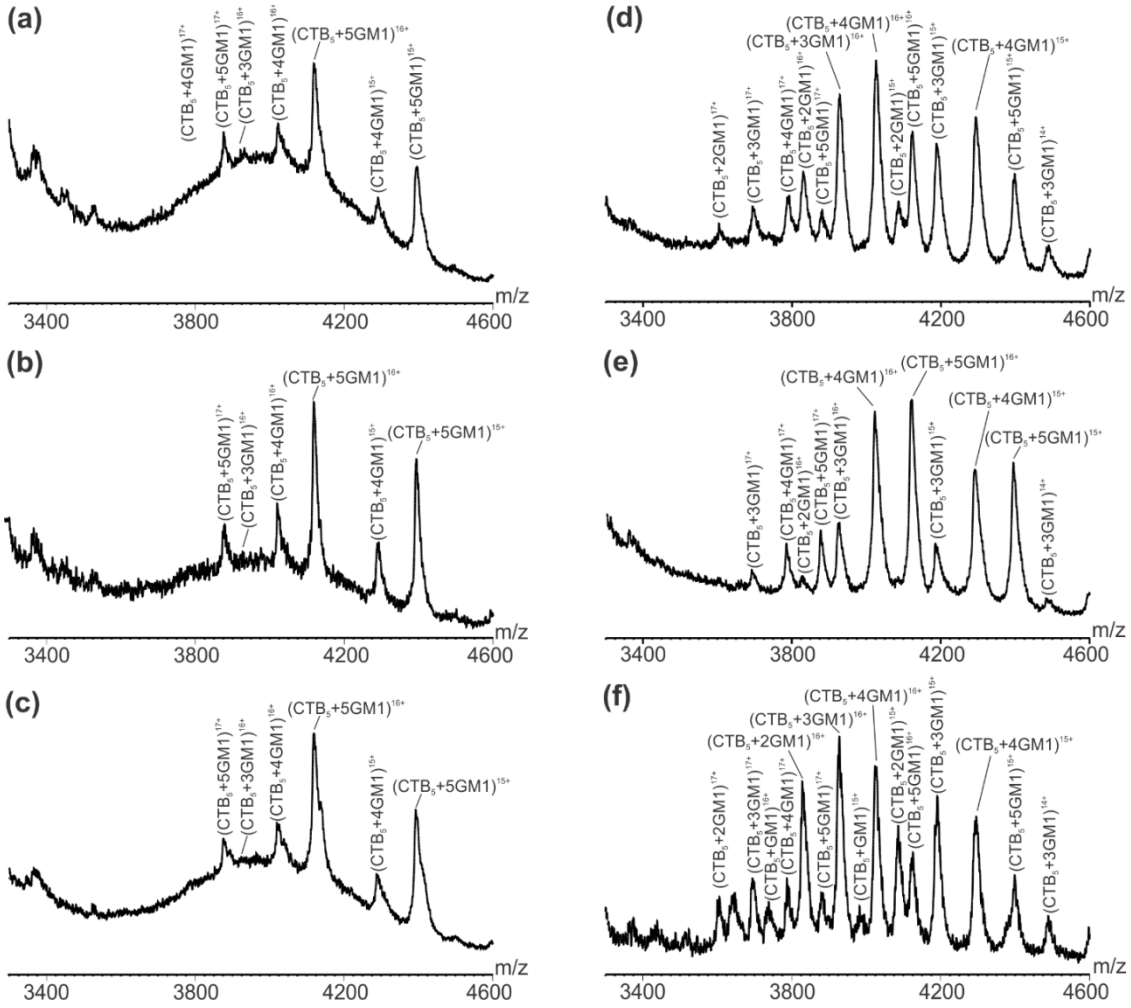

Figure 4.6 ESI mass spectra acquired in positive ion mode for aqueous ammonium acetate solutions (200 mM, pH 6.8, 22 °C) of CTB_5 (6 μM) and GM1 (40 μM) in the presence of POPC-PDs (10 μM). The GM1 and POPC-PDs were incubated at room temperature for (a) 14 d, (b) 17

d or (c) 20 d before adding CTB_5. ESI mass spectra acquired in positive ion mode for a 200 mM aqueous ammonium acetate solution (pH 6.8, 22 °C) of CTB_5 (6 µM) and GM1 (40 µM) in the presence of DMPC-PDs (10 µM). The GM1 and DMPC-PDs were incubated at room temperature for (d) 14 d, (e) 17 d or (f) 20 d before adding CTB_5.

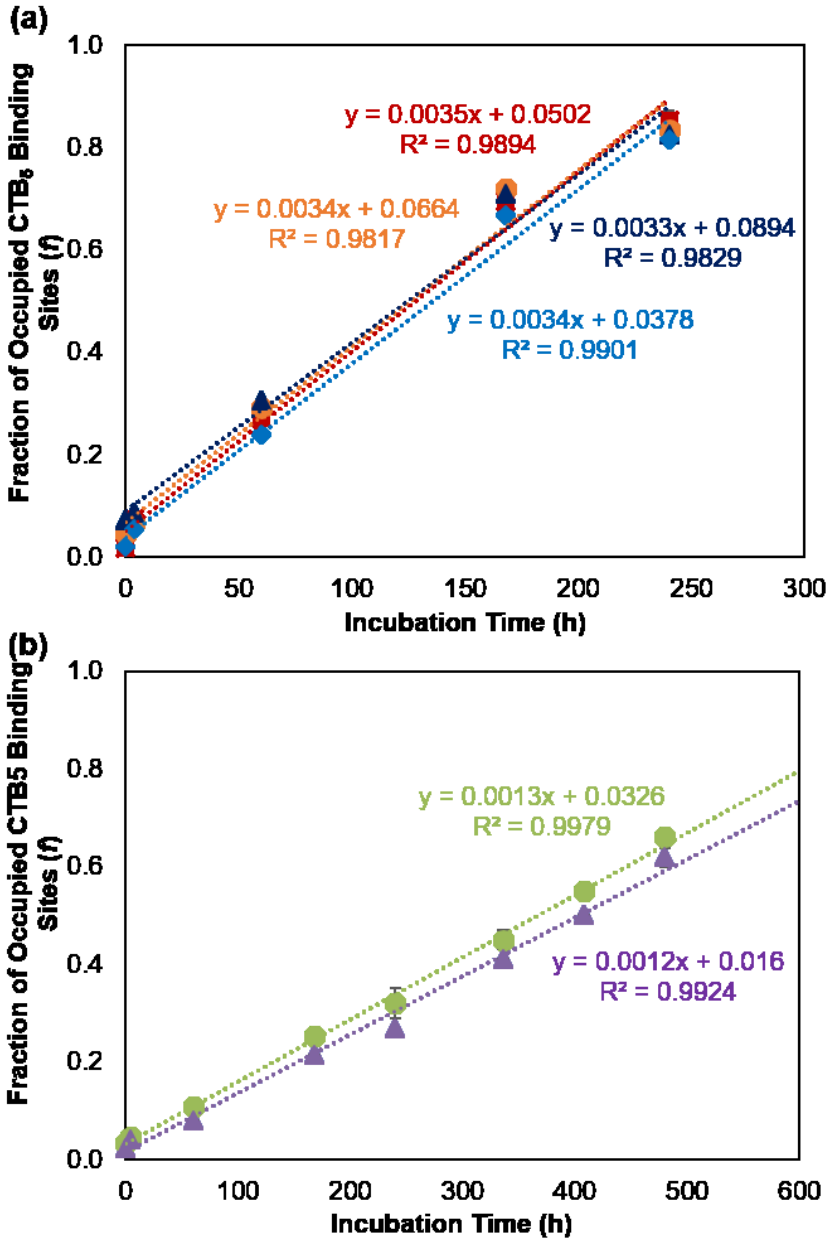

Figure 4.7 (a) Linear fitting (dashed lines) to the fraction of occupied CTB_5 binding sites (f) versus incubation time data measured by ESI-MS for solutions of CTB_5 (6 μM) and ^{PL}PDs produced from: (■) POPC-PDs (10 μM) and GM1 (40 μM); (●) POPC-PDs (10 μM) and GM1 (50 μM); (▲) POPC-PDs (20 μM) and GM1 (40 μM) and (◆) DMPC-PDs (10 μM) and GM1 (40 μM). (b) Linear fitting (dashed lines) to the fraction of occupied CTB_5 binding sites (f) versus incubation time data measured by ESI-MS for solutions of CTB_5 (6 μM) and ^{PL}NDs produced from: (●) POPC-NDs (10 μM) and GM1 (40 μM) and (▲) DMPC-NDs (20 μM) and GM1 (40 μM). The error bars correspond to one standard deviation.

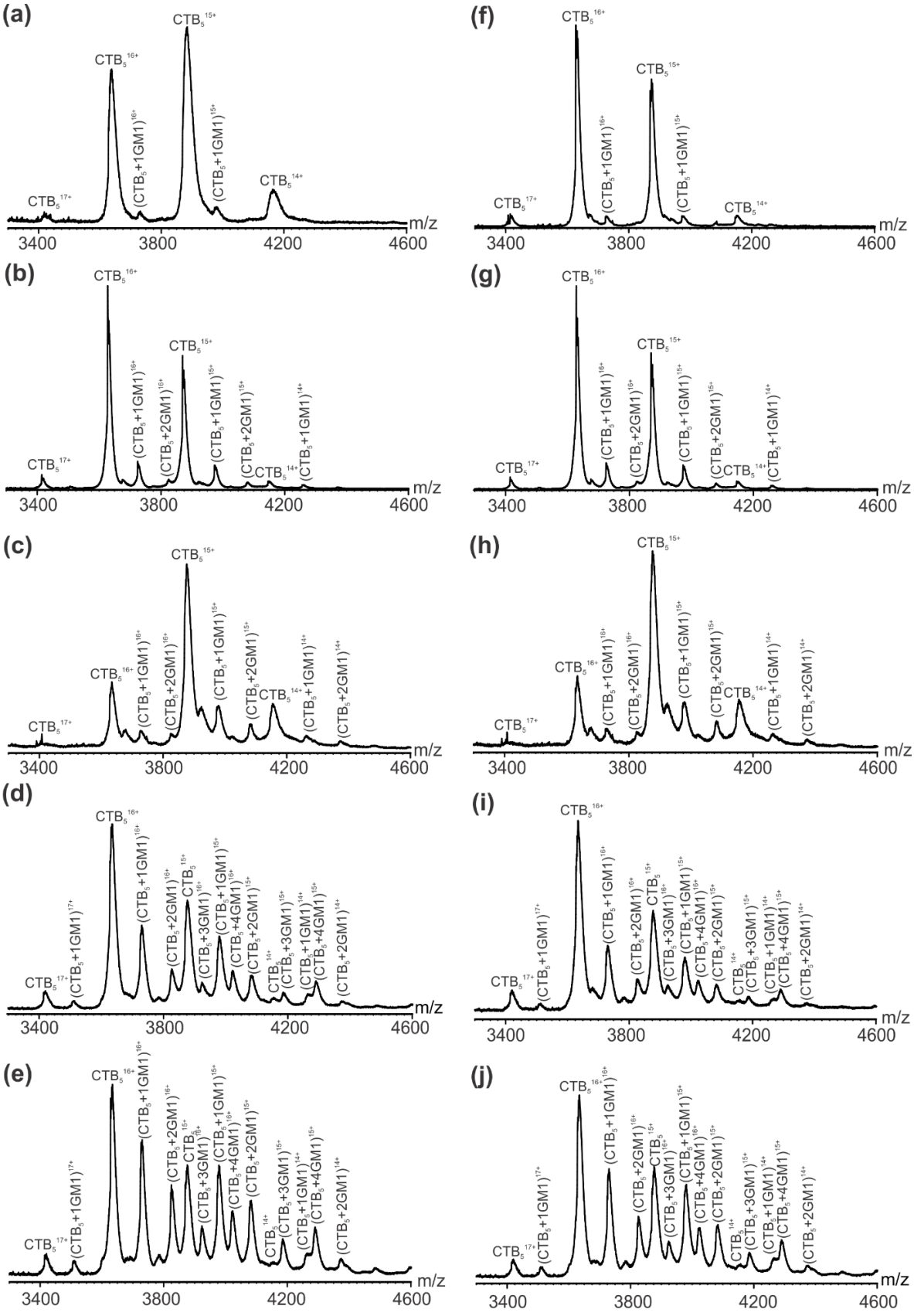
(a)
(b)
(c)
(d)
(e)
(f)
(g)
(h)
(i)
(j)
m/z
3400
3800
4200
4600

Figure 4.8 ESI mass spectra acquired in positive ion mode for a 200 mM aqueous ammonium acetate solution (pH 6.8, 22 °C) of CTB_5 (6 μM) and GM1 (40 μM) in the presence of POPC-NDs (10 μM). The GM1 and POPC-NDs were incubated at room temperature for (a) 5 min, (b) 4 h, (c) 2.5 d, (d) 7 d or (e) 10 d before adding CTB_5. ESI mass spectra acquired in positive ion mode for a 200 mM aqueous ammonium acetate solution (pH 6.8, 22 °C) of CTB_5 (6 μM) and GM1 (40 μM) in the presence of DMPC-NDs (10 μM). The GM1 and DMPC-NDs were incubated at room temperature for (f) 5 min, (g) 4 h, (h) 2.5 d, (i) 7 d or (j) 10 d before adding CTB_5.

Taken together, these results demonstrate that it is possible to incorporate GM1 into phospholipid-containing PDs and NDs through incubation with GM1 glycomicelles in aqueous solution. Moreover, comparative binding measurements performed with CTB_5 revealed that, given sufficiently long incubation times (for the preparation of ^{PL}PDs), it is possible to achieve the same extent of GM1-CTB_5 binding (as measured by ESI-MS) with ^{PL}PDs as with pre-formed PDs (produced using the same GM1 concentration). The GM1 incorporation process (into the MMs), inferred from the rate of change of CTB_5 binding site occupancy, appears to be relatively slow and is somewhat sensitive to the nature of the lipid discs but independent of structural differences in the structures of the two phosphatidylcholines used to prepare the PDs. The reasons for the apparent zero-order transfer kinetics, as well as the slower incorporation rates measured for NDs compared to PDs, are not fully understood and require further investigation.

4.3.3 Comparison of CTB_5 binding to ganglioside libraries in pre- and passively-loaded PDs

Because the CTB_5-GM1 interactions are high affinity,[31] it was of interest to test whether similar results are obtained with lower affinity GL ligands. With this in mind, the binding of CTB_5 with ^{PL}PDs produced by incubating POPC-PDs with an equimolar library of seven purified gangliosides (7G library) in aqueous solution was analyzed by CaR-ESI-MS and the results compared to those obtained using PDs directly prepared from the library.[17] As reported previously, the oligosaccharides of GM2, GM3, GD1a, GD1b and GT1b bind to CTB_5 with low affinity (~500 M^{-1}).[17] The GD2 pentasaccharide does not bind and, therefore, GD2 served as a negative control.[17,32]

Shown in Figure 4.9 are representative post-IMS mass spectra acquired in negative ion mode for aqueous ammonium acetate solutions (200 mM, pH 6.8, 25 °C) of CTB_5 (6 μM) and ^{PL}PDs (10 μM) produced through incubation (4 h, 2.5 d, 5 d or 10 d) with the 7G library (10 μM each ganglioside). For the solution containing the ^{PL}PDs produced at 4 h incubation, ion signal corresponding to free CTB_5 and CTB_5 bound to one ganglioside (L), i.e., $(CTB_5 + qL)^{n-}$ with q = 0 – 1 and n = 12 – 14, were detected (Figure 4.9a). To establish which gangliosides were bound to CTB_5, CID was performed on the $(CTB_5 + qL)^{n-}$ ions in the Transfer region (75 V). Collisional activation resulted in the appearance of singly deprotonated GM1 ions, as well as CTB monomer ions (Figure 4.9e). At longer incubation times, signal corresponding to CTB_5 bound to two ganglioside ligands was also detected and CID resulted in the appearance GM1, as well as other gangliosides, although with much lower abundances (Figures 4.9b – 4.9d). For the ^{PL}PDs produced at 2.5 d incubation, GM3 and GD1 (GD1a and/or GD1b) were detected (Figure 4.9f); for the ^{PL}PDs produced at 5 d and 10 d incubation, GM1, GM2, GM3, GD1 and GT1b ligands were detected (Figures 4.9g and 4.9h). No GD2 was detected in any of the measurements. Notably, the results

obtained for the ^{PL}PDs produced from ≥5 d incubation are consistent with those obtained for POPC-PDs prepared directly from the 7G library (Figure 4.10).[17]

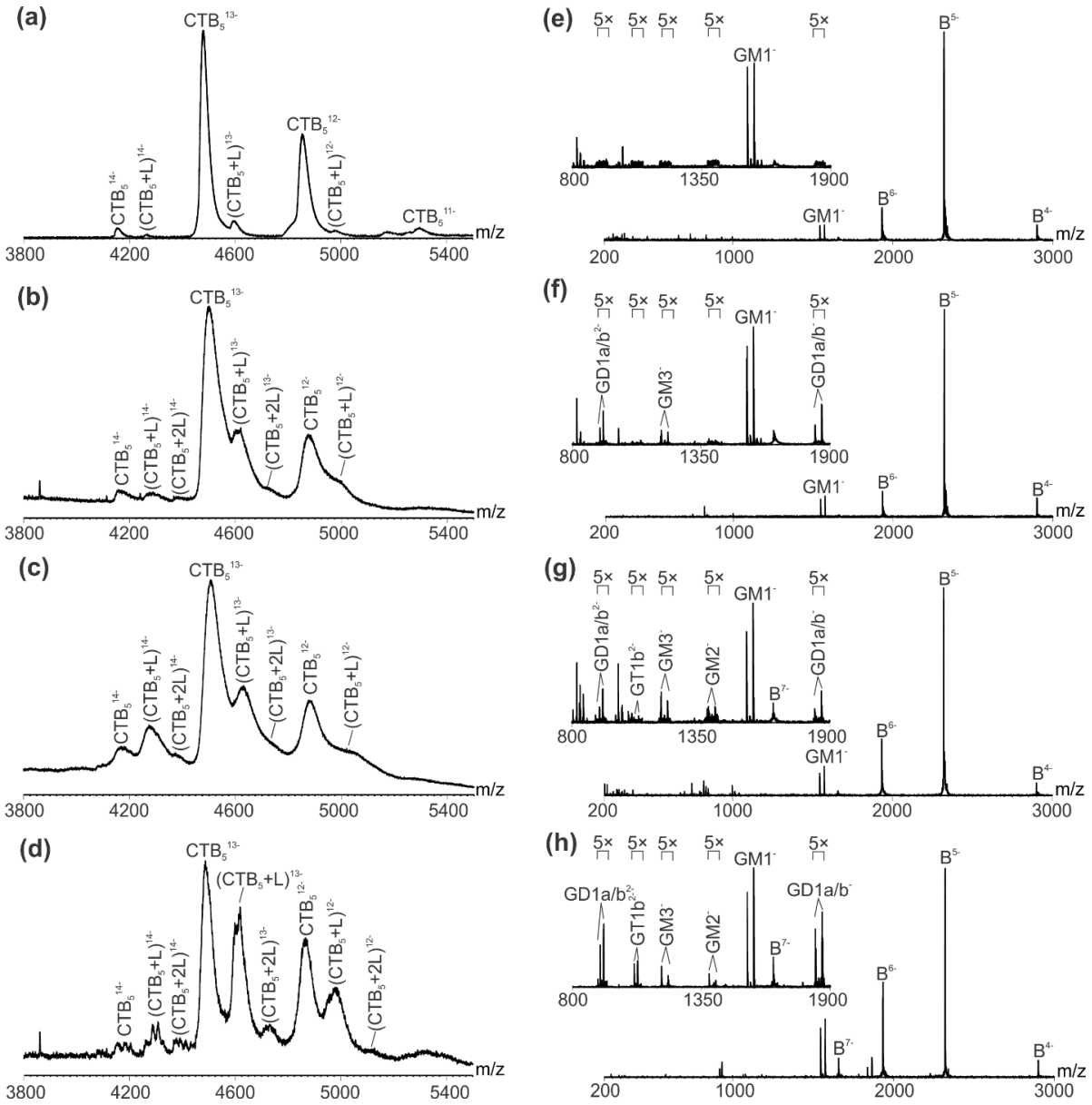

Figure 4.9 ESI mass spectra acquired in negative ion mode for a 200 mM aqueous ammonium acetate solution (pH 6.8, 22 °C) containing CTB_5 (6 μM) and POPC-PDs (10 μM) produced by incubation of POPC-PDs with an equimolar (10 μM each) of seven gangliosides (GM1, GM2,

GM3, GD1a, GD1b, GD2 and GT1b) at room temperature for (a) 4 h, (b) 2.5 d, (c) 5 d or (d) 10 d. (e), (f), (g) and (h) are CID mass spectra acquired in the Transfer region (post-IMS separation) using a collision voltage of 75 V for the CTB_5 ions produced from the solutions described in (a), (b), (c) and (d), respectively.

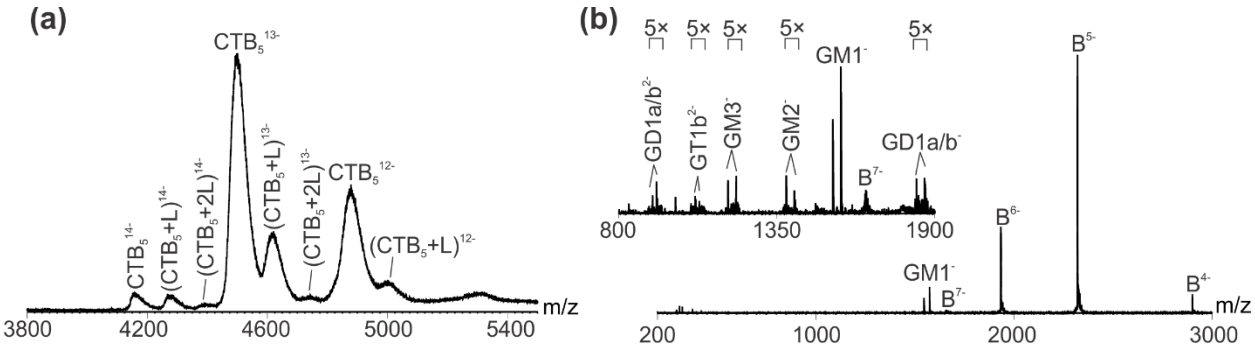

Figure 4.10 (a) ESI mass spectrum acquired in negative ion mode for a 200 mM aqueous ammonium acetate solution (pH 6.8, 22 °C) of CTB_5 (6 μM) and PDs prepared from an equimolar mixture (10 μM each) of seven gangliosides (GM1, GM2, GM3, GD1a, GD1b, GD2 and GT1b). (b) CID mass spectrum acquired in the Transfer region using a collision voltage of 75 V for all CTB_5 ions produced from the solution in (a).

Analogous measurements were performed using natural libraries of GLs extracted from pig and mouse brains. The commercial pig brain extract is known to contain the gangliosides GM1a, GM1b, GM2, GM3, GD1a, GD1b, GD1c, GD2, GD3, GT1a, GT1b, GT1c, GT2, GT3 and GQ1 (structures shown in Figure 4.1.[33] The presence of fucosylated-GM1 (Fuc-GM1, structure shown in Figure 4.1) in the extract was also recently reported.[17] An ESI mass spectrum acquired in negative mode for a methanol solution of the pig brain extract is shown in Figure 4.11. Assuming similar ESI-MS response factors, GD1, GT1, GM1 and Fuc-GM1 are the most abundant

gangliosides present in the mixture. Other gangliosides, including GM2 and GM3, appear to be at much lower concentrations based on the ESI-MS data. For the mouse brain extract, which was prepared in-house, ESI-MS analysis revealed abundant ions corresponding to glycerophospholipids, as well as GM1, GD1 and GT1 ions (Figure 4.11).[34] Ganglioside identification was based on the measured MWs and CID fragmentation patterns (Figures 4.12-4.15).[34] Assuming similar ESI-MS response factors, this analysis suggests that GD1 is the most abundant ganglioside type in the mixture, followed by GM1 and GT1.

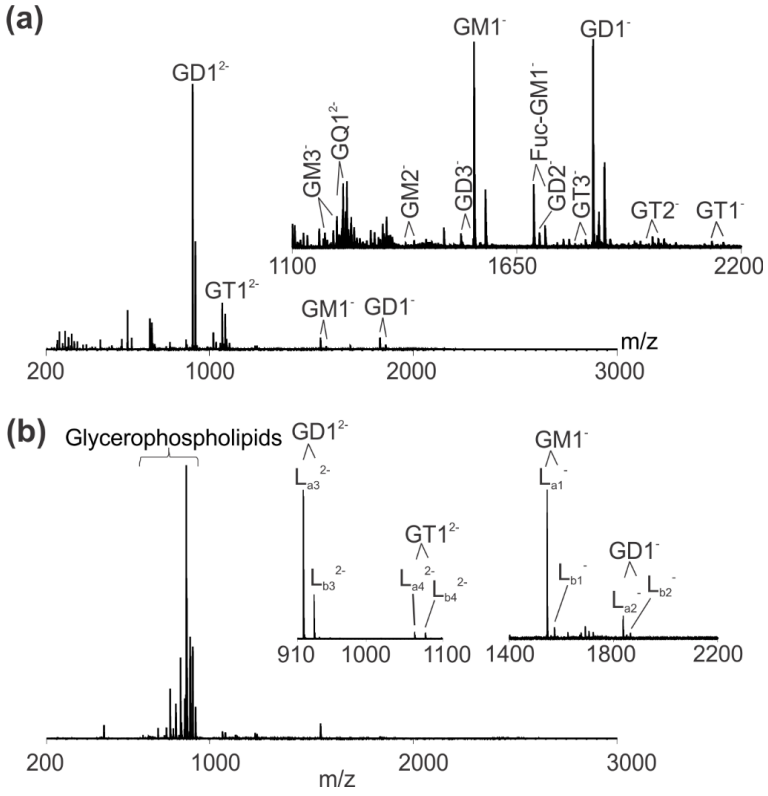

Figure 4.11 ESI mass spectra acquired in negative ion mode for methanol solutions of GL extract from (a) pig brain (0.01 mg/mL) and (b) mouse brain (0.01 mg/mL). The structures of the gangliosides present in the mouse brain extract (L_{a1}^-, L_{b1}^-, L_{a2}^-, L_{b2}^-, L_{a3}^{2-}, L_{b3}^{2-}, L_{a4}^{2-}, L_{b4}^{2-}) were established by CID (Figures 4.12–4.15).

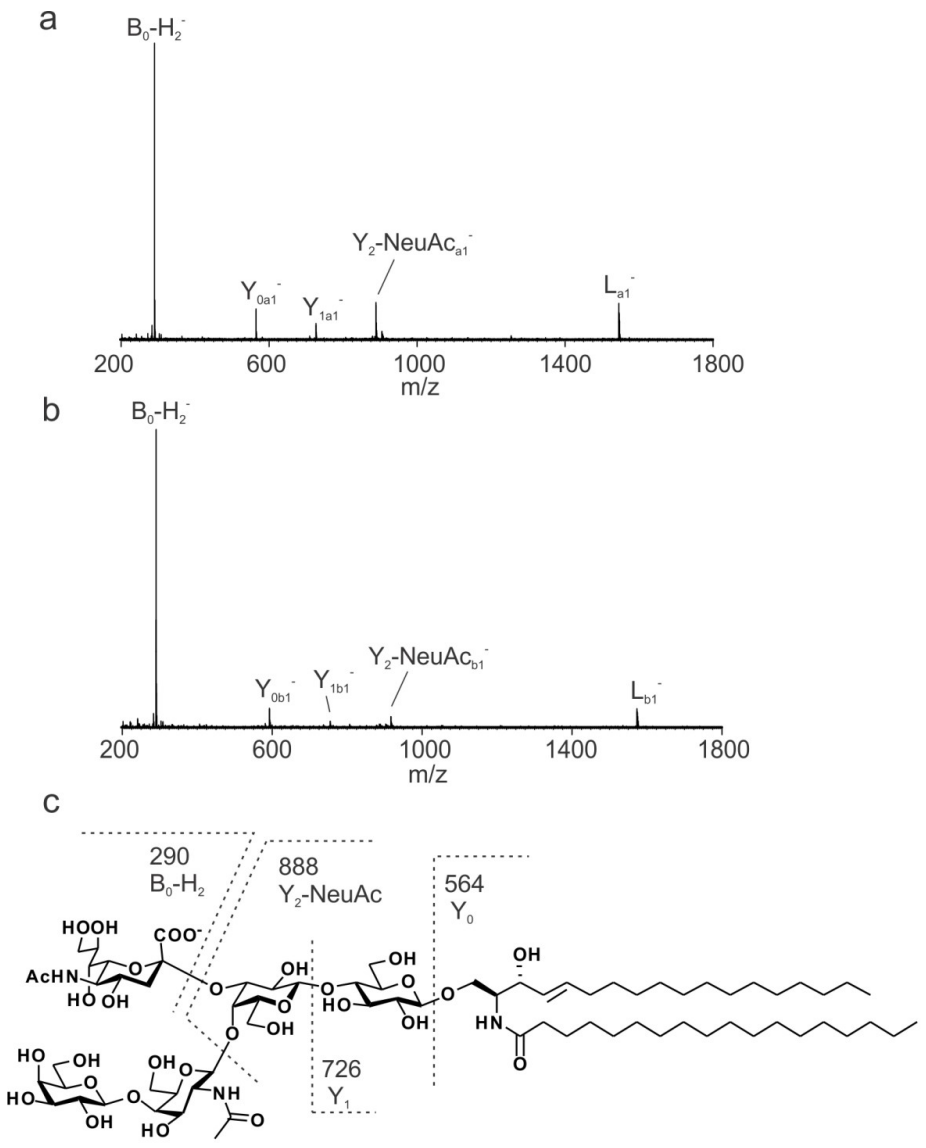

Figure 4.12 CID mass spectra acquired for (a) the L_{a1}^- (at *m/z* 1544.8) and (b) L_{b1}^- (at *m/z* 1572.8) ions, produced by ESI performed in negative ion mode on a methanol solution of mouse brain extract. B_0-H_2^- corresponds to deprotonated 5-N-acetyl-neuraminic acid (Neu5Ac); Y_2-$Neu5Ac_{a1}^-$ and Y_2-$NeuA5c_{b1}^-$ result from loss of the Gal, GalNAc and Neu5Ac residues from L_{a1}^- and L_{b1}^-, respectively; Y_{1a1}^- and Y_{1b1}^- result from the loss of Gal residue from Y_2-$NeuAc_{a1}^-$ and Y_2-$NeuAc_{b1}^-$, respectively; and Y_{0a1}^- and Y_{0b1}^- result from the loss of Glc residue from Y_{1a1}^- and Y_{1b1}^-, respectively. (c) Fragmentation scheme shown for L_{a1}^- (d18:1-18:0).

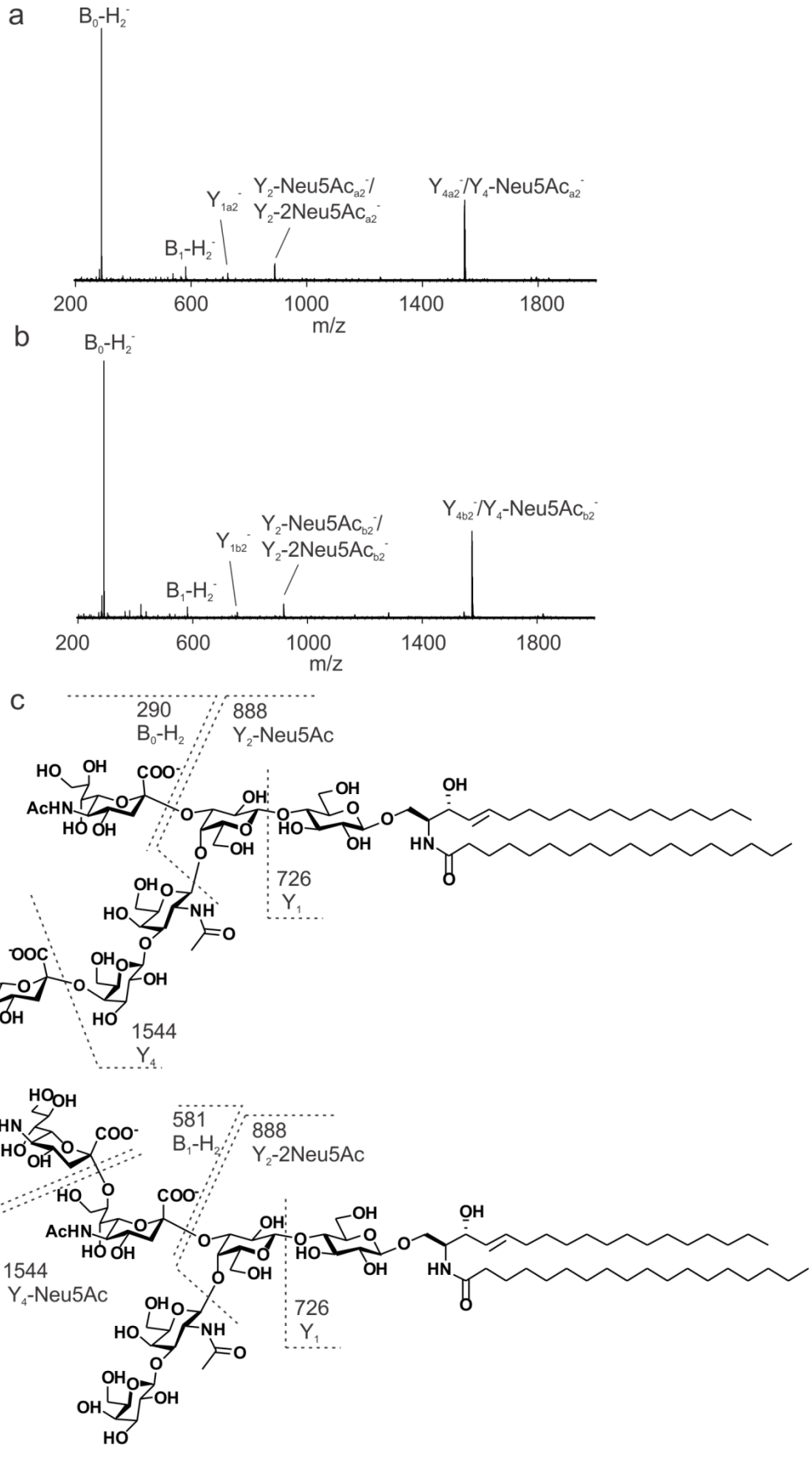
a
B0-H2-
Y1a2-
Y2-Neu5Aca2-/
Y2-2Neu5Aca2-
Y4a2-/Y4-Neu5Aca2-
B1-H2-
200
600
1000
1400
1800
m/z
b
B0-H2-
Y1b2-
Y2-Neu5Acb2-/
Y2-2Neu5Acb2-
Y4b2-/Y4-Neu5Acb2-
B1-H2-
200
600
1000
1400
1800
m/z
c
290
B0-H2
888
Y2-Neu5Ac
726
Y1
1544
Y4
581
B1-H2
888
Y2-2Neu5Ac
290
B0-H2
1544
Y4-Neu5Ac
726
Y1

Figure 4.13 CID mass spectra acquired for (a) the L_{a2}^- (at *m/z* 1836.1) and (b) L_{b2}^- (at *m/z* 1864.1) ion, produced by ESI performed in negative ion mode on a methanol solution of mouse brain extract. B_0-H_2^- corresponds to deprotonated Neu5Ac; B_1-H_2^- corresponds to deprotonated α-D-Neu5Ac-(2→8)-α-D-Neu5Ac; Y_{4a2}^-/Y_4-$Neu5Ac_{a2}^-$ and Y_{4b2}^-/Y_4-$NeuA5c_{b2}^-$ result from loss of the Neu5Ac from L_{a2}^- and L_{b2}^-, respectively; Y_2-$Neu5Ac_{a2}^-$ and Y_2-$NeuA5c_{b2}^-$ result from loss of the Gal, GalNAc and Neu5Ac residues from L_{a2}^- and L_{b1}^-, respectively; Y_2-$2Neu5Ac_{a2}^-$ and Y_2-$2NeuA5c_{b2}^-$ result from loss of the Gal, GalNAc and α-D-Neu5Ac-(2→8)-α-D-Neu5Ac residues from L_{a2}^- and L_{b2}^-, respectively; Y_{1a2}^- and Y_{1b2}^- result from the loss of Gal residue from Y_2-$NeuAc_{a2}^-$ and Y_2-$NeuAc_{b2}^-$, respectively. (c) Fragmentation scheme shown for L_{a2}^- (d18:1-18:0).

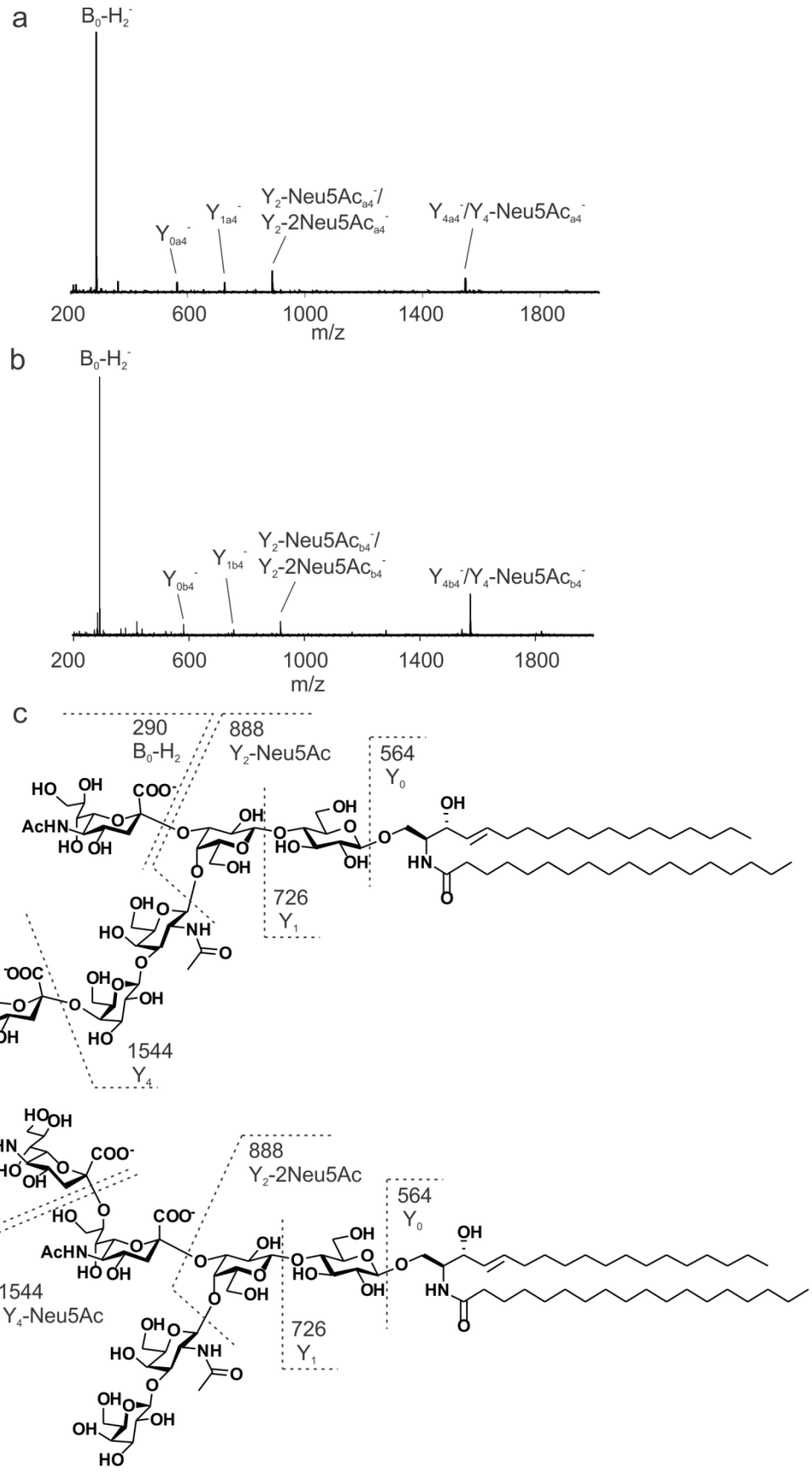
a
B_0-H_2^-
Y_{0a4}^-
Y_{1a4}^-
Y_2-$Neu5Ac_{a4}^-$/
Y_2-$2Neu5Ac_{a4}^-$
Y_{4a4}^-/Y_4-$Neu5Ac_{a4}^-$
200
600
1000
1400
1800
m/z
b
B_0-H_2^-
Y_{0b4}^-
Y_{1b4}^-
Y_2-$Neu5Ac_{b4}^-$/
Y_2-$2Neu5Ac_{b4}^-$
Y_{4b4}^-/Y_4-$Neu5Ac_{b4}^-$
200
600
1000
1400
1800
m/z
c
290
B_0-H_2
888
Y_2-Neu5Ac
564
Y_0
726
Y_1
1544
Y_4
888
Y_2-2Neu5Ac
290
B_0-H_2
564
Y_0
1544
Y_4-Neu5Ac
726
Y_1

Figure 4.14 CID mass spectra acquired for the (a) the L_{a3}^{2-} (at *m/z* 917.5) and (b) L_{b3}^{2-} (at *m/z* 931.5) ion, produced by ESI performed in negative ion mode on a methanol solution of mouse brain extract. B_0-H_2^- corresponds to deprotonated Neu5Ac; Y_{4a4}^-/Y_4-$Neu5Ac_{a4}^-$ and Y_{4b4}^-/Y_4-$NeuA5c_{b4}^-$ result from loss of the Neu5Ac from L_{a4}^- and L_{b4}^-, respectively; Y_2-$Neu5Ac_{a4}^-$ and Y_2-$NeuA5c_{b4}^-$ result from loss of the Gal, GalNAc and Neu5Ac residues from L_{a4}^{2-} and L_{b4}^{2-}, respectively; Y_2-$2Neu5Ac_{a4}^-$ and Y_2-$2NeuA5c_{b4}^-$ result from loss of the Gal, GalNAc and α-D-Neu5Ac-(2→8)-α-D-Neu5Ac residues from L_{a4}^{2-} and L_{b4}^{2-}, respectively; Y_{1a4}^- and Y_{1b4}^- result from the loss of Gal residue from Y_2-$NeuAc_{a4}^-$ and Y_2-$NeuAc_{b4}^-$, respectively; and Y_{0a4}^- and Y_{0b4}^- result from the loss of Glc residue from Y_{1a4}^- and Y_{1b4}^-, respectively. (c) Fragmentation scheme shown for L_{a4}^{2-} (d18:1-18:0).

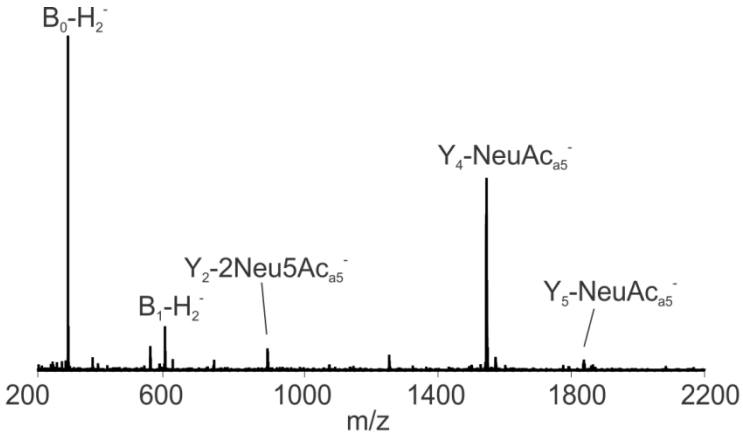
B0-H2-
Y4-NeuAca5-
Y2-2Neu5Aca5-
B1-H2-
Y5-NeuAca5-
200
600
1000
1400
1800
2200
m/z

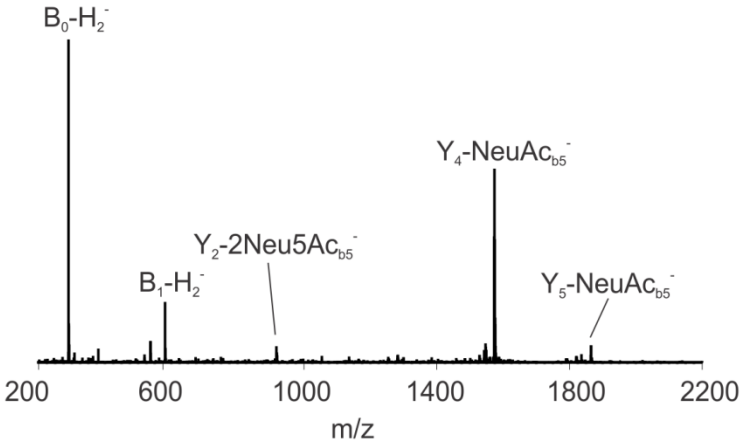
B0-H2-
Y4-NeuAcb5-
Y2-2Neu5Acb5-
B1-H2-
Y5-NeuAcb5-
200
600
1000
1400
1800
2200
m/z

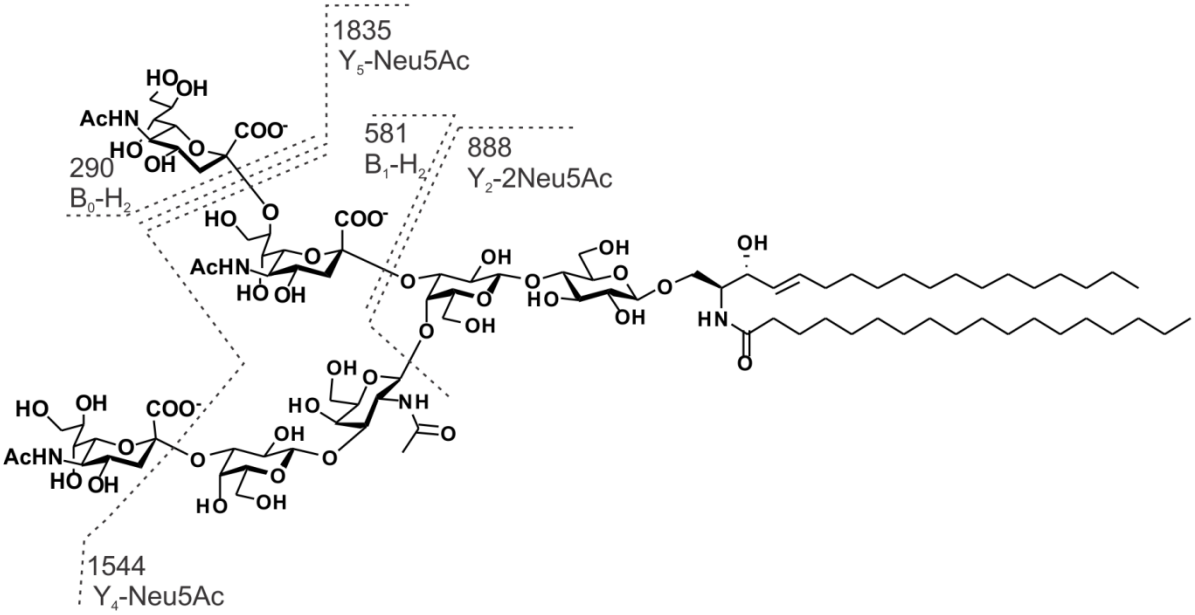
1835
Y5-Neu5Ac
581
B1-H2
888
Y2-2Neu5Ac
290
B0-H2
1544
Y4-Neu5Ac

Figure 4.15 CID mass spectra acquired for (a) the L_{a4}^{2-} (at *m/z* 1063.0) and (b) L_{b4}^{2-} (at *m/z* 1077.0) ion, produced by ESI performed in negative ion mode on a methanol solution of mouse brain extract. B_0-H_2^- corresponds to deprotonated Neu5Ac; B_1-H_2^- corresponds to deprotonated α-D-Neu5Ac-(2→8)-α-D-Neu5Ac; Y_5-$Neu5Ac_{a3}^-$ and Y_5-$NeuA5c_{b3}^-$ result from loss of the Neu5Ac from L_{a3}^- and L_{b3}^-, respectively; Y_4-$Neu5Ac_{a3}^-$ and Y_4-$NeuA5c_{b3}^-$ result from loss of two Neu5Ac from L_{a3}^- and L_{b3}^-, respectively; Y_2-$2Neu5Ac_{a3}^-$ and Y_2-$2NeuA5c_{b3}^-$ result from loss of the Gal, GalNAc, Neu5Ac and α-D-Neu5Ac-(2→8)-α-D-Neu5Ac residues from L_{a3}^- and L_{b3}^-, respectively. (c) Fragmentation scheme shown for L_{a5}^- (d18:1-18:0).

Shown in Figure 4.16a is a representative ESI mass spectrum acquired for aqueous ammonium acetate solutions (200 mM, pH 6.8 and 25 °C) of CTB_5 (3 μM) and the pig brain extract (at an estimated concentration of 80 μM). Under these conditions, only signal corresponding to free CTB_5 ions, i.e., CTB_5^{n-} at n = 11 – 15, was detected. ESI mass spectra acquired for aqueous ammonium acetate solutions (200 mM, pH 6.8, 25 °C) of CTB_5 (3 μM) and ^{PL}PDs (20 μM) produced by incubating for 4 h, 2.5 d, 5 d and 10 d, at room temperature, with the extract (at an estimated concentration of 80 μM). Analysis of the solution with ^{PL}PDs produced after 4 h incubation identified ions corresponding to free CTB_5 and CTB_5 bound to one ganglioside ligand (Figure 4.17a). CID of the $(CTB_5 + L)^{n-}$ ions in the Transfer region (75 V) produced abundant GM1 and fucosyl-GM1 anions (Figure 4.17e). These results are consistent with data acquired using pre-loaded POPC-PDs produced from the same lipid extract (Figure 4.18).[17] For the ^{PL}PDs produced at longer incubation times (≥2.5 d), gaseous ions of CTB_5 bound to up to two gangliosides were detected (Figures 4.17b–4.17d). In addition to GM1 and fucosyl-GM1, deprotonated ions corresponding to GD1 and GT1 were detected (Figures 4.17f–4.17h). No GD1

or GT1 ions were detected by CaR-ESI-MS performed using pre-loaded PDs produced using this extract (at the same concentration) (Figure 4.18). It should also be noted that neither the ^{PL}PDs nor the PDs yielded evidence of GM2 or GM3 binding. The absence of binding is attributed to the low concentrations of these (low affinity) gangliosides in the extract.

Shown in Figure 4.16b is an illustrative ESI mass spectrum acquired in negative ion mode for aqueous ammonium acetate solutions (200 mM, pH 6.8, 25 °C) of CTB_5 (3 μM) with GLs extracted from mouse brain (at an estimated concentration of 80 μM). Similar to what was observed for the analysis of the solution of pig brain extract, only free CTB_5 ions were detected. Measurements performed on the solution containing the pre-loaded PDs, produced directly from the mouse brain extract, resulted in the detection of ions corresponding to free CTB_5 and CTB_5 bound to one molecule of GM1 (Figure 4.18). In contrast, analysis of the solutions containing ^{PL}PDs produced by incubating POPC-PDs with the extract for 5 d or 10 d revealed ions corresponding to CTB_5 bound up to two ganglioside ligands, which were identified as GM1 and GD1 (Figure 4.19). The binding of GT1 gangliosides was not detected, presumably due to its low concentration in the extract*, vide supra*.

Taken together, the CTB_5 binding results obtained for the pig and mouse extracts revealed notable differences in the performance of ^{PL}PDs and conventionally-prepared PDs for screening natural libraries of GLs against GBPs using the CaR-ESI-MS assay. The use of ^{PL}PDs produced using incubation times of ≥5 d led to a higher occupancy of the CTB_5 binding sites and the identification of more GL ligands than the use of pre-loaded PDs produced directly from the lipid extract.

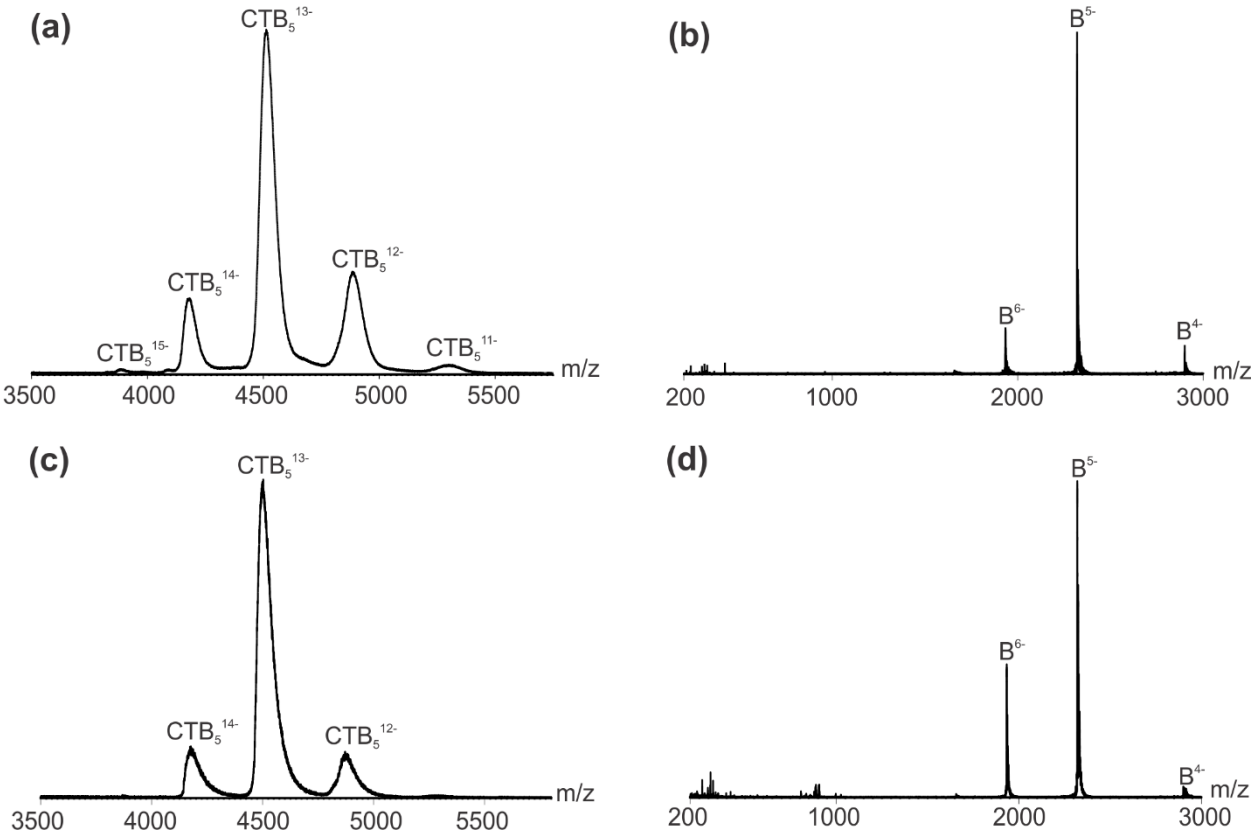

Figure 4.16 (a) ESI mass spectra acquired in negative ion mode for a 200 mM aqueous ammonium acetate solution (pH 6.8, 22 °C) containing CTB_5 (3 μM) and GL extract from pig brain (80 μM estimated concentration). (b) CID spectrum acquired for all CTB_5 ions in solution (a) in Transfer region using a collision energy of 75 V. (c) ESI mass spectra acquired in negative ion mode for a 200 mM aqueous ammonium acetate solution (pH 6.8, 22 °C) containing CTB_5 (3 μM) and GL extract from pig brain (20 μM estimated concentration). (d) CID spectrum acquired for all CTB_5 ions in solution (c) in Transfer region using a collision energy of 75 V.

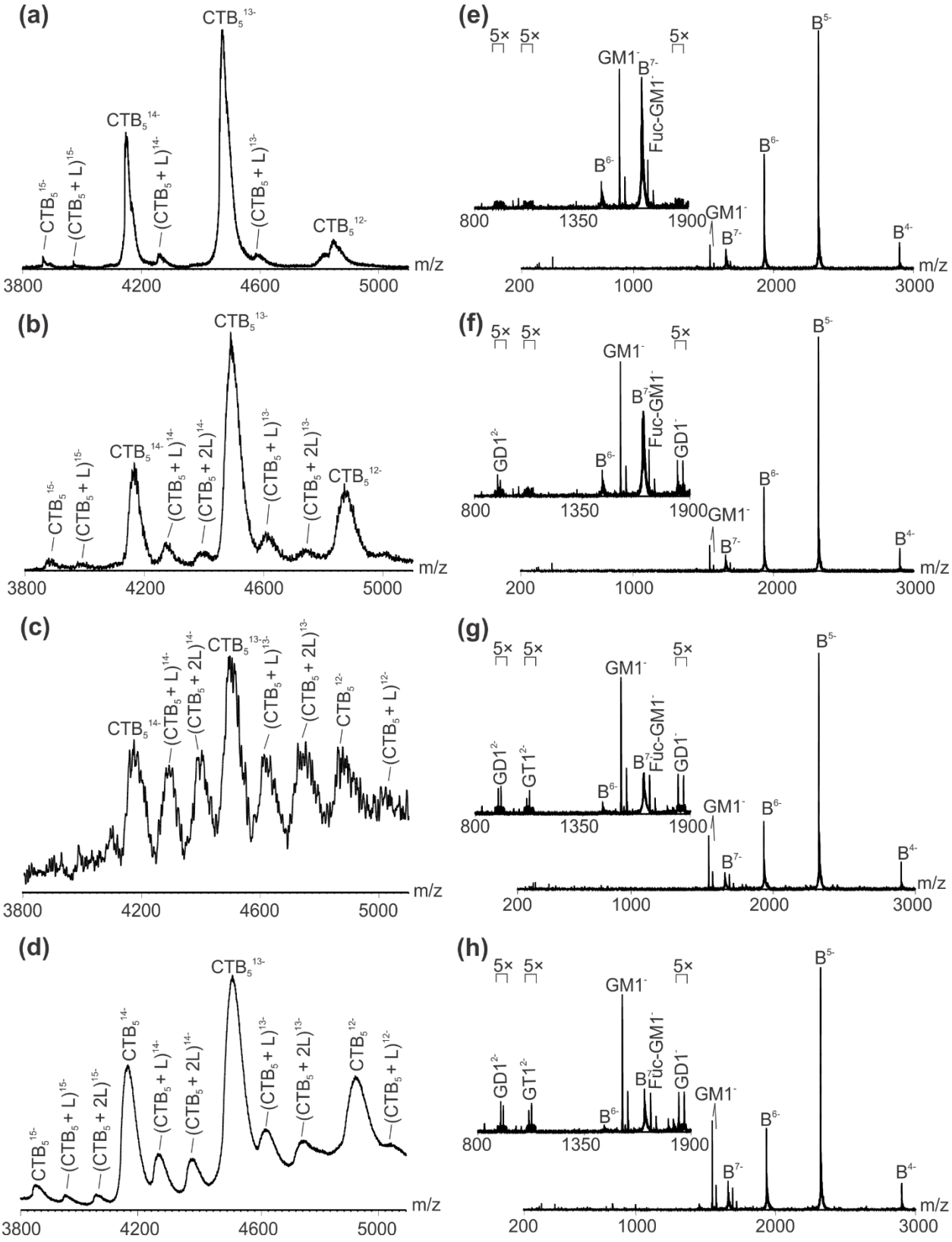
(a)
(b)
(c)
(d)
(e)
(f)
(g)
(h)
m/z
3800
4200
4600
5000
200
1000
2000
3000
800
1350
1900
5×

Figure 4.17 ESI mass spectra acquired in negative ion mode for a 200 mM aqueous ammonium acetate solution (pH 6.8, 22 °C) containing CTB_5 (3 μM) and GL extract from pig brain (at an estimated concentration of 80 μM) in the presence of POPC-PDs (20 μM). The GL extract and POPC-PDs were incubated at room temperature for (a) 4 h, (b) 2.5 d, (c) 5 d or (d) 10 d before the adding of CTB_5. (e), (f), (g) and (h) are CID mass spectra acquired in the Transfer region (post-IMS separation) using a collision voltage of 75 V for the CTB_5 ions produced from the solutions described in (a), (b), (c) and (d), respectively.

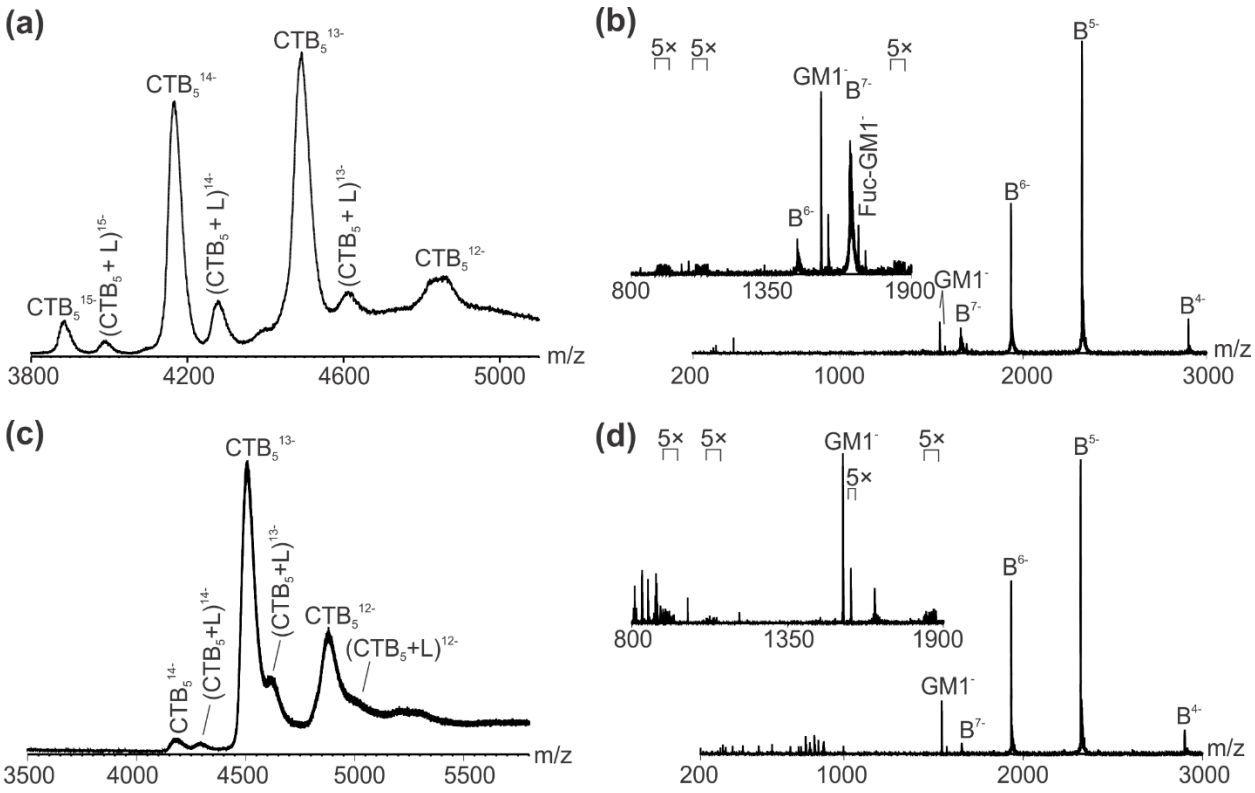

Figure 4.18 (a) ESI mass spectrum acquired in negative ion mode for a 200 mM aqueous ammonium acetate solution (pH 6.8, 22 °C) of CTB_5 (3 μM) and PDs prepared from the GL extract from pig brain (80 μM estimated concentration for extract). (b) CID spectrum acquired for all CTB_5 complexes ions in solution (a) in Transfer region using a collision energy of 75 V. (c) ESI mass spectruma acquired in negative ion mode for a 200 mM aqueous ammonium acetate solution (pH 6.8, 22 °C) of CTB_5 (3 μM) and PDs prepared from GL extract from mouse brain (80 μM estimated concentration for extract). (d) CID spectrum acquired for all CTB_5 complexes ions solution (c) in Transfer region using a collision energy of 75 V.

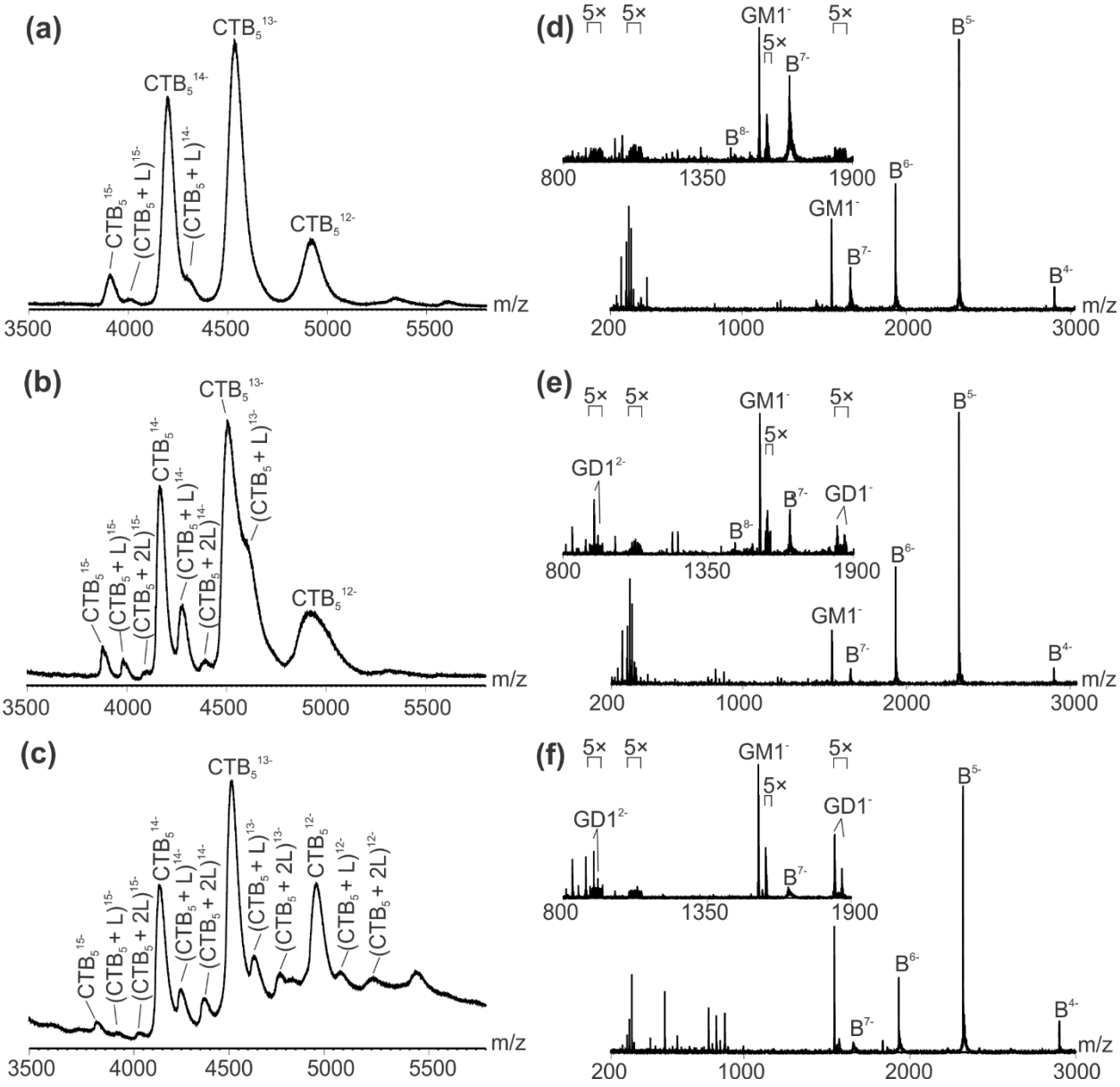

Figure 4.19 ESI mass spectra acquired in negative ion mode for a 200 mM aqueous ammonium acetate solution (pH 6.8) containing CTB_5 (3 μM) and GL extract from mouse brain (80 μM) in the presence of POPC-PDs (20 μM). The GL extract and POPC-PDs were incubated at room temperature for (a) 2.5 d, (b) 5 d or (c) 10 d before the adding of CTB_5. (d), (e) and (f) are CID mass spectra acquired in the Transfer region (post-IMS separation) using a collision voltage of 75 V for the CTB_5 ions produced from the solutions described in (a), (b) and (c), respectively.

4.4 Conclusions

This work describes the use of ^{PL}PDs, prepared by incubating phospholipid PDs with GL-containing lipid mixtures in aqueous solution, for CaR-ESI-MS screening of GLs against GBPs and compares their performance with conventional, pre-loaded PDs, prepared directly from a mixture of phospholipid and GL(s). Experiments carried out on GM1 glycomicelles revealed evidence of GM1 incorporation into ^{PL}PDs within a few hours of incubation and increased with increasing incubation time. At ≥10 d, GM1 binding to CTB_5 was indistinguishable from that observed with pre-loaded PDs produced directly from GM1 (at the same initial concentration). The transfer of GM1 from glycomicelles to NDs was also observed, although the apparent rate of incorporation is slower than for PDs. Comparison of ganglioside binding to CTB_5 measured for pre-loaded PDs and ^{PL}PDs prepared from a ganglioside library or GLs extracted from pig or mouse brain revealed that ^{PL}PDs allows for the detection of a greater number of ganglioside ligands than the pre-loaded PD. However, low abundance, low affinity ligands were not detected with either the ^{PL}PDs or PDs. Together, the results of this study suggest ^{PL}PDs may have advantages over conventionally prepared PDs for screening GLs against GBPs using CaR-ESI-MS.

4.5 References

1. Malhotra, R. *Biochem. Anal. Biochem*. **2012**, *1*, 108.
2. Varki, A.; Cummings, R. D.; Esko, J. D.; Freeze, H. H.; Stanley, P.; Bertozzi, C. R.; Hart, G. W.; Etzler, M. E. *Essentials of Glycobiology*, 2nd ed.; Cold Spring Harbor Laboratory Press: Cold Spring Harbor, NY, 2009.
3. Evans, S. V.; Roger MacKenzie. C. *J. Mol. Recognit*. **1999**, *12*, 155–68.

4. Lingwood, C. A.; Manis, A.; Mahfoud, R.; Khan, F.; Binnington, B.; Mylvaganam, M. *Chem. Phys. Lipids*. **2010**, *163*, 27–35.

5. Shi, J.; Yang, T.; Kataoka, S.; Zhang, Y.; Diaz, A. J.; Cremer, P. S. *J. Am. Chem. Soc*. **2007**, *129*, 5954−5961.

6. Sanghera, N.; Correia, B. E.; Correia, J. R.; Ludwig, C.; Agarwal, S.; Nakamura, H. K.; Kuwata, K.; Samain, E.; Gill, A. C.; Bonev, B. B.; Pinheiro, T. J. *Chem. Biol.* **2011**, *18*, 1422–1431.

7. Lingwood, D.; Binnington, B.; Rog, T.; Vattulainen, I.; Grzybek, M.; Coskun, U.; Lingwood, C. A.; Simons, K. *Nat. Chem. Biol.* **2011**, *7*, 260–262.

8. Czogalla, A.; Grzybek, M.; Jones, W.; Coskun, U. *Biochim. Biophys. Acta*. **2014**, *1841*, 1049–1059.

9. Bayburt, T. H.; Grinkova, Y. V.; Sligar, S. G. *Nano Lett*. **2002**, *2*, 853−856.

10. Zhang, Y.; Liu, L.; Daneshfar, R.; Kitova, E. N.; Li, C.; Jia, F.; Cairo, C.W.; Klassen, J. S. *Anal. Chem.* **2012**, *84*, 7618−7621.

11. Popovic, K.; Holyoake, J.; Pomès, R.; Privé, G. G. *Prot. Natl. Acad. Sci.* **2012**, *109*, 2908−2912.

12. Leney, A. C.; Darestani, R. R.; Li, J.; Nikjah, S.; Kitova, E. N.; Zou, C.; Cairo, C. W.; Xiong, Z. J.; Privé, G. G.; Klassen, J. S. *Anal. Chem.* **2015**, *87*, 4402−4408.

13. Borch, J.; Torta, F.; Sligar, S. G.; Roepstorff, P. *Anal. Chem.* **2008**, *80*, 6245–6252.

14. Bally, M.; Rydell, G. E.; Zahn, R.; Nasir, W.; Eggeling, C.; Breimer, M. E.; Svensson, L.; Hook, F.; Larson, G. *Angew. Chem. Int. Ed*. **2012**, *51*, 12020–12024.

15. Lauer, S.; Goldstein, B.; Nolan, R. L.; Nolan, J. P. *Biochemistry*. **2002**, *41*, 1742–1751.

16. Leney, A.; Fan, X.; Kitova, E.N.; Klassen, J. S. *Anal. Chem.* **2014**, *86*, 5271–5277.

17. Li, J.; Fan, X.; Kitova, E. N.; Zou, C.; Cairo, C. W.; Eugenio, L.; Ng, K. K. S.; Xiong, Z. J.; Privé, G. G.; Klassen, J. S. *Anal. Chem.* **2016**, *88*, 4742–4750.

18. Nakano, M.; Fukuda, M.; Kudo, T.; Miyazaki, M.; Wada, Y.; Matsuzaki, N.; Endo, H., Handa, T. *J. Am. Chem. Soc*. **2009**, *131*, 8308–8312.

19. Brown, R. E.; Thompson, T. E. *Biochemistry*. **1987**, *26*, 5454–5460.

20. Brown, R. E. *Biochim. Biophys. Acta*. **1992**, *1113*, 375–389.

21. Nichols, J. W. *Biochemistry*. **1988**, *27*, 3925–3931.

22. Han, L.; Kitova, E. N.; Li, J.; Nikjah, S.; Lin, H.; Pluvinage, B.; Boraston, A. B.; Klassen, J. S. *Anal. Chem*. **2015**, *87*, 4888–4896.

23. Zhou, D.; Cantu, C. 3rd.; Sagiv, Y.; Schrantz, N.; Kulkarni, A. B.; Qi, X.; Mahuran, D. J.; Morales, C. R.; Grabowski, G. A.; Benlagha, K.; Savage, P.; Bendelac, A.; Teyton, L. *Science*. **2004**, *303*, 523–527.

24. Locatelli-Hoops, S.; Remmel, N.; Klingenstein, R.; Breiden, B.; Rossocha, M.; Schoeniger, M.; Koenigs, C.; Saenger, W.; Sandhoff, K. *J Biol Chem*. **2006**, *281*, 32451–3260.

25. Han, L.; Kitova, E. N.; Klassen, J. S. *J Am Soc Mass Spectrom*. **2016**, *27*, 1878–1886.

26. Sturqill, E. R.; Aoki, K.; Lopez, P. H.; Colacurcio, D.; Vajn, K.; Lorenzini, I.; Majic, S.; Yang, W. H.; Heffer, M.; Tiemeyer, M.; Marth, J. D.; Schnaar, R. L. *Glycobiology*. **2012**, *22*, 1289–1301.

27. Yagi-Utsumi, M.; Kameda, T.; Yamaguchi, Y.; Kato, K. *FEBS Lett*. **2010**, *584*, 831–836.

28. Li, J.; Richards, M. R.; Bagal, D.; Campuzano, I. D. G.; Kitova, E. N.; Xiong, Z. J.; Privé, G. G.; Klassen, J. S. *Anal. Chem*. **2016**, *88*, 9524–9531.

29. Han, L.; Morales, L. C.; Richards, M. R.; Kitova, E. N.; Sipione, S.; Klassen, J. S. *Anal. Chem*. **2017**, *89*, 9330–9338.

30. Bayburt, T. H., Sligar, S. G. *FEBS Lett*. **2010**, *584*, 1721−1727.

31. Lin, H.; Kitova, E. N.; Klassen, J. S. *J. Am. Soc. Mass Spectrom*. **2014**, *25*, 104−110.

32. Kuziemko, G. M.; Stroh, M.; Stevens, R. C. *Biochemistry*. **1996**, *35*, 6375–6384.

33. Ikeda, K.; Shimizu, T.; Taguchi, R. *J. Lipid Res*. **2008**, *49*, 2678−2689.

34. Whitehead, S. N.; Chan, K. H. N.; Gangaraju, S.; Slinn, J.; Li, J.; Hou, S. T. *PLoS ONE*. **2011**, *6*, e20808.

Chapter 5

Delivering Transmembrane Peptide Complexes to the Gas Phase Using Nanodiscs and Electrospray Ionization[§]

5.1 Introduction

Membrane peptides and proteins (MPs) are implicated in many critical cellular processes, including signal transduction, transport and metabolism.[1,2] Although their biological significance is well-established, the structural and functional analysis of MPs and their complexes in a native lipid bilayer environment remains experimentally challenging. Commonly used approaches involve the incorporation of the peptide/protein into model membranes (e.g., micelles, bicelles, lipid bilayers and vesicles)[3-6] or detergent systems,[7] which provide both a native-like membrane environment and allow for integration with conventional structural and biophysical techniques. Nanodiscs (NDs), which are water-soluble discoidal phospholipid bilayers surrounded by two copies of an amphipathic membrane scaffold protein (MSP), represent a popular alternative to present MPs.[8,9] NDs, combined with diverse structural and biophysical techniques, including X-ray crystallography and nuclear magnetic resonance (NMR), optical and surface plasmon resonance (SPR) spectroscopies, as well as electrochemistry,[9-13] have been used to probe the properties of isolated MPs, as well as their complexes with other proteins, peptides and lipids. Recently, electrospray ionization-mass spectrometry (ESI-MS), implemented with NDs, has emerged as a promising tool for studying the binding properties of MPs in a lipid environment.[14-

[§] A version of this chapter has been published: Li, J.; Richards, M. R.; Kitova, E. N.; Klassen, J. S. *J. Am. Soc. Mass. Spectrom*. **2017**, *28*, 2054–2065.

[16] Moreover, collision cross sections (Ω), measured using ion mobility separation (IMS), provides a means of assessing possible conformations of the gaseous peptide/protein ions produced from the NDs.[17] However, the extent to which the structures of the gaseous ions reflect the conformations present in the membrane remains unclear, in particular for small peptide complexes, for which electrostatic effects may influence conformation in the gas phase.

Here, we describe the application of ESI-MS and IMS to investigate the conformations of the gas-phase ions of dimers of the transmembrane peptide gramicidin A (GA) produced from NDs. Homodimers of GA are known to act as monovalent cation-selective channels in membranes.[18] Due to its small size and ready availability (from the soil bacteria *Bacillus brevis*), GA has been extensively used as a model to study the organization, dynamics and function of transmembrane peptide channels.[19,20] The GA peptide (HCO-Val-Gly-Ala-D-Leu-Ala-D-Val-Val-D-Val-Trp-D-Leu-Trp-D-Leu-Trp-D-Leu-Trp-$NHCH_2CH_2OH$) consists of aliphatic and aromatic amino acids, with a protected N-terminus (formylated) and C-terminus (ethanolamide). The alternating L- and D-amino acids sequence causes the peptides to adopt β-helical conformers, with the side chains projecting out from the exterior surface of the helix formed by the peptide backbone.[18] The distribution of monomeric and dimeric GA, as well as the dimer conformations, are strongly influenced by environment. In polar solvents, such as dimethyl sulfoxide, GA exists predominantly as monomer.[21] In alcohols, GA forms parallel and antiparallel double-stranded double helix (DSDHp and DSDHap, respectively) dimers and the extent of GA dimerization varies from ~5% to ~85% (with dimerization increasing with increasing hydrophobicity).[22-24] The DSDH dimers are stabilized by intermolecular H-bonds between backbone amide groups.[18] When incorporated into lipid membranes, GA forms monovalent cation channels. The results of electrophysiological experiments performed on the GA ion channel in lipid bilayers suggest that

there is single ion conducting structure.[18] Based on solution NMR spectroscopy data measured for GA-containing micelles and high-resolution solid-state NMR data acquired for GA dimers in a lipid bilayer, it has been proposed that the antiparallel single stranded head-to-head helical (SSHH) dimer is the ion conducting form of GA.[25,26] The SSHH structure is formed by transmembrane dimerization, stabilized by intermolecular H-bonds between the two N-termini, of two nearly cylindrical monomers residing in opposite leaflets with their axes aligned to form a channel across the bilayer. The four Trp residues in the C-termini are positioned such that they can form H-bonds to polar residues at the bilayer/solution interface.[19]

Recently, ESI-IMS-MS was used to probe the conformations of gaseous GA dimer ions produced using the phospholipid vesicle capture-freeze-drying (VCFD) method.[27,28] Briefly, vesicles containing GA are freeze-dried and then re-suspended in isobutanol for ESI-IMS-MS analysis.[27,28] Three different conformations of the gaseous GA dimers, detected as $(2GA + 2Na)^{2+}$ ions, were identified from phospholipid vesicles sprayed out of isobutanol; these were assigned as DSDHp, DSDHap, and SSHH based on a comparison of the Ω measured for these ions and values calculated from molecular dynamics (MD) simulations carried out on structures measured using X-ray crystallography and NMR spectroscopy.[27] It was later reported that the nature of the phospholipid and the presence of cholesterol influences the relative abundances of the three conformations.[28] Implementation of the VCFD method using a mixing tee ESI setup, which allows fast mixing between aqueous vesicles and organic solvent and reduces sample preparation time, was also recently described.[29] Although relatively straightforward to implement, a potential weakness of the VCFD method is that the original conformation(s) of the peptide dimer in the phospholipid bilayer may be altered prior to the IMS measurements due to exposure to isobutanol.

In the present study, the conformations of GA dimer ions produced by ESI performed on aqueous solutions of GA-containing NDs composed of 1,2-dimyristoyl-sn-glycero-3-phosphocholine (DMPC) or 1-palmitoyl-2-oleoyl-*sn*-glycero-3-phosphocholine (POPC) were analyzed by ESI-IMS-MS and the measured Ω compared to those obtained using the VCFD method. Measurements were also performed on GA dimer ions produced from isobutanol solutions to probe whether the conformations present in the gas phase exhibit any dependence on the nature of the ESI charging agents. The Ω determined experimentally for the gaseous GA dimer ions were compared with values calculated for structures obtained by X-ray and NMR spectroscopy and from MD simulations.

5.2 Experimental Section

5.2.1 Proteins, peptides and lipids

Gramicidin A (GA, ≥90% purity, MW 1882.33 Da) was purchased from Sigma-Aldrich Canada (Oakville, Canada) and used without further purification. As described below, the GA sample also contained gramicidin B (GB, HCO-Val-Gly-Ala-D-Leu-Ala-D-Val-Val-D-Val-Trp-D-Leu-Phe-D-Leu-Trp-D-Leu-Trp-$NHCH_2CH_2OH$, MW 1843.30 Da) as an impurity. Recombinant membrane scaffold protein (MSP1E1, MW 27,494 Da) was expressed and purified as previously described.[8] Cytochrome c from equine heart (Cyt c, MW 12,384 Da), myoglobin from equine heart (myo, MW 16,951 Da), which were used to construct the Ω calibration curve for IMS measurements, were purchased from Sigma-Aldrich Canada (Oakville, Canada). The phospholipids DMPC (MW 677.9 Da) and POPC (MW 760.08 Da) was purchased from Avanti Polar Lipids Inc. (Alabaster, AL). The structures of the phospholipids are shown in Figure 5.1.

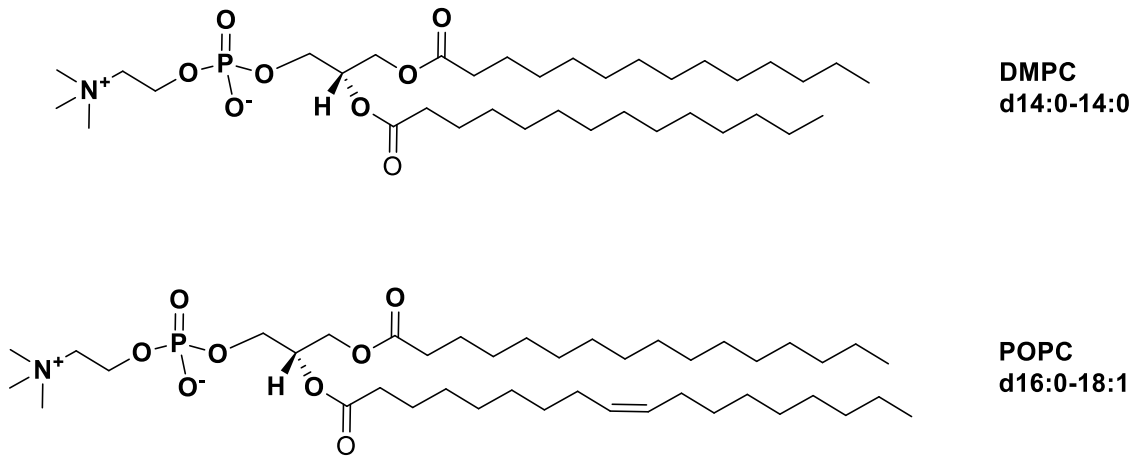

Figure 5.1 Structures of the phospholipids 1,2-dimyristoyl-sn-glycero-3-phosphocholine (DMPC) and 1-palmitoyl-2-oleoyl-sn-glycero-3-phosphocholine (POPC).

5.2.2 Nanodisc preparation

GA-containing NDs were prepared according to a protocol reported previously.[8,9] Briefly, DMPC or POPC (dissolved in chloroform) was mixed with GA (dissolved in ethanol) in the desired ratio (160:1 molar ratio of phospholipid-to-GA) for ND preparation and a more detailed description was provided in Chapter 2, section 2.2.5. The corresponding size exclusion chromatograms are shown in Figure 5.2.[30] The purified NDs were concentrated using a 30 kDa MW cut-off filter, to approximately 30 μM, and stored at –80 °C until needed.

5.2.3 Mass spectrometry

All MS measurements were performed in positive ion mode using a Synapt G2-S mass spectrometer and a more detailed description was given in Chapter 2, section 2.2.6. To dissociate GA dimers, the *m/z* region corresponding to GA dimer ions was selected by quadrupole mass filter and the ions subjected to collision-induced dissociation (CID) in Transfer region following IMS,

at voltages ranging from 2 V to 50 V. For IMS, a wave height of 38 V and a wave velocity of 800 m s^{-1} were applied and the helium and nitrogen gas flow rates were 190 mL min^{-1} and 60 mL min^{-1}, respectively. The Ω of the GA dimer ions were determined from the IMS measurements using a protocol described previously.[31,32] and detailed information was given in Chapter3, section 3.2.4. A calibration plot was constructed (Figure 5.3) from ATs for calibrant ions – doubly protonated tryptic peptides obtained from cytochrome c and myoglobin with, with known Ω (in He, Table 5.1).[33,34] All data was processed using the Waters MassLynx software (*v*4.1) in combination with Driftscope *v*2.5. Gaussian functions, fit using the multipeak fitting function of Igor pro 6.22A, were used to describe the IMS arrival time distributions (ATDs) and the fitting was evaluated from an analysis of the residuals.

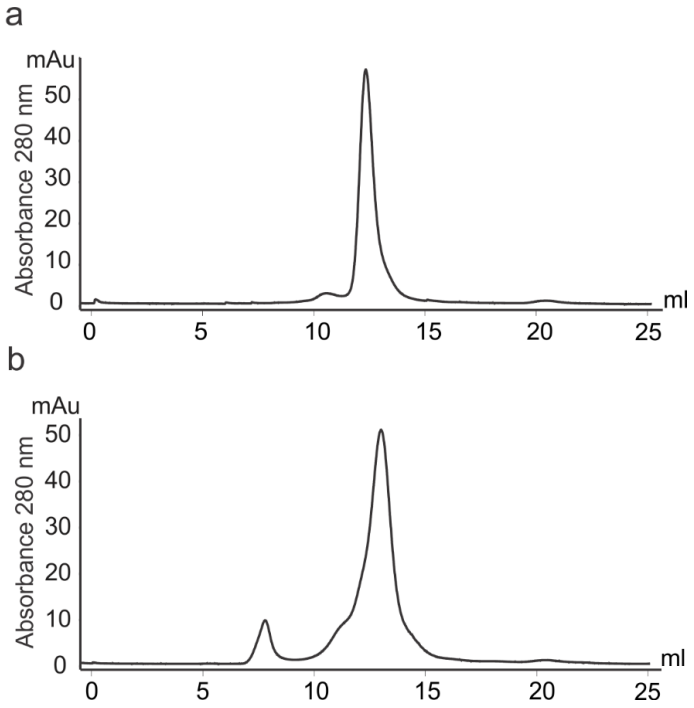

Figure 5.2 Size exclusion chromatograms measured for (a) GA-containing DMPC NDs and (b) GA-containing POPC NDs. The elution volume of intact NDs is ~12.5 mL.

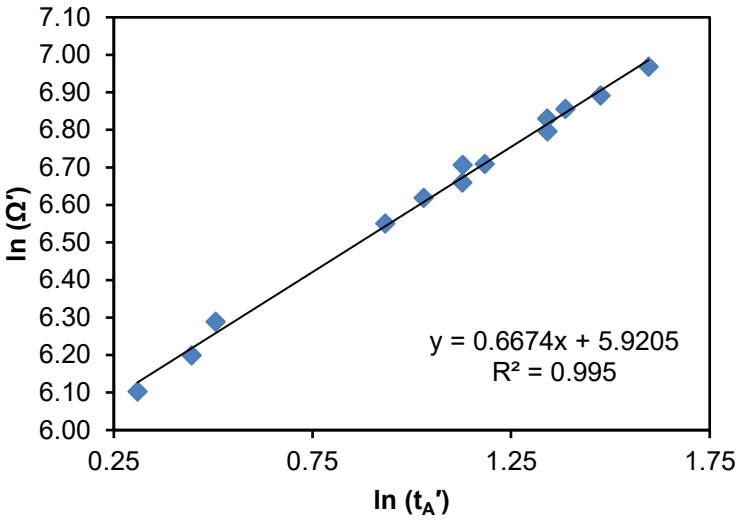

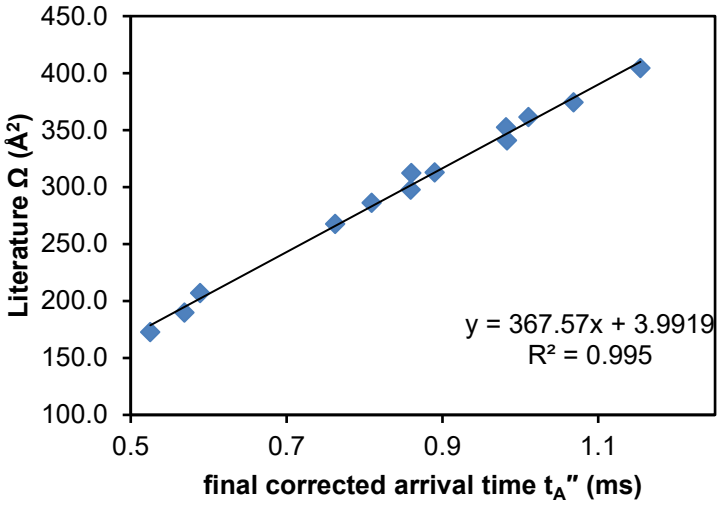

Figure 5.3 (a) Plot of ln(Ω′) versus ln(t_A′) for the doubly protonated trypic peptides from cytochrome c and myoglobin. An exponential factor (X) of 0.6674 was determined from the slope of the plot. (b) Plot of literature Ω values versus final corrected arrival times (t_A″).

Table 5.1 Ion mobility separation arrival times (IMS-ATs) measured for the doubly protonated tryptic peptides of cytochrome c and myoglobin and their reported collision cross sections (**Ω**, in He).

Peptide	*m/z*	AT (ms)	**Ω** (Å^2) [a]
Cytochrome c			
GITWK	302.85	1.95	172.82
YIPGTK	339.90	2.15	189.88
MIFAGIK	390.50	2.25	207.03
TGPNLHGLFGR	585.17	3.14	267.56
EETLMEYLENPK	748.84	3.87	312.71
TGQAPGFTYTDANK	736.30	3.69	297.61
Myoglobin			
ASEDLKK	395.95	2.21	238.09
LFTGHPETLEK	636.72	3.40	286.2
HGTVVLTALGGILK	690.40	3.69	312.22
VEADIAGHGQEVLIR	804.41	4.43	340.95
GLSDGEWQQVLNVWGK	909.01	4.43	352.48
YLEFISDAIIHVLHSK	943.60	5.54	404.45
GHHEAELKPLAQSHATK	928.03	4.61	361.52
KGHHEAELKPLAQSHATK	992.12	4.98	374.41

a. **Ω** values taken from references 35 and 36.

5.2.4 Molecular dynamics (MD) simulations

MD simulations were performed on GA dimer ions charged with two Na^+ or two NH_4^+ cations. A total of twelve different GA dimer ion structures were investigated. The starting structures were based on reported structures for DSDHp, DSHHap and SSHH GA dimers. For the DSDHp GA dimer, two models (models 1 and 4) taken from the NMR spectroscopy results reported by Chen *et al.* were used (PDB ID: 1MIC, Figure 5.4);[37] for the DSDHap GA dimer, two different X-ray structures – one crystalized from ethanol (PDB ID: 1ALZ, Figure 5.5)[38] and another in complex with CsCl (PDB ID: 1AV2, Figure 5.5)[39] – were used; for the SSHH GA dimer, two different NMR spectroscopy structures – one with GA in a DMPC bilayer (PDB ID: 1MAG, Figure 5.6)[40] and another with GA in a DDPC micelle with excess Na^+ present (PDB ID: 1NRU, Figure 5.6)[41] – were used. For all the simulations performed on GA dimers charged with Na^+, except the ones involving 1AV2, the cations were added using the *addIons* command in the *tleap* module of AmberTools15.[42] For the 1AV2 structure, the two Cs^+ ions associated with chain A in the PDB file were replaced with either Na^+. For the simulations performed on GA dimers charged with NH_4^+, the Na^+ ions were replaced with the nitrogen atom of NH_4^+ ions, and the hydrogens were added using the *tleap* module of AmberTools15.[42]

All simulations were run in the gas phase using the *sander* module in AMBER12.[43] The *ff14SB* force field[44] was used for both the L- and D-amino acids, as well as for NH_4^+ ions, and Joung-Cheatham parameters were used for Na^+.[45] Partial charges for the N-terminal formyl group, the C-terminal ethanolamine, and the NH_4^+ ion were assigned using the AM1 with bond charge correction (AM1-BCC) model[46] in the *antechamber* module of AmberTools15.[42] The systems were first minimized using 5000 steps of steepest decent, followed by 5000 steps of conjugate gradient. The systems were heated from 5 K to 300 K over 100 ps, then allowed to run at 300 K

for 100 ps before the 500 ns production simulations were started. The timestep was 2 fs, bonds to hydrogen were constrained with the SHAKE[47] algorithm, and the cutoff for non-bonded interactions was infinite (999.0 Å). The temperature was maintained with the Berendsen thermostat[48] (*ntt* = 1) with velocities rescaled every 1 ps.

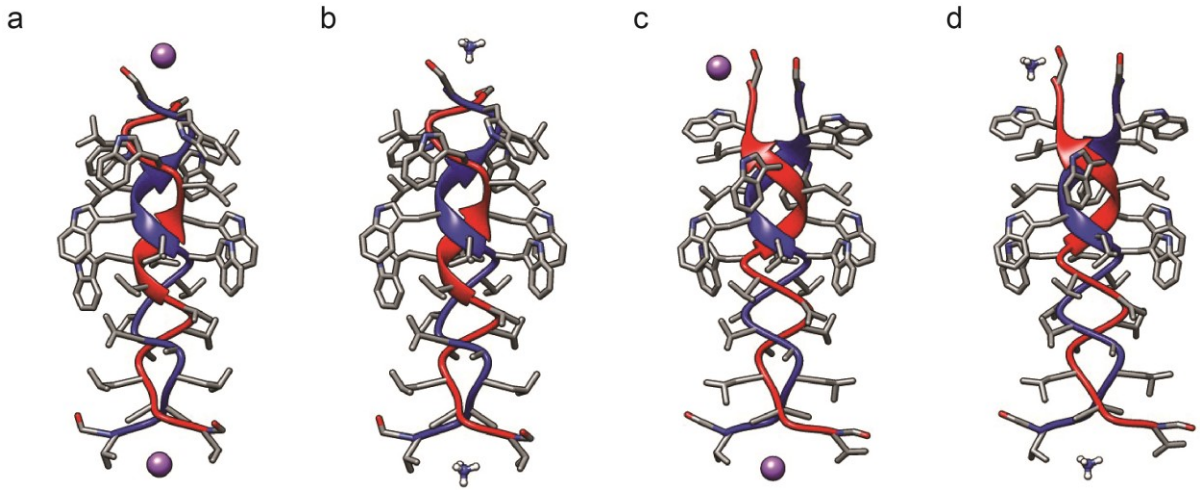

Figure 5.4 Starting structures of the DSDHp form of GA dimer, showing the initial placement of the charging agents, for MD simulations: (a) 1MIC, model 1, with 2 Na^+; (b) 1MIC, model 1, with 2 NH_4^+; (c) 1MIC, model 4, with 2 Na^+; (d) 1MIC, model 4, with 2 NH_4^+.

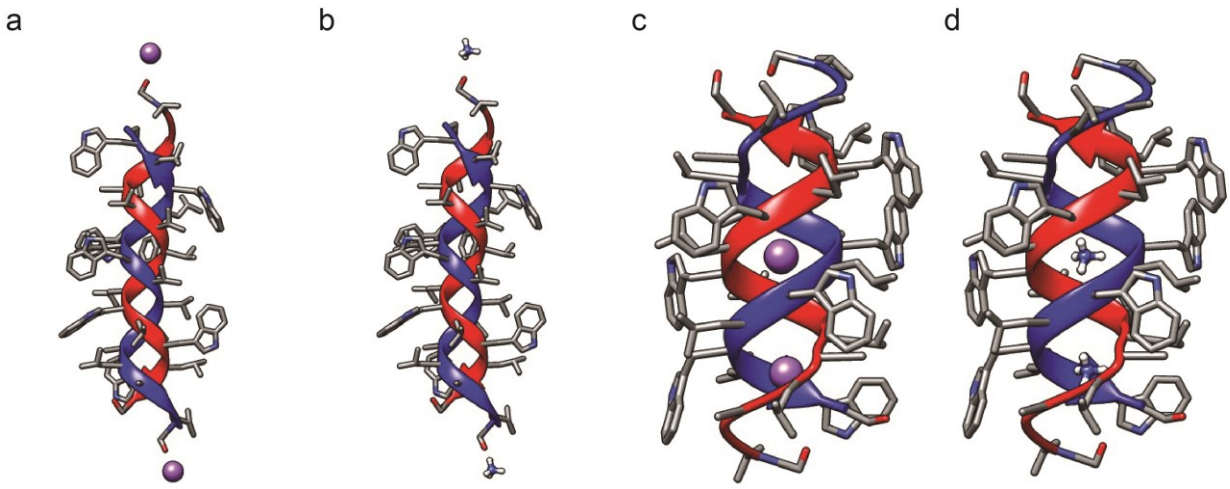

Figure 5.5 Starting structures of the DSDHap form of GA dimer, showing the initial placement of the charging agents, for MD simulations: (a) 1ALZ with 2 Na^+; (b) 1ALZ with 2 NH_4^+; (c) 1AV2 with 2 Na^+; (d) 1AV2 with 2 NH_4^+.

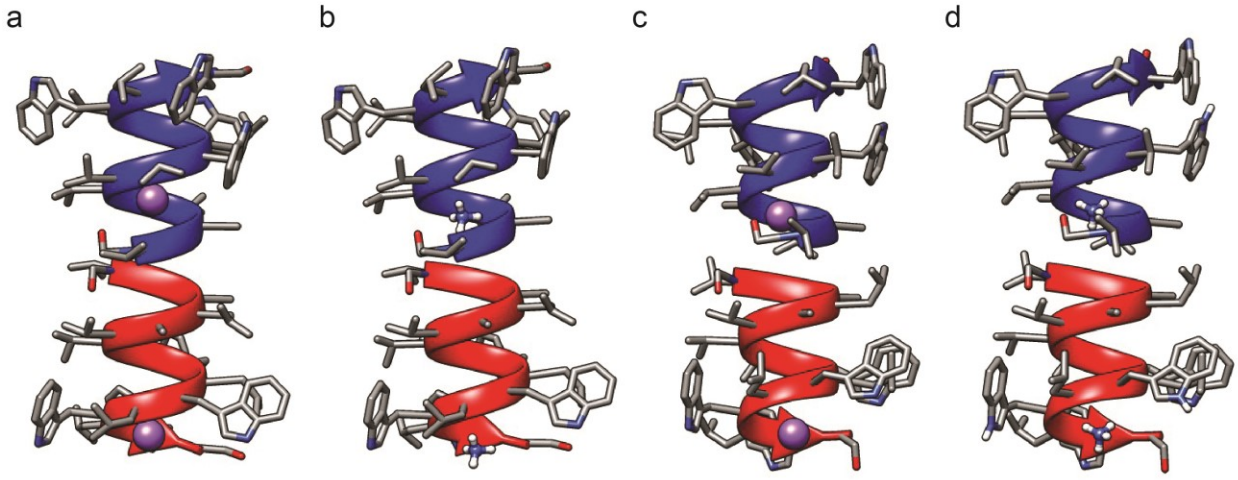

Figure 5.6 Starting structures of the SSHH form of GA dimer, showing the initial placement of the charging agents, for MD simulations: (a) 1MAG with 2 Na^+; (b) 1MAG with 2 NH_4^+; (c) 1MAG with 2 Na^+; (d) 1MAG with 2 NH_4^+.

5.2.5 Theoretical collision cross sections

Theoretical Ω values were calculated for GA dimer structures produced over the course of the MD simulations using the MOBCAL trajectory method.[49,50] Fifty structures were chosen from the 500 ns production simulation, one structure every 10 ns, and the Ω values were calculated with the MOBCAL software parameter *imp* set to 50. Theoretical Ω values were also calculated for GA dimer structures taken directly from Protein Data Bank (PDB).[51] For DSDHap GA dimer, structures 1AL4, 1ALX, 1ALZ were used,[38,39] for DSDHp GA dimer, the 10 models in 1MIC were used[37] and for SSHH GA dimer, structures 1JNO, 1MAG, 1NRM and 1NRU were used.[40,41,52,53] Because each PDB structure was a single set of coordinates, the Ω values were calculated with the MOBCAL software parameter *imp* set to 1000.

5.3 Results and Discussion

5.3.1 GA dimer ions produced from isobutanol

Prior to investigating the conformations of gaseous GA dimers produced from NDs, ESI-IMS-MS was used to analyze isobutanol solutions of GA. Shown in Figure 5.7a is a representative mass spectrum acquired for an isobutanol solution of 5 μM GA (equilibrated for 48 h at 25 °C). The major species detected were the sodiated adducts of the GA monomer and homodimer, i.e., $(GA + 2Na)^{2+}$ (*m/z* 963.54, based on monoisotopic mass), and $(GA + Na)^{+}$ and $(2GA + 2Na)^{2+}$ (*m/z* 1904.08) ions. Also detected were ions corresponding to the sodiated adducts of the heterodimer of GA and GB, i.e., $(GA + GB + 2Na)^{2+}$ (*m/z* 1884.56), and the mixed sodium and potassium adducts of the GA homodimer, i.e., $(2GA + Na + K)^{2+}$ (*m/z* 1912.07).

A plot of IMS arrival time (ATs) measured for *m/z* 1904.08 ions (and the corresponding isotopomers) revealed two features (Figure 5.7b). The dominant feature, attributed to (2GA +

$2Na)^{2+}$ ions, exhibited three distinct (but only partially resolved) arrival time distributions (ATDs), with ATs centred at 10.82 ms (referred to as conformation 1, C1), 11.38 ms (conformation 2, C2), and 12.20 ms (conformation 3, C3), and a lower abundance feature, centred at 15.74 ms, corresponding to $(GA + Na)^{+}$ ions. The mass spectra corresponding to each of these ATs are shown in Figures 5.7c-5.7f , along with the expected theoretical isotopomer distributions calculated for the $(2GA + 2Na)^{2+}$ and $(GA + Na)^{+}$ ions (Figures 5.7g-5.7h). The full width at half maximum (FWHM) for the deconvoluted ATDs (represented as Gaussian functions) for the three $(2GA + 2Na)^{2+}$ conformations are relatively small, 0.44 ms (C1), 0.50 ms (C2) and 0.31 ms (C3), consistent with the presence of three well-defined dimer conformations. In contrast, the broad feature observed for the $(GA + Na)^{+}$ ions (FWHM 1.3 ms) is suggestive of ions with significant conformational flexibility. This finding is consistent with reported results obtained from MD simulations.[54] The IMS-AT data measured for the $(2GA + Na + K)^{2+}$ ions (*m/z* 1912.07) is also suggestive of three distinct conformations, with ATDs centred at 10.92 ms, 11.53 ms and 12.40 ms (Figure 5.7j). In contrast, the IMS-AT data for $(GA + GB + 2Na)^{2+}$ (*m/z* 1884.56) consists of a single broad feature (FWHM 0.95 ms) centred at 11.05 ms (Figure 5.7o), which suggests the presence of multiple, but structurally-similar conformations. A single IMS-ATD, centred at 4.95 ms (FWHM of 0.34), was measured for $(GA + 2Na)^{2+}$ (*m/z* 963.54) (Figure 5.7r).

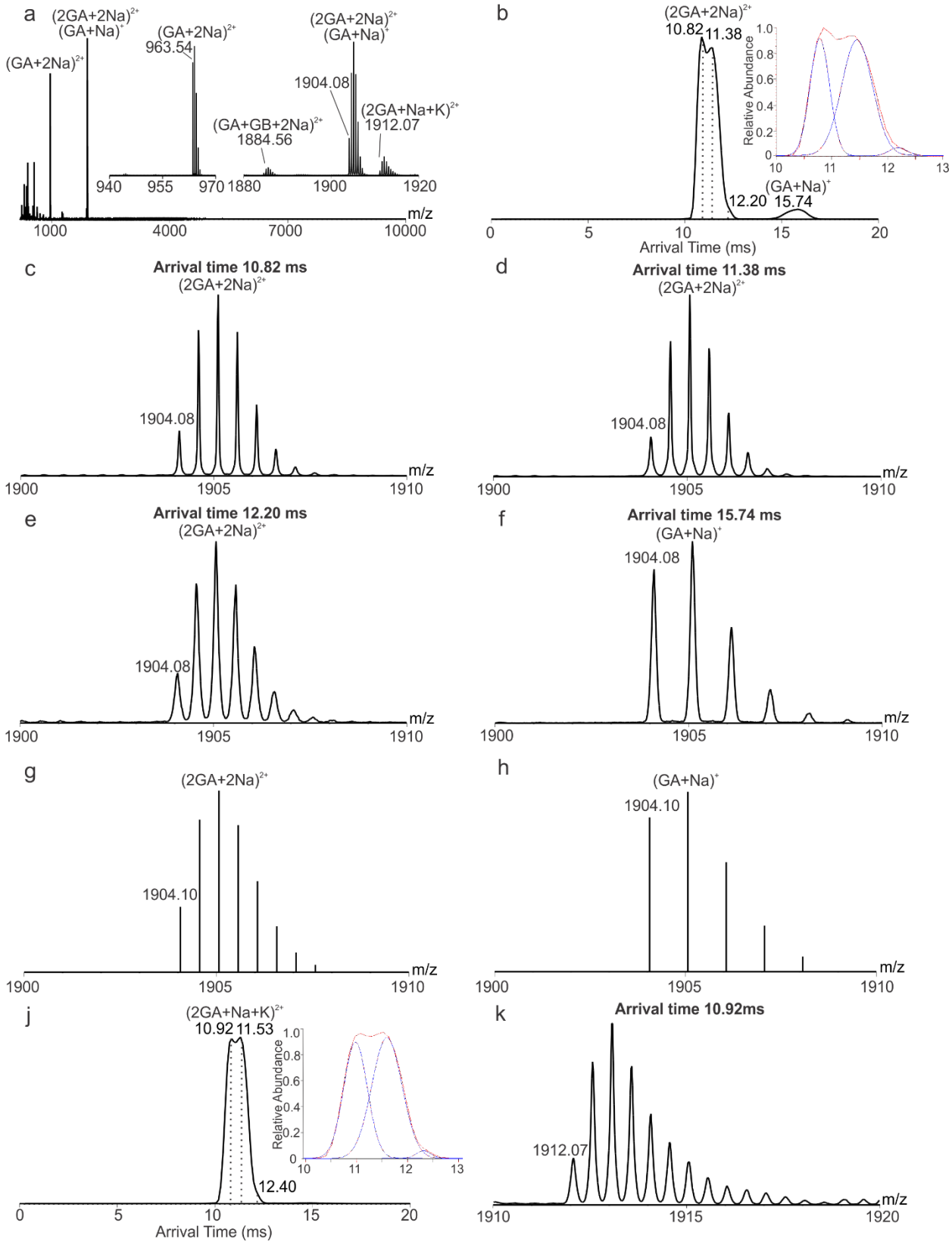
a
(2GA+2Na)2+
(GA+Na)+
(GA+2Na)2+
963.54
(2GA+2Na)2+
(GA+Na)+
(GA+2Na)2+
1904.08
(GA+GB+2Na)2+
1884.56
(2GA+Na+K)2+
1912.07
940 955 970 1880 1900 1920
m/z
1000 4000 7000 10000
b
(2GA+2Na)2+
10.82 11.38
Relative Abundance
(GA+Na)+
12.20 15.74
Arrival Time (ms)
c
Arrival time 10.82 ms
(2GA+2Na)2+
1904.08
m/z
d
Arrival time 11.38 ms
(2GA+2Na)2+
1904.08
m/z
e
Arrival time 12.20 ms
(2GA+2Na)2+
1904.08
m/z
f
Arrival time 15.74 ms
(GA+Na)+
1904.08
m/z
g
(2GA+2Na)2+
1904.10
m/z
h
(GA+Na)+
1904.10
m/z
j
(2GA+Na+K)2+
10.92 11.53
Relative Abundance
12.40
Arrival Time (ms)
k
Arrival time 10.92ms
1912.07
m/z

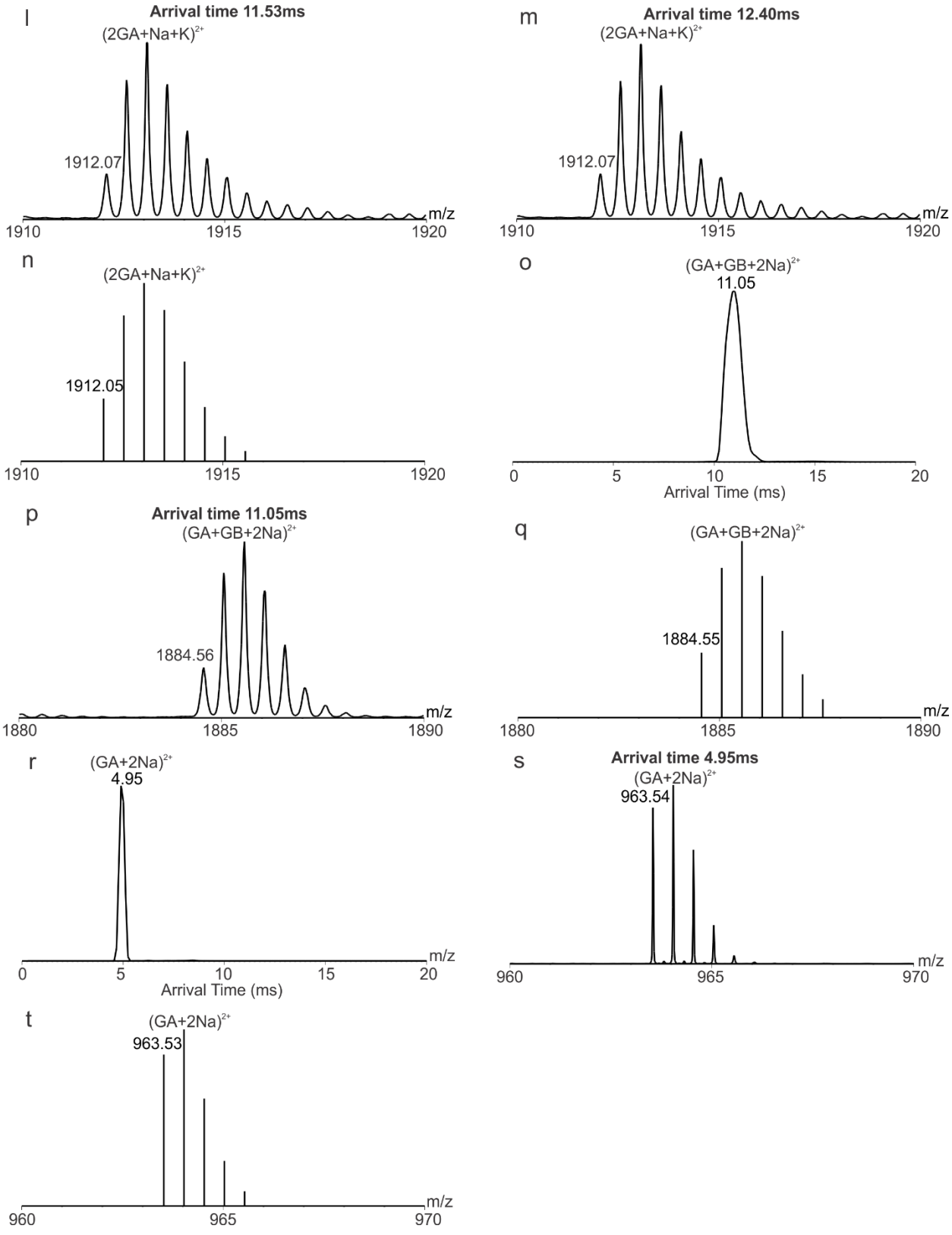
l
Arrival time 11.53ms
(2GA+Na+K)2+
1912.07
m/z
1910
1915
1920
m
Arrival time 12.40ms
(2GA+Na+K)2+
1912.07
m/z
1910
1915
1920
n
(2GA+Na+K)2+
1912.05
1910
1915
1920
o
(GA+GB+2Na)2+
11.05
0
5
10
15
20
Arrival Time (ms)
p
Arrival time 11.05ms
(GA+GB+2Na)2+
1884.56
m/z
1880
1885
1890
q
(GA+GB+2Na)2+
1884.55
m/z
1880
1885
1890
r
(GA+2Na)2+
4.95
m/z
0
5
10
15
20
Arrival Time (ms)
s
Arrival time 4.95ms
(GA+2Na)2+
963.54
m/z
960
965
970
t
(GA+2Na)2+
963.53
m/z
960
965
970

Figure 5.7 (a) ESI mass spectrum of a solution of GA (5 μM) in isobutanol (equilibrated for 48 h at 25 °C). (b) IMS-ATDs measured for ions at *m/z* 1904.08 (monoisotopic mass); inset shows the contribution of three $(2GA + 2Na)^{2+}$ ions conformations to the ATD. (c), (d) and (e) Mass spectra corresponding to AT 10.82 ms, 11.38 ms and 12.20 ms, respectively. (f) Mass spectrum corresponding to AT 15.74 ms. (g) and (h) Theoretical isotopic distributions for $(2GA + 2Na)^{2+}$ and $(GA + Na)^{+}$ ions, respectively. (j) IMS-ATDs measured for ions at *m/z* 1912.07; inset shows the contribution of three $(2GA + Na + K)^{2+}$ ion conformations to the ATD. (k), (l) and (m) Mass spectra corresponding to AT of 10.92 ms, 11.53 ms and 12.40 ms, respectively. (n) Theoretical isotopic distribution for $(2GA + Na + K)^{2+}$. (o) IMS-ATDs measured for ions at *m/z* 1884.56. (p) Mass spectrum corresponding to AT 11.05 ms. (q) Theoretical isotopic distribution of $(GA + GB + 2Na)^{2+}$. (r) IMS-ATDs measured for ions at *m/z* 963.54. (s) Mass spectrum corresponding to AT 4.95 ms. (t) Theoretical isotopic distribution for $(GA + 2Na)^{2+}$.

The IMS-ATs measured for the GA monomer and dimer ions were converted to **Ω** (in He) using the calibration plot constructed from the tryptic peptide calibrant ions (Figure 5.3).[33,34] Using this calibration approach, the **Ω** of the three conformations of $(2GA + 2Na)^{2+}$ were found to be 683 $Å^2$ (C1), 708 $Å^2$ (C2), and 737 $Å^2$ (C3), respectively (Table 5.2). These values agree, within 2%, with values reported previously by Russell and co-workers.[55] Similar **Ω** were also found for the three conformations of $(2GA + Na + K)^{2+}$ ions (688 $Å^2$, 714 $Å^2$, and 749 $Å^2$, Table 5.2), suggesting that the $(2GA + Na + K)^{2+}$ ions adopt the same C1, C2 and C3 conformations. The **Ω** for the $(GA + GB + 2Na)^{2+}$ ions, based on the averaged IMS-AT, is 694 $Å^2$ (Table 5.2). This value is somewhat smaller than the weighted average of the C1, C2 and C3 values, suggesting that the replacement of Trp (GA) with Phe (GB) influences dimer conformation in isobutanol.

Table 5.2 Ion mobility separation arrival times (IMS-ATs) and corresponding collision cross sections (**Ω**, in He) measured for GA dimer and monomer ions produced by ESI from isobutanol solutions (with and without ammonium acetate) and aqueous ammonium acetate solutions of GA-containing NDs.

Solvent	GA ions	*m/z*	Arrival time (ms)	FWHM (ms)	**Ω** ($Å^2$)
Isobutanol	$(2GA+2Na)^{2+}$	1904.08	10.82	0.44	683
			11.38	0.50	708
			12.20	0.31	737
	$(GA+GB+2Na)^{2+}$	1884.56	11.05	0.95	694
	$(2GA+Na+K)^{2+}$	1912.07	10.92	0.52	688
			11.53	0.78	714
			12.40	0.38	749
	$(GA+Na)^{+}$	1904.08	15.74	1.30	441
	$(GA+2Na)^{2+}$	963.54	4.95	0.34	407
Isobutanol saturated $NH_4CH_3CO_2$	$(2GA+2H)^{2+}$	1882.11	11.45	0.60	711
	$(2GA+H+NH_4)^{2+}$	1890.63	11.55	0.56	715
	$(2GA+H+Na)^{2+}$	1893.11	11.19	0.44	700
			11.63	0.41	718
			12.07	0.43	736
	$(2GA+2NH_4)^{2+}$	1899.15	11.55	0.64	715
	$(2GA+2Na)^{2+}$	1904.08	10.95	0.40	690
			11.52	0.67	714
			12.32	0.31	746
	$(GA+H)^{+}$	1882.11	15.31	0.81	434
	$(GA+NH_4)^{+}$	1899.15	14.50	0.75	419
	$(GA+Na)^{+}$	1904.08	15.65	1.18	441
	$(GA+2H)^{2+}$	941.57	4.94	0.23	408

	$(GA+H+Na)^{2+}$	952.57	4.95	0.25	407
	$(GA+2Na)^{2+}$	963.54	4.95	0.27	407
Aqueous $NH_4CH_3CO_2$ solution of GA-containing DMPC ND	$(2GA+2NH_4)^{2+}$	1899.15	10.15	0.43	656
	$(2GA+2H)^{2+}$	1882.11	11.44	0.56	710
	$(GA+NH_4)^{+}$	1899.15	14.96	0.73	428
	$(GA+H)^{+}$	1882.11	15.68	0.83	442
	$(GA+2H)^{2+}$	941.57	4.95	0.23	408
Aqueous $NH_4CH_3CO_2$ solution of GA-containing POPC ND	$(2GA+2NH_4)^{2+}$	1899.15	10.15	0.48	656
	$(GA+NH_4)^{+}$	1899.15	14.77	1.67	425
	$(GA+H)^{+}$	1882.11	16.05	0.72	448
	$(GA+2H)^{2+}$	941.57	4.95	0.32	408

The ESI-IMS-MS data, taken on their own, suggest that ~59% of GA exists as dimer in isobutanol. This value is in good agreement with a value of ~55% determined previously by ESI-MS.[55] However, given the possibility that the GA monomer and dimer have different ionization and detection efficiencies (i.e., ESI-MS response factors), the distribution of GA monomer and dimer present in solution may not be quantitatively reflected in the ESI-MS data. Similarly, assuming that the multiple conformations detected for the $(2GA + 2Na)^{2+}$ and $(2GA + Na + K)^{2+}$ ions are reflective of solution structures and that they have uniform response factors, the ESI-MS data suggest that the GA homodimer exists in three distinct conformations (i.e., C1, C2 and C3) in isobutanol, with relative abundances of 30%, 68% and 2%, respectively. These results are in reasonable agreement with the distribution of $(2GA + 2Na)^{2+}$ conformers reported previously (36%, 61% and 3%).[55]

5.3.2 GA dimer ions produced from isobutanol saturated with ammonium acetate

To investigate whether charging in the ESI process affects the conformations of gaseous GA dimer ions detected from isobutanol, the measurements were repeated using solutions containing ammonium acetate. Shown in Figure 5.8a is a representative mass spectrum acquired for GA (5 μM) in isobutanol (equilibrated for 48 h at 25 °C) saturated with ammonium acetate. In addition to the $(2GA + 2Na)^{2+}$, $(GA + Na)^{+}$ and $(GA + 2Na)^{2+}$ ions, the mass spectrum revealed signal corresponding to $(2GA + 2H)^{2+}$ and $(GA + H)^{+}$ (*m/z* 1882.11), $(2GA + H + NH_4)^{2+}$ (*m/z* 1890.63), $(2GA + H + Na)^{2+}$ (*m/z* 1893.11), $(2GA + 2NH_4)^{2+}$ and $(GA + NH_4)^{+}$) (*m/z* 1899.15), $(GA + 2H)^{2+}$ (*m/z* 941.57) and $(GA + 2Na)^{2+}$ ions (*m/z* 952.57). The IMS-AT data measured for $(2GA + 2Na)^{2+}$ are similar to those described above; the **Ω** for the three conformations (690 $Å^2$, 714 $Å^2$ and 746 $Å^2$, Table 5.2) are within 2% of values measured in the absence of ammonium acetate (Figure 5.8b). This result, on its own, suggests that the presence of ammonium acetate ions does not perturb the GA dimer structures in isobutanol. Three conformations were also detected for the $(2GA + H + Na)^{2+}$ ions, with **Ω** (700 $Å^2$, 718 $Å^2$ and 736 $Å^2$, Table 5.2) similar to those of the $(2GA + 2Na)^{2+}$ ions (Figure 5.8y). In contrast, the IMS-AT data acquired for the $(2GA + 2H)^{2+}$, $(2GA + H + NH_4)^{2+}$ and $(2GA + 2NH_4)^{2+}$ ions are suggestive of a single conformation in the gas phase (Figures 5.8j, 5.8o and 5.8v), with **Ω** values (711 $Å^2$, 715 $Å^2$ and 715 $Å^2$, respectively, Table 5.2), similar to that of C2. The IMS-AT data measured for the $(GA + H)^{+}$ and $(GA + NH_4)^{+}$ ions give **Ω** in the range of 419 $Å^2$ to 434 $Å^2$, which is slightly smaller than that of $(GA + Na)^{+}$. Likewise, the **Ω** measured for the $(GA + 2H)^{2+}$ and $(GA + H + Na)^{2+}$ ions (407 $Å^2$ and 408 $Å^2$, respectively, Table 5.2) are indistinguishable from that of $(GA + 2Na)^{2+}$.

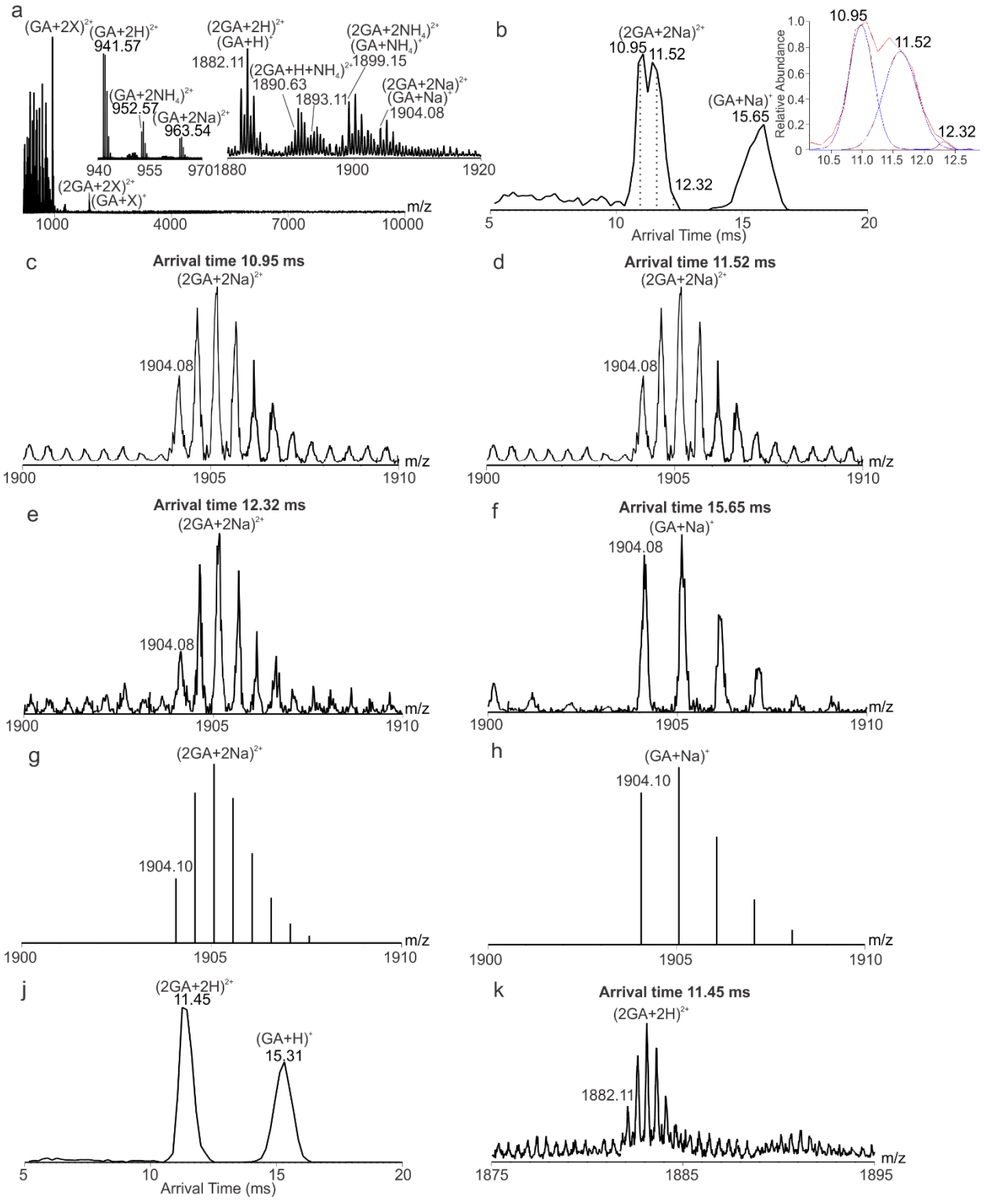
a
(GA+2X)2+
(GA+2H)2+
941.57
(2GA+2H)2+
(GA+H)+
1882.11
(2GA+2NH4)2+
(GA+NH4)+
1899.15
(2GA+H+NH4)2+
1890.63
1893.11
(2GA+2Na)2+
(GA+Na)+
1904.08
(GA+2NH4)2+
952.57
(GA+2Na)2+
963.54
(2GA+2X)2+
(GA+X)+
m/z
b
(2GA+2Na)2+
10.95
11.52
12.32
(GA+Na)+
15.65
Relative Abundance
Arrival Time (ms)
c
Arrival time 10.95 ms
(2GA+2Na)2+
1904.08
d
Arrival time 11.52 ms
(2GA+2Na)2+
1904.08
e
Arrival time 12.32 ms
(2GA+2Na)2+
1904.08
f
Arrival time 15.65 ms
(GA+Na)+
1904.08
g
(2GA+2Na)2+
1904.10
h
(GA+Na)+
1904.10
j
(2GA+2H)2+
11.45
(GA+H)+
15.31
Arrival Time (ms)
k
Arrival time 11.45 ms
(2GA+2H)2+
1882.11
m/z

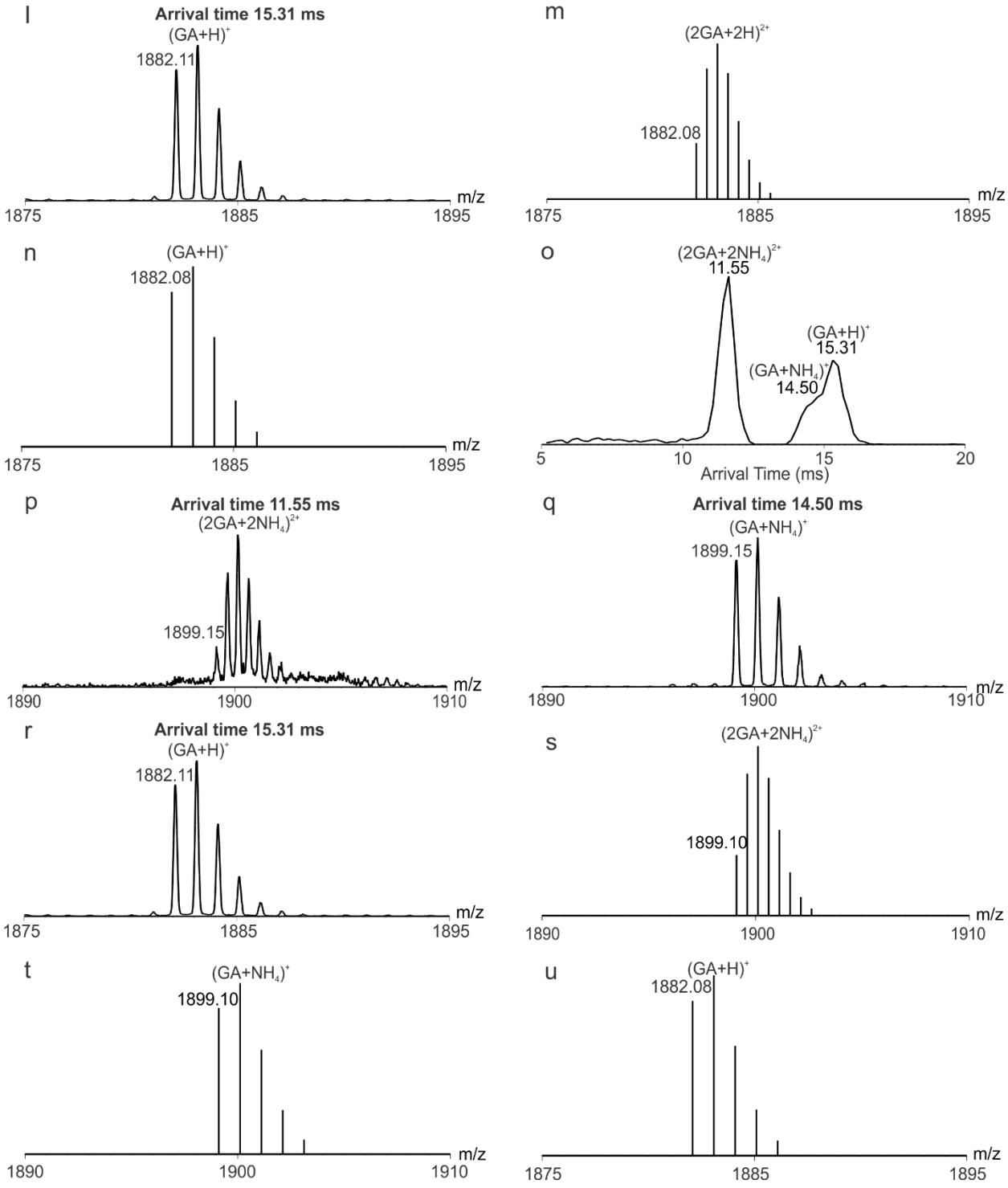
l
Arrival time 15.31 ms
(GA+H)+
1882.11
m/z
1875
1885
1895
m
(2GA+2H)2+
1882.08
m/z
1875
1885
1895
n
(GA+H)+
1882.08
m/z
1875
1885
1895
o
(2GA+2NH4)2+
11.55
(GA+H)+
15.31
(GA+NH4)+
14.50
5
10
15
20
Arrival Time (ms)
p
Arrival time 11.55 ms
(2GA+2NH4)2+
1899.15
m/z
1890
1900
1910
q
Arrival time 14.50 ms
(GA+NH4)+
1899.15
m/z
1890
1900
1910
r
Arrival time 15.31 ms
(GA+H)+
1882.11
m/z
1875
1885
1895
s
(2GA+2NH4)2+
1899.10
m/z
1890
1900
1910
t
(GA+NH4)+
1899.10
m/z
1890
1900
1910
u
(GA+H)+
1882.08
m/z
1875
1885
1895

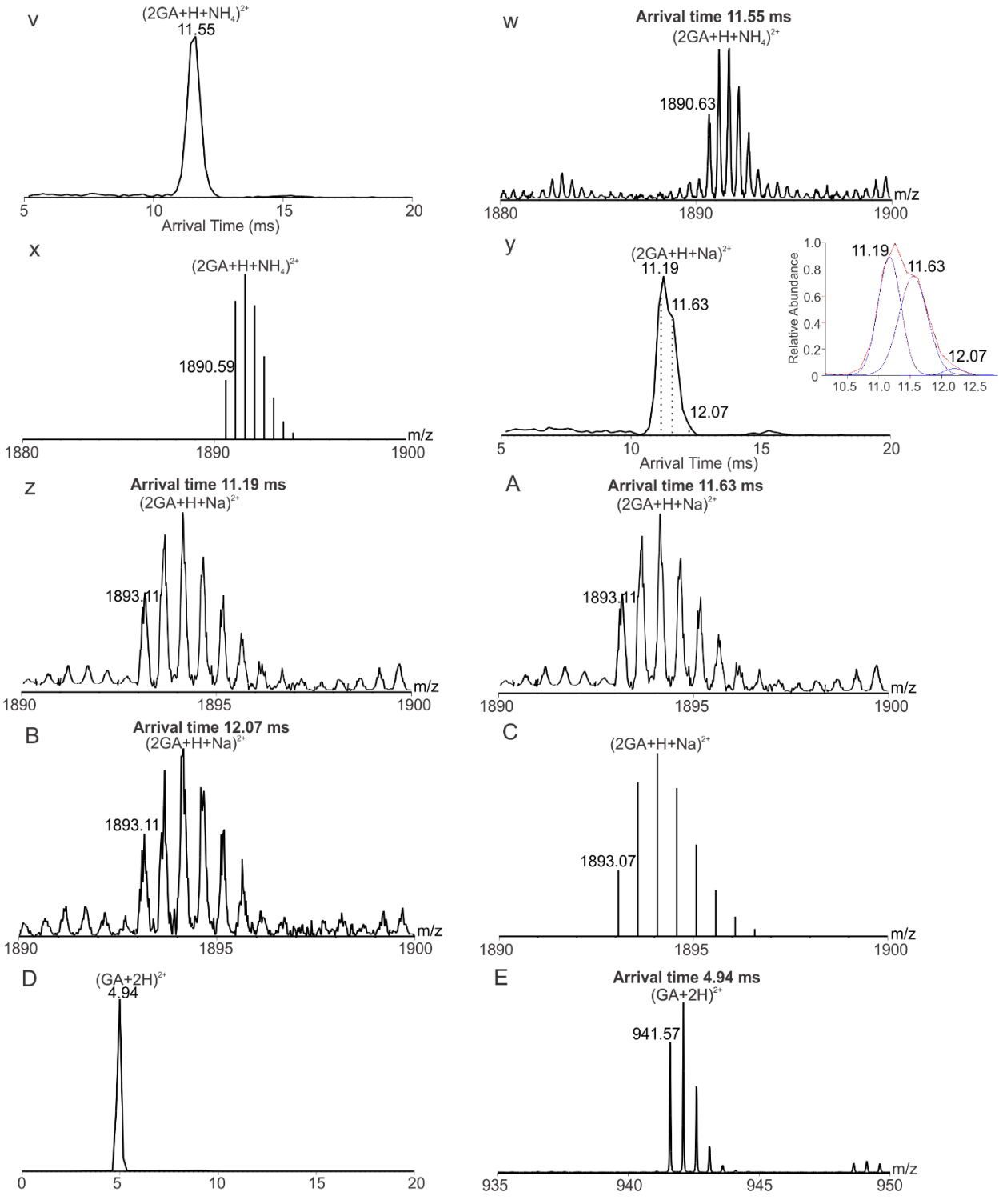
v
(2GA+H+NH4)2+
11.55
5
10
15
20
Arrival Time (ms)
w
Arrival time 11.55 ms
(2GA+H+NH4)2+
1890.63
1880
1890
1900
m/z
x
(2GA+H+NH4)2+
1890.59
1880
1890
1900
m/z
y
(2GA+H+Na)2+
11.19
11.63
12.07
5
10
15
20
Arrival Time (ms)
Relative Abundance
1.0
0.8
0.6
0.4
0.2
0
10.5
11.0
11.5
12.0
12.5
z
Arrival time 11.19 ms
(2GA+H+Na)2+
1893.11
1890
1895
1900
m/z
A
Arrival time 11.63 ms
(2GA+H+Na)2+
1893.11
1890
1895
1900
m/z
B
Arrival time 12.07 ms
(2GA+H+Na)2+
1893.11
1890
1895
1900
m/z
C
(2GA+H+Na)2+
1893.07
1890
1895
1900
m/z
D
(GA+2H)2+
4.94
0
5
10
15
20
E
Arrival time 4.94 ms
(GA+2H)2+
941.57
935
940
945
950
m/z

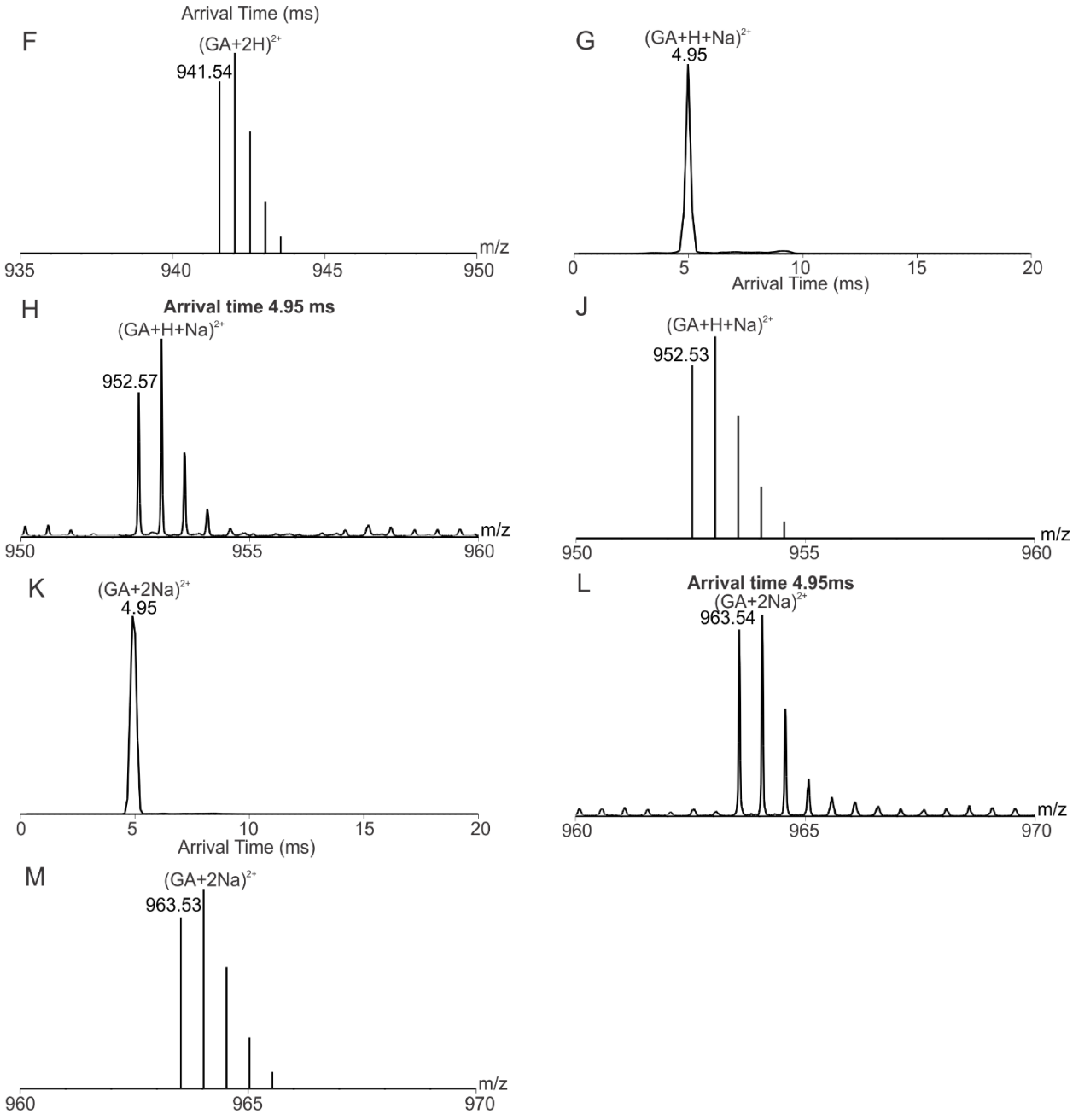

Figure 5.8 (a) ESI mass spectrum of a solution of GA (5 μM) in isobutanol (equilibrated for 48 h at 25 °C) saturated with ammonium acetate. (b) IMS-ATDs measured for ions at *m/z* 1904.08 (monoisotopic mass); inset shows the contribution of three $(2GA + 2Na)^{2+}$ ions conformations to the ATD. (c), (d), (e) and (f) Mass spectra corresponding to AT 10.95 ms, 11.52 ms, 12.32 ms and

15.65 ms, respectively. (g) and (h) Theoretical isotopic distributions of $(2GA + 2Na)^{2+}$ and $(GA + Na)^{+}$, respectively. (j) IMS-ATDs measured for ions at *m/z* 1882.11. (k) and (l) Mass spectra corresponding to AT 11.45 ms and 15.31 ms, respectively. (m) and (n) Theoretical isotopic distributions for $(2GA + 2H)^{2+}$ and $(GA + H)^{2+}$, respectively. (o) IMS-ATDs measured for ions at *m/z* 1899.15. (p), (q) and (r) Mass spectra corresponding to AT 11.55 ms, 14.5 ms and 14.5 ms, respectively. (s), (t) and (u) Theoretical isotopic distributions for $(2GA + 2NH_4)^{2+}$, $(GA + NH_4)^{+}$ and $(GA + H)^{+}$, respectively. (v) IMS-ATDs measured for ions at *m/z* 1890.63. (w) Mass spectrum corresponding to AT 11.55 ms. (x) Theoretical isotopic distribution for $(2GA + H + NH_4)^{2+}$. (y) IMS-ATDs measured for ions at *m/z* 1893.11. (z), (A) and (B) Mass spectra corresponding to AT 11.63 ms, and 12.07 ms, respectively. (C) Theoretical isotopic distribution for $(2GA + H + Na)^{2+}$. (D) IMS-ATDs measured for ions at *m/z* 941.54. (E) Mass spectrum corresponding to AT 4.94 ms. (F) Theoretical isotopic distribution for $(GA + 2H)^{2+}$. (G) IMS-ATDs measured for ions at *m/z* 952.57. (H) Mass spectrum corresponding to AT 4.95 ms. (J) Theoretical isotopic distribution for $(GA + H + Na)^{2+}$. (K) IMS-ATDs measured for ions at *m/z* 963.54. (L) Mass spectrum corresponding to AT 4.95 ms. (M) Theoretical isotopic distribution of $(GA + 2Na)^{2+}$.

Taken together, the IMS results obtained for the GA ions produced from isobutanol solutions, alone or with ammonium acetate, provide experimental evidence that the nature of the ESI charging agent can influence the conformations of GA dimer ions detected in the gas phase. Despite being produced from the same solution, three distinct conformations were observed for GA dimer ions charged by one or two Na^{+}, but only a single conformation for GA dimer ions charged by H^{+} or NH_4^{+}. While the origin of these structural differences could not be conclusively

established, *vide infra*, they presumably arise from differences in the nature of the interactions between the different charging agents with the peptides. As described in more detail below, the results of MD simulations performed on desolvated, doubly charged GA dimers revealed that both Na^+ and NH_4^+ are solvated predominantly by carbonyl oxygens, although the average number of interactions is significantly different for the two cations. Regardless of the exact origin of the conformational differences in the GA dimer ions, the present findings highlight a potential complication in using IMS-derived Ω as a probe of the conformations of peptide complexes in solution.

5.3.3 GA dimer ions produced from NDs

According to available structural data, the GA dimer exists preferentially in the SSHH form when present in a lipid bilayer and the DSDHp and DSDHap forms when present in organic solvents.[22,23,25,26] Consequently, it was of interest to probe the Ω of gas-phase GA dimer ions produced directly from ND lipid bilayers in aqueous solution and to compare them to values measured for dimer ions produced from isobutanol. Shown in Figures 5.9 and 5.10 are representative ESI mass spectra and corresponding IMS data acquired for an aqueous ammonium acetate (200 mM, pH 6.8) solution of GA-containing DMPC ND (Figure 5.9) or GA-containing POPC ND (Figure 5.10). In both cases, the major species detected correspond to protonated DMPC or POPC ions. For the DMPC NDs, the GA dimer ions, $(2GA + 2H)^{2+}$ and $(2GA + 2NH_4)^{2+}$, were detected, along with monomeric species, $(GA + H)^+$, $(GA + NH_4)^+$ and $(GA + 2H)^{2+}$ (Figure 5.9). It is proposed that the GA dimers are spontaneously ejected from the NDs upon transfer to the gas phase in a process that is analogous to what has been previously reported in ESI-MS studies of protein–glycolipid complexes involving water soluble lectins and glycolipids incorporated into

NDs.[30] The broad feature centred at *m/z* ~8000 is attributed to intact ND ions.[56] Collisional activation of these ions (at *m/z* ≥6000) in the Trap region (20 V) resulted in the appearance of $(GA + NH_4)^+$ monomer ions, indicating the incomplete release of GA from the NDs in the source (Figure 5.11). For the POPC NDs, only the $(2GA + 2NH_4)^{2+}$ dimer ion were detected; monomeric $(GA + H)^+$ ions and $(GA + NH_4)^+$ ions were also produced (Figure 5.10). Similar to what was observed for the DMPC ND ions, collisional activation of the POPC ND ions (at *m/z* ≥6000) in the Trap region (20 V) resulted in the appearance of $(GA + NH_4)^+$ monomer ions (Figure 5.12).

The **Ω** measured for the monomeric GA ions, $(GA + H)^+$, $(GA + NH_4)^+$ and $(GA + 2H)^{2+}$, (442 $Å^2$, 428 $Å^2$, 408 $Å^2$, respectively, Table 5.2), as well as the $(2GA + 2H)^{2+}$ dimer ion (710 $Å^2$, Table 5.2), produced from DMPC NDs, are similar to the values measured for these ions produced from the isobutanol solution containing ammonium acetate. In contrast, the **Ω** measured for the $(2GA + 2NH_4)^{2+}$ ions (656 $Å^2$, Table 5.2) is significantly smaller than that measured for the $(2GA + 2NH_4)^{2+}$ ions produced from isobutanol (715 $Å^2$, Table 5.2). Similar findings were obtained from the IMS analysis of the GA-containing POPC NDs. The results indicate that the GA dimer present in the NDs exist predominantly in a conformation (referred to here as C4) that is distinct from those adopted in isobutanol. Furthermore, given that this conformation was only observed when GA was present in a lipid bilayer, it may be further speculated that C4 originates from the native, ion conducting SSHH form of GA. The observation of a compact GA dimer produced from NDs contrasts recent results, obtained using the VCFD method, where the same three conformations (with **Ω** of 673 $Å^2$, 697 $Å^2$, and 725 $Å^2$, respectively) were detected for $(2GA + 2Na)^{2+}$ ions from DMPC and POPC vesicles.[27] While the reason behind these differences is not fully understood, these results show that the nature of the method used to deliver the GA dimers from a lipid bilayer to the gas phase can influence the conformation(s) of the gaseous ions.

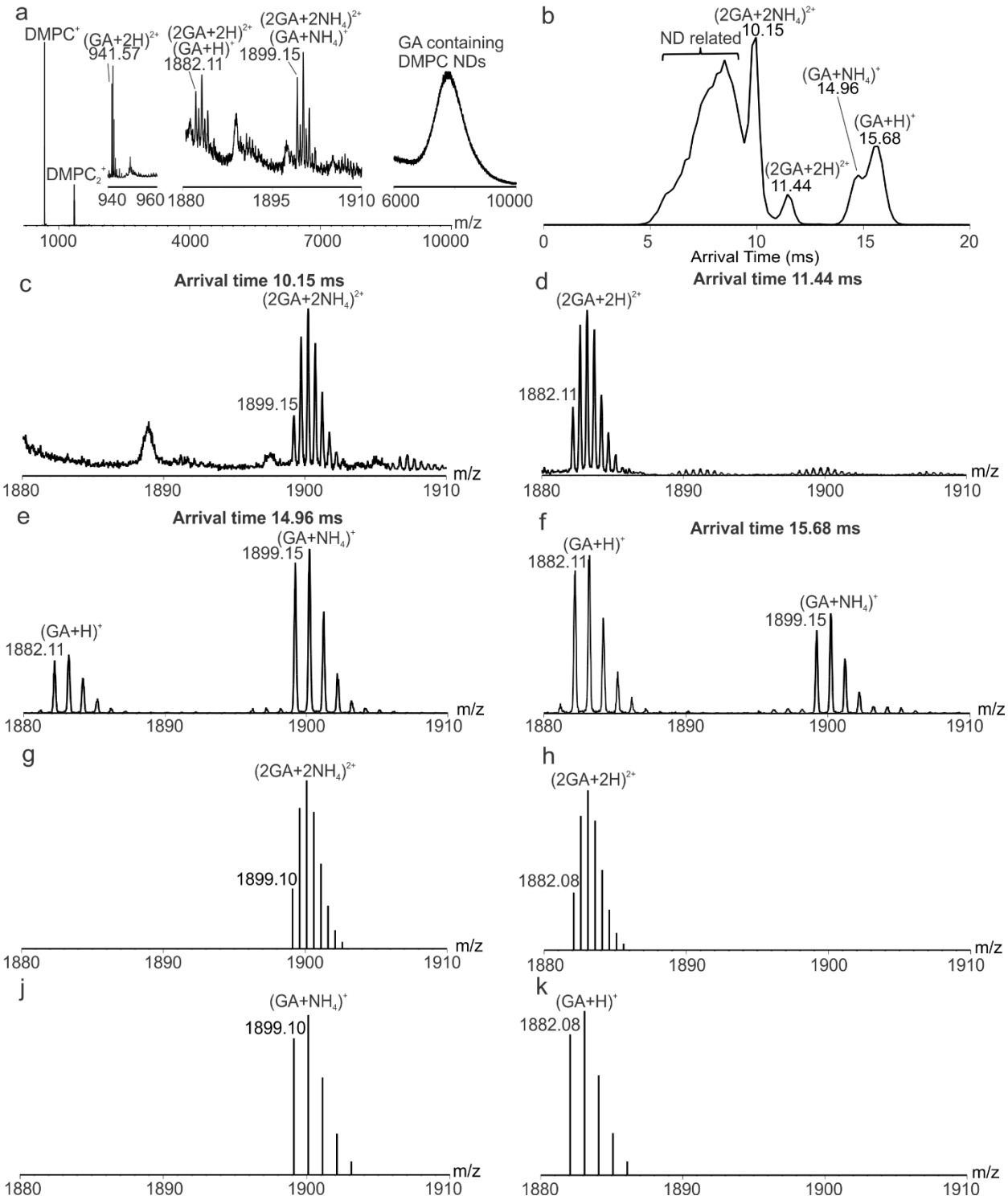
a
DMPC+
(GA+2H)2+
941.57
DMPC2+
(2GA+2H)2+
(GA+H)+
1882.11
(2GA+2NH4)2+
(GA+NH4)+
1899.15
GA containing
DMPC NDs
940 960
1880 1895 1910
6000 10000
1000 4000 7000 10000
m/z
b
(2GA+2NH4)2+
10.15
ND related
(GA+NH4)+
14.96
(GA+H)+
15.68
(2GA+2H)2+
11.44
0 5 10 15 20
Arrival Time (ms)
c
Arrival time 10.15 ms
(2GA+2NH4)2+
1899.15
m/z
1880 1890 1900 1910
d
Arrival time 11.44 ms
(2GA+2H)2+
1882.11
m/z
1880 1890 1900 1910
e
Arrival time 14.96 ms
(GA+NH4)+
1899.15
(GA+H)+
1882.11
m/z
1880 1890 1900 1910
f
Arrival time 15.68 ms
(GA+H)+
1882.11
(GA+NH4)+
1899.15
m/z
1880 1890 1900 1910
g
(2GA+2NH4)2+
1899.10
m/z
1880 1890 1900 1910
h
(2GA+2H)2+
1882.08
m/z
1880 1890 1900 1910
j
(GA+NH4)+
1899.10
m/z
1880 1890 1900 1910
k
(GA+H)+
1882.08
m/z
1880 1890 1900 1910

Figure 5.9 (a) ESI mass spectrum acquired for aqueous ammonium acetate solution (200 mM, pH 6.8, 25 °C) of GA-containing DMPC NDs (15 μM). (b) Plot of IMS-ATs measured for all ions between *m/z* 1880 and *m/z* 1910. (c) and (d) ESI mass spectra corresponding to IMS-AT 10.15 ms and 11.44 ms, respectively. (e) and (f) ESI mass spectra corresponding to AT 14.96 ms and 15.68 ms, respectively. (g), (h), (j) and (k) Theoretical isotopic distributions for $(2GA + 2NH_4)^{2+}$, $(2GA + 2H)^{2+}$, $(GA + NH_4)^{+}$ and $(GA + H)^{+}$, respectively.

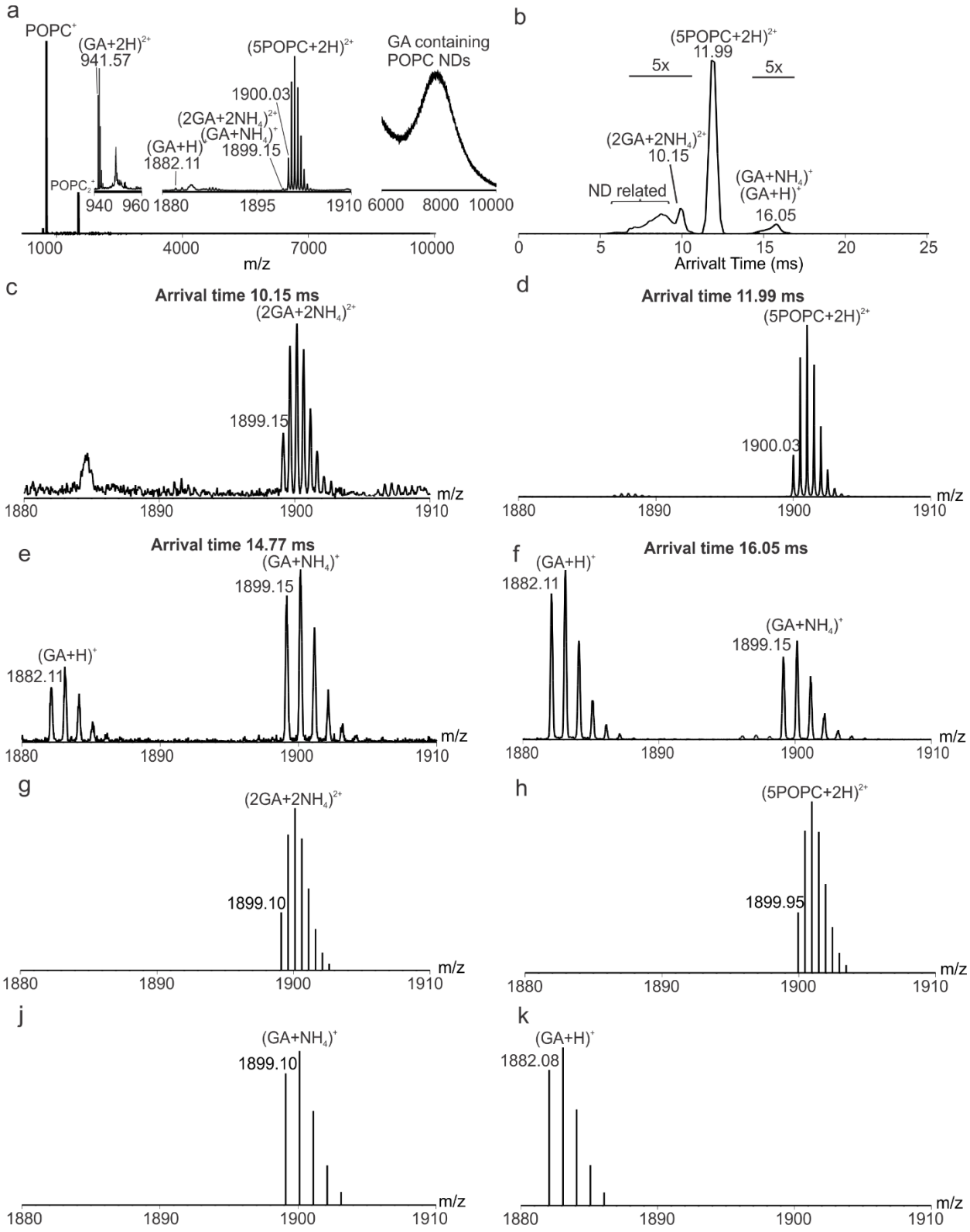
a
POPC+
(GA+2H)2+
941.57
(5POPC+2H)2+
GA containing
POPC NDs
1900.03
(2GA+2NH4)2+
(GA+NH4)+
1899.15
(GA+H)+
1882.11
POPC2+
940 960 1880 1895 1910 6000 8000 10000
1000 4000 7000 10000
m/z
b
(5POPC+2H)2+
11.99
5x
5x
(2GA+2NH4)2+
10.15
ND related
(GA+NH4)+
(GA+H)+
16.05
0 5 10 15 20 25
Arrivalt Time (ms)
c
Arrival time 10.15 ms
(2GA+2NH4)2+
1899.15
m/z
1880 1890 1900 1910
d
Arrival time 11.99 ms
(5POPC+2H)2+
1900.03
m/z
1880 1890 1900 1910
e
Arrival time 14.77 ms
(GA+NH4)+
1899.15
(GA+H)+
1882.11
m/z
1880 1890 1900 1910
f
Arrival time 16.05 ms
(GA+H)+
1882.11
(GA+NH4)+
1899.15
m/z
1880 1890 1900 1910
g
(2GA+2NH4)2+
1899.10
m/z
1880 1890 1900 1910
h
(5POPC+2H)2+
1899.95
m/z
1880 1890 1900 1910
j
(GA+NH4)+
1899.10
m/z
1880 1890 1900 1910
k
(GA+H)+
1882.08
m/z
1880 1890 1900 1910

Figure 5.10 (a) ESI mass spectrum acquired for aqueous ammonium acetate solution (200 mM, pH 6.8, 25 °C) of GA-containing POPC NDs (15 μM). (b) Plot of IMS-ATs measured for all ions between *m/z* 1880 and *m/z* 1910. (c), (d), (e) and (f) ESI mass spectra corresponding to IMS-AT 10.15 ms, 11.99 ms, 14.77 ms and 16.05 ms, respectively. (g), (h), (j) and (k) Theoretical isotopic distributions for $(2GA + 2NH_4)^{2+}$, $(5POPC + 2H)^{2+}$, $(GA + NH_4)^{+}$ and $(GA + H)^{+}$, respectively.

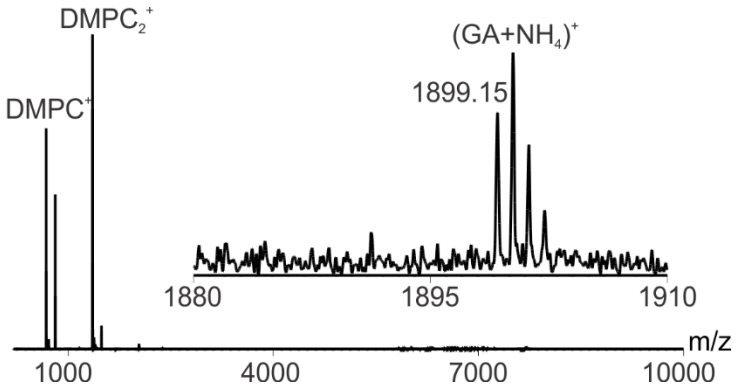

Figure 5.11 CID mass spectrum acquired for ND ions at *m/z* ≥6000, produced from GA-containing DMPC NDs in 200 mM aqueous ammonium acetate solutions (pH 6.8), in the Trap region at 20 V.

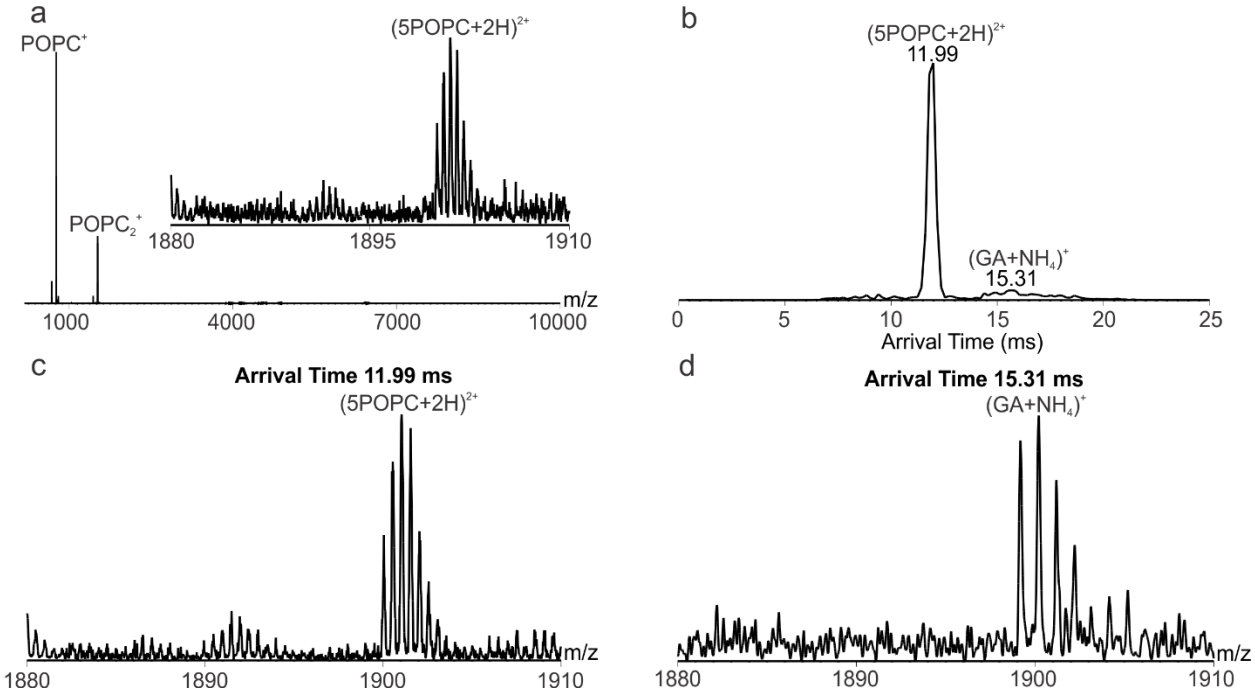

Figure 5.12 (a) CID mass spectrum acquired for ND ions at *m/z* ≥6000, produced from GA-containing DMPC NDs in 200 mM aqueous ammonium acetate solutions (pH 6.8) in the Trap region at 20 V. (b) IMS-ATD measured for ions from *m/z* 1880 to *m/z* 1910 in (c). (c) and (d) Mass spectrum corresponding to AT 11.99 ms and 15.31 ms, respectively.

It is also curious that the $(2GA + 2NH_4)^{2+}$ and $(2GA + 2H)^{2+}$ ions produced from the DMPC NDs exhibit significantly different **Ω**. This observation has, at least, two possible explanations – there are two GA dimer conformers present in the DMPC NDs or the larger $(2GA + 2H)^{2+}$ ions originate from the loss of NH_3 from the more compact $(2GA + 2NH_4)^{2+}$ ions. To test the latter, CID was performed on the $(2GA + 2NH_4)^{2+}$ ions in the Transfer region at voltages ranging from 2 V to 50 V (Figure 5.13). It can be seen that the $(2GA + 2NH_4)^{2+}$ ions dissociate preferentially into $(GA + NH_4)^{+}$ ions, which in turn convert to give $(GA + H)^{+}$ ions; there is no evidence of (2GA +

$2H)^{2+}$ ion formation. This results, together with the absence of $(2GA + 2H)^{2+}$ ion produced from the POPC NDs, suggests that there are two different GA dimer structures in the solutions of DMPC ND, but only one dominant structure in the POPC ND solution.

Additional, albeit indirect, insights into the differences in GA dimer structures in the ND solutions can be found from the results obtained when sodium acetate was added to the aqueous ammonium acetate solutions of GA-containing NDs (Figures 5.14 and 5.15). Notably, $(2GA + H + Na)^{2+}$, $(2GA + 2Na)^{2+}$ ions were produced, in addition to $(2GA + 2H)^{2+}$ and $(2GA + 2NH_4)^{2+}$ ions, from the DMPC NDs. The Ω of the $(2GA + H + Na)^{2+}$ and $(2GA + 2Na)^{2+}$ ions (710 $Å^2$) are indistinguishable from the value measured for $(2GA + 2H)^{2+}$ (Figure 5.14). In contrast, no Na^+ adducts of GA dimers were detected for the POPC NDs (Figure 5.15); however, $(GA + Na)^+$ ions were observed. Taken together, these results suggest that the mechanism of ESI charging of the compact GA dimer (i.e., $(2GA + 2NH_4)^{2+}$) is distinct from that of GA monomer ions and $(2GA + 2H)^{2+}$ produced from the ND solutions. One possible explanation is that the GA dimer exists in the ion conducting SSHH form in the ND bilayer and is associated with NH_4^+ cations, present at high concentration in solution, which are retained in the gas phase. An alternative explanation would see the compact GA dimer ionized, post-transfer of the ND to the gas phase. In this case, ESI charging of the dimer will reflect the available charging agents associated with the gaseous ND ions. If the ESI droplets and, correspondingly, the NDs are primarily charged by NH_4^+ ions, then these will be the main charging agents for the GA ions released from the NDs. According to the proposed models, the less compact GA dimer exists either in a structure that does not bind cations in solution or is more "exposed" to the charging agents in the ESI droplets.

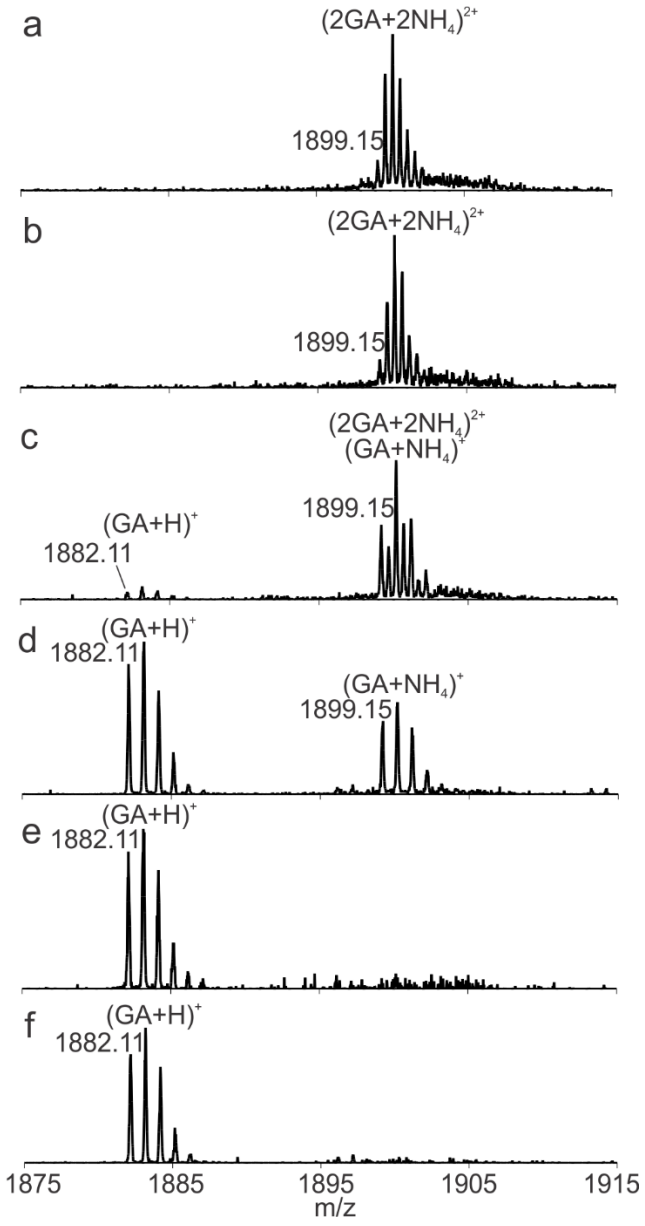

Figure 5.13 CID mass spectra acquired in the Transfer region for $(2GA + 2NH_4)^{2+}$, produced from aqueous ammonium acetate solution (200 mM, pH 6.8, 25 °C) of GA-containing DMPC NDs (15 μM), at voltages of (a) 2 V, (b) 10 V, (c) 20 V, (d) 30 V, (e) 40 V and (f) 50 V.

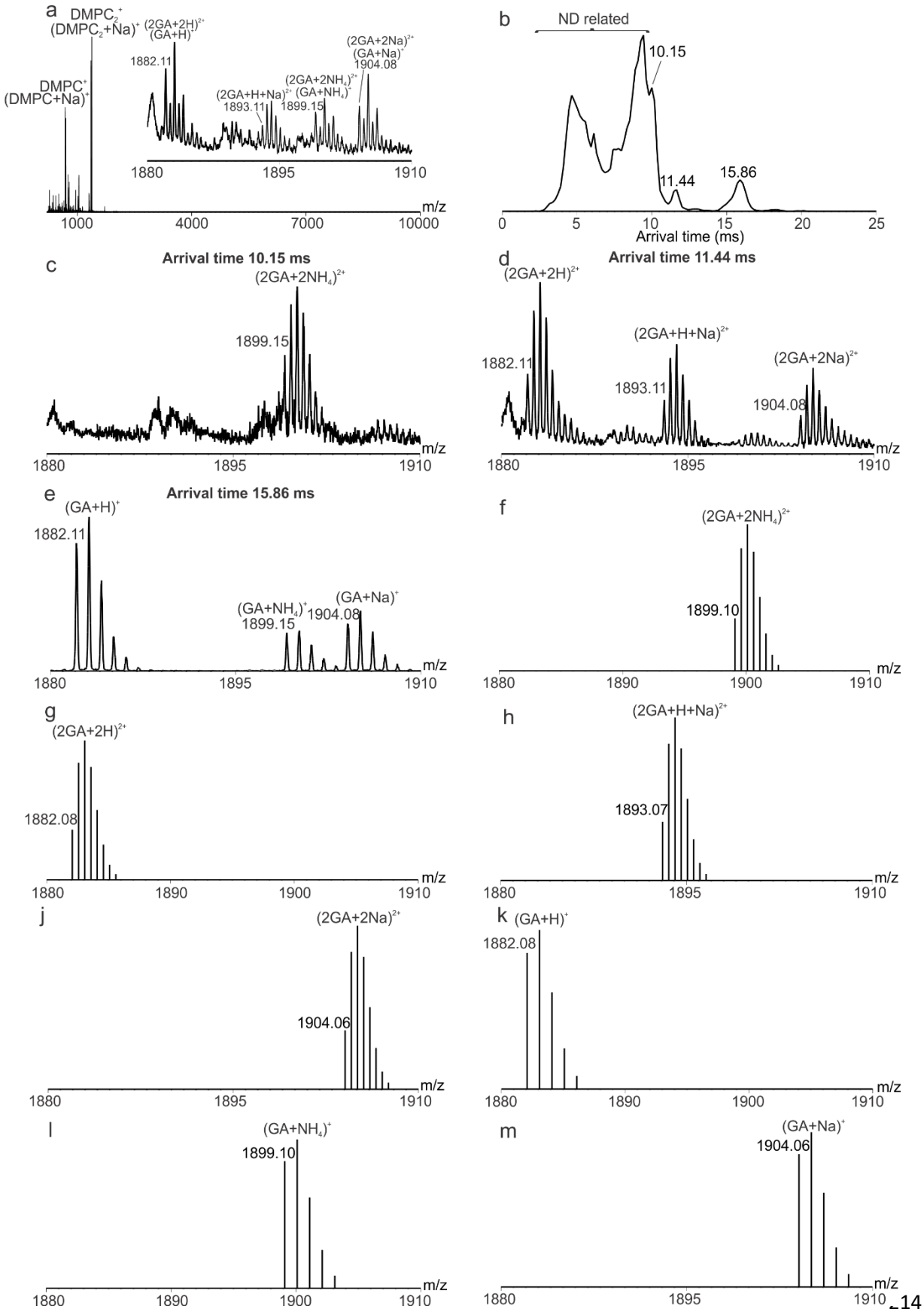
a
DMPC2+
(DMPC2+Na)+
(2GA+2H)2+
(GA+H)+
1882.11
DMPC+
(DMPC+Na)+
(2GA+H+Na)2+
1893.11
(2GA+2NH4)2+
(GA+NH4)+
1899.15
(2GA+2Na)2+
(GA+Na)+
1904.08
1880
1895
1910
m/z
1000
4000
7000
10000
b
ND related
10.15
11.44
15.86
0
5
10
15
20
25
Arrival time (ms)
c
Arrival time 10.15 ms
(2GA+2NH4)2+
1899.15
m/z
1880
1895
1910
d
Arrival time 11.44 ms
(2GA+2H)2+
(2GA+H+Na)2+
(2GA+2Na)2+
1882.11
1893.11
1904.08
m/z
1880
1895
1910
e
Arrival time 15.86 ms
(GA+H)+
1882.11
(GA+NH4)+
1899.15
1904.08
(GA+Na)+
m/z
1880
1895
1910
f
(2GA+2NH4)2+
1899.10
m/z
1880
1890
1900
1910
g
(2GA+2H)2+
1882.08
m/z
1880
1890
1900
1910
h
(2GA+H+Na)2+
1893.07
m/z
1880
1895
1910
j
(2GA+2Na)2+
1904.06
m/z
1880
1895
1910
k
(GA+H)+
1882.08
m/z
1880
1890
1900
1910
l
(GA+NH4)+
1899.10
m/z
1880
1890
1900
1910
m
(GA+Na)+
1904.06
m/z
1880
1895
1910

Figure 5.14 (a) ESI mass spectrum acquired for aqueous ammonium acetate solution (200 mM, pH 6.8, 25 °C) of GA-containing DMPC NDs (15 μM) with addition of sodium acetate (10 mM). (b) Plot of IMS-ATs measured for all ions between *m/z* 1880 and *m/z* 1910. (c), (d) and (e) ESI mass spectrum corresponding to AT 10.15 ms, 11.44 ms, and 15.86 ms, respectively. (f), (g), (h), (j), (k), (l) and (m) Theoretical isotopic distribution of $(2GA + 2NH_4)^{2+}$, $(2GA + 2H)^{2+}$, $(2GA + H + Na)^{2+}$, $(2GA + 2Na)^{2+}$, $(GA + H)^{+}$, $(GA + NH_4)^{+}$ and $(GA + Na)^{+}$, respectively.

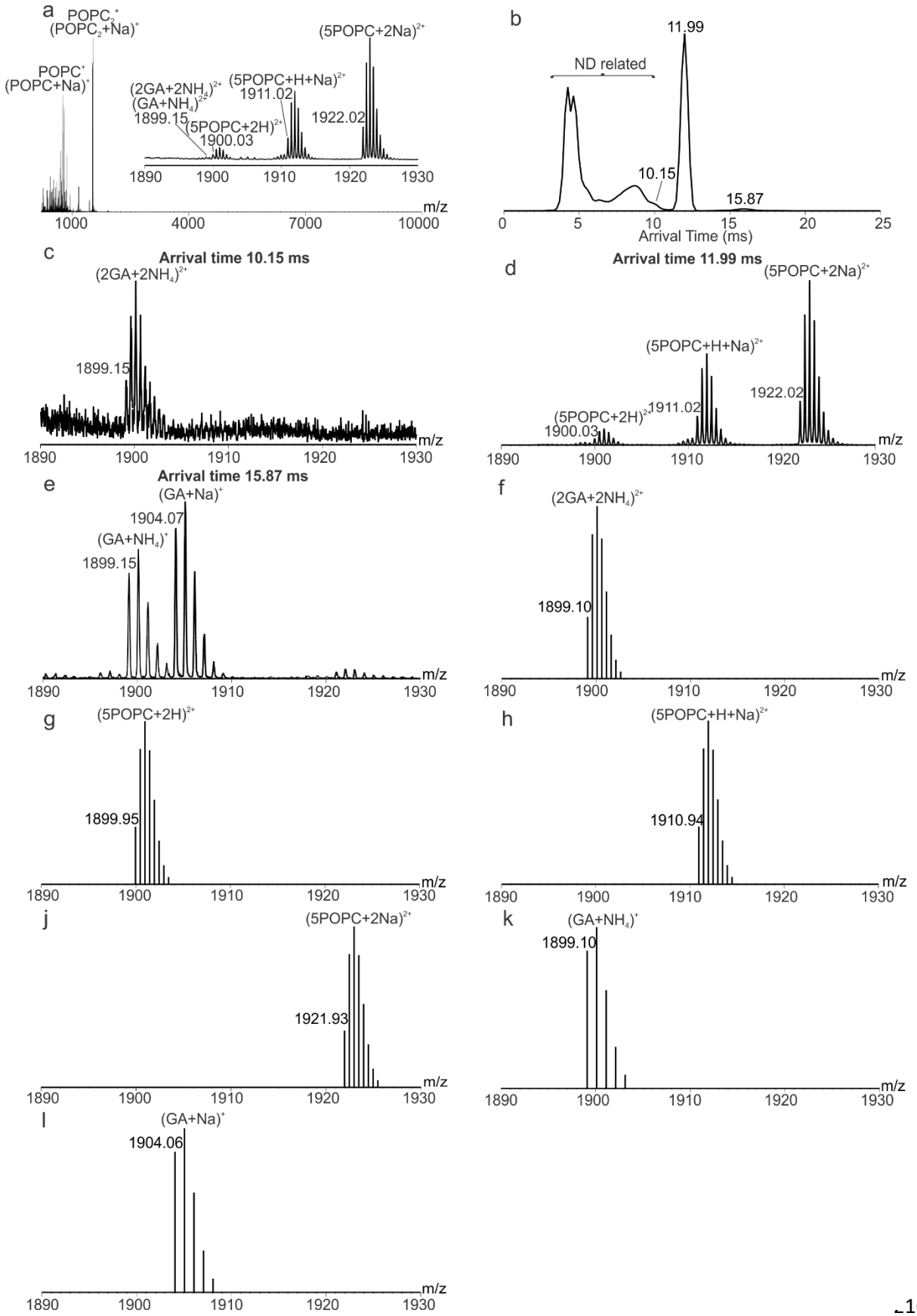
a
POPC2+
(POPC2+Na)+
POPC+
(POPC+Na)+
(2GA+2NH4)2+
(GA+NH4)2+
1899.15
(5POPC+2H)2+
1900.03
(5POPC+H+Na)2+
1911.02
1922.02
(5POPC+2Na)2+
m/z
b
11.99
ND related
10.15
15.87
Arrival Time (ms)
c
Arrival time 10.15 ms
(2GA+2NH4)2+
1899.15
d
Arrival time 11.99 ms
(5POPC+2Na)2+
(5POPC+H+Na)2+
1922.02
1911.02
(5POPC+2H)2+
1900.03
e
Arrival time 15.87 ms
(GA+Na)+
1904.07
(GA+NH4)+
1899.15
f
(2GA+2NH4)2+
1899.10
g
(5POPC+2H)2+
1899.95
h
(5POPC+H+Na)2+
1910.94
j
(5POPC+2Na)2+
1921.93
k
(GA+NH4)+
1899.10
l
(GA+Na)+
1904.06

Figure 5.15 (a) ESI mass spectrum acquired for aqueous ammonium acetate solution (200 mM, pH 6.8, 25 °C) of GA-containing POPC NDs (15 μM) with addition of sodium acetate (10 mM). (b) Plot of IMS-ATs measured for all ions between *m/z* 1890 and *m/z* 1930 (c), (d) and (e) ESI mass spectrum corresponding to AT 10.15 ms, 11.99 ms and 15.87 ms respectively. (f), (g), (h), (j), (k) and (l) Theoretical isotopic distribution of $(2GA + 2NH_4)^{2+}$, $(5POPC + 2H)^{2+}$, $(5POPC + H + Na)^{2+}$, $(5POPC + 2Na)^{2+}$, $(GA + NH_4)^{+}$ and $(GA + Na)^{+}$, respectively.

5.3.4 Computational results

Motivated by the observation of the compact $(2GA + 2NH_4)^{2+}$ ions produced from the NDs, a series of MD simulations were carried out on $(2GA + 2Na)^{2+}$ and $(2GA + 2NH_4)^{2+}$ ions and their Ω calculated at various times points along the trajectory. As described in the Experimental Section, 500 ns simulations were performed using two different initial structures, taken from the PDB, for each the three helical classes of GA dimer.[51]

Analysis of the MD results revealed that the overall helical structure of each ion was preserved throughout the simulations. The length of the helices, as measured along the helical axis, exhibited modest fluctuations that were independent of charging agent, with values ranging from 2.5 nm to 3.2 nm (DSDHp), 2.4 nm to 3.0 nm (DSDHap) and 1.6 nm to 3.2 nm (SSHH). It was also found that, regardless of initial placement, the charging agents ended up in the interior of the helix (Figure 5.16). Both the Na^+ and NH_4^+ cations interact preferentially with backbone carbonyl oxygens; the Na^+ ions were almost fully solvated, with an average of 5.8 interactions per ion, over the simulation, while each NH_4^+ participated, on average, in 2.7 H-bonds.

The Ω calculated for the $(2GA + 2Na)^{2+}$ and $(2GA + 2NH_4)^{2+}$ ions over the course of the simulation for each helical class (Figure 5.17) were found to span a significant and overlapping

range of values, 616 to 690 Å^2 (DSDHp), 590 to 688 Å^2 (DSDHap) and 616 to 702 Å^2 (SSHH). The average Ω values are listed in Table 5.3. Interestingly, the nature of the charging agent did not have any significant effect on the Ω values. Moreover, the calculated Ω are similar in magnitude to the Ω values measured for C4 and C1, but consistently smaller than those corresponding to C2 and C3. Finally, it is notable that the Ω values determined from the MD simulations are reasonably similar in magnitude to the theoretical Ω values calculated for seventeen different GA dimer structures taken from the PDB (613–658 Å^2 (DSDHp), 642–680 Å^2 (DSDHap) and 641–654 Å^2 (SSHH) (Figure 5.17).

Two significant findings emerge from this analysis. First, the structures of the GA dimers, regardless of conformation (i.e., DSDHp, DSDHap or SSHH), span a wide range of overlapping Ω values. Secondly, these Ω values are consistently lower than the experimental values measured for C2 and C3. Consequently, it would seem that it is not possible to unambiguously infer dimer conformation from a comparison the Ω measured for the gaseous ions and values calculated from structures available in the PDB or from MD simulations (as performed in the present study). That the measured Ω of C2 and C3 are consistently larger than the calculated values raises the possibility that the helices are partially disordered in the gas phase. Indeed, the structures of the C2 and C3 conformations of the $(2GA + 2Na)^{2+}$ ions proposed by Russell and coworkers exhibit some fraying of the helices, suggestive of partial unfolding of the peptides, which could be caused by collisional heating of the gaseous ions.[28,57]

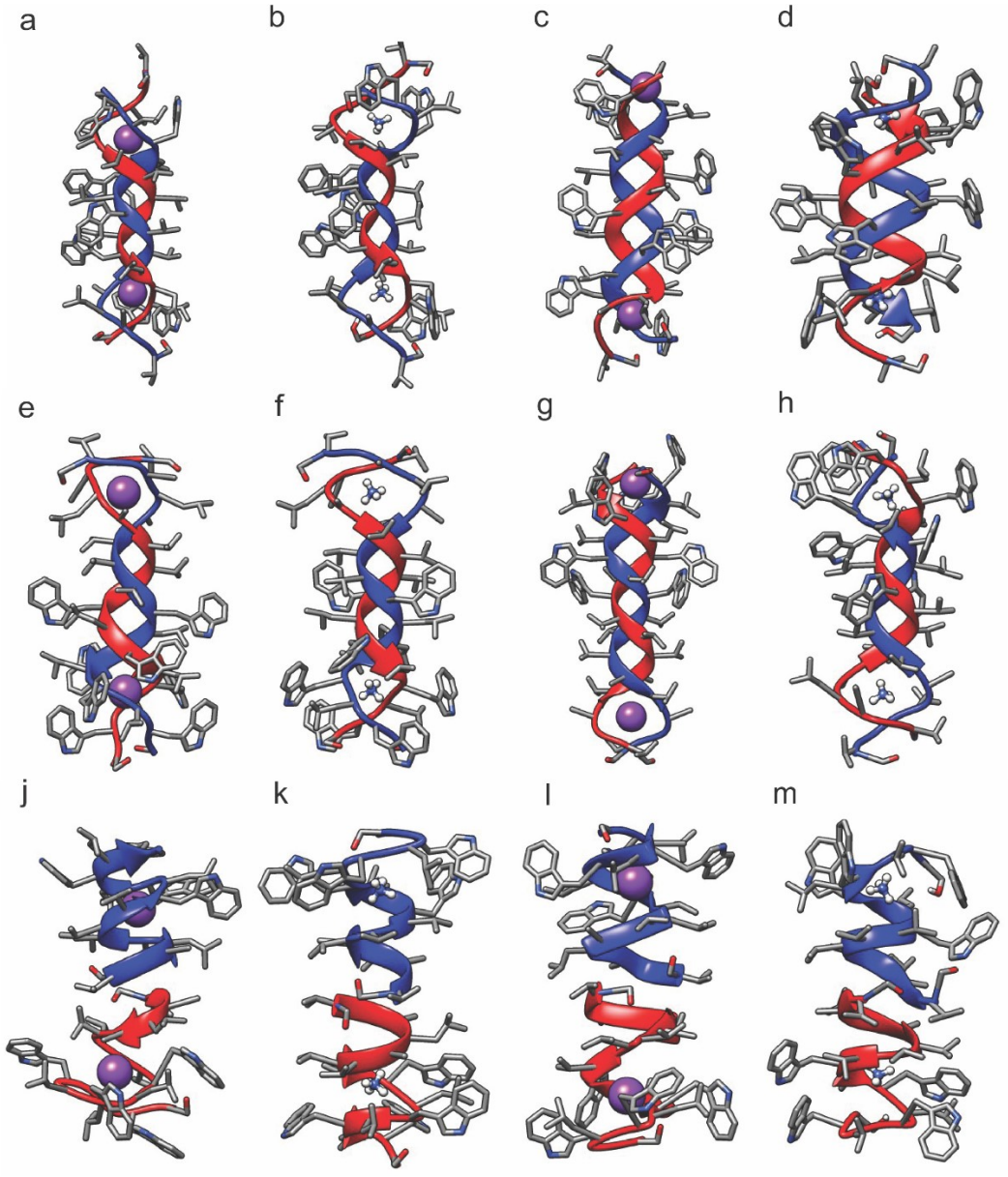

Figure 5.16 Average structures of the DSDHap form of GA dimer from MD simulations: (a) 1ALZ with 2 Na^+; (b) 1ALZ with 2 NH_4^+; (c) 1AV2 with 2 Na^+; (d) 1AV2 with 2 NH_4^+. Average structures of the DSDHp form of GA dimer from MD simulations: (e) 1MIC, model 1, with 2 Na^+; (f) 1MIC, model 1, with 2 NH_4^+; (g) 1MIC, model 4, with 2 Na^+; (h) 1MIC, model 4, with 2 NH_4^+.

Average structures of the SSHH form of GA dimer from MD simulations: (j) 1MAG with 2 Na^+; (k) 1MAG with 2 NH_4^+; (l) 1MAG with 2 Na^+; (m) 1MAG with 2 NH_4^+.

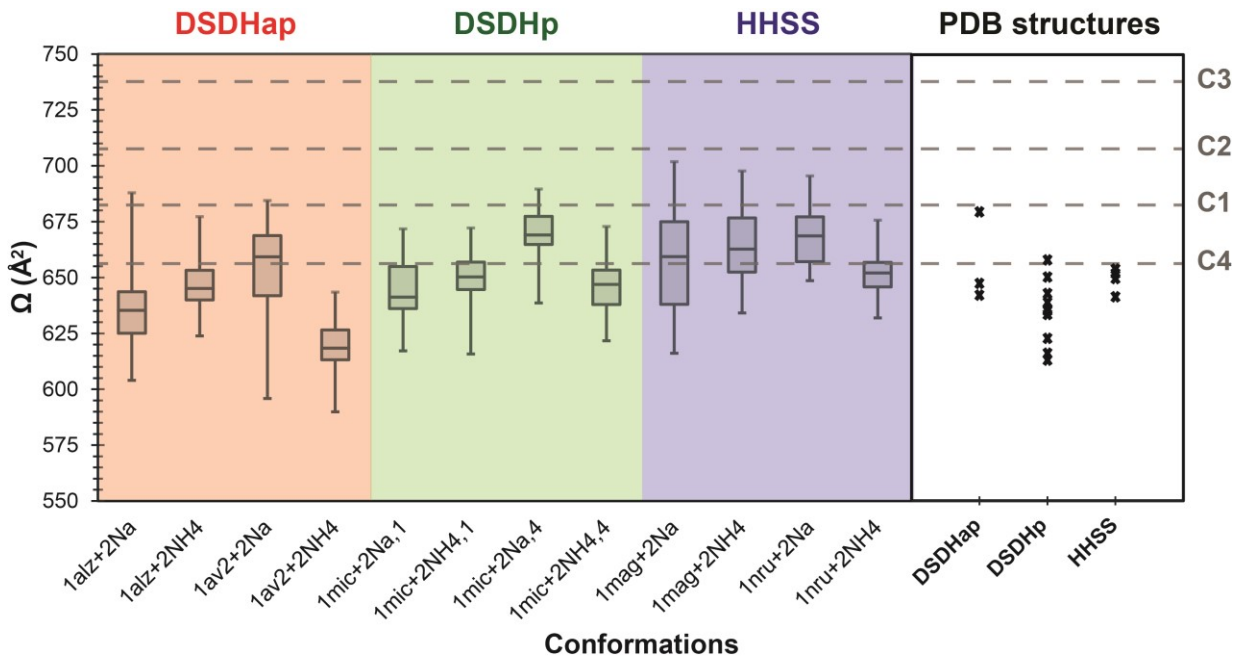

Figure 5.17 Ω calculated using the MOBCAL trajectory method for GA dimer structures taken from the PDB and structures generated from MD simulations. The Ω values calculated for the structures from MD simulations are shown as box plots, in which the error bars represent the entire range Ω values, the boxes show the 25^{th}–75^{th} percentile, and the interior line represents the median value. The Ω values calculated for the structures from the PDB are represented by an X in the plot. For the DSDHap GA dimer, the PDB structures used are 1AL4, 1ALX and 1ALZ; for the DSDHp GA dimer the PDB structures used are the ten models in 1MIC; and for SSHH GA dimer the PDB structures used are 1JNO, 1MAG, 1NRM and 1NRU. The Ω values for C1 (683 $Å^2$), C2 (708 $Å^2$), C3 (737 $Å^2$) and C4 (656 $Å^2$) are shown as dashed horizontal lines.

Table 5.3 Collision cross sections (Ω) of GA dimer structures taken from the PDB and average values calculated for doubly charged GA dimer ions obtained from MD simulations.

PDB starting structure	Description	Ω (Å^2) [a]	Charging agent	Ω (Å^2) from MD simulations [b]
1ALZ	Double stranded, antiparallel helix	642	2 Na^+	638 ± 18
			2 NH_4^+	647 ± 11
1AV2	Double stranded, antiparallel helix	611	2 Na^+	655 ± 20
			2 NH_4^+	619 ± 10
1MIC (Model 1)	Double stranded, parallel helix	616	2 Na^+	644 ± 13
			2 NH_4^+	650 ± 11
1MIC (Model 4)	Double stranded, parallel helix	658	2 Na^+	669 ± 10
			2 NH_4^+	646 ± 12
1MAG	Head-to-head	652	2 Na^+	657 ± 23
			2 NH_4^+	664 ± 15
1NRU	Head-to-head	654	2 Na^+	668 ± 12
			2 NH_4^+	652 ± 10

a. Ω determined using MOBCAL trajectory method with imp=1000.
b. Ω determined using 50 structures, as described in the Experimental Section. The value shown is the average Ω ± one standard deviation.

5.4 Conclusions

The results of the present study provide useful insights into the application of ESI-IMS-MS to probe the influence of solvent environment on the conformations of MP complexes. Importantly, it is found that the transmembrane GA dimer is readily transferred from phospholipid NDs to the gas phase by ESI. However, the Ω values measured for GA dimers produced from NDs differ from those determined for DMPC or POPC vesicles using the VCFD method.[27] While the origin of these conformational differences is not fully understood and requires further investigation, this finding suggests that the method used to deliver the peptide complexes from the lipid bilayer to the gas phase may influence the conformations of the gaseous ions. Moreover, the results acquired for GA dimer ions produced from solutions of isobutanol with and without ammonium acetate, suggest that the nature of the charging agents imparted by the ESI process can influence dimer conformation in the gas phase, potentially complicating the structural interpretation of measured Ω values.

5.5 References

1. Nath, A.; Atkins, W. M.; Sligar, S. G. *Biochemistry*. **2007**, *46*, 2059–2069.
2. Denisov, I. G.; Sligar, S.G. *Nat. Struct. Mol. Biol*. **2016**, *23*, 481–486.
3. Sanders, C. R.; Prosser, R. S. *Structure*. **1998**, *6*, 1227–1234.
4. Sanders, C. R.; Landis, G. C. *Biochemistry*. **1995**, *34*, 4030–4040.
5. Kashara, M.; Hinkle, P. C. *J. Biol. Chem*. **1977**, *252*, 7384–7390.
6. Rigaud, J. L.; Paternostre, M. T.; Bluzat, A. 2. *Biochemistry*. **1988**, *27*, 2677–2688.
7. Seddon, A. M.; Curnow, P.; Booth, P. J. *Biophys. Acta*. **2004**, *1666*, 105–117.
8. Bayburt, T. H.; Grinkova, Y. V.; Sligar, S. G. *Nano Lett*. **2002**, *2*, 853−856.

9. Bayburt, T. H.; Sligar, S. G. *FEBS Lett*. **2010**, *584*, 1721−1727.

10. Hagn, F.; Etzkorn, M.; Raschle, T.; Wagner, G. *J. Am. Chem. Soc*. **2013**, *135*, 1919–1925.

11. Wang, X.; Mu, Z.; Li, Y.; Bi, Y.; Wang, Y. *Protein J*. **2015**, *34*, 205–211.

12. Ritchie, T. K.; Kwon, H.; Atkins, W. M. *J. Biol. Chem*. **2011**, *286*, 39489–39496.

13. Mak, P. J.; Gregory, M. C.; Denisov, I. G.; Sligar, S. G.; Kincaid, J. R. *Proc. Natl. Acad. Sci. USA.* **2015**, *112*, 15856–15861.

14. Hopper, J. T.; Yu, Y. T.; Li, D.; Raymond, A.; Bostock, M.; Liko, I.; Mikhailov, V.; Laganowsky, A.; Benesch, J. L.; Caffrey, M.; Nietlispach, D.; Robinson, C. V. *Nat Methods*. **2013**, *10*, 1206**–**1208.

15. Hebling, C. M.; Morgan, C. R.; Stafford, D. W.; Jorgenson, J. W.; Rand, K. D.; Engen, J. R. *Anal. Chem*. **2010**, *82*, 5415–5419.

16. Marty, M. T.; Hoi, K. K.; Gault, J.; Robinson, C. V. *Angew. Chem., Int. Ed*. **2016**, *55*, 550−554.

17. Bernstein, S. L.; Dupuis, N. F.; Lazo, N. D.; Wyttenbach, T.; Condron, M. M.; Bitan, G.; Teplow, D. B.; Shea, J. E.; Ruotolo, B. T.; Robinson, C. V.; Bowers, M. T. *Nature Chem*. **2009**, *1*, 326−331.

18. Andersen, O. S.; Koeppe, R. E. 2nd; Roux, B. *IEEE Trans Nanobioscience*. **2005**, *4*, 10**–**20.

19. Kelkar, D. A.; Chattopadhyay, A. *Biochim. Biophys. Acta, Biomembr*. **2007**, *1768*, 2011−2025.

20. Miloshevsky, G. V.; Jordan, P. C. *Trends Neurosci*. **2004**, *27*, 308–314.

21. Veatch, W. R.; Blout, E. R. *Biochemistry*. **1974**, *13*, 5257–5264.

22. Veatch, W. R.; Fossel, E. T.; Blout. E. R. *Biochemistry*. **1974**, *13*, 5249–5256.

23. Bystrov, V. F.; Arseniev, A. S. *Tetrahedron*. **1988**, *44*, 925–940.

24. Braco, L.; Bano, C.; Chillaron, F.; Abad, C. *Int. J. Biol. Macromol*. **1988**, *10*, 343−348.

25. Arseniev, A. S.; Barsukov, I. L.; Bystrov, V. F.; Lomize, A. L.; Ovchinnikov, Y. A. *FEBS Lett*. **1985**, *186*, 168–174.

26. Ketchem, R. R.; Hu, W.; Cross, T. A. *Science.* **1993**, *261*, 1457–1460.

27. Patrick, J. W.; Gamez, R. C.; Russell, D. H. *Anal. Chem*. **2015**, *87*, 578–583.

28. Patrick, J. W.; Gamez, R. C.; Russell, D. H. *Biophys. J*. **2016**, *110*, 1826**–**1835.

29. Patrick. J. W.; Zerfas, B.; Gao, J.; Russell, D. H. *Analyst*. **2017**, *142*, 310**–**315.

30. Leney, A. C.; Fan, X.; Kitova, E. K.; Klassen, J. S. *Anal. Chem*. **2014**, *86,* 5271**–**5277.

31. Ruotolo, B. T.; Benesch, J. L. P.; Sandercock, A. M.; Hyung, S. J.; Robinson, C. V. *Nat. Protoc*. **2008**, *3*, 1139–1152.

32. Bush, M. F.; Hall, Z.; Giles, K.; Hoyes, J.; Robinson, C. V.; Ruotolo, B. T. *Anal. Chem*. **2010**, *82*, 9557−9565.

33. Hoaglund, C. S.; Valentine, S. J.; Sporleder, C. R.; Reily, J. P.; Clemmer, D. E. *Anal. Chem*. **1998**, *70*, 2236−2242.

34. Henderson, S. C.; Valentine, S. J.; Counterman, A. E.; Clemmer, D. E. *Anal. Chem*. **1999**, *71*, 291−301.

35. Hoaglund, C. S.; Valentine, S. J.; Sporleder, C. R.; Reily, J. P., Clemmer, D. E. *Anal. Chem*. **1998**, *70*, 2236−2242.

36. Henderson, S. C.; Valentine, S. J.; Counterman, A. E.; Clemmer, D. E. *Anal. Chem*. **1999**, *71*, 291−301.

37. Chen, Y.; Tucker, A.; Wallace, B. A. *J. Mol. Biol*. **1996**, *264*, 757–769.

38. Burkhart, B. M.; Gassman, R. M.; Langs, D. A.; Pangborn, W. A.; Duax, W. L. *Biophys. J*. **1998**, *75*, 2135–2146.

39. Burkhart, B. M.; Li, N.; Langs, D. A.; Pangborn, W. A.; Duax, W. L. *Proc. Natl. Acad. Sci. U.S.A*. **1998**, *95*, 12950–12955.

40. Ketchem, R. R.; Lee, K.-C.; Huo, S.; Cross, T. A. *J. Biomol. NMR*. **1996**, *8*, 1–14.

41. Townsley, L. E. (PDB ID: 1NRU). 2003.

42. Case, D. A.; Berryman, J. T.; Betz, R. M.; Cerutti, D. S.; Cheatham III, T. E.; Darden, T. A.; Duke, R. E.; Giese, T. J.; Gohlke, H.; Goetz, A. W.; Homeyer, N.; Izadi, S.; Janowski, P.; Kaus, J.; Kovalenko, A.; Lee, T. S.; LeGrand, S.; Li, P.; Luchko, T.; Luo, R.; Madej, B.; Merz, K. M.; Monard, G.; Needham, P.; Nguyen, H.; Nguyen, H. T.; Omelyan, I.; Onufriev, A.; Roe, D. R.; Roitberg, A.; Salomon-Ferrer, R.; Simmerling, C. L.; Smith, W.; Swails, J.; Walker, R. C.; Wang, J.; Wolf, R. M.; Wu, X.; York, D. M.; Kollman, P. A. AMBER 15, University of California: San Francisco, CA, 2015.

43. Case, D. A.; Darden, T. A.; Cheatham III, T. E.; Simmerling, C. L.; Wang, J.; Duke, R. E.; Luo, R.; Walker, R. C.; Zhang, W.; Merz, K. M.; Roberts, B.; Hayik, S.; Roitberg, A.; Seabra, G.; Swails, J.; Götz, A. W.; Kolossváry, I.; Wong, K. F.; Paesani, F.; Vanicek, J.; Wolf, R. M.; Liu, J.; Wu, X.; Brozell, S. R.; Steinbrecher, T.; Gohlke, H.; Cai, Q.; Ye, X.; Wang, J.; Hsieh, M.-J.; Cui, G.; Roe, D. R.; Mathews, D. H.; Seetin, M. G.; Salomon-Ferrer, R.; Sagui, C.; Babin, V.; Luchko, T.; Gusarov, S.; Kovalenko, A.; Kollman, P. A. AMBER 12, University of California: San Fancisco, CA, 2012.

44. Hornak, V.; Abel, R.; Okur, A.; Strockbine, B.; Roitberg, A.; Simmerling, C. *Proteins*, **2006**, *65*, 712–725.

45. Joung, I. S.; Cheatham, T. E. *J. Phys. Chem. B*. **2008**, *112*, 9020–9041.

46. Jakalian, A.; Bush, B. L.; Jack, D. B.; Bayly, C. I. *J. Comput. Chem*. **2000**, *21*, 132–146.

47. Ryckaert, J.-P.; Ciccotti, G.; Berendsen, H. J. C. *J. Comput. Phys*. **1977**, *23*, 327–341.

48. Berendsen, H. J. C.; Postma, J. P. M.; Gunsteren, W. F. V.; DiNola, A.; Haak, J. R. *J. Chem. Phys*. **1984**, *81*, 3684–3690.

49. Shvartsburg, A. A.; Jarrold, M. F. *Chem. Phys. Lett*. **1996**, *261*, 86–91.

50. Mesleh, M. F.; Hunter, J. M.; Shvartsburg, A. A.; Schatz, G. C.; Jarrold, M. F. *J. Phys. Chem*. **1996**, *100*, 16082–16086.

51. RSCB Protein Data Bank. www.rcsb.org (accessed 3/14/2017).

52. Townsley, L. E.; Tucker, W. A.; Sham, S.; Hinton, J. F. *Biochemistry*. **2001**, *40*, 11676–11686.

53. Townsley, L. E. (PDB ID: 1NRM). 2003

54. Chen, L.; Gao, Y. Q.; Russell, D. H. *J. Phys. Chem. A*. **2012**, *116*, 689**–**696.

55. Chen, L.; Chen, S. H.; Russell, D. H. *Anal. Chem*. **2013**, *85*, 7826–7833.

56. Zhang, Y.; Liu, L.; Daneshfar, R.; Kitova, E. N.; Li, C.; Jia, F.; Cairo, C. W.; Klassen, J. S. *Anal. Chem*. **2012**, *84*, 7618**–**7621.

57. Chen, L. Ph.D. thesis, Texas A&M University, College Station, TX, 2012.

Chapter 6

Conclusions and Future Work

6.1 Conclusions

This thesis describes the development and application of electrospray ionization mass spectrometry (ESI-MS) based techniques combined with model membranes (MMs) for discovery and characterization of glycan-binding protein (GBP)–glycolipid (GL) interactions and gas phase conformation investigation of membrane peptides (MPs). The first and third research projects (Chapter 2 and Chapter 4) describes the development of the catch-and-release (CaR)-ESI-MS assay, combined with picodiscs (PDs) or passively-loaded PDs (^{PL}PDs) for screening interactions between GBPs and GLs. The second project (Chapter 3) demonstrates the characterization of the size and composition of PDs. The last research project (Chapter 5) focuses on investigation on the gas phase conformations of dimers of a channel-forming transmembrane peptide using ESI-MS and nanodiscs (NDs).

Chapter 2 demonstrates the utility of the CaR-ESI-MS assay, implemented with PDs, for screening libraries of GLs against water-soluble GBPs *in vitro* to detect specific interactions. Screening PDs containing a small library of purified gangliosides against the B subunit homopentamer of cholera toxin (CTB_5) and a sub-fragment of toxin A from *Clostridium difficile* (TcdA-A2) demonstrates the simultaneous detection of both high and low affinity interactions. The CaR-ESI-MS results are consistent with the measured binding specificities of these GBPs for ganglioside oligosaccharides. Screening mixtures of lipids extracted from porcine brain and a human epithelial cell line against CTB_5 successfully identified high affinity GL ligands present in both GL mixtures. Finally, a comparison of the present results with data obtained with the CaR-

ESI-MS assay implemented using NDs revealed that the PDs exhibited similar or superior performance to NDs for GBP-GL binding measurements and that PDs are to be preferred over NDs for detection of low affinity GBP–GL interactions.

The results described in Chapter 2 suggest that PDs could play a significant role in the discovery and characterization of GBP-GL interactions. However, the structural composition of PDs have not been thoroughly investigated. Chapter 3 reports the first detailed investigation into the size, composition, heterogeneity and structure of 1-palmitoyl-2-oleoyl-*sn*-glycero-3-phosphocholine-containing PDs (POPC-PDs) in aqueous solutions using high resolution ESI-MS, multi-angle laser light scattering (MALLS) and molecular dynamics (MD) simulations. ESI-MS data suggest that the size and composition of POPC-PDs at neutral pH differs from those of *N,N*-dimethyldodecylamine *N*-oxide (LDAO)-containing PDs determined by X-ray crystallography. The ESI-MS and MALLS data revealed that the size and composition of POPC-PDs are dependent on pH – predominantly as SapA dimer at acidic pH; predominantly as SapA tetramer in freshly prepared solutions at neutral pH 6.8 and converts to SapA trimer over a period of hours. The results of molecular modelling suggest spheroidal structures for all the three complexes in solution. Comparison of measured collision cross sections (Ω) with values calculated for gaseous ions produced from modelling suggests that the solution structures are largely preserved in the gas phase, although the lipids do not maintain regular bilayer orientations.

The CaR-ESI-MS has been successfully implemented with PDs for screening GLs against soluble GBPs. However, the non-uniform incorporation efficiencies of the various GL present in the mixture is one of the outstanding challenges to using PDs as GL arrays for screening. Chapter 4 describes the use of ^{PL}PDs, prepared by incubating phospholipid PDs with GL or GL mixture (in the form of glycomicelle) in aqueous solution, for CaR-ESI-MS screening of GLs against GBPs

and compares their performance with conventional, pre-loaded PDs, prepared directly from a mixture of purified phospholipid and GL(s) or GL extract. Time-dependent changes in the composition of the ^{PL}PDs produced by incubation with GM1 micelle were monitored using collision-induced dissociation (CID) of the gaseous PDs ions and from the extent of GM1 binding to CTB_5 measured by ESI-MS. The ESI-MS results measured for ^{PL}PDs (≥ 10 d incubation) is indistinguishable from that observed with pre-loaded PDs produced directly from GM1 at the same concentration. The transfer of GM1 from micelles to NDs for ^{PL}NDs was also observed, although the apparent rate of incorporation is slower than for PDs. Comparison of ganglioside binding to CTB_5 measured for pre-loaded PDs and ^{PL}PDs prepared from GLs extracted from pig and mouse brain revealed that the ^{PL}PDs allow for the detection of a greater number of ganglioside ligands. Together, the results of this study suggest ^{PL}PDs may have advantages over conventionally prepared PDs for screening GLs against GBPs using CaR-ESI-MS.

NDs and PDs have been successfully used to solubilize GLs for their CaR-ESI-MS screening against GBPs described in above Chapters. They have also been shown to have utility for solubilizing MPs in a native like environment for structural and functional studies. In Chapter 5, the gas-phase conformations of dimers of the channel-forming membrane peptide gramicidin A (GA) in NDs are investigated using ESI-IMS-MS and MD simulations. The transmembrane GA dimer is readily transferred from phospholipid NDs to the gas phase by ESI and it suggested that the ion conducting single stranded head-to-dead helical conformation of the dimer was preserved in the gas phase. These findings highlight the potential of NDs, combined with ESI, for transferring transmembrane peptide complexes directly from lipid bilayers to the gas phase. However, the Ω values measured for GA dimers produced from NDs differ from those determined for phospholipid vesicles. While the origin of these conformational differences is not fully understood and requires

further investigation, this finding suggests that the method used to deliver the peptide complexes from the lipid bilayer to the gas phase may influence the conformations of the gaseous ions. Moreover, the ESI-IMS-MS results acquired for GA dimer ions produced from isobutanol with and without ammonium acetate suggest that the nature of the charging agents, imparted by the ESI process, can influence dimer conformation in the gas phase.

6.2 Future Work

Our lab has demonstrated the use of CaR-ESI-MS implemented with NDs and PDs for discovery and characterization of GBP-GL interactions.[1-3] The CaR-ESI-MS assay described in Chapter 2 and 4 showed that both low and high affinity GBP–GL interactions can be simultaneous detected for GL mixtures. However, almost no binding or multivalent binding (for multivalent protein) was observed when low affinity GL ligand was the only receptor in NDs and PDs. A useful screening tool needs to be able to reliably detect low affinity GBP-GL interaction. Therefore a further investigation for the fundamental understanding of low affinity GBP–GL interactions is proposed in section 6.2.1 in order to enhance detection of low affinity GBP-GL interaction. The discovery of GL receptors is also hindered by the limited availability of many GLs in purified form or from tissues and cell lines. Recently, another MM styrene maleic acid copolymer lipid particles (SMALPs) was used to solubilize endogenous MPs and lipids directly from cell membranes.[4,5] It allows us to generate a series of endogenous glycan receptors libraries (including GLs and glycosylated MPs) for receptor discovery proposed in section 6.2.2. In Chapter 4 we demonstrated that ^{PL}PDs have advantageous over conventionally prepared PDs for screening GLs. However, the mechanism controlling the GL transfer process is not fully understand. Therefore the kinetic studies of the GL transfer using high resolution MS is proposed in section 6.2.3.

6.2.1 Fundamental studies of low affinity protein–glycolipid interactions

The CaR-ESI-MS assay described in Chapter 2 and 4 showed that both low and high affinity of GBP–GL interactions can be detected. CTB_5 could bind to low affinity binding receptors such as GM2 (with apparent K_a = 580 ± 130 M^{-1} between CTB_5 and GM2 oligosaccharide) when 7 different gangliosides were mixed in PDs. However, almost no binding was observed when GM2 was the only receptor in NDs and PDs. Moreover, even though the direct detection of low affinity binding between Shiga toxin type 1 (Stx1) and its native globotriaosylceramide receptor Gb3 in PDs was observed, no multivalent Stx1-Gb3 complexes were detected in ESI-MS.[3] It is proposed that the off kinetics between GBP and low affinity GL ligand is too fast to allow the detecting of low affinity GL binding (Figure 6.1). Recently, it was also demonstrated that the GM2 can contribute to CTB_5 binding when it is mixed with a strong binding receptor GM1 using a nanocube based lipid bilayer sensor and localized SPR.[6] With the binding of GBP to a high affinity GL on the surface, the off kinetics between GBP and low affinity GL could be largely reduced to enhance the detection of their binding.

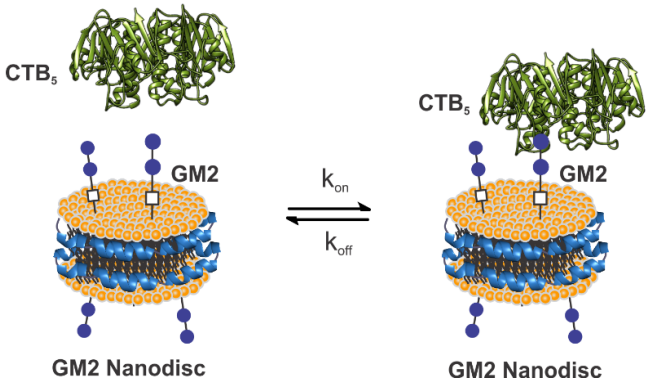

Figure 6.1 A schematic representation of the kinetics between CTB_5 binding to GM2 solubilized in ND.

For this project, a direct detection on heterogeneous cooperativity of low affinity GBP-GL binding by addition of a high affinity GL would be demonstrated using ESI-MS assay combined with MMs (NDs and PDs). NDs and PDs containing high affinity receptor (such as GM1) alone, low affinity receptor (such as GM2) alone, and a series of mixtures of these two receptors with different percentage would be prepared and screened against CTB_5 using a high resolution ESI-MS (a recently purchased high field FT-ICR MS instrument). High resolution MS allows the direct detection of resolved complexes of CTB_5 with different GL with small difference (such as GM1 and GM2) to monitor the hetero-multivalent binding. The stoichiometry and fraction of bound low affinity GL in the absence and presence of a high affinity GL can be quantified and compared. With the heterogeneous binding cooperativity proven, a more general crosslinking reagent will be introduced into the MMs, which can covalent bind to target GBP to enhance the detection of low affinity GBP-GL interaction.

6.2.2 Receptor discovery from endogenous glycan receptors libraries

In Chapter 2 and 4, we demonstrate the screening of GLs against GBPs using a small library of purified ganglioside and some GLs extract from tissue and human cell line. However, the limited availability of purified GLs hinders the discovery of GL receptors. The incorporation of GLs into MMs also have some limitations, such as failure incorporation of some GLs, the non-uniform incorporation efficiencies of the various GLs present in the mixture, and long incubation time required for passively-loading of GLs. Recently, another MM styrene maleic acid copolymer lipid particles (SMALPs) was used to solubilize endogenous MPs and lipids directly from cell membranes. SMALPs, which are quite similar with NDs, is a phospholipid bilayer surrounded by

a styrene maleic acid copolymer (SMA) instead of scaffold protein.[4,5] The polymer SMA binds to the surface of membrane, spontaneous self-inserts into cell membrane and extracts intact membrane pitches (MPs as well as lipids) in the form of discoidal particles (SMALPs).[4,5] A series of SMALP-based endogenous glycan libraries (GLs as well as glycosylated MPs) would be made directly from tissue and cell lines, which, when combined with the CaR-ESI-MS assay, will accelerate the discovery of glycan receptors for bacterial and viral GBPs.

The starting point for this project will be the preparation of well-defined SMALPs using purified gangliosides such as the small library of 7 ganglioside described in Chapter 2 and 4. These will then be screened against soluble GBPs, such as CTB_5 by CaR-ESI-MS to validate the method. Efforts will then focus on the production of tissue and cell line-specific SMALP-based glycan libraries directly from tissue (e.g. murine, porcine and human brain) and human cell lines (e.g. HT29, T84 and Caco-2). Once in hand, the SMALP-based glycan libraries will be characterized and screened against a series of bacterial and viral GBPs for which the native human receptors have not been conclusively identified. Preliminary efforts will focus on CTB_5 and strains of human norovirus. Recent data suggest that glycans, other than the ganglioside GM1a, may be responsible for cellular recognition by CTB_5.[7] Similarly, the glycan receptors of certain strains of human norovirus (e.g. VA115 (GI.3)) have yet to be identified.[8] The discovery of the functional receptors will serve as the basis for the development of new treatments for these infectious diseases.

6.2.3 Kinetic studies of lipid transfer involved in passively-loaded model membranes

In Chapter 4 we developed the use of passively-loaded GL PDs (^{PL}PDs), prepared by incubating phospholipid PDs with GLs (in the form of GL micelles), as shown in Figure 6.2. However, the time-dependent changes in the composition of the produced ^{PL}PDs were indirectly monitored using

CID of the gaseous PDs ions and from the extent of ganglioside binding to CTB_5 measured by ESI-MS, which limits the illustration of the mechanism of lipid transfer and the observed differences in GL uptake when using GL mixture extracted from tissues. There are mainly two mechanisms for lipid exchange and one of them is a lipid monomer diffusion model, whereby lipid monomers partition between the lipid assemblies and aqueous solution and, through diffusion, are taken up by other assemblies,[9-11] In most cases of this model, the monomer lipid departure from the assemble is the rate limiting step.[10] However, the experimental data in Chapter 4 showed that the apparent rate constants were dependent on the nature of lipis discs, which means this mechanism is not likely to be the case or the take up of GLs by discs also contribute. Another model is a collision model, whereby a collision complex forms between different lipid assemblies and allowing for lipid diffusion within the complex.[9-11] The difference of GL transfer between PD and ND can be explained by their difference in diffusion rate constant, however, no conclusion could be drawn. Here, in order to further investigate the mechanism controlling the GL transfer process, we would like to meaure the kinetics directly by performing a direct measurement of the composition of the ^{PL}PDs along incubation time using high resolution mass spectrometry (MS). Recently, it was reported that SMALPs represent highly dynamic equilibrium and phospholipids exchange between SMALPs occurs within seconds via two mechanisms – lipid monomer diffusion and fast collisional transfer.[12] Here we can also make passively-loaded SMALPs by incubating phospholipid SMALPs and GLs and moniter the kinetics of GL transfer to SMALPs. It should dramatically decrease incubation time required for lipid transfer.

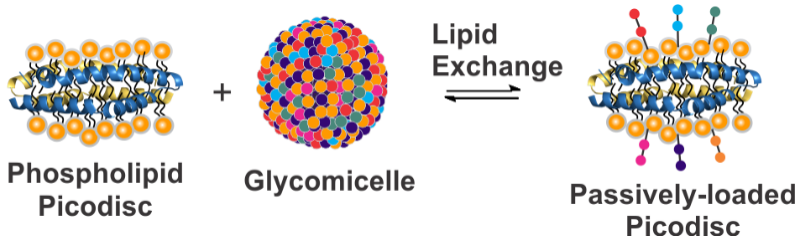

Figure 6.2 The schematic figure of passively-loaded PD formation through lipid transfer between phospholipid PD with GLs in the form of glycomicelle.

In this project, time-dependent changes in the composition of the ^{PL}MMs (^{PL}PDs, ^{PL}NDs, ^{PL}SMALPs) produced by incubating phospholipid MMs (PDs, NDs, SMALPs) and ganglioside GM1 micelle would be monitored using high resolution MS (FT-ICR MS instrument). High resolution MS allows for the direct detection of the intact ^{PL}PDs in a highly resolved form, which makes the measurement of the lipid composition of ^{PL}PDs possible through mass deconvolution. The time-dependent changes of the amount of GM1 in ^{PL}MMs (PDs, NDs, SMALPs) along incubation would be used to calculate the kinetics of GM1 transfer. The composition of ^{PL}MMs (PDs, NDs, SMALPs) with ganglioside libraries from porcine and mouse brains will also be measured to investigate the transfer rates of each ganglioside in the mixture in order to give more explanation on the different GLs uptake. And the understanding of lipid transfer between MMs also lay a foundation of characterization of bound lipids to MPs on MM surface through a passively-loaded way of selective lipid transfer to MPs for binding.

6.3 References

1. Zhang, Y.; Liu, L.; Daneshfar, R.; Kitova, E. N.; Li, C.; Jia, F.; Cairo, C.W.; Klassen, J. S. *Anal. Chem.* **2012**, *84*, 7618–7621.

2. Leney, A.; Fan, X.; Kitova, E.N.; Klassen, J. S. *Anal. Chem.* **2014**, *86*, 5271–5277.

3. Leney, A. C.; Darestani, R. R.; Li, J.; Nikjah, S.; Kitova, E. N.; Zou, C.; Cairo, C. W.; Xiong, Leney, A.; Fan, X.; Kitova, E. N.; Klassen, J. S. *Anal. Chem.* **2015**, *87*, 4402–4408.

4. Dörr, J. M. Scheidelaar, S.; Koorengevel, M. C.; Dominguez, J. J.; Schäfer, M.; van Walree, C. A.; Killian, J. A. *Eur. Biophys. J*. **2016**, *45*, 3–21.

5. Lee, S. C.; Knowles, T. J.; Postis, V. L.; Jamshad, M.; Parslow, R. A.; Lin, Y. P.; Goldman, A.; Sridhar, P.; Overduin, M.; Muench, S. P.; Dafforn, T. R.; *Nat. Protoc.* **2016**, *11*, 1149–62.

6. Wu, H. J.; Henzie, J.; Lin, W. C.; Rhodes, C.; Li, Z.; Sartorel, E.; Thorner, J.; Yang, P.; Groves, J. T. *Nat Methods*. **2012**, *9*, 1189.

7. Wands, A. M.; Fujita, A.; McCombs, J. E.; Cervin, J.; Dedic, B.; Rodriguez, A. C.; Nischan, N.; Bond, M. R.; Mettlen, M.; Trudgian, D. C.; Lemoff, A.; QuidingJärbrink, M.; Gustavsson, B.; Steentoft, C.; Clausen, H.; Mirzaei, H.; Teneberg, S.; Yrlid, U.; Kohler. J. J. *Elife* **2015**, 10.7554/eLife.09545.

8. Huang, P.; Farkas, T.; Zhong, W.; Thornton, S.; Morrow, A. L.; Jiang, X. *J. Virol*. **2005**, *79*, 6714.

9. Brown, R. E.; Thompson, T. E. *Biochemistry*. **1987**, *26*, 5454-5460.

10. Brown, R. E. *Biochim. Biophys. Acta*. **1992**, *1113*, 375-389.

11. Nichols, J. W. *Biochemistry*. **1988**, *27*, 3925-3931.

12. Arenas, R. C.; Danielczak, B.; Martel, A.; Porcar, L.; Breyton, C.; Ebel, C.; Kellera, S. *Scientific Reports*. **2017**, 7, 45875.

List of References

Chapter 1

1. Singleton, P. *Bacteria in Biology, Biotechnology and Medicine*, 5th ed.; Wiley: New York, 1999.
2. Noutsi, P.; Gratton, E.; Chaieb, S. (2016-06-30). *PLoS ONE*. **2016**, *11*, e0158313.
3. Lodish, H.; Berk, A.; Zipursky, L. S.; Matsudaira, P.; Baltimore, D.; Darnell, J. (2000). Biomembranes: Structural Organization and Basic Functions. *Molecular Cell Biology*, 4th ed.; Freeman, W. H: New York, 2000.
4. Zachowski, A. *Biochem. J*. **1993**, *294*, 1–14.
5. Brown, B. *Biological Membranes*. The Biochemical Society: London, U. K; p. 21.
6. van Meer, G.; Voelker, D. R.; Feigenson, G. W. *Nat. Rev. Mol. Cell Biol*. **2008**, *9*, 112–24.
7. D'Avanzo, N. *Curr. Top. Membr*. **2016**, *78*, 353-407.
8. Alberts, B.; Johnson, A.; Lewis, J.; Raff, M.; Roberts, K.; Walter, P. *Molecular Biology of the Cell*, 4th ed. Garland Science: New York, 2002.
9. Varki, A.; Cummings, R. D.; Esko, J. D.; Freeze, H. H.; Stanley, P.; Bertozzi, C. R.; Hart, G. W.; Etzler, M. E. *Essentials of Glycobiology*, 2nd ed.; Cold Spring Harbor Laboratory Press: Cold Spring Harbor, NY, 2009.
10. Nath, A.; Atkins, W. M.; Sligar, S. G. *Biochemistry*. **2007**, *46*, 2059–2069.
11. von Heijne, G. *J. Intern. Med*. **2007**, *261*, 543–557.
12. Bakheet, T. M.; Doig, A. J. *Bioinformatics* **2009**, *25*, 451–457.
13. Holgersson, J.; Gustafsson, A.; Breimer, M. E. *Immunol. Cell Biol.* **2005**, *83*, 694.
14. Weis, W. I.; Drickamer, K. *Annu. Rev. Biochem.* **1996**, *65*, 441.

15. Larsen, K.; Thygesen, M. B.; Guillaumie, F.; William, G. T.; Willats, W. G. T.; Jensen, K. J. *Carb. Res*. **2006**, *341*, 1209.

16. Homola, J. *Anal. Bioanal. Chem*. **2003**, *377*, 528.

17. Daghestani, H. N.; Day, B. W. *Sensors* **2010**, *10*, 9630.

18. De Crescenzo, G.; Boucher, C.; Durocher, Y.; Jolicoeur, M. *Cell. Mol. Bioeng.* **2008**, *1*, 204.

19. Wang, D. N.; Liu, S. Y.; Trummer, B. J.; Deng, C.; Wang, A. L. *Nat. Biotechnol.* **2002**, *20*, 275.

20. Liu, Y.; Palma, A. S.; Feizi, T. *Biol. Chem.* **2009**, *390*, 647.

21. Grant, O. C.; Smith, H. M.; Firsova, D.; Fadda, E.; Woods, R. J. *Glycobiology* **2014**, *24*, 17.

22. Fais, M.; Karamanska, R.; Russell, D. A.; Field, R. A. *J. Cereal Sci.* **2009,** *50*, 306–311.

23. Saboury, A. A. *J. Iran. Chem. Soc.* **2006**, *3*, 1.

24. Wilcox, D. E. *Inorg. Chim. Acta* **2008**, *361*, 857.

25. Wishart, D. *Curr. Pharm. Biotechnol.* **2005**, *6*, 105.

26. Mayer, M.; Meyer, B. *J. Am. Chem. Soc.* **2001,** *123*, 6108.

27. Haselhorst, T.; Lamerz, A. C.; Itzstein, M. *Methods Mol. Biol.* **2009,** *534*, 375.

28. Viegas, A.; Manso, J.; Nobrega, F. L.; Cabrita, E. J. *J. Chem. Educ.* **2011,** *88*, 990.

29. Wishart, D. *Curr. Pharm. Biotechnol.* **2005**, *6*, 105-120.

30. Ganem, B.; Li, Y. T.; Henion, J. D. *J. Am. Chem. Soc.* **1991**, *113*, 6294.

31. Van Dongen, W. D.; Heck, A. J. R. *Analyst* **2000**, *125*, 583.

32. Kitova, E. N.; Kitov, P. I.; Bundle, D. R.; Klassen, J. S. *Glycobiology* **2001**, *11*, 605.

33. Cederkvist, F. H.; Zamfir, A. D.; Bahrke, S.; Eijsink, V. G.; Sorlie, M.; Peter-Katalinic, J.; Peter, M. G., *Angew. Chem. Int. Ed.* **2006,** *45*, 2429.

34. Jecklin, M. C.; Touboul, D.; Jain, R.; Toole, E. N.; Tallarico, J.; Drueckes, P.; Ramage, P.; Zenobi, R. *Anal. Chem.* **2009**, *81*, 408.

35. Shi, J.; Yang, T.; Kataoka, S.; Zhang, Y.; Diaz, A. J.; Cremer, P. S. *J. Am. Chem. Soc*. **2007**, *129*, 5954−5961.

36. Sanghera, N.; Correia, B. E.; Correia, J. R.; Ludwig, C.; Agarwal, S.; Nakamura, H. K.; Kuwata, K.; Samain, E.; Gill, A. C.; Bonev, B. B.; Pinheiro, T. J. *Chem. Biol.* **2011**, *18*, 1422–1431.

37. Lingwood, D.; Binnington, B.; Rog, T.; Vattulainen, I.; Grzybek, M.; Coskun, U.; Lingwood, C. A.; Simons, K. *Nat. Chem. Biol.* **2011**, *7*, 260–262.

38. Lopez, H. H. H.; Schnaar, R. L. *Methods Enzymol*. **2006**, *417*, 205–220.

39. Lipid–Protein Interactions. In *Methods and Protocols*; Kleinschmidt, J. H., Ed.; Springer: New York, 2014; Vol. *974*.

40. Evans, S. V.; Roger MacKenzie. C. *J. Mol. Recognit*. **1999**, *12*, 155–68.

41. Feizi, T.; Chai, W. *Nat. Rev. Mol. Cell Biol.* **2004**, *5*, 582.

42. Song, X.; Lasanajak, Y.; Xia, B.; Heimburg–Molinaro, J.; Rhea, J. M.; Ju, H.; Zhao, C.; Molinaro, R. J.; Cummings, R. D.; Smith, D. F. *Nat Methods*. **2011**, *8*, 85–90

43. Lingwood, C. A.; Manis, A.; Mahfoud, R.; Khan, F.; Binnington, B.; Mylvaganam, M. *Chem. Phys. Lipids*. **2010**, *163*, 27–35.

44. Bayburt, T. H.; Grinkova, Y. V.; Sligar, S. G. *Nano Lett*. **2002**, *2*, 853−856.

45. Popovic, K.; Holyoake, J.; Pomès, R.; Privé, G.G. *Prot. Natl. Acad. Sci.* **2012**, *109*, 2908–2912.

46. Borch, J.; Torta, F.; Sligar, S. G.; Roepstorff, P. *Anal. Chem.* **2008**, *80*, 6245–6252.

47. Wu, H. J.; Henzie, J.; Lin, W. C.; Rhodes, C.; Li, Z.; Sartorel, E.; Thorner, J.; Yang, P.; Groves, J. T. *Nat Methods*. **2012**, *9*, 1189.

48. Zhang, Y.; Liu, L.; Daneshfar, R.; Kitova, E. N.; Li, C.; Jia, F.; Cairo, C.W.; Klassen, J. S. *Anal. Chem.* **2012**, *84*, 7618–7621.

49. Leney, A.; Fan, X.; Kitova, E.N.; Klassen, J. S. *Anal. Chem.* **2014**, *86*, 5271–5277.

50. Han, L.; Kitova, E. N.; Li, J.; Nikjah, S.; Lin, H.; Pluvinage, B.; Boraston, A. B.; Klassen, J. S. *Anal. Chem.* **2015,** *87,* 4888–4896.

51. Leney, A. C.; Darestani, R. R.; Li, J.; Nikjah, S.; Kitova, E. N.; Zou, C.; Cairo, C. W.; Xiong, Leney, A.; Fan, X.; Kitova, E. N.; Klassen, J. S. *Anal. Chem.* **2015**, *87*, 4402–4408.

52. Garavito, R. M.; Ferguson-Miller, S. *J. Biol. Chem*. **2001**, *276*, 32403–32406.

53. Seddon, A. M.; Curnow, P.; Booth, P. J. *Biochim. Biophys. Acta.* **2004**, *1666*, 105–117.

54. Duquesne, K.; Sturgis, J. N. *Humana Press*. **2010**, *601*, 205–217.

55. Popot, J. L. *Annu. Rev. Biochem*. **2010**, *79*, 737–775.

56. Calabrese, A. N.; Watkinson, T. G.; Henderson, P. J. F.; Radford, S. E.; Ashcroft, A. E. *Anal. Chem*. **2015**, *87*, 1118–1126.

57. Frauenfeld, J.; Löving, R.; Armache, J. P.; Sonnen, A. F.; Guettou, F.; Moberg, P.; Zhu, L.; Jegerschöld, C.; Flayhan, A.; Briggs, J. A.; Garoff, H.; Löw, C.; Cheng, Y.; Nordlund, P. *Nat Methods*. **2016**, *13*, 345–51.

58. Lyons, J. A.; Bøggild, A.; Nissen, P.; Frauenfeld, J. *Methods Enzymol*. **2017**, *594*, 85–99.

59. Hagn, F.; Etzkorn, M.; Raschle, T.; Wagner, G. J. *Am. Chem. Soc*. **2013**, *135*, 1919-1925.

60. Kijac, A.; Shih, A. Y.; Nieuwkoop, A. J.; Schulten, K.; Sligar, S. G.; Rienstra, C. M. *Biochemistry.* **2010**, *49*, 9190–9198.

61. Wang, X.; Mu, Z.; Li, Y.; Bi, Y.; Wang, Y. *Protein J*. **2015**, *34*, 205–211.

62. Baas, B. J.; Denisov, I. G.; Sligar, S. G. *Arch. Biochem. Biophys*. **2004**, *430*, 218–228.

63. Bayburt, T. H.; Grinkova, Y. V.; Sligar, S. G. *Arch. Biochem. Biophys*. **2006**, *450*, 215–222.

64. Mak, P. J.; Gregory, M. C.; Denisov, I. G.; Sligar, S. G.; Kincaid, J. R. *Proc. Natl. Acad. Sci. USA.* **2015**, *112*, 15856–15861.

65. Bayburt, T. H.; Vishnivetskiy, S. A.; McLean, M. A.; Morizumi, T.; Huang, C.-C.; Tesmer, J. J. G.; Ernst, O. P.; Sligar, S. G.; Gurevich, V. V. *J. Biol. Chem*. **2011**, *286*, 1420–1428.

66. Chougnet, A.; Grinkova, Y.; Ricard, D.; Sligar, S.; Woggon, W.-D. *ChemMedChem.* **2007**, *2*, 717–724.

67. Nath, A.; Trexler, A. J.; Koo, P.; Miranker, A. D.; Atkins, W. M.; Rhoades, E. *Methods Enzymol*. **2010**, *472*, 89–117.

68. Mak, P. J.; Denisov, I. G.; Grinkova, Y. V.; Sligar, S. G.; Kincaid, J. R. *J. Am. Chem. Soc*. **2011**, *133*, 1357–1366.

69. Gregory, M.; Mak, P. J.; Sligar, S. G.; Kincaid, J. R. *Angew. Chem. Int. Ed*. **2013**, *52*, 5342–5345.

70. Ye, F.; Hu, G.; Taylor, D.; Ratnikov, B.; Bobkov, A. A.; McLean, M. A.; Sligar, S. G.; Taylor, K. A.; Ginsberg, M. H. *J. Cell Biol*. **2010**, *188*, 157–173.

71. Akkaladevi, N.; Hinton-Chollet, L.; Katayama, H.; Mitchell, J.; Szerszen, L.; Mukherjee, S.; Gogol, E. P.; Pentelute, B. L.; Collier, R. J.; Fisher, M. T. *Protein Sci*. **2013**, *22*, 492–501.

72. Civjan, N. R.; Bayburt, T. H.; Schuler, M. A.; Sligar, S. G. *Biotechniques.* **2003**, *35*, 556–563.

73. Skar-Gislinge, N.; Arleth, L. *Phys. Chem. Chem. Phys*. **2011**, *13*, 3161–3170.

74. Denisov, I. G.; McLean, M. A.; Shaw, A. W.; Grinkova, Y. V.; Sligar, S. G. *J. Phys. Chem. B.* **2005**, *109*, 15580–15588.

75. Das, A.; Sligar, S. G. *Biochemistry.* **2009**, *48*, 12104–12112.

76. Das, A.; Grinkova, Y. V.; Sligar, S. G. *J. Am. Chem. Soc*. **2007**, *129*, 13778–13779.

77. Hopper, J. T.; Yu, Y. T.; Li, D.; Raymond, A.; Bostock, M.; Liko, I.; Mikhailov, V.; Laganowsky, A.; Benesch, J. L.; Caffrey, M.; Nietlispach, D.; Robinson, C. V. *Nat Methods*. **2013**, *10*, 1206–1208.

78. Hebling, C. M.; Morgan, C. R.; Stafford, D. W.; Jorgenson, J. W.; Rand, K. D.; Engen, J. R. *Anal. Chem*. **2010**, *82*, 5415–5419.

79. Marty, M. T.; Hoi, K. K.; Gault, J.; Robinson, C. V. *Angew. Chem., Int. Ed*. **2016**, *55*, 550−554.

80. Bernstein, S. L.; Dupuis, N. F.; Lazo, N. D.; Wyttenbach, T.; Condron, M. M.; Bitan, G.; Teplow, D. B.; Shea, J. E.; Ruotolo, B. T.; Robinson, C. V.; Bowers, M. T. *Nature Chem*. **2009**, *1*, 326−331.

81. Kebarle, P.; Tang, L. *Anal. Chem*. **1993**, *65*, 972A–986A.

82. Fenn, J. B. *Angew. Chem. Int. Ed.* **2003**, *42*, 3871.

83. Kebarle, P. *J. Mass Spectrom.* **2000,** *35*, 804.

84. Kebarle, P.; Verkerk, U. H. *Mass Spectrom. Rev.* **2009***, 28*, 898.

85. Taylor, G. I. *J. Fluid Mech.* **1965***, 2*, 1.

86. Iribarne, J. V.; Thomson, B. A. *J. Chem. Phys.* **1976***, 64*, 2287.

87. Iribarne, J. V.; Thomson, B. A. *J. Chem. Phys.* **1979***, 71*, 4451.

88. Dole, M.; Mack, L. L.; Hines, R. L. *J. Chem. Phys.* **1968**, *49*, 2240.

89. Smith, J. N.; Flagan, R. C.; Beauchamp, J. L. *J. Phys. Chem. A* **2002**, *106*, 9957.

90. Peschke, M.; Verkerk, U. H.; Kebarle, P. *J. Am. Soc. Mass Spectrom.* **2004**, *15*, 1424.

91. de la Mora, J. F. *Anal. Chim. Acta* **2000**, *406*, 93.

92. Konermann, L.; Rodriguez, A. D.; Liu, J. *Anal. Chem.* **2012**, *84*, 6798.

93. Ahadi, E.; Konermann, L. *J. Phy. Chem. B* **2012**, *116*, 104.

94. Konermann, L.; Ahadi, E.; Rodriguez, A. D.; Vahidi, S. *Anal. Chem.* **2013**, *85*, 2.

95. Wilm, M. S.; Mann, M. *Int J Mass Spectrom Ion Processes*. **1994**, *136*, 167–180.

96. Wilm, M.; Mann, M. *Anal. Chem.* **1996**, *68*, 1.

97. Karas, M.; Bahr, U.; Dulcks, T. *Fresenius J. Anal. Chem.* **2000**, *366*, 669.

98. Juraschek, R.; Dulcks, T.; Karas, M. *J. Am. Soc. Mass Spectrom.* **1999**, *10*, 300.

99. Jecklin, M. C.; Touboul, D.; Bovet, C.; Wortmann, A.; Zenobi, R. *J. Am. Soc. Mass Spectrom*. **2008**, *19*, 332.

100. Benesch, J. L. P.; Ruotolo, B. T.; Simmons, D. A.; Robinson, C. V. *Chem Rev*. **2007**, 107, 3544–3567.

101. Dawson, P. H. *Quadrupole Mass Spectrometry and Its Applications*. Springer: New York, 1995.

102. March, R. E.; Hughes, R. J. *Quadrupole Storage Mass Spectrometry*. John Wiley & Sons: New York, 1989.

103. De Hoffmann, E.; Stroobant, V. *Mass Spectrometry Principles and Applications,* 3th ed.; John Wiley & Sons: New York, 2007.

104. Pedder, R. E. *Ardara Technologies Technical Note* **2009**, TN_3005A.

105. Wilfried, M. A.; Niessen, Ricardo A.; Correa C. Interpretation of MS-MS Mass Spectra of Drugs and Pesticides.; John Wiley & Sons: New York, 2017.

106. Lu, D. PhD. Dissertation, University of Alberta, 2013.

107. Pringle, S. D.; Giles, K.; Wildgoose, J. L.; Williams, J. P.; Slade, S. E.; Thalassinos, K.; Bateman, R. H.; Bowers, M. T.; Scrivens, J. H. *Int. J. Mass Spectrom.* **2007***, 261*, 1.

108. Giles, K.; Pringle, S. D.; Worthington, K. R.; Little, D.; Wildgoose, J. L.; Bateman, R. H. *Rapid Commun. Mass Spectrom.* **2004***, 18*, 2401–2414.

109. Karasek, F. W. *Anal. Chem.* **1974***, 46*, 710A.

110. McCullough, B. J.; Kalapothakis, J.; Eastwood, H.; Kemper, P.; MacMillan, D.; Taylor, K.; Dorin, J.; Barran, P. E. *Anal. Chem.* **2008**, *80*, 6336.

111. Sergio, A.; Manel, A.; Marcelo, B. *Anal. Chim. Acta.* **2011***, 703*, 114.

112. Cohen, M. J.; Karasek, F. W. *J. Chromatogr. Sci.* **1970***, 8*, 330.

113. Buryakov, I. A.; Krylov, E. V.; Nazarov, E. G.; Rasulev, U. K. *Int. J. Mass Spectrom. Ion Processes.* **1993***, 128*, 143.

114. Shvartsburg, A. A.; Smith, R. D. *Anal. Chem.* **2008**, *80*, 9689.

115. Wildgoose, J.; McKenna, T.; Hughes, C.; Giles, K.; Pringle, S.; Campuzano, I.; Langridge, J.; Bateman, R. H. *Mol. Cell. Proteomics.* **2006**, *5*, S14.

116. Ruotolo, B. T.; Benesch, J. L. P.; Sandercock, A. M.; Hyung, S.-J.; Robinson, C. V. *Nat. Protocols.* **2008**, *3*, 1139.

117. Giles, K.; Williams, J. P.; Campuzano, I. *Rapid Commun. Mass Spectrom.* **2011**, *25*, 1559.

118. McLuckey, S. A. *J. Am. Soc. Mass. Spectrom.* **1992**, *3*, 599.

119. Papayannopoulos, I. A. *Mass Spectrom. Rev.* **1995**, *14*, 49.

120. Dongre, A. R.; Somogyi, A.; Wysocki, V. H. *J. Mass Spectrom.* **1996,** *31*, 339.

121. Price, W. D.; Schnier, P. D.; Jockusch, R. A.; Strittmatter, E. F.; Williams, E. R. *J. Am. Chem. Soc.* **1996**, *118*, 10640.

122. Dunbar, R. C.; McMahon, T. B. *Science* **1998**, *279*, 194.

123. Price, W. D.; Schnier, P. D.; Williams, E. R. *Anal. Chem.* **1996**, *68*, 859.

124. Polfer, N. C. *Chem. Soc. Rev.* **2011**, *40*, 2211.

125. Madsen, J. A.; Boutz, D. R.; Brodbelt, J. S. *J. Proteome Res.* **2010,** *9*, 4205.

126. Shaw, J. B.; Li, W.; Holden, D. D.; Zhang, Y.; Griep-Raming, J.; Fellers, R. T.; Early, B. P.; Thomas, P. M.; Kelleher, N. L.; Brodbelt, J. S. *J. Am. Chem. Soc.* **2013,** *135*, 12646.

127. Zubarev, R. A.; Kelleher, N. L.; McLafferty, F. W. *J. Am. Chem. Soc.* **1998**, *120*, 3265.

128. Zubarev, R. A.; Kruger, N. A.; Fridriksson, E. K.; Lewis, M. A.; Horn, D. M.; Carpenter, B. K.; McLafferty, F. W. *J. Am. Chem. Soc.* **1999**, *121*, 2857.

129. Syka, J. E. P.; Coon, J. J.; Schroeder, M. J.; Shabanowitz, J.; Hunt, D. F. *Proc. Natl. Acad. Sci. U. S. A.* **2004,** *101*, 9528.

130. Wyttenbach, T.; Bowers, M. T. *Annu. Rev. Phys. Chem.* **2007**, *58*, 511.

131. Sharon, M.; Taverner, T.; Ambroggio, X. I.; Deshaies, R. J.; Robinson, C. V. *PLoS. Biol.* **2006,** *4*, 1314.

132. Benesch, J. L. P.; Aquilina, J. A.; Ruotolo, B. T.; Sobott, F.; Robinson, C. V. *Chem. Biol*. **2006**, *13*, 597.

133. Lorenzen, K.; Vannini, A.; Crarner, P.; Heck, A. J. R. *Structure.* **2007,** *15*, 1237.

134. Tešić, M.; Wicki, J.; Poon, D. K. Y.; Withers, S. G.; Douglas, D. J. *J. Am. Soc. Mass Spectrom.* **2007**, *18*, 64. El-Hawiet, A.;

135. Shoemaker, G. K.; Daneshfar, R.; Kitova, E. N.; Klassen, J. S. *Anal. Chem.* **2012,** *84*, 50.

136. Guilhaus, M.; Selby, D.; Mlynski, V. *Mass Spectrom. Rev.* **2000**, *19*, 65.

137. Chernushevich, I. V.; Loboda, A. V.; Thomson, B. A. J Mass Spectrom. **2001**, *36*, 849–865.

138. Mamyrin, B. A. *Int. J. Mass Spectrom.* **2001,** *206*, 251.

139. Kitova, E. N.; El-Hawiet, A.; Schnier, P. D.; Klassen, J. S. *J. Am. Soc. Mass Spectrom.* **2012**, *23*, 431–441.

140. Kitova, E. N.; Kitov, P. I.; Paszkiewicz, E.; Kim, J.; Mulvey, G. L.; Armstrong, G. D.; Bundle, D. R.; Klassen, J. S. *Glycobiology* **2007**, *17*, 1127.

141. Han, L.; Kitova, E. N.; Klassen, J. S. *J. Am. Soc. Mass Spectrom*. **2016**, *27*, 1878–1886.

142. Abzalimov, R. R.; Dubin, P. L.; Kaltashov, I. A. *Anal. Chem.* **2007**, *97*, 6055–6063.

143. Cederkvist, F.; Zamfir, A. D.; Bahrke, S.; Eijsink, V. G. H.; Sorlie, M.; Peter-Katalinic, J.; Peter, M. G. *Angew. Chem. Int. Ed.* **2006,** *45*, 2429–2434.

144. El-Hawiet, A.; Shoemaker, G. K.; Daneshfar, R.; Kitova, E. N.; Klassen, J. S. *Anal. Chem.* **2012,** *84*, 50–58.

145. Creaser, C. S. ; Griffiths, J. R.; Bramwell, C. J.; Noreen, S.; Hill, C. A. ; Paul Thomas, C. L. *Analyst.* **2004***, 129*, 984.

146. Uetrecht, C., Rose, R. J., van Duijn, E., Lorenzen, K., Heck, A. J. R. *Chem. Sov. Rev*. **2010**, *39*, 1633–1655.

147. Scarff, C. A.; Thalassinos, K.; Hilton, G. R.; Scrivens, J. H. *Rapid Commun. Mass Spectrom*. **2008**, *22*, 3297–3304.

148. Thalassinos, K.; Slade, S. E.; Jennings, K.R.; Scrivens, J. H.; Giles, K.; Wildgoose, J.; Hoyes, J.; Bateman, R. H.; Bowers, M. T. *Int. J. Mass Spectrom*. **2004**, *236*, 55–63.

149. Smith, D. P.; Giles, K.; Bateman, R. H.; Radford, S. E.; Ashcroft, A. E. *J. Am. Soc. Mass Spectrom*. **2007**, *18*, 2180–2190.

150. Ruotolo, B. T.; Giles, K.; Campuzano, I.; Sandercock, A. M.; Bateman, R. H.; Robinson, C. V. *Science*, **2005**, *310*,1658–1661.

151. Uetrecht, C.; Versluis, C.; Watts, N. R.; Wingfield, P. T.; Steven, A. C.; Heck, A. J. *Angew. Chem. Int. Ed*. **2008**, *47*, 6247–6251.

152. Pacholarz, K. J.; Garlish, R. A.; Taylor, R. J.; Barran, P. E. *Chem. Soc. Rev.* **2012**, *41*, 4335–4355.

153. Arteca, G. A.; Reimann, C. T.; Tapia, O.; *Mass Spectrom. Rev*. **2001**, *20*, 402–422.

154. Daggett, V. *Chem. Rev*. **2006**, *106*, 1898–1916.

155. Clemmer, D. E.; Jarrold, M. F. *J. Mass Spectrom.* **1997**, *32*, 577–592.

156. Wyttenbach, T.; Witt, M.; Bowers, M. T. *J. Am. Chem. Soc.* **2000**, *122*, 3458–3464.

157. Sun, J.; Kitova, E. N.; Klassen, J. S. *Anal. Chem*. **2006**, *79*, 416–425.

158. Sun, J.; Kitova, E. N.; Klassen, J. S. *Anal. Chem*. **2007**, *79*, 416.

159. Bagal, D.; Kitova, E. N.; Liu, L.; El-Hawiet, A.; Schnier, P. D.; Klassen, J. S. *Anal. Chem.* **2009**, *81*, 7801.

160. Robinson, C. V.; Chung, E. W.; Kragelund, B. B.; Knudsen, J.; Aplin, R. T.; Poulsen, F. M.; Dobson, C. M. *J. Am. Chem. Soc.* **1996***, 118*, 8646.

161. El-Hawiet, A.; Kitova, E. N.; Liu, L.; Klassen J. S. *J. Am. Soc. Mass Spectrom.* **2010**, *21*, 1893.

162. Sakamoto, S.; Fujita, M.; Kim, K.; Yamaguchi, K. *Tetrahedron*. **2000**, *56*, 955–964.

163. Nishimura, S. -I.; Nagahori, N.; Takaya, K.; Tachibana, Y.; Miura, N.; Monde, K. *Angew. Chem. Int. Ed*. **2005**, *44*, 571–575.

164. Miras, H. N.; Wilson, E. F.; Cronin, L. *Chem. Commun*. **2009**, *11*, 1297–1311.

165. Hunter, E. P.; Lias, S. G. *Phys. Chem. Ref. Data.* **1998**, *27*, 413.

166. Liu, L.; Kitova, E. N.; Klassen, J. S. *J. Am. Soc. Mass Spectrom*. **2011**, *22*, 310–318.

167. Wang, W.; Kitova, E. N.; Klassen, J. S. *Anal. Chem.* **2005,** *77*, 3060.

168. Hossain, B. M.; Konermann, L. *Anal. Chem.* **2006**, *78*, 1613.

169. Daubenfeld, T.; Bouin, A. P.; van der Rest, G. *J. Am. Soc. Mass Spectrom.* **2006**, *17*, 50 1239.

170. Lane, L. A.; Ruotolo, B. T.; Robinson, C. V.; Favrin, G.; Benesch, J. L. P. *J. Mass Spectrom.* **2009**, *283*, 169.

171. Shimon, L.; Sharon, M.; Horovitz, A. *Biophys. J.* **2010,** *99*, 1645.

172. Sun, N.; Sun, J.; Kitova, E. N.; Klassen, J. S. J. *Am. Soc. Mass Spectrom.* **2009**, *20*, 1242.

173. Kitova, E. N.; Soya, N.; Klassen, J. S. *Anal. Chem.* **2011**, *83*, 5160.

174. Wilcox, J. M.; Rempel, D. L.; Gross, M. L. *Anal. Chem.* **2008**, *80*, 2365.

175. Gabelica, V.; Galic, N.; Rosu, F.; Houssier, C.; De Pauw, E. *J. Mass Spectrom.* **2003**, *38*, 491.

176. Gabelica, V.; Rosu, F.; De Pauw, E. *Anal. Chem.* **2009**, *81*, 6708.

177. Mathur, S.; Badertscher, S.; Scott, M.; Zenobi, R. *Phys. Chem. Chem. Phys.* **2007**, *9*, 6187.

178. Wang, W.; Kitova, E. N.; Klassen, J. S. *Anal. Chem.* **2003**, *75*, 4945.

179. Van Berkel, G. J.; Asano, K. G.; Schnier, P. D. *J. Am. Soc. Mass Spectrom.* **2001**, *12*, 853.

180. Yao, Y.; Shams-Ud-Doha, K.; Daneshfar, R.; Kitova, E. N.; Klassen, J. S. *J. Am. Soc. Mass. Spectrom.* **2015,** *26*, 98.

181. Susa, A. C.; Xia, Z.; Williams, E. R. *Anal. Chem*. **2017**, *89*, 3116.

182. Konermann, L. *J. Am. Soc. Mass Spectrom*. **2017**, *28*, 1827–1835.

183. Lide, D. R. *CRC Handbook of chemistry and physics*, 82nd ed. CRC Press: Boca Raton, London, New York, Washington, 2001.

184. Zhuang, X.; Gavriilidou, A. F. M.; Zenobi, R. *J. Am. Soc. Mass Spectrom*. **2017**, *28*, 341–346.

185. Hedges, J. B.; Vahidi, S.; Yue, X.; Konermann, L. *Anal. Chem*. **2013**, *85*, 6469–6476.

Chapter 2

1. Hakomori, S. *Curr. Opin. Hematol.* **2003**, *10*, 16–24.

2. Varki, A.; Cummings, R. D.; Esko, J. D.; Freeze, H. H.; Stanley, P.; Bertozzi, C. R.; Hart, G. W.; Etzler, M. E. *Essentials of Glycobiology*, 2nd ed.; Cold Spring Harbor Laboratory Press: Cold Spring Harbor, NY, 2009.

3. Malhotra, R. *Biochem Anal Biochem* **2012**, *1*, 108.

4. Schulze, H.; Sandhoff, K. *Biochim. Biophys. Acta* **2014**, *1841*, 799–810.

5. Lopez, H. H. H.; Schnaar, R. L. *Methods Enzymol*. **2006**, *417*, 205–220.

6. Lipid-Protein Interactions. In *Methods and Protocols*; Kleinschmidt, J. H., Ed.; Springer: New York, 2014; Vol. *974*.

7. Evans, S. V.; Roger MacKenzie. C. *J. Mol. Recognit*. **1999**, *12*, 155–68.

8. Lingwood, C. A.; Manis, A.; Mahfoud, R.; Khan, F.; Binnington, B.; Mylvaganam, M. *Chem. Phys. Lipids*. **2010**, *163*, 27–35.

9. Czogalla, A.; Grzybek, M.; Jones, W.; Coskun, U. *Biochim. Biophys. Acta* **2014**, *1841*, 1049–1859.

10. Zhang, Y.; Liu, L.; Daneshfar, R.; Kitova, E. N.; Li, C.; Jia, F.; Cairo, C.W.; Klassen, J. S. *Anal. Chem.* **2012**, *84*, 7618–7621.

11. Leney, A.; Fan, X.; Kitova, E.N.; Klassen, J. S. *Anal. Chem.* **2014**, *86*, 5271–5277.

12. Han, L.; Kitova, E. N.; Li, J.; Nikjah, S.; Lin, H.; Pluvinage, B.; Boraston, A. B.; Klassen, J. S. *Anal. Chem.* **2015,** *87,* 4888–4896.

13. Leney, A. C.; Darestani, R. R.; Li, J.; Nikjah, S.; Kitova, E. N.; Zou, C.; Cairo, C. W.; Xiong, Leney, A.; Fan, X.; Kitova, E. N.; Klassen, J. S. *Anal. Chem.* **2015**, *87*, 4402–4408.

14. Bayburt, T. H.; Grinkova, Y. V.; Sligar, S. G. *Nano Lett*. **2002**, *2*, 853−856.

15. Popovic, K.; Holyoake, J.; Pomès, R.; Privé, G.G. *Prot. Natl. Acad. Sci.* **2012**, *109*, 2908–2912.

16. Merritt, E. A.; Sarfaty, S.; Van Den Akker, F.; L'Hoir, C.; Martial, J. A.; Hol, W. G. J. *Protein Sci*. **1994**, *3*, 166−175.

17. Holmgren, J.; Lö nnroth, I.; Svennerholm, L. *Infect. Immun*. **1973**, *8*, 208–214.

18. Kuziemko, G. M.; Stroh, M.; Stevens, R. C. *Biochemistry* **1996**, *35*, 6375–6384.

19. Lin, H.; Kitova, E. N.; Klassen, J. S. *J. Am. Soc. Mass Spectrom*. **2014**, *25*, 104−110.

20. Just, I.; Gerhard, R. Large clostridial cytotoxins. In *Reviews of Physiology, Biochemistry and Pharmacology*, Springer Berlin Heidelberg: **2005**, *152*, 23–47.

21. Dallas, S. D.; Rolfe, R. D. *J. Med. Microbiol*. **1998**, *47*, 879–888.

22. Krivan, H. C.; Clark, G. F.; Smith, D. F.; Wilkins, T. D. *Infect. Immun*. **1986**, *53*, 573–581.

23. Smith, J. A.; Cooke, D. L.; Hyde, S.; Borriello, S. P.; Long, R. G. *J. Med. Microbiol*. **1997**, *46*, 953–958.

24. Tucker, K. D.; Wilkins, T. D. *Infect. Immun*. **1991**, *59*, 73–78.

25. Karlsson, K. A. *Curr. Opin. Struct. Biol*. **1995**, *5*, 622–635.

26. Teneberg, S.; Lonnroth, I.; Lopez, J. F. T.; Galili, U.; Halvarsson, M. O.; Angstrom, J.; Karlsson, K. A. *Glycobiology* **1996**, *6*, 599–609.

27. Fan, X.; Kitova, E. N.; Eugenio, L.; Ng, K. K. S; Klassen, J. S. *manuscript in preparation*

28. Greco, A.; Ho, J. G. S.; Lin, S. J.; Palcic, M. M.; Rupnik, M.; Ng, K. K. S. *Nat. Struct. Mol. Biol.* **2006**, *13*, 460–461.

29. Zdanov, A.; Li Y.; Bundle, D. R.; Deng, S. J.; Mackenzie, C. R.; Narang, S. A.; Young, N. M.; Cygler, M. *Proc. Natl. Acad. Sci. USA.* **1994**, *91*, 6423–6427.

30. Bayburt, T. H.; Grinkova, Y. V.; Sligar, S. G. *Nano Lett*. **2002**, *2*, 853−856.

31. Borch, J.; Torta, F.; Sligar, S. G.; Roepstorff, P. *Anal. Chem*. **2008**, *80*, 6245−6252.

32. Bayburt, T. H.; Sligar, S. G. *FEBS Lett*. **2010**, *584*, 1721−1727.

33. Kitova, E. N.; El-Hawiet, A.; Schnier, P. D.; Klassen, J. S. *J. Am. Soc. Mass Spectrom.* **2012**, *23*, 431–441.

34. Sun, J.; Kitova, E. N.; Wang, W.; Klassen, J. S. *Anal. Chem*. **2006**, *78*, 3010–3018.

35. Teneberg, S.; Hirst, T. R.; Angström, J.; Karlsson, K. A.; *Glycoconj. J*. **1994**, *11*, 533–540.

36. MacKenzie, C. R.; Hirama, T.; Lee, K. K.; Altman, E.; Young, N. M. *J. Biol. Chem*. **1997**, *272*, 5533–5538.

37. Ikeda, K.; Shimizu, T.; Taguchi, R. *J. Lipid Res*. **2008**, *49*, 2678−2689.

38. Masserini, M.; Freire, E.; Palestini, P.; Calappi, E.; Tettamanti, G. *Biochemistry*. **1992**, *31*, 2422–2426.

Chapter 3

1. Malhotra, R. *Biochem. Anal. Biochem.* **2012**, *1*, 108.

2. Hakomori, S. *Curr. Opin. Hematol.* **2003**, *10*, 16−24.

3. Sharon, N.; Lis, H. *Sci. Am*. **1993**, *268*, 82−89.

4. Varki, A.; Cummings, R. D.; Esko, J. D.; Freeze, H. H.; Stanley, P.; Bertozzi, C. R.; Hart, G. W.; Etzler, M. E. *Essentials of Glycobiology*, 2nd ed.; Cold Spring Harbor Laboratory Press: Cold Spring Harbor, NY, 2009.

5. Lopez, H. H. H.; Schnaar, R. L. *Methods Enzymol*. **2006**, *417*, 205–220.

6. Feizi, T. *Ann. N.Y. Acad. Sci*. **2013**, *1292*, 33−44.

7. Grant, O. C.; Smith, H. M.; Firsova, D.; Fadda, E.; Woods, R. J. *Glycobiology* **2014**, *24*, 17−25.

8. Shi, J.; Yang, T.; Kataoka, S.; Zhang, Y.; Diaz, A. J.; Cremer, P. S. *J. Am. Chem. Soc*. **2007**, *129*, 5954−5961.

9. Jayaraman, N.; Maiti, K.; Naresh, K. *Chem. Soc. Rev*. **2013**, *42*, 4640 −4656.

10. Bayburt, T. H.; Grinkova, Y. V.; Sligar, S. G. *Nano Lett*. **2002**, *2*, 853−856.

11. Zhang, Y.; Liu, L.; Daneshfar, R.; Kitova, E. N.; Li, C.; Jia, F.; Cairo, C.W.; Klassen, J. S. *Anal. Chem.* **2012**, *84*, 7618−7621.

12. Leney, A. C.; Darestani, R. R.; Li, J.; Nikjah, S.; Kitova, E. N.; Zou, C.; Cairo, C. W.; Xiong, Z. J.; Privé, G. G.; Klassen, J. S. *Anal. Chem.* **2015**, *87*, 4402−4408.

13. Li, J.; Fan, X.; Kitova, E. N.; Zou, C.; Cairo, C. W.; Eugenio, L.; Ng, K. K. S.; Xiong, Z. J.; Privé, G. G.; Klassen, J. S. *Anal. Chem.* **2016**, *88*, 4742**–**4750.

14. Locatelli-Hoops, S.; Remmel, N.; Klingenstein, R.; Breiden, B.; Rossocha, M. Schoeniger, M.; Koenigs, C.; Saenger, W.; Sandhoff, K. *J. Biol. Chem*. **2006**, *281*, 32451.

15. Popovic, K.; Holyoake, J.; Pomès, R.; Privé, G. G. *Prot. Natl. Acad. Sci.* **2012**, *109*, 2908−2912.

16. Sun, J.; Kitova, E.N.; Wang, W.; Klassen, J. S. *Anal. Chem.* **2006**, *78*, 3010−3018.

17. Rose, R. J.; Damoc, E,; Denisov, E.; Makarov, A.; Heck, A. J. R. *Nat. Methods* **2012**, *9*, 1084−1086.

18. Rosati, S.; Rose, R. J.; Thompson, N. J.; Van Duijn, E.; Damoc, E.; Denisov, E.; Makarov, A.; Heck, A. J. *Angew. Chem. Int. Ed*. **2012**, *51*, 12992−12996.

19. Michalski, A.; Damoc, E.; Hauschild, J. P.; Lange, O.; Wieghaus, A.; Makarov, A.;

Nagaraj, N.; Cox, J.; Mann, M.; Horning, S. *Mol. Cell. Proteomics*. **2011**, *10*, M111.011015.

20. Marty, M. T.; Baldwin, A. J.; Marklund, E. G.; Hochberg, G. K.; Benesch, J. L.; Robinson, C. V. *Anal. Chem.* **2015**, *87*, 4370–4376.

21. Bush, M. F.; Hall, Z.; Giles, K.; Hoyes, J.; Robinson, C. V.; Ruotolo, B. T. *Anal. Chem*. **2010**, *82*, 9557−9565.

22. Ruotolo, B. T.; Benesch, J. L. P.; Sandercock, A. M.; Hyung, S. J.; Robinson, C. V. *Nat. Protoc*. **2008**, *3*, 1139−1152.

23. Pettersen, E. F.; Goddard, T. D.; Huang, C. C.; Couch, G. S.; Greenblatt, D. M.; Meng, E. C.; Ferrin, T. E. *J. Comput. Chem.* **2004**, *25*, 1605–1612.

24. Balabin, I. Membrane Plugin, Version 1.1. http://www.ks.uiuc.edu/Research/vmd/plugins/membrane/ (accessed 11/21/2014).

25. Humphrey, W.; Dalke, A.; Schulten, K. *J. Mol. Graphics* **1996**, *14*, 33–38.

26. Case, D. A.; Darden, T. A.; Cheatham III, T. E.; Simmerling, C. L.; Wang, J.; Duke, R. E.; Luo, R.; Walker, R. C.; Zhang, W.; Merz, K. M.; Roberts, B.; Hayik, S.; Roitberg, A.; Seabra, G.; Swails, J.; Götz, A. W.; Kolossváry, I.; Wong, K. F.; Paesani, F.; Vanicek, J.; Wolf, R. M.; Liu, J.; Wu, X.; Brozell, S. R.; Steinbrecher, T.; Gohlke, H.; Cai, Q.; Ye, X.; Wang, J.; Hsieh, M.-J.; Cui, G.; Roe, D. R.; Mathews, D. H.; Seetin, M. G.; Salomon-Ferrer, R.; Sagui, C.; Babin, V.; Luchko, T.; Gusarov, S.; Kovalenko, A.; Kollman, P. A. AMBER 12, University of California: San Fancisco, CA, 2012.

27. Jorgensen, W. L.; Chandrasekhar, J.; Madura, J. D.; Impey, R. W.; Klein, M. L. *J. Chem. Phys.* **1983**, *79*, 926–935.

28. Duan, Y.; Wu, C.; Chowdhury, S.; Lee, M. C.; Xiong, G.; Zhang, W.; Yang, R.; Cieplak,

P.; Luo, R.; Lee, T.; Caldwell, J.; Wang, J.; Kollman, P. *J. Comput. Chem*. **2003**, *24*, 1999−2012.

29. Skjevik, Å. A.; Madej, B. D.; Walker, R. C.; Teigen, K. *J. Phys. Chem. B* **2012**, *116*, 11124−11136.

30. Berendsen, H. J. C.; Postma, J. P. M.; Gunsteren, W. F. v.; DiNola, A.; Haak, J. R. *J. Chem. Phys*. **1984**, *81*, 3684–3690.

31. Ryckaert, J.-P.; Ciccotti, G.; Berendsen, H. J. C. *J. Comput. Phys*. **1977**, *23*, 327–341.

32. Contributors to Amber. http://ambermd.org/contributors.html (accessed 1/26/2016).

33. Larriba, C.; Hogan, C. J. Jr. *J. Phys. Chem. A* **2013**, *117*, 3887–3901.

34. Antonietti, M.; Bremser, W.; Schmidt, M. *Macromolecules* **1990**, *23*, 3796−3805.

35. Tande, B. M.; Wagner, N. J.; Mackay, M. E.; Hawker, C. J.; Jeong, M. *Macromolecules* **2001**, *34*, 8580−8585.

Chapter 4

1. Malhotra, R. *Biochem. Anal. Biochem*. **2012**, *1*, 108.

2. Varki, A.; Cummings, R. D.; Esko, J. D.; Freeze, H. H.; Stanley, P.; Bertozzi, C. R.; Hart, G. W.; Etzler, M. E. *Essentials of Glycobiology*, 2nd ed.; Cold Spring Harbor Laboratory Press: Cold Spring Harbor, NY, 2009.

3. Evans, S. V.; Roger MacKenzie. C. *J. Mol. Recognit*. **1999**, *12*, 155–68.

4. Lingwood, C. A.; Manis, A.; Mahfoud, R.; Khan, F.; Binnington, B.; Mylvaganam, M. *Chem. Phys. Lipids*. **2010**, *163*, 27–35.

5. Shi, J.; Yang, T.; Kataoka, S.; Zhang, Y.; Diaz, A. J.; Cremer, P. S. *J. Am. Chem. Soc*. **2007**, *129*, 5954−5961.

6. Sanghera, N.; Correia, B. E.; Correia, J. R.; Ludwig, C.; Agarwal, S.; Nakamura, H. K.; Kuwata, K.; Samain, E.; Gill, A. C.; Bonev, B. B.; Pinheiro, T. J. *Chem. Biol.* **2011**, *18*, 1422–1431.

7. Lingwood, D.; Binnington, B.; Rog, T.; Vattulainen, I.; Grzybek, M.; Coskun, U.; Lingwood, C. A.; Simons, K. *Nat. Chem. Biol.* **2011**, *7*, 260–262.

8. Czogalla, A.; Grzybek, M.; Jones, W.; Coskun, U. *Biochim. Biophys. Acta*. **2014**, *1841*, 1049–1059.

9. Bayburt, T. H.; Grinkova, Y. V.; Sligar, S. G. *Nano Lett*. **2002**, *2*, 853−856.

10. Zhang, Y.; Liu, L.; Daneshfar, R.; Kitova, E. N.; Li, C.; Jia, F.; Cairo, C.W.; Klassen, J. S. *Anal. Chem.* **2012**, *84*, 7618−7621.

11. Popovic, K.; Holyoake, J.; Pomès, R.; Privé, G. G. *Prot. Natl. Acad. Sci.* **2012**, *109*, 2908−2912.

12. Leney, A. C.; Darestani, R. R.; Li, J.; Nikjah, S.; Kitova, E. N.; Zou, C.; Cairo, C. W.; Xiong, Z. J.; Privé, G. G.; Klassen, J. S. *Anal. Chem.* **2015**, *87*, 4402−4408.

13. Borch, J.; Torta, F.; Sligar, S. G.; Roepstorff, P. *Anal. Chem.* **2008**, *80*, 6245–6252.

14. Bally, M.; Rydell, G. E.; Zahn, R.; Nasir, W.; Eggeling, C.; Breimer, M. E.; Svensson, L.; Hook, F.; Larson, G. *Angew. Chem. Int. Ed*. **2012**, *51*, 12020–12024.

15. Lauer, S.; Goldstein, B.; Nolan, R. L.; Nolan, J. P. *Biochemistry*. **2002**, *41*, 1742–1751.

16. Leney, A.; Fan, X.; Kitova, E.N.; Klassen, J. S. *Anal. Chem.* **2014**, *86*, 5271–5277.

17. Li, J.; Fan, X.; Kitova, E. N.; Zou, C.; Cairo, C. W.; Eugenio, L.; Ng, K. K. S.; Xiong, Z. J.; Privé, G. G.; Klassen, J. S. *Anal. Chem.* **2016**, *88*, 4742–4750.

18. Nakano, M.; Fukuda, M.; Kudo, T.; Miyazaki, M.; Wada, Y.; Matsuzaki, N.; Endo, H., Handa, T. *J. Am. Chem. Soc*. **2009**, *131*, 8308–8312.

19. Brown, R. E.; Thompson, T. E. *Biochemistry*. **1987**, *26*, 5454–5460.

20. Brown, R. E. *Biochim. Biophys. Acta*. **1992**, *1113*, 375–389.

21. Nichols, J. W. *Biochemistry*. **1988**, *27*, 3925–3931.

22. Han, L.; Kitova, E. N.; Li, J.; Nikjah, S.; Lin, H.; Pluvinage, B.; Boraston, A. B.; Klassen, J. S. *Anal. Chem*. **2015**, *87*, 4888–4896.

23. Zhou, D.; Cantu, C. 3rd.; Sagiv, Y.; Schrantz, N.; Kulkarni, A. B.; Qi, X.; Mahuran, D. J.; Morales, C. R.; Grabowski, G. A.; Benlagha, K.; Savage, P.; Bendelac, A.; Teyton, L. *Science*. **2004**, *303*, 523–527.

24. Locatelli-Hoops, S.; Remmel, N.; Klingenstein, R.; Breiden, B.; Rossocha, M.; Schoeniger, M.; Koenigs, C.; Saenger, W.; Sandhoff, K. *J Biol Chem*. **2006**, *281*, 32451–3260.

25. Han, L.; Kitova, E. N.; Klassen, J. S. *J Am Soc Mass Spectrom*. **2016**, *27*, 1878–1886.

26. Sturqill, E. R.; Aoki, K.; Lopez, P. H.; Colacurcio, D.; Vajn, K.; Lorenzini, I.; Majic, S.; Yang, W. H.; Heffer, M.; Tiemeyer, M.; Marth, J. D.; Schnaar, R. L. *Glycobiology*. **2012**, *22*, 1289–1301.

27. Yagi-Utsumi, M.; Kameda, T.; Yamaguchi, Y.; Kato, K. *FEBS Lett*. **2010**, *584*, 831–836.

28. Li, J.; Richards, M. R.; Bagal, D.; Campuzano, I. D. G.; Kitova, E. N.; Xiong, Z. J.; Privé, G. G.; Klassen, J. S. *Anal. Chem*. **2016**, *88*, 9524–9531.

29. Han, L.; Morales, L. C.; Richards, M. R.; Kitova, E. N.; Sipione, S.; Klassen, J. S. *Anal. Chem*. **2017**, *89*, 9330–9338.

30. Bayburt, T. H., Sligar, S. G. *FEBS Lett*. **2010**, *584*, 1721−1727.

31. Lin, H.; Kitova, E. N.; Klassen, J. S. *J. Am. Soc. Mass Spectrom*. **2014**, *25*, 104−110.

32. Kuziemko, G. M.; Stroh, M.; Stevens, R. C. *Biochemistry*. **1996**, *35*, 6375–6384.

33. Ikeda, K.; Shimizu, T.; Taguchi, R. *J. Lipid Res*. **2008**, *49*, 2678−2689.

34. Whitehead, S. N.; Chan, K. H. N.; Gangaraju, S.; Slinn, J.; Li, J.; Hou, S. T. *PLoS ONE*. **2011**, *6*, e20808.

Chapter 5

1. Nath, A.; Atkins, W. M.; Sligar, S. G. *Biochemistry*. **2007**, *46*, 2059–2069.

2. Denisov, I. G.; Sligar, S.G. *Nat. Struct. Mol. Biol*. **2016**, *23*, 481–486.

3. Sanders, C. R.; Prosser, R. S. *Structure*. **1998**, *6*, 1227–1234.

4. Sanders, C. R.; Landis, G. C. *Biochemistry*. **1995**, *34*, 4030–4040.

5. Kashara, M.; Hinkle, P. C. *J. Biol. Chem*. **1977**, *252*, 7384–7390.

6. Rigaud, J. L.; Paternostre, M. T.; Bluzat, A. 2. *Biochemistry*. **1988**, *27*, 2677–2688.

7. Seddon, A. M.; Curnow, P.; Booth, P. J. *Biophys. Acta*. **2004**, *1666*, 105–117.

8. Bayburt, T. H.; Grinkova, Y. V.; Sligar, S. G. *Nano Lett*. **2002**, *2*, 853−856.

9. Bayburt, T. H.; Sligar, S. G. *FEBS Lett*. **2010**, *584*, 1721−1727.

10. Hagn, F.; Etzkorn, M.; Raschle, T.; Wagner, G. *J. Am. Chem. Soc*. **2013**, *135*, 1919–1925.

11. Wang, X.; Mu, Z.; Li, Y.; Bi, Y.; Wang, Y. *Protein J*. **2015**, *34*, 205–211.

12. Ritchie, T. K.; Kwon, H.; Atkins, W. M. *J. Biol. Chem*. **2011**, *286*, 39489–39496.

13. Mak, P. J.; Gregory, M. C.; Denisov, I. G.; Sligar, S. G.; Kincaid, J. R. *Proc. Natl. Acad. Sci. USA.* **2015**, *112*, 15856–15861.

14. Hopper, J. T.; Yu, Y. T.; Li, D.; Raymond, A.; Bostock, M.; Liko, I.; Mikhailov, V.; Laganowsky, A.; Benesch, J. L.; Caffrey, M.; Nietlispach, D.; Robinson, C. V. *Nat Methods*. **2013**, *10*, 1206–1208.

15. Hebling, C. M.; Morgan, C. R.; Stafford, D. W.; Jorgenson, J. W.; Rand, K. D.; Engen, J. R. *Anal. Chem*. **2010**, *82*, 5415–5419.

16. Marty, M. T.; Hoi, K. K.; Gault, J.; Robinson, C. V. *Angew. Chem., Int. Ed*. **2016**, *55*, 550−554.

17. Bernstein, S. L.; Dupuis, N. F.; Lazo, N. D.; Wyttenbach, T.; Condron, M. M.; Bitan, G.; Teplow, D. B.; Shea, J. E.; Ruotolo, B. T.; Robinson, C. V.; Bowers, M. T. *Nature Chem*. **2009**, *1*, 326−331.

18. Andersen, O. S.; Koeppe, R. E. 2nd; Roux, B. *IEEE Trans Nanobioscience*. **2005**, *4*, 10–20.

19. Kelkar, D. A.; Chattopadhyay, A. *Biochim. Biophys. Acta, Biomembr*. **2007**, *1768*, 2011−2025.

20. Miloshevsky, G. V.; Jordan, P. C. *Trends Neurosci*. **2004**, *27*, 308–314.

21. Veatch, W. R.; Blout, E. R. *Biochemistry*. **1974**, *13*, 5257–5264.

22. Veatch, W. R.; Fossel, E. T.; Blout. E. R. *Biochemistry*. **1974**, *13*, 5249–5256.

23. Bystrov, V. F.; Arseniev, A. S. *Tetrahedron*. **1988**, *44*, 925–940.

24. Braco, L.; Bano, C.; Chillaron, F.; Abad, C. *Int. J. Biol. Macromol*. **1988**, *10*, 343−348.

25. Arseniev, A. S.; Barsukov, I. L.; Bystrov, V. F.; Lomize, A. L.; Ovchinnikov, Y. A. *FEBS Lett*. **1985**, *186*, 168–174.

26. Ketchem, R. R.; Hu, W.; Cross, T. A. *Science.* **1993**, *261*, 1457–1460.

27. Patrick, J. W.; Gamez, R. C.; Russell, D. H. *Anal. Chem*. **2015**, *87*, 578–583.

28. Patrick, J. W.; Gamez, R. C.; Russell, D. H. *Biophys. J*. **2016**, *110*, 1826–1835.

29. Patrick. J. W.; Zerfas, B.; Gao, J.; Russell, D. H. *Analyst*. **2017**, *142*, 310–315.

30. Leney, A. C.; Fan, X.; Kitova, E. K.; Klassen, J. S. *Anal. Chem*. **2014**, *86,* 5271–5277.

31. Ruotolo, B. T.; Benesch, J. L. P.; Sandercock, A. M.; Hyung, S. J.; Robinson, C. V. *Nat. Protoc*. **2008**, *3*, 1139–1152.

32. Bush, M. F.; Hall, Z.; Giles, K.; Hoyes, J.; Robinson, C. V.; Ruotolo, B. T. *Anal. Chem*. **2010**, *82*, 9557−9565.

33. Hoaglund, C. S.; Valentine, S. J.; Sporleder, C. R.; Reily, J. P.; Clemmer, D. E. *Anal. Chem*. **1998**, *70*, 2236−2242.

34. Henderson, S. C.; Valentine, S. J.; Counterman, A. E.; Clemmer, D. E. *Anal. Chem*. **1999**, *71*, 291−301.

35. Hoaglund, C. S.; Valentine, S. J.; Sporleder, C. R.; Reily, J. P., Clemmer, D. E. *Anal. Chem*. **1998**, *70*, 2236−2242.

36. Henderson, S. C.; Valentine, S. J.; Counterman, A. E.; Clemmer, D. E. *Anal. Chem*. **1999**, *71*, 291−301.

37. Chen, Y.; Tucker, A.; Wallace, B. A. *J. Mol. Biol*. **1996**, *264*, 757–769.

38. Burkhart, B. M.; Gassman, R. M.; Langs, D. A.; Pangborn, W. A.; Duax, W. L. *Biophys. J*. **1998**, *75*, 2135–2146.

39. Burkhart, B. M.; Li, N.; Langs, D. A.; Pangborn, W. A.; Duax, W. L. *Proc. Natl. Acad. Sci. U.S.A*. **1998**, *95*, 12950–12955.

40. Ketchem, R. R.; Lee, K.-C.; Huo, S.; Cross, T. A. *J. Biomol. NMR*. **1996**, *8*, 1–14.

41. Townsley, L. E. (PDB ID: 1NRU). 2003.

42. Case, D. A.; Berryman, J. T.; Betz, R. M.; Cerutti, D. S.; Cheatham III, T. E.; Darden, T. A.; Duke, R. E.; Giese, T. J.; Gohlke, H.; Goetz, A. W.; Homeyer, N.; Izadi, S.; Janowski, P.; Kaus, J.; Kovalenko, A.; Lee, T. S.; LeGrand, S.; Li, P.; Luchko, T.; Luo, R.; Madej, B.; Merz, K. M.; Monard, G.; Needham, P.; Nguyen, H.; Nguyen, H. T.; Omelyan, I.; Onufriev, A.; Roe, D. R.; Roitberg, A.; Salomon-Ferrer, R.; Simmerling, C. L.; Smith, W.;

Swails, J.; Walker, R. C.; Wang, J.; Wolf, R. M.; Wu, X.; York, D. M.; Kollman, P. A. AMBER 15, University of California: San Francisco, CA, 2015.

43. Case, D. A.; Darden, T. A.; Cheatham III, T. E.; Simmerling, C. L.; Wang, J.; Duke, R. E.; Luo, R.; Walker, R. C.; Zhang, W.; Merz, K. M.; Roberts, B.; Hayik, S.; Roitberg, A.; Seabra, G.; Swails, J.; Götz, A. W.; Kolossváry, I.; Wong, K. F.; Paesani, F.; Vanicek, J.; Wolf, R. M.; Liu, J.; Wu, X.; Brozell, S. R.; Steinbrecher, T.; Gohlke, H.; Cai, Q.; Ye, X.; Wang, J.; Hsieh, M.-J.; Cui, G.; Roe, D. R.; Mathews, D. H.; Seetin, M. G.; Salomon-Ferrer, R.; Sagui, C.; Babin, V.; Luchko, T.; Gusarov, S.; Kovalenko, A.; Kollman, P. A. AMBER 12, University of California: San Fancisco, CA, 2012.

44. Hornak, V.; Abel, R.; Okur, A.; Strockbine, B.; Roitberg, A.; Simmerling, C. *Proteins*, **2006**, *65*, 712–725.

45. Joung, I. S.; Cheatham, T. E. *J. Phys. Chem. B*. **2008**, *112*, 9020–9041.

46. Jakalian, A.; Bush, B. L.; Jack, D. B.; Bayly, C. I. *J. Comput. Chem*. **2000**, *21*, 132–146.

47. Ryckaert, J.-P.; Ciccotti, G.; Berendsen, H. J. C. *J. Comput. Phys*. **1977**, *23*, 327–341.

48. Berendsen, H. J. C.; Postma, J. P. M.; Gunsteren, W. F. V.; DiNola, A.; Haak, J. R. *J. Chem. Phys*. **1984**, *81*, 3684–3690.

49. Shvartsburg, A. A.; Jarrold, M. F. *Chem. Phys. Lett*. **1996**, *261*, 86–91.

50. Mesleh, M. F.; Hunter, J. M.; Shvartsburg, A. A.; Schatz, G. C.; Jarrold, M. F. *J. Phys. Chem*. **1996**, *100*, 16082–16086.

51. RSCB Protein Data Bank. www.rcsb.org (accessed 3/14/2017).

52. Townsley, L. E.; Tucker, W. A.; Sham, S.; Hinton, J. F. *Biochemistry*. **2001**, *40*, 11676–11686.

53. Townsley, L. E. (PDB ID: 1NRM). 2003

54. Chen, L.; Gao, Y. Q.; Russell, D. H. *J. Phys. Chem. A*. **2012**, *116*, 689–696.

55. Chen, L.; Chen, S. H.; Russell, D. H. *Anal. Chem*. **2013**, *85*, 7826–7833.

56. Zhang, Y.; Liu, L.; Daneshfar, R.; Kitova, E. N.; Li, C.; Jia, F.; Cairo, C. W.; Klassen, J. S. *Anal. Chem*. **2012**, *84*, 7618–7621.

57. Chen, L. Ph.D. thesis, Texas A&M University, College Station, TX, 2012.

Chapter 6

1. Zhang, Y.; Liu, L.; Daneshfar, R.; Kitova, E. N.; Li, C.; Jia, F.; Cairo, C.W.; Klassen, J. S. *Anal. Chem.* **2012**, *84*, 7618–7621.

2. Leney, A.; Fan, X.; Kitova, E.N.; Klassen, J. S. *Anal. Chem.* **2014**, *86*, 5271–5277.

3. Leney, A. C.; Darestani, R. R.; Li, J.; Nikjah, S.; Kitova, E. N.; Zou, C.; Cairo, C. W.; Xiong, Leney, A.; Fan, X.; Kitova, E. N.; Klassen, J. S. *Anal. Chem.* **2015**, *87*, 4402–4408.

4. Dörr, J. M. Scheidelaar, S.; Koorengevel, M. C.; Dominguez, J. J.; Schäfer, M.; van Walree, C. A.; Killian, J. A. *Eur. Biophys. J*. **2016**, *45*, 3–21.

5. Lee, S. C.; Knowles, T. J.; Postis, V. L.; Jamshad, M.; Parslow, R. A.; Lin, Y. P.; Goldman, A.; Sridhar, P.; Overduin, M.; Muench, S. P.; Dafforn, T. R.; *Nat. Protoc.* **2016**, *11*, 1149–62.

6. Wu, H. J.; Henzie, J.; Lin, W. C.; Rhodes, C.; Li, Z.; Sartorel, E.; Thorner, J.; Yang, P.; Groves, J. T. *Nat Methods*. **2012**, *9*, 1189.

7. Wands, A. M.; Fujita, A.; McCombs, J. E.; Cervin, J.; Dedic, B.; Rodriguez, A. C.; Nischan, N.; Bond, M. R.; Mettlen, M.; Trudgian, D. C.; Lemoff, A.; QuidingJärbrink, M.;

Gustavsson, B.; Steentoft, C.; Clausen, H.; Mirzaei, H.; Teneberg, S.; Yrlid, U.; Kohler. J. J. *Elife* **2015**, 10.7554/eLife.09545.

8. Huang, P.; Farkas, T.; Zhong, W.; Thornton, S.; Morrow, A. L.; Jiang, X. *J. Virol*. **2005**, *79*, 6714.

9. Brown, R. E.; Thompson, T. E. *Biochemistry*. **1987**, *26*, 5454-5460.

10. Brown, R. E. *Biochim. Biophys. Acta*. **1992**, *1113*, 375-389.

11. Nichols, J. W. *Biochemistry*. **1988**, *27*, 3925-3931.

12. Arenas, R. C.; Danielczak, B.; Martel, A.; Porcar, L.; Breyton, C.; Ebel, C.; Kellera, S. *Scientific Reports*. **2017**, 7, 45875.